Advancing Fluoroalkylation Methodologies with Copper, Nickel, and Cobalt

Advancing Fluoroalkylation Methodologies with Copper, Nickel, and Cobalt

by

Scott T. Shreiber

A Dissertation

Presented to the Graduate and Research Committee

of Lehigh University

in Candidacy for the Degree of

Doctor of Philosophy

in

Department of Chemistry

Lehigh University

May 23, 2022

Approved and recommended for acceptance as a dissertation in partial fulfillment of the requirements for the degree of Doctor of Philosophy

Scott T. Shreiber
Advancing Fluoroalkylation Methodologies with Copper, Nickel, and Cobalt

03/23/2022 Committee Director/Advisor

Defense Date

Dr. David A. Vicic

03/24/2022

Approved Date

Committee Members

Dr. Gregory S. Ferguson

Dr. Xiaoji Xu

Dr. Robert Syvret

ACKNOWLEDGMENTS

Throughout my career I have had many incredible people help and support me, and I would like to take this opportunity to give my appreciation. To start at the true beginning, my family. I owe an incredible amount of indebted gratitude and appreciation to my mom and dad (Traci and Morgan) who have helped me in countless ways, and my brother Alex who has always set a positive example for me. I am forever grateful for my fiancé Kiera Jeschke, who has been an amazing supporter during my time in graduate school. She has exhaustively listened to countless stories, some even multiple times, and I couldn't be more thankful to have her support. I am further thankful for the Jeschke family for their support, Eric, Cheryl, Dana, and Evan.

I offer my gratitude and appreciation to my advisor, Professor David A. Vicic. You provided me with the proper guidance and mentorship to lead me to become an independent scientist, and supported me in my research and career endeavors. I am thankful to all the former Vicic Group members I have overlapped with: Dr. Mikhail Khrizanforov, Dr. Yulia Dudkina, Dr. Siqi Yu, Fatema Amin, John Scudder, and Renee Fang, and all the current members: Lydia Yorks, Gabby Puchall, and Lindsay Adler. I would like to specifically name current fellow graduate student Teng Xue – who has been in the group during my entire tenure, and has been a great colleague and friend.

I would be remiss if I did show my utter appreciation to the support and training I received prior to my time in graduate school. I am thankful to the chemistry faculty at Lock Haven University, the Neufedlt Group at Montana State University, and my colleagues during my time at Avery Dennison Performance Polymers.

TABLE OF CONTENTS

LIST OF FIGURES

LIST OF TABLES

LIST OF SCHEMES

LIST OF ABBREVIATIONS

%	percent
°	degrees
°C	degrees Celsius
^{19}F	fluorine-19
^{1}H	proton
$^{31}P\{^{1}H\}$	phosphorous-31 proton decoupled
Å	angstrom
Ar	aryl
bpy	bipyridine
Bu	butyl
CCDC	Cambridge Crystallographic Data Centre
CCSD(T)	coupled-cluster single doubles triples
COSY	correlated spectroscopy
Cp	cyclopentadienyl
CV	cyclic voltammetry
DFT	density functional theory
dme	diemethoxyethane
DMSO	dimethyl sulfoxide
dppp	1,2-bis(diphenylphosphino)ethane
equiv	equivalents
Et	ethyl
fac	facial
Fc	ferrocene
Fc^{+}	ferrocenium
g	gram
hr	hour
IEFPCM	integral equation formalism polarizable continuum model
IMes	1,3-bis(2,4,6-trimethylphenyl)imidazole-2-ylidene
M	molar
Me	methyl
Me_3-tacn	1,4,7-trimethyl-1,4,7-triazacyclononane
MeCN	acetonitrile
MeOH	methanol
mer	meridional
Mes	mesityl
mg	milligram
MHz	megahertz
min	minute
mL	milliliters

mM	millimolar
mmol	millimoles
mnt	maleonitriledithiolate
MO	molecular orbitals
NBu_4^+	tetrbutylammonium
NEt_4^+	tetraethylammonium
NHC	N-heterocyclic carbene
NMe_4^+	tetramethylammonium
NMR	nuclear magnetic resonance
OMe	methoxy
ORTEP	Oak Ridge Thermal Ellipsoid Plot
O^{t}Bu	*tert*-butoxide
OTf	triflate
Ph	phenyl
Phen	phenanthroline
PhO	phenoxide
PMe_3	trimethylphosphine
PPh_4^+	tetraphenylphosphonium
ppm	parts per million
PPN^+	bis(triphenylphosphine)iminium chloride
Py	pyridine
Pyr	pyridine
SIMes	1,3-dimesitylimidazolin-2-ylidene
SO_4^{2-}	sulfate
SORCI	spectroscopy oriented configuration interaction
TD-DFT	time dependent density functional theory
TEMPO	(2,2,6,6-tetramethypiperidine-1-yl)oxyl
THF	tetrahydrofuran
TMS	trimethylsilane
Tp	trispyrazoylborate
tpy	terpyridine
UV-Vis	ultraviolet-visible
XAS	x-ray absorption spectroscopy
δ	parts per million
μL	microliters

Abstract

The introduction of fluoroalkyl groups into organic molecules is well-known to alter various chemical and physical properties that are important to the life sciences and materials fields. Evidence is observed in the pharmaceutical field where over 40% of new small molecule drugs in 2018 and 2019 contained fluorine. Likewise, over 50% of new agrochemicals since 1998 contained fluoroalkyl functionalities. Therefore, the development of synthetic strategies for introducing fluoroalkyl groups is imperative in organic synthesis. In this dissertation, new advances towards enabling fluoroalkylation with earth-abundant first-row transition metals copper, cobalt, and nickel, are described. With copper, a methodology for rapidly accessing and analyzing mixed fluoroalkyl cuprates is described. A family of fluoroalkyl cobalt(III) complexes have been prepared, and their solution and oxidative properties have been studied. Finally, a new strategy for fluoroalkylation is reported using simple nickel salts supported by solvato ligands.

Chapter 1: Introduction

1.1 Importance of Fluorine in Organic Compounds

The introduction of fluorine into organic molecules is now well-known to alter various chemical and physically properties. The high electronegativity and electron-withdrawing abilities of fluoroalkyl groups decrease basicity of neighboring functionalities and ultimately alter the acidity (pK_a) of the molecule.[1] Fluorine has the ability to control conformational bias from hyperconjugation interactions of C-F σ^* orbitals accepting electron density from adjacent C-H σ bonds.[2] Fluoroalkyl groups offer the ability to increase a molecules lipophilicity, thus increasing membrane permeability and absorption.[3, 4] Further, fluoroalkyl groups have been shown to increase a molecule's stability by preventing metabolic decomposition.[4, 5]

Because of these unique properties, fluorine now plays a critical role in almost every aspect of human life. Products such as refrigerants[6], toothpaste[7], uranium purification[8], etchants[9], and cookware[10] all contain fluorine and fluorinated molecules. One of the most impactful roles that fluorine plays is in pharmaceuticals and agrochemicals. Over 50% of new agrochemicals introduced on the market from 1998-2020 contained fluorine.[11] Further, over 40% of new small molecule drugs introduced on the market in 2018 and 2019, contained fluorine (Figure 1a contains examples of fluorine containing pharmaceuticals).[12] A representative example for the unique effect of fluorine in drugs can be seen in the small molecule drug aprepitant (Figure 1a), where the added fluorinated functionalities are found to increase central nervous system permeability and potency in comparison to non-fluorinated counterparts.[13] Ezetimibe, a drug used for the treatments of high blood cholesterol was developed from **1a** (Figure 1b).[14] Compound **1a** was a potent lead

cholesterol absorption inhibitor, though it suffered from metabolic degradation at multiple sites.[14] However, incorporation of fluorinated groups produced the metabolically stable drug Ezetimibe, without affecting the potency (Figure 1b).[14]

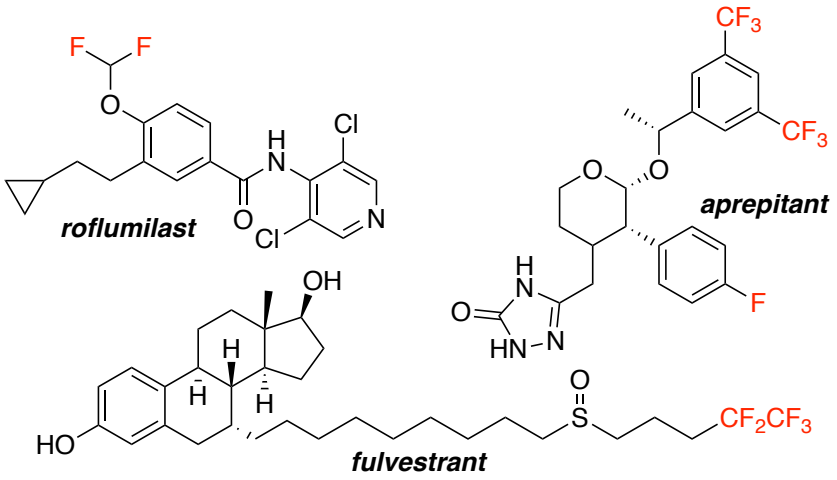

Figure 1a. Examples of fluorine containing drugs.

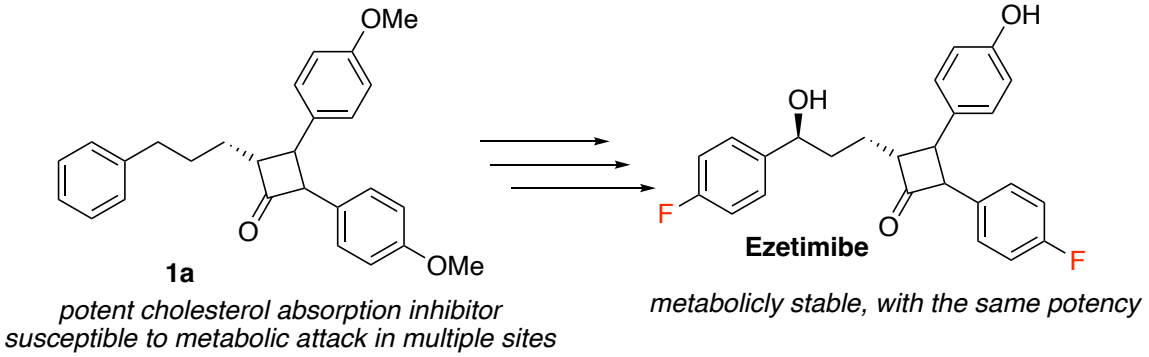

Figure 1b. Design of fluorinated Ezetimibe from cholesterol absorption inhibitor **1a**.

1.2 Methods for Incorporating Fluorine

While it is clear that incorporation of fluorine into organic molecules is important, synthetic methodologies are still needed for basic fluorinated groups. To exemplify the need, shown in Scheme 1a is the current industrial method to prepare one of the simplest trifluoromethyl containing molecules, trifluorotoluene. The method requires two synthetic steps and the

use of harsh chlorine gas and HF.[15] This method is very advantageous from an atom economy and cost perspective on the industrial scale. However, the method is not useful for fine chemical production of new products like pharmaceuticals, where late-stage functionalization can be beneficial. In the literature, there exist a number of different types of fluorinated groups, therefore, the focus of this section and this thesis is on perfluoroalkyl groups. The trifluoromethyl group has been regarded as one of the most important of the fluorinated functionalities, as it is the most common fluorinated group in agrochemicals,[11] and the second most common in pharmacueticals.[12]

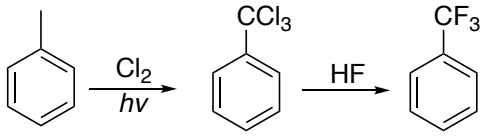

Scheme 1a. Industrial synthesis of trifluorotoluene

First-row transition metals are desirable catalysts for new synthetic methodologies for fluoroalkylations due to their low cost and higher natural abundance in comparison to second- and third-row metals. For example, nickel is over 2000x cheaper than palladium, rhodium, iridium, platinum, and gold. Furthermore, first-row transition metals tend to be lower in toxicity.[16] An additional benefit of first-row transition metals is they typically react under mild reaction conditions. If mild, catalytic method with first-row metals can be developed, and late-stage fluoroalkylations would be more accessible. The following three sections describe representations of the pioneering work with copper, nickel, and cobalt that has motivated the research in this thesis.

1.2.1 Methodologies Using Copper

For copper, a number of fundamental studies utilizing stoichiometric reactions with in-situ generated or isolable LCu-CF_3 (or C_nF_{2n+1}, L = ancillary ligand) complexes have been

reported to generate aryl-CF_3 products from aryl halides.[17-19] Examples of copper-catalyzed trifluoromethylations utilizing traditional cross-coupling approaches also have appeared in the literature.[20-22] For example, Hideki Amii's group reported a copper-catalyzed protocol for the trifluoromethylation of aryl iodides (Scheme 1b).[20] However, methods like those reported by Amii's group had low substrate scopes, gave moderate yields, required elevated temperatures, and often only worked for aryl iodides. The general proposed mechanism for these reactions is shown in Scheme 1b. Here, first a transmetalation of the trifluoromethyl group to copper(I) occurs, followed by an oxidative addition of the aryl halide, leading to reductive elimination from a copper(III) center to yield the desired product and complete the cycle.

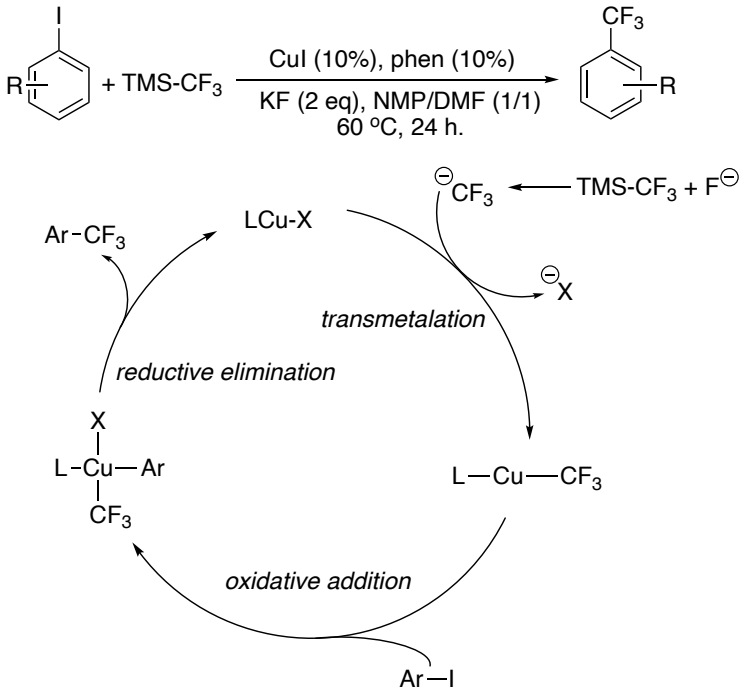

Scheme 1b. Early example of copper catalyzed trifluoromethylation strategy

Key takeaways of these fundamental and stoichiometric studies have now taught us that reductive elimination from copper(III) occurs quite readily, and oxidative addition at a copper(I) center with aryl iodides and bromides is difficult, but can occur at elevated

temperatures. However, aryl chlorides are rather unreactive. MacMillan's group used these known limitations and made a significant advance by using a copper-catalyzed radical approach for the trifluromethyaltion of aryl bromides (Scheme 1c).[23] Instead of requiring a discrete oxidative-addition step, they relied on the addition of aryl radicals adding to a [$L_nCu(II)$-CF_3] (generated from radical CF_3 addition to Cu(I)) species to generate an arylated copper(III) species that can quickly reductively eliminate aryl-CF_3 product (Scheme 1c). The method had a much broader substrate scope, operated at lower temperatures, and used the more widely available aryl bromides. Novel alternative approaches utilizing knowledge gained from fundamental studies will be critical to circumventing limitations in future methods developments.

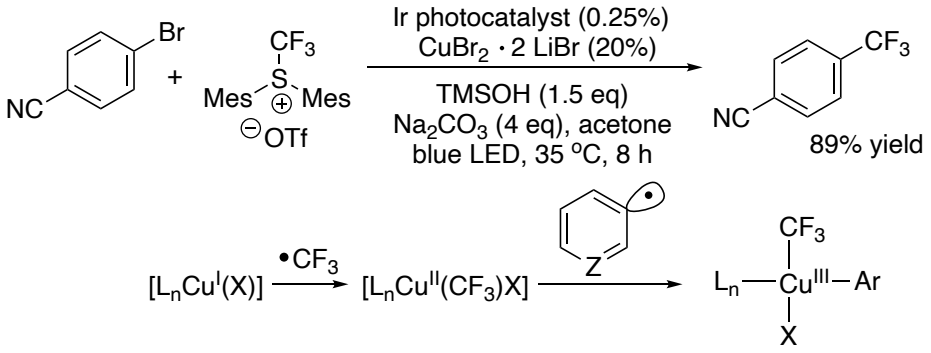

Scheme 1c. Radical approach to the copper oxidative-addition problem

1.2.2 Methodologies Using Nickel

Methodologies for the incorporation of perfluoroalkyl groups with nickel have suffered a different problem than copper. Oxidative addition of aryl halides occurs quite rapidly with nickel, and transmetalation is rather facile (Scheme 1d left).[24, 25] Rather the reductive elimination of aryl-CF_3 has proven to be quite challenging, particularly with nickel in the +2 oxidation state.[25] A fundamental study in 2008 found that nickel complexes of the type

[(dippe)Ni(aryl)(CF_3)] were stubborn to undergo reductive elimination, and rather underwent redistribution reactions (Scheme 1d right).[25] Hydrocarbon derivatives underwent reductive elimination quantitatively, in contrast (Scheme 1d right).[25] The work demonstrated an inherent challenge with developing nickel catalyzed fluoroalkylations - the ability to circumvent the need for discrete reductive elimination from nickel in the +2 oxidation state.

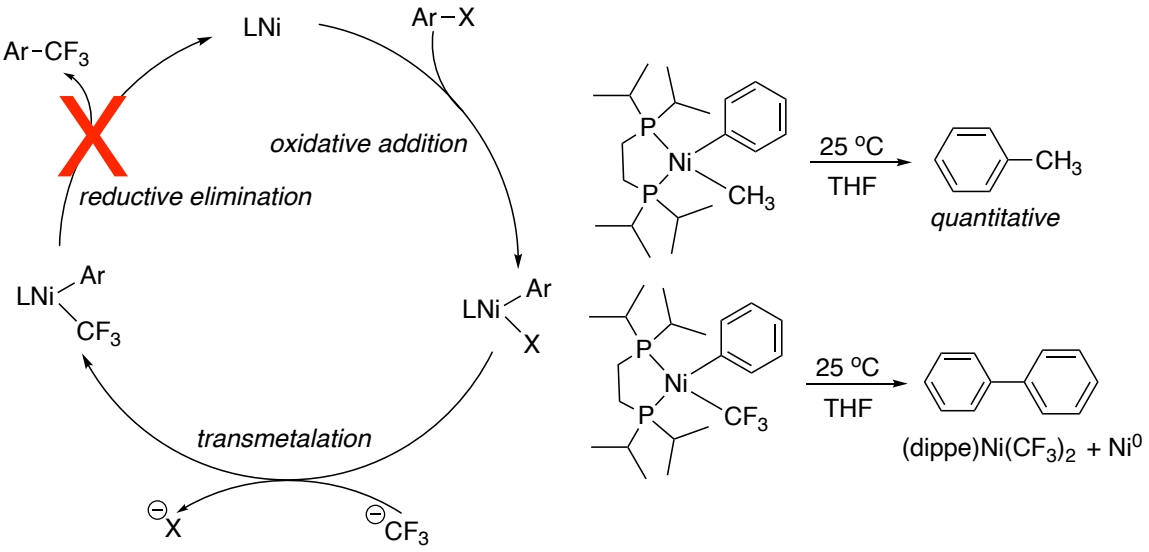

Scheme 1d. Left: Common catalytic cycle attempted for nickel-catalyzed trifluoromethylations of aryl halides. Right: Fundamental reactions comparing the difference between hydrocarbon and fluorocarbons in reductive eliminations from nickel

More recently, groups have begun to develop new approaches in order to circumvent this challenge, by accessing the high-valent states of nickel in order to enable reductive eliminations of aryl-CF_3 groups. The Sanford group found that using ligands like dppf, [(L)Ni(aryl)(CF_3)] species could be oxidized to formally nickel(III) states that could do reductive eliminations generating aryl-CF_3 products (Scheme 1e top).[26] However, in this reaction, the nickel containing byproducts were unidentified. While it is proposed that a nickel(I) species would be generated from the reductive elimination, other groups have

found that nickel(I) with wide-bite angles like dppf are detrimental to catalysis.[27] Sanford's group also has found using the Tp ligand, nickel(II) complexes can be oxidized with Umemoto Reagent II (2,8-difluoro-5-(trifluoromethyl)-5H-dibenzo[b,d]thiopehen-5-ium) to generate formally nickel(IV) complexes (Scheme 1e bottom).[28] Further, these complexes can indeed undergo reductive elimination of aryl-CF_3 products, and the nickel containing by products were a result of a ligand redistribution reaction ($[Ni(Tp)_2]$ and $[(MeCN)_2Ni(CF_3)_2]$, Scheme 1e bottom). Thus, it is clear that oxidation of nickel to higher valent states enables the difficult reductive eliminations, but the coordinated ligand on nickel is problematic for turning systems catalytic.

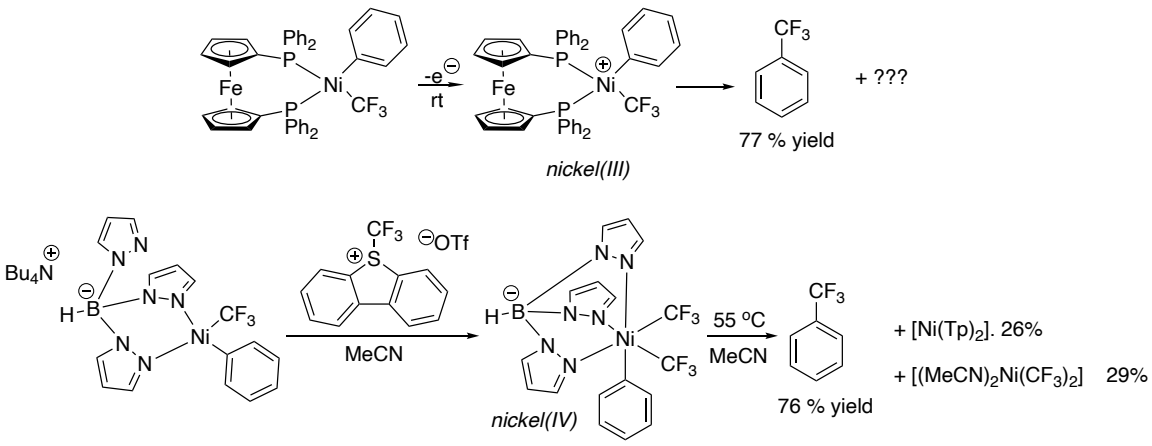

Scheme 1e. Trifluoromethylations enabled by accessing high-valent nickel

1.2.3 Methodologies Using Cobalt

Reactivity studies of well-defined cobalt fluoroalkyl complexes has only started to appear in the literature, and initial studies have shown great promise for developing new fluoroalkylation methodologies. For example, Soper's group has shown that Co-CF_3 complexes can undergo photolytic homolysis reactions leading to trifluoromethyl radicals that perform C-H bond trifluoromethyaltions of arenes (Scheme 1f top).[29] Further Baker's

group has found that Co-R_f complexes can undergo alpha-fluoride eliminations leading to difluorocarbene motifs (Co=CF_2), that then undergo migratory insertions (Scheme 1f bottom).[30, 31] These alternative reaction pathways are of high value in future methods developments, as the chemistry can complement what is known for copper and nickel.

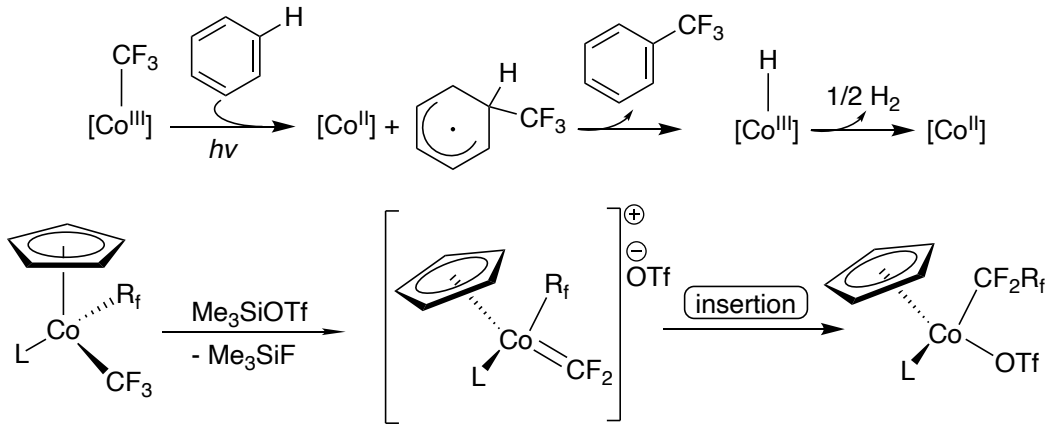

Scheme 1f. Unique reactivities of cobalt fluoroalkyl complexes

1.3 Overview of Thesis

The following chapters describe my recent efforts for developing new approaches for developing fluoroalkyaltions with copper, cobalt, and nickel. Each chapter is presented with its own introduction, followed by a presentation of the new chemistry I discovered. Chapter 2 describes my work focused on developing a method for preparing mixed fluoroalkyl cuprates that can be rapidly analyzed and screened by ^{19}F NMR for use in new synthetic methodology developments. Chapter 3-5 document the preparation of a family of new fluoroalkylated cobalt(III) complexes, and their characterization, including oxidative stabilities towards accessing formally cobalt(IV) fluoroalkyls. Chapter 6-9 show my work towards developing fluoroalkylations at nickel using a solvated nickel platform.

1.4 Comment on Per- and Polyfluoroalkyl Substances (PFAS)

Currently there exist a growing concern over the existence of per- and polyfluoroalkyl substances (PFAS) in the environment. The PFAS are long lasting chemicals that break down slowly and have now been found in the water, air, fish, and soil. Some PFAS in the environment have now been linked to harmful effects on humans and animals.[32] Generally the six or more fluorinated carbon chains are the class PFAS that have been well-studied, and linked to such harms.[33] Therefore, industries started to stop using the longer chain fluoroalkyls and began using smaller fluoroalkyl carbon chains (four). However, more recent research has suggested that even these molecules are also harmful to the environment.[33] Currently, fluoroalkyl groups studied in this dissertation (one or two carbon chains) are not of the class of harmful PFAS however, it is important to note that these substances exist and are harmful to the environment. Further as described in this thesis, the ability to synthesize and characterize fluoroalkyl organometallic complexes however, does provide a potential opportunity to use fundamental organometallic chemistry to study the removal or break down of PFAS in the future.

1.5 References

1. O'Hagan, D. Understanding Organofluorine Chemistry. An Introduction to the C–F Bond. *Chem. Soc. Rev.* **2008,** *37*, 308-319.
2. Gillis, E. P.; Eastman, K. J.; Hill, M. D.; Donnelly, D. J.; Meanwell, N. A. Applications of Fluorine in Medicinal Chemistry. *J. Med. Chem.* **2015,** *58*, 8315-8359.
3. Zhou, Y.; Wang, J.; Gu, Z.; Wang, S.; Zhu, W.; Aceña, J. L.; Soloshonok, V. A.; Izawa, K.; Liu, H. Next Generation of Fluorine-Containing Pharmaceuticals, Compounds Currently in Phase II–III Clinical Trials of Major Pharmaceutical Companies: New Structural Trends and Therapeutic Areas. *Chem. Rev.* **2016,** *116*, 422-518.
4. Kirk, K. L. Fluorination in Medicinal Chemistry: Methods, Strategies, and Recent Developments. *Org. Process Res. Dev.* **2008,** *12*, 305-321.
5. Müller, K.; Faeh, C.; Diederich, F. Fluorine in Pharmaceuticals: Looking Beyond Intuition. *Science* **2007,** *317*, 1881-1886.
6. Sicard, A. J.; Baker, R. T. Fluorocarbon Refrigerants and their Syntheses: Past to Present. *Chem. Rev.* **2020,** *120*, 9164-9303.

7. Williams, K. R., Behind the Scenes at the Toothpaste Aisle: The Chemistry of Dental Materials. *J. Chem. Ed.* **2010,** *87*, 1007-1008.
8. Barbour, A. K.; Barlow, G. B.; Tatlow, J. C. The Fluorination of Hydrocarbons with Cobalt Trifluoride. *J. Appl. Chem.* **1952,** *2*, 127-133.
9. Kolasinski, K. W. Etching of Silicon in Fluoride Solutions. *Surf. Sci.* **2009,** *603*, 1904-1911.
10. Sajid, M.; Ilyas, M. PTFE-Coated Non-Stick Cookware and Toxicity Concerns: a Perspective. *Environ. Sci. Pollut. Res.* **2017,** *24*, 23436-23440.
11. Ogawa, Y.; Tokunaga, E.; Kobayashi, O.; Hirai, K.; Shibata, N. Current Contributions of Organofluorine Compounds to the Agrochemical Industry. *iScience* **2020,** *23*, 101467.
12. Inoue, M.; Sumii, Y.; Shibata, N. Contribution of Organofluorine Compounds to Pharmaceuticals. *ACS Omega* **2020,** *5*, 10633-10640.
13. Hale, J. J.; Mills, S. G.; MacCoss, M.; Finke, P. E.; Cascieri, M. A.; Sadowski, S.; Ber, E.; Chicchi, G. G.; Kurtz, M.; Metzger, J.; Eiermann, G.; Tsou, N. N.; Tattersall, F. D.; Rupniak, N. M. J.; Williams, A. R.; Rycroft, W.; Hargreaves, R.; MacIntyre, D. E. Structural Optimization Affording 2-(R)-(1-(R)-3,5-Bis(trifluoromethyl)phenylethoxy)-3-(S)-(4-fluoro)phenyl-4- (3-oxo-1,2,4-triazol-5-yl)methylmorpholine, a Potent, Orally Active, Long-Acting Morpholine Acetal Human NK-1 Receptor Antagonist. *J. Med. Chem.* **1998,** *41*, 4607-4614.
14. Shah, P.; Westwell, A. D. The Role of Fluorine in Medicinal Chemistry. *J. Enzyme Inhib. Med. Chem.* **2007,** *22*, 527-540.
15. Swarts, F. *Bull. Akad. R. Belg.* **1898,** *45*, 875.
16. Gandeepan, P.; Müller, T.; Zell, D.; Cera, G.; Warratz, S.; Ackermann, L. 3d Transition Metals for C–H Activation. *Chem. Rev.* **2019,** *119*, 2192-2452.
17. Dubinina, G. G.; Furutachi, H.; Vicic, D. A. Active Trifluoromethylating Agents From Well-Defined Copper(I)-CF_3 Complexes. *J. Am. Chem. Soc.* **2008,** *130*, 8600-8601.
18. Morimoto, H.; Tsubogo, T.; Litvinas, N. D.; Hartwig, J. F. A Broadly Applicable Copper Reagent for Trifluoromethylations and Perfluoroalkylations of Aryl Iodides and Bromides. *Angew. Chem. Int. Ed.* **2011,** *50*, 3793-3798.
19. Tomashenko, O. A.; Escudero-Adán, E. C.; Belmonte, M. M.; Grushin, V. V. Simple, Stable, and Easily Accessible Well Defined $CuCF_3$ Aromatic Trifluoromethylating Agents. *Angew. Chem. Int. Ed.* **2011,** *50*, 7655-7659.
20. Oishi, M.; Kondo, H.; Amii, H. Aromatic Trifluoromethylation Catalytic in Copper. *Chem. Commun.* **2009,** *14*, 1909-1911.
21. Weng, Z.; Lee, R.; Jia, W.; Yuan, Y.; Wang, W.; Feng, X.; Huang, K.-W. Cooperative Effect of Silver in Copper-Catalyzed Trifluoromethylation of Aryl Iodides Using Me_3SiCF_3. *Organometallics* **2011,** *30*, 3229-3232.
22. Schareina, T.; Wu, X.-F.; Zapf, A.; Cotté, A.; Gotta, M.; Beller, M. Towards a Practical and Efficient Copper-Catalyzed Trifluoromethylation of Aryl Halides. *Top. Catal.* **2012,** *55*, 426-431.
23. Le, C.; Chen, T. Q.; Liang, T.; Zhang, P.; MacMillan, D. W. C. A Radical Approach to the Copper Oxidative Addition Problem: Trifluoromethylation of Bromoarenes. *Science* **2018,** *360*, 1010-1014.

24. Bajo, S.; Laidlaw, G.; Kennedy, A. R.; Sproules, S.; Nelson, D. J. Oxidative Addition of Aryl Electrophiles to a Prototypical Nickel(0) Complex: Mechanism and Structure/Reactivity Relationships. *Organometallics* **2017,** *36*, 1662-1672.
25. Dubinina, G. G.; Brennessel, W. W.; Miller, J. L.; Vicic, D. A. Exploring Trifluoromethylation Reactions at Nickel: A Structural and Reactivity Study. *Organometallics* **2008,** *27*, 3933-3938.
26. Bour, J. R.; Roy, P.; Canty, A. J.; Kampf, J. W.; Sanford, M. S., Oxidatively Induced Aryl-CF_3 Coupling at Diphosphine Nickel Complexes. *Organometallics* **2020,** *39*, 3-7.
27. Mohadjer Beromi, M.; Nova, A.; Balcells, D.; Brasacchio, A. M.; Brudvig, G. W.; Guard, L. M.; Hazari, N.; Vinyard, D. J. Mechanistic Study of an Improved Ni Precatalyst for Suzuki–Miyaura Reactions of Aryl Sulfamates: Understanding the Role of Ni(I) Species. *J. Am. Chem. Soc.* **2017,** *139*, 922-936.
28. Bour, J. R.; Camasso, N. M.; Sanford, M. S. Oxidation of Ni(II) to Ni(IV) with Aryl Electrophiles Enables Ni-Mediated Aryl-CF_3 Coupling. *J. Am. Chem. Soc.* **2015,** *137*, 8034-8037.
29. Harris, C. F.; Kuehner, C. S. B., J.; Soper, J. D. Photoinduced Cobalt(III)-Trifluoromethyl Bond Activation Enables Arene C-H Trifluoromethylation. *Angew. Chem. Int. Ed.* **2018,** *57*, 1311-1315.
30. Harrison, D. J.; Gorelsky, S. I.; Lee, G. M.; Korobkov, I.; Baker, R. T. Cobalt Fluorocarbene Complexes. *Organometallics* **2013,** *32*, 12-15.
31. Leclerc, M. C.; Bayne, J. M.; Lee, G. M.; Gorelsky, S. I.; Vasiliu, M.; Korobkov, I.; Harrison, D. J.; Dixon, D. A.; Baker, R. T. Perfluoroalkyl Cobalt(III) Fluoride and Bis(perfluoroalkyl) Complexes: Catalytic Fluorination and Selective Difluorocarbene Formation. *J. Am. Chem. Soc.* **2015,** *137*, 16064-16073.
32. *EPA PFAS Explained.* https://www.epa.gov/pfas/pfas-explained (accessed 2022-03-23)
33. Kwiatkowski, C. F.; Andrews, D. Q.; Birnbaum, L. S.; Bruton, T. A.; DeWitt, J. C.; Knappe, D. R. U.; Maffini, M. V.; Miller, M. F.; Pelch, K. E.; Reade, A.; Soehl, A.; Trier, X.; Venier, M.; Wagner, C. C.; Wang, Z.; Blum, A. Scientific Basis for Managing PFAS as a Chemical Class. *Environ. Sci. Technol. Lett.* **2020**, *7*, 532-543.

Chapter 2: Synthesis, Solution Behavior, and Computational Bond Length Analyses of Trifluoromethyl and Perfluoroethyl Cuprate Salts

The following chapter has been adapted (reprinted) with permission from: Shreiber, S. T.; Kaplan, P. T.; Hughes, R. P.; Vasiliu, M.; Dixon, D. A.; Cramer, R. E.; Vicic, D. A. *J. Fluorine Chem.* **2020**, *234*, 109518.

2.1 Abstract: Heteroleptic cuprate salts of the form [X-Cu-Y][$(SIMes)_2Cu$] (SIMes = 1,3-dimesitylimidazolin-2-ylidene, X and Y = permutations of Cl, CF_3, C_2F_5) were generated by equilibrating mixtures of [(SIMes)Cu-X] and [(SIMes)Cu-Y] in CD_2Cl_2 solvent. The solubility features of the cuprates relative to the neutral species permitted the structural characterizations of new cuprates, including the first example of a mixed fluoroalkylated cuprate [$(CF_3)Cu(C_2F_5)$][$(SIMes)_2Cu$]. Computational studies (DFT and CCSD(T)) of fluorinated cuprates generate Cu-C distances that are shorter than those in hydrocarbon analogues, in conflict with crystallographically determined values, which show the reverse trend.

2.2 Introduction: There is a continuous demand to develop better ways to incorporate fluoroalkyl groups into organic molecules. The trifluoromethyl group, in particular, has become an important replacement for metabolically sensitive CH_3 groups attached to aromatic and heteroaromatic rings in drug candidates.[1-3] Pentafluoroethyl and longer-chained fluoroalkyl groups are also emerging as novel functionalities in medicinal chemistry,[4-7] and thus the transition-metal-mediated fluoroalkylation of organic halides has become a topic of intense research in the past two decades. Many such reactions have been developed with copper, and the active fluoroalkylating agents commonly take on the form [LCu-R_f], where L = solvent or another type of ancillary ligand (Scheme 2a, eq a). Mechanistic studies of fluoroalkylation reactions with copper have established that, for

certain ligand frameworks, [LCu-R_f] can exist in equilibria with its cuprate form as described in Scheme 2a, eq b.[8-12]

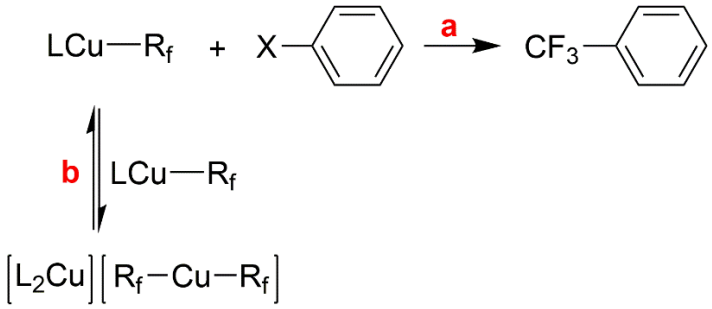

Scheme 2a. Equilibrium of fluoroalkyl cuprates and their reactivity towards aryl halides.

Vicic provided the first kinetic evidence that the charge neutral form (and not the cuprate) is the more active species in copper-mediated trifluoromethylation of aryl halides.[8] Others have recently provided additional experimental and computational support for this assignment.[12,13] Despite displaying a lower reactivity towards organic halides, the generation of [R_f-Cu-R_f]$^-$ cuprates can be important for providing stable reservoirs of the more sensitive [LCu-R_f] at higher temperatures[14] or even providing precursors of [LCu-R_f] at lower temperatures[12] in copper-mediated fluoroalkylation reactions.

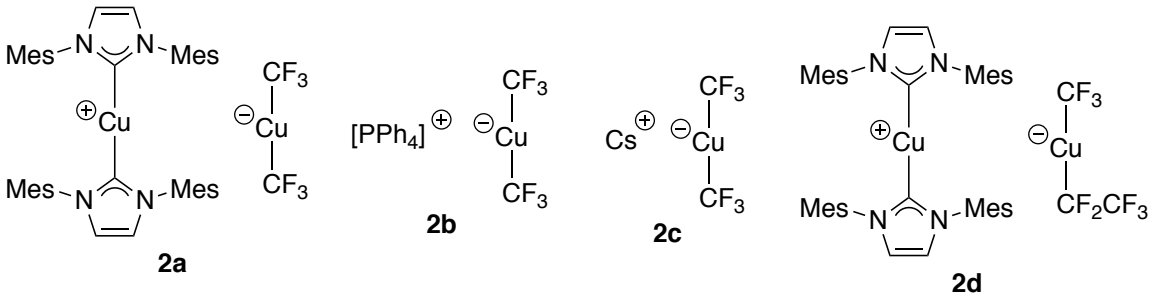

Scheme 2b. Examples of known fluoroalkyl cuprates.

The characterization of bis(trifluoromethyl)cuprates began in 1986, when Burton reported that addition of [CuBr] to [CF_3-Cd-X] led to the formation of [Cu-CF_3], which upon heating

gave rise to two new and additional NMR peaks.[15] Formal assignment of one of these peaks as a bis(trifluoromethyl)cuprate salt was later reported in 1989 by the same research group.[16] The first crystal structure of a bis(trifluoromethyl)cuprate salt was that of complex **2a**, whose separation from the neutral form was enabled by solubility differences afforded by the NHC (N-heterocyclic carbene) ligand.[8] The copper-carbon bond lengths of **2a** were reported to be 1.970(6) Å, which were significantly longer than any of the known $[CH_3\text{-}Cu\text{-}CH_3]^-$ derivatives **2e**-**2g** (Table 2a). Recently, two more crystal structures of a bis(trifluoromethyl)cuprate appeared in the literature. Complex **2b** bears a tetraphenylphosphonium counter-ion, and the copper-carbon bond lengths of **2b** were reported to be 1.930(3) Å.[12] The cesium complex **2c** has also been disclosed, however the structure is somewhat complicated due to the presence of intermolecular Cs···F and Cu···Cu contacts.[13] Complex **2c** has copper-carbon bond lengths of 1.940(10) Å. Because of the substantial differences in copper-carbon bond distances between **2a** and **2b**, both of which contain no intermolecular atom···atom contacts that could influence the bond lengths, we were interested in obtaining insights from electronic structure theory methods about what the bond lengths in bis(trifluoromethyl)cuprates would be in gas phase structures. Gas phase structures would also not be influenced by crystal packing forces,[17-19] and thus more accurate bond length comparisons could be obtained computationally. Additionally, we were curious to see how the copper-carbon bond length would vary in 'mixed' $[X\text{-}Cu\text{-}CF_3]^-$ cuprates. To this end, we explored the development of a new synthetic route to prepare such mixed cuprates, including one that bears one trifluoromethyl and one perfluoroethyl ligand, namely $[CF_3\text{-}Cu\text{-}C_2F_5][(SIMes)_2Cu]$ (**2d**).

Table 2a. Crystallographically determined bond lengths of various cuprates.

Compound	*Experimentally Determined Cu-CX_3 Bond Length (Å)*	*Reference*
$[(CF_3)_2Cu][(SIMes)_2Cu]$ (**2a**)	1.970(6)	[8]
$[(CF_3)_2Cu][PPh_4]$ (**2b**)	1.930(3)	[12]
$[(CF_3)_2Cu][Cs]$ (**2c**)	1.940(10)	[13]
$[(CF_3)Cu(C_2F_5)][(SIMes)_2Cu]$ (**2d**)	1.927(2)	this work
$[Me_2Cu][Li(12\text{-crown-}4)_2]$ (**2e**)	1.935(8)	[20]
$[Me_2Cu][Cu(PMe_3)_4]$ (**2f**)	1.94(1)	[21]
$[Me_2Cu][Li(dme)_3]$ (**2g**)	1.933(4) avg	[22]

2.3 Results and Discussion

2.3.1. Synthesis of the Pentafluoroethyl Cuprate: Addition of $[Me_3Si\text{-}C_2F_5]$ to the known [(SIMes)Cu-O^{t}Bu] (**2h**) led to the production of $[(SIMes)Cu\text{-}C_2F_5]$ (**2i**) in 41% isolated yield (Scheme 2c). The solution behavior of **2i** is similar to that of $[(SIMes)Cu\text{-}CF_3]$ whereby an equilibration with the cuprate form **2j** could be observed by NMR spectroscopy (Scheme 2c). The ^{19}F NMR signals of the neutral species **2i** appear at δ = 85.64 and 119.43 in CD_2Cl_2, and the signals of **2j** appear at δ = 85.01 and 118.04.

Solubility differences between **2i** and **2j** enabled the selective crystallization of **2j** from THF/pentane, and X-ray crystallography confirmed the structure (See Appendix A).

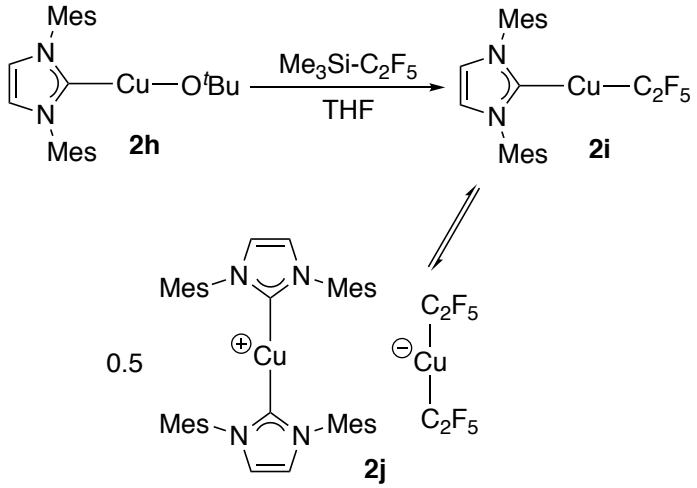

Scheme 2c. Preparation of [(SIMes)Cu(C_2F_5)] (**2i**), and its equilibration with the cuprate.

2.3.2. Generation of the First Mixed Fluoroalkyl Cuprate: Having established that both [(SIMes)Cu-C_2F_5] (**2i**) and [(SIMes)Cu-CF_3] (**2k**) equilibrate into the cuprate forms, we wondered whether mixtures of **2i** and **2k** would give rise to the mixed cuprate [CF_3-Cu-C_2F_5][$(SIMes)_2Cu$] (**2d**, Scheme 2d). To our knowledge, such a mixed perfluoroalkyl cuprate is unknown. Indeed, dissolution of a 1:1 mixture of **2i** and **2k** in CD_2Cl_2 gave rise to a set of NMR signals (δ = 32.14, 84.98, and 118.01) that didn't correspond to either of the established [CF_3-Cu-CF_3]$^-$ or [C_2F_5-Cu-C_2F_5]$^-$ salts (the ratio of the fluorinated copper complexes in solution can be found in the experimental section). Fortuitous crystallization of this new product from THF/pentane enabled its unambiguous structural assignment by X-ray diffraction, which confirmed the structure to be the mixed cuprate **2d** (Figure 2a). In the solid state, the Cu-CF_3 bond length of 1.927(2) Å in **2d** was found to be longer than the Cu-CF_2CF_3 bond length (1.916(2) Å), suggesting the perfluoroethyl exhibits larger

trans influencing properties than the trifluoromethyl group. However, gas-phase calculations conflict with these crystallographically determined bond lengths (see below).

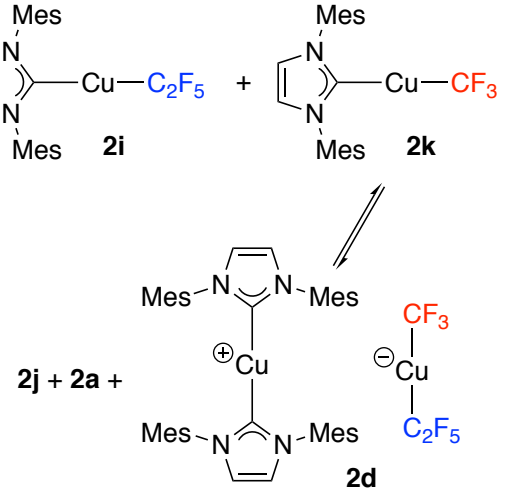

Scheme 2d. Equilibration of a mixture of **2i** and **2k** with all possible cuprate forms.

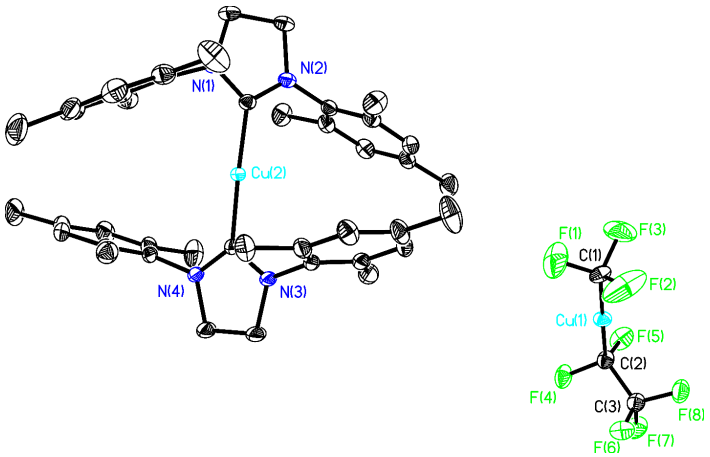

Figure 2a. ORTEP diagram of **2d**. Hydrogens are omitted for clarity. Selected bond lengths (Å): Cu1-C1 1.927(2); Cu1-C2 1.916(2). Selected bond angle (˚): C2-Cu1-C1 178.10(10).

2.3.3. General Method to Preparing Mixed Cuprates: To examine whether the [(SIMes)Cu] system can also be used to characterize mixed cuprates of the type [X-Cu-R_f]$^-$, where X=halides (Scheme 2e), we allowed [(SIMes)CuCl] (**2l**) and [(SlMes)Cu(CF_2CF_3)] (**2i**) to react. Gratifyingly, the mixture gave rise to a new set of signals in the ^{19}F NMR spectrum in CD_2Cl_2 at δ = -85.10 and -113.56, which corresponds

to the known $[Cl\text{-}Cu\text{-}C_2F_5)]^-$ anion.[23] In accordance with Nolan's prior results, complex **2l** also shows minor traces of the $[(SIMes)_2Cu]^+$ cation, suggestive that **2l** is also in equilibrium with $[(SIMes)_2Cu][Cl\text{-}Cu\text{-}Cl]$ (**2o**). The ability of **2l** to equilibrate into its cuprate form **2o** would then be similar to [(SIMes)AgCl],[24,25] although we are unaware of any reports that specifically refer to an equilibrium process for the copper derivative.

Importantly, the [(SIMes)Cu] system may be useful to characterize previously unknown mixed cuprates. A SciFinder search of the $[Cl\text{-}Cu\text{-}CF_3)]^-$ anion gave no hits (at the time this work was conducted and published), so we exploited the equilibrium properties of the[(SIMes)Cu] system to determine its NMR spectrum. Reaction of $[(SIMes)Cu(CF_3)]$ (**2k**) with [(SIMes)CuCl] (**2l**) indeed led to the generation of the new cuprate $[(SIMes)_2Cu][Cl\text{-}Cu\text{-}CF_3)]$ (**2n**) which displayed a new resonance in ^{19}F NMR spectrum in CD_2Cl_2 at δ = -28.17. Table 2b summarizes the ^{19}F NMR chemical shifts of the SIMes copper complexes in CD_2Cl_2.

Table 2b. ^{19}F NMR chemical shifts (ppm) of copper complexes in CD_2Cl_2.

compound	Cu-CF_3 resonance	Cu-CF_2CF_3 resonance	Cu-CF_2CF_3 resonance
[(SIMes)Cu(CF_3)] (**2k**)	-33.25	-	-
[(SIMes)$_2$Cu][Cu(CF_3)$_2$] (**2a**)	-32.06	-	-
[(SIMes)Cu(CF_2CF_3)] (**2i**)	-	-85.64	-119.43
[(SIMes)$_2$Cu][Cu(CF_2CF_3)$_2$] (**2j**)	-	-85.01	-118.04
[(SIMes)$_2$Cu][Cu(CF_3)(C_2F_5)] (**2d**)	-32.14	-84.98	-118.01
[(SIMes)$_2$Cu][Cu(Cl)(C_2F_5)] (**2m**)	-	-85.10	-113.56
[(SIMes)$_2$Cu][Cu(Cl)(CF_3)] (**2n**)	-28.17	-	-

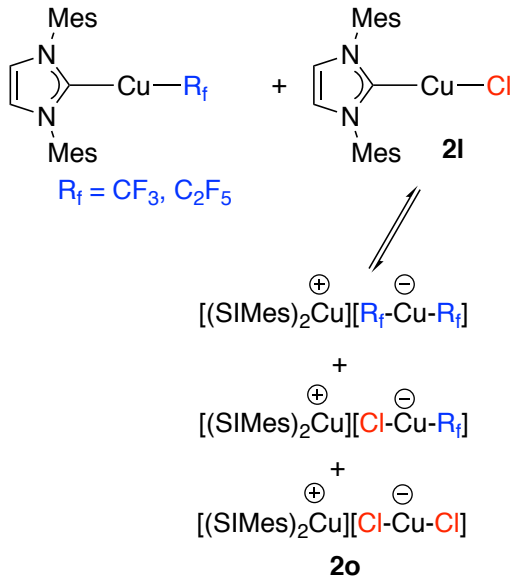

Scheme 2e. Equilibration of a mixture of a [(SIMes)Cu-R_f] complex and **2l** with all possible cuprate forms.

2.3.4. Computational Bond Length Analysis: Based on of the interesting discrepancy in experimental bond length between **2a** and **2b** (Table 2a), in collaboration from Russell P. Hughes (*Dartmouth),* and David A. Dixon's group (*Alabama)*, a computational bond length analysis of various hydrocarbon and fluorocarbon cuprates was performed. In summary of their combined efforts, gas-phase structures of cuprate anions was performed, and compared to crystallographic results. They found that fluorinated cuprates generate Cu-C distances that are shorter than those in hydrocarbon analogous, the opposite of which is seen in experimentally determined values. According to Dixon and Hughes, it is plausible that adventitious intermolecular packing forces in the crystal would be more than sufficient to results in intramolecular bond length variations that would confound the predictions of gas phase electronic structure calculations. Caveats concerning crystalographically determined structures have been discussed in the literature[26,27], and should serve as a caution when using experimentally determined solid state data to validate

gas-phase computational metrics. Analogously, a discrepancy between the mixed fluoroalkyl cuprate **2d**, found a longer Cu-CF_3 in the crystallography data, than the Cu-C_2F_5 distance, and the opposite was found in the computed structure.

2.4. Conclusions: Here we describe a procedure to prepare heteroleptic cuprate salts of the form [X-Cu-Y][$(SIMes)_2$Cu] (where X and Y = permutations of Cl, CF_3, C_2F_5) by equilibrating mixtures of [(SIMes)Cu-X] and [(SIMes)Cu-Y] in CD_2Cl_2 solvent. The solubility features of the cuprates relative to the neutral species permitted the structural characterizations of new cuprates, including the first example of a mixed fluoroalkylated cuprate [$(CF_3)Cu(C_2F_5)$][$(SIMes)_2$Cu]. Computational studies (DFT and CCSD(T)) of fluorinated cuprates generate Cu-C distances that are shorter than those in hydrocarbon analogues, in conflict with crystallographically determined values, which show the reverse trend. Given these observations, along with the additional caveat that the trifluoromethyl group is quite often disordered in X-ray crystal structures, we strongly encourage the use of electronic structure methods to supplement crystallography data in discussions of metal-CF_3 distances.

2.5. Experimental

2.5.1. General Information: All manipulations were performed using standard Schlenk and high vacuum techniques or in a nitrogen-filled glovebox. Solvents were purified by passing through activated alumina and/or copper in a solvent purification system supplied by Pure Process Technology. Solution ^{1}H NMR spectra were recorded at ambient temperature on a Bruker DRX 400 MHz spectrometer and referenced to residual proton solvent signals. ^{19}F spectra were recorded on the Bruker NMR spectrometer operating at 376 MHz and referenced to α,α,α-trifluorotoluene as an internal standard (δ = -63.7). A

Bruker D8 Quest diffractometer was used for X-ray crystal structure determinations. The CCDC numbers 1986498, 1986499, and 1986500 contain the supplementary crystallographic data for compounds **10**, **4**, and **13**, respectively, for this paper. These data can be obtained free of charge via www.ccdc.cam.ac.uk/data_request/cif, or by e-mailing data_request@ccdc.cam.ac.uk, or by contacting The Cambridge Crystallographic Data Centre, 12 Union Road, Cambridge CB2 1EZ, UK; fax: +44 1223 336033.

2.5.2. Preparation of [(SIMes)Cu(C_2F_5)] (2i): In a nitrogen glovebox, [(SIMes)Cu(O-*t*-Bu)] (0.22 g, 0.50 mmol) and TMS-C_2F_5 (0.13 mL, 0.75 mmol) were stirred in 6 mL of THF. After 3 hours, the volatiles were removed and the resulting solid was washed twice with 5 mL of toluene, and twice with 5 mL of pentane to yield 100 mg (41% yield) of white solid. The thermal and air-sensitivity of **2i** precluded elemental analysis. ^{1}H NMR (CD_2Cl_2, 400 MHz): δ: 7.00 (s, 4H), 3.97 (s, 4H), 2.46 – 2.20 (br s, 18H). ^{19}F NMR (CD_2Cl_2, 376 MHz): δ: -85.64 (s, 3F), -119.43 (s, 2F).

2.5.3. NMR Spectra of [(SIMes)$_2$Cu][Cu(C_2F_5)$_2$] (2j) Present in Solutions of 2i: ^{1}H NMR (CD_2Cl_2, 400 MHz): δ: 6.89 (s, 4H), 3.79 (s, 4H), 2.38 (s, 6H), 1.83 (s, 12H). ^{19}F NMR (CD_2Cl_2, 376 MHz): δ : -85.01 (s, 3F), -118.04 (s, 2F).

2.5.4. Generation of [(SIMes)$_2$Cu][Cu(CF_3)(C_2F_5)] (2d) for NMR Analysis: In a nitrogen filled glovebox, 20 mg (0.05 mmol) of [(SIMes)Cu(C_2F_5)] and 10 mg (0.02 mmol) of [(SIMes)Cu(CF_3)] were dissolved in CD_2Cl_2 inside a NMR tube and mixed. Three new unique NMR signals were observed corresponding to **2d**. ^{19}F NMR (CD_2Cl_2, 376 MHz): δ : -32.14 (s, 3F), -84.98 (s, 3F), -118.01 (s, 2F). 23% converted to [F_3C-Cu-CF_2CF_3]$^-$ based on [(SlMes)Cu-CF_3] added. The ratio of each species in solution was: 0.07 [F_3C-Cu-

$CF_2CF_3]^-$: 0.02 $[F_3C\text{-}Cu\text{-}CF_3]^-$: 0.21 [(SlMes)Cu-CF_3 : 0.05 $[CF_3CF_2\text{-}Cu\text{-}CF_2CF_3]^-$: 0.65 [(SlMes)Cu-CF_2CF_3.

2.5.5. Generation of $[(SIMes)_2Cu][Cu(Cl)(C_2F_5)]$ (2m) for NMR Analysis: In a nitrogen-filled glovebox, 10 mg (0.02 mmol) of both [(SIMes)Cu(C_2F_5)] and [(SIMes)Cu(Cl)] were dissolved in CD_2Cl_2 inside a NMR tube and mixed. Two new unique NMR signals were observed corresponding to **2m**. ^{19}F NMR (CD_2Cl_2, 376 MHz): δ : -85.10 (s, 3F), -113.56 (s, 2F). 36% converted to $[Cl\text{-}Cu\text{-}CF_2CF_3]^-$ based on [(SlMes)Cu-CF_2CF_3] added. The ratio of each species in solution was: 0.36 $[Cl\text{-}Cu\text{-}CF_2CF_3]^-$: 0.17 $[CF_3CF_2\text{-}Cu\text{-}CF_2CF_3]^-$: 0.47 [(SlMes)Cu-CF_2CF_3].

2.5.6 Generation of $[(SIMes)_2Cu][Cu(Cl)(CF_3)]$ (2n) for NMR Analysis: In a nitrogen filled glovebox, 10 mg of both [(SIMes)Cu(CF_3)] and [(SIMes)Cu(Cl)] were dissolved in CD_2Cl_2 inside a NMR tube and mixed. One new unique NMR signal was observed corresponding to **2n**. ^{19}F NMR (CD_2Cl_2, 376 MHz): δ : -28.17 (s, 3F). 51% converted to $[Cl\text{-}Cu\text{-}CF_3]^-$ based on [(SlMes)Cu-CF_3] added. The ratio of each species in solution was: 0.51 $[Cl\text{-}Cu\text{-}CF_3]^-$: 0.23 $[CF_3\text{-}Cu\text{-}CF_3]^-$: 0.26 [(SlMes)Cu-CF_3.

2.6 References

1. Müller, K.; Faeh, C.; Diederich, F. Fluorine in Pharmaceuticals: Looking Beyond Intuition. *Science* **2007**, *317,* 1881-1886.
2. Heidelberger, C.; Boohar, J.; Kampschroer, B. Fluorinated Pyrimidines, XXIV. In Vivo Metabolism of 5-Trifluoromethyluracil-2-C14 and 5-Trifluoromethyl-2'-deoxyuridine-2-C14. *Cancer Res.* **1965**, *25*, 377-381.
3. Zhu, W.; Wang, J.; Wang, S.; Gu, Z.; Aceña, J.L.; Izawa, K.; Liu, H.; Soloshonok, V. A. Recent Advances in the Trifluoromethylation Methodology and New CF_3-Containing Frugs. *J. Fluorine Chem.* **2014**, *167,* 37-54.
4. Xie, Q.; Li, L.; Zhu, Z.; Zhang, R.; Ni, C.; Hu, J. From C1 to C2: $TMSCF_3$ as a Precursor for Pentafluoroethylation. *Angew. Chem., Int. Ed.* **2018**, *57,* 13211-13215.
5. Ohashi, M.; Ishida, I.; Ando, K.; Hashimoto, Y.; Shigaki, A.; Kikushima, K.; Ogoshi, S. CuI-Catalyzed Pentafluoroethylation of Aryl Iodides in the Presence of Tetrafluoroethylene and Cesium Fluoride: Determining the Route to the Key Pentafluoroethyl CuI Intermediate. *Chem. - Eur. J.* **2018**, *24,* 9794-9798.

6. Serizawa, H.; Aikawa, K.; Mikami, K. Direct Synthesis of Pentafluoroethyl Copper from Pentafluoropropionate as an Economical C_2F_5 Source: Application to Pentafluoroethylation of Arylboronic Acids and Aryl Bromides. *Org. Lett.* **2014**, *16,* 3456-3459.
7. Ma, J.-A.; Cahard, D. Asymmetric Fluorination, Trifluoromethylation, and Perfluoroalkylation Reactions. *Chem. Rev.* **2004**, *16,* 6119-6146.
8. Dubinina, G. G.; Ogikubo, J.; Vicic, D. A. Structure of Bis(trifluoromethyl)cuprate and Its Role in Trifluoromethylation Reactions *Organometallics* **2008**, *27,* 6233-6235.
9. Litvinas, N. D.; Fier, P. S.; Hartwig, J. F. A General Strategy for the Perfluoroalkylation of Arenes and Arylbromides by Using Arylboronate Esters and [(phen)CuRF]. *Angew. Chem., Int. Ed.* **2012**, *51* 536-539.
10. Panferova, L. I.; Miloserdov, F. M.; Lishchynskyi, A.; Martinez Belmonte, M.; Benet-Buchholz, J.; Grushin, V.V.; Well-Defined CuC_2F_5 Complexes and Pentafluoroethylation of Acid Chlorides. *Angew. Chem., Int. Ed.* **2015**, *54,* 5218-5222.
11. Kuett, A.; Movchun, V.; Rodima, T.; Dansauer, T.; Rusanov, E. B.; Leito, I.; Kaljurand, I.; Koppel, J.; Pihl, V.; Koppel, I.; Ovsjannikov, G.; Toom, L.; Mishima, M.; Medebielle, M.; Lork, E.; Roeschenthaler, G.-V.; Koppel, I. A.; Kolomeitsev, A.A. Pentakis(trifluoromethyl)phenyl, a Sterically Crowded and Electron-withdrawing Group: Synthesis and Acidity of Pentakis(trifluoromethyl)benzene, -toluene, -phenol, and –aniline. *J. Org. Chem.* **2008**, *73,* 2607-2620.
12. Liu, H.; Shen, Q. Bistrifluoromethylated organocuprate $[Ph_4P]^+[Cu(CF_3)_2]^-$: synthesis, characterization and its application for trifluoromethylation of activated heteroaryl bromides, chlorides and iodides. *Organic Chemistry Frontiers* **2019**, *6* 2324-2328.
13. Martinez de Salinas S.; Mudarra, A.L.; Odena, C.; Martinez Belmonte, M.; Benet-Buchholz, J.; Maseras, F.; Perez-Temprano, M.H. Exploring the Role of Coinage Metalates in Trifluoromethylation: A Combined Experimental and Theoretical Study. *Chem. - Eur. J.* **2019**, *25,* 9390-9394.
14. Fier, P. S.; Hartwig, J. F. Copper-Mediated Difluoromethylation of Aryl and Vinyl Iodides. *J. Am. Chem. Soc.* **2012**, *134,* 5524-5527.
15. Wiemers, D. M.; Burton, D. J. Pregeneration, spectroscopic detection and chemical reactivity of (trifluoromethyl)copper, an elusive and complex species. *J. Am. Chem. Soc.* **1986**, *108,* 832-834.
16. Willert-Porada, M.A.; Burton, D.J.; Baenziger, N.C. Synthesis and X-ray Structure of bis(trifluoromethyl)(N,N-diethyldithiocarbamato)copper; a Remarkably Stable Perfluoroalkylcopper(III) Complex. *J. Chem. Soc., Chem. Commun.* **1989**, 1633-1634.
17. Dance, I. Intermolecular Embraces and Intermolecular Energies. *Mol. Cryst. Liq. Cryst.* **2005**, *440*, 265-293.
18. Karle, J.; Huang, L. The Glue that Holds Crystals Together: a Review. *J. Mol. Struct.* **2003**, *647,* 9-16.
19. Dunitz, J.D.; Gavezzotti, A. How Molecules Stick Together in Organic Crystals: Weak Intermolecular Interactions. *Chem. Soc. Rev.* **2009**, *38,* 2622-2633.
20. Hope, H.; Olmstead, M.M.; Power, P.P.; Sandell, J.; Xu, X. Isolation and X-Ray Crystal Structures of the Mononuclear Cuprates $[CuMe_2]^-$, $[CuPh_2]^-$, and $[Cu(Br)CH(SiMe_3)_2]$. *J. Amer. Chem. Soc.* **1985**, *107*, 4337-8.

21. Dempsey, D.F.; Girolami, G.S. Copper(I) alkyls. Synthesis and Characterization of Tertiary Phosphine Adducts and the Crystal Structure of the Dimethylcuprate Complex [Cu(PMe3)4][CuMe2]. *Organometallics* **1988,** *7*, 1208-1213.
22. John, M.; Auel, C,; Behrens, C.; Marsch, M.; Harms, K.; Bosold, F.; Gschwind, R.M.; Rajamohanan, P. R.; Boche, G. The Relation Between Ion Pair Structures and Reactivities of Lithium Cuprates. *Chem. - Eur. J.* **2000**, *6*, 3060-3068.
23. Popov, I.; Lindeman, S.; Daugulis, O. Copper-Catalyzed Arylation of 1H-Perfluoroalkanes. *J. Amer. Chem. Soc.* **2011**, *133*, 9286-9289.
24. de Frémont, P.; Scott, N.M.; Stevens, E.D.; Ramnial, T.; Lightbody, O.C.; Macdonald, C.L.B.; Clyburne, J.A.C.; Abernethy, C.D.; Nolan, S.P. Synthesis of Well-Defined N-Heterocyclic Carbene Silver(I) Complexes. *Organometallics* **2005**, *24*, 6301-6309.
25. Caytan, E.; Roland, S.; Structure of Silver–N-Heterocyclic Carbenes in Solution: Evidence of Equilibration in DMSO at Very Different Time Scales by 1H NMR Experiments. *Organometallics* **2014**, *33*, 2115-2118.
26. Orpen, A.G.; Brammer, L.; Allen, F. H.; Kennard, O.; Watson, D. G.; Taylor, R. Supplement. Tables of Bond Lengths Determined by X-ray and Neutron Diffraction. Part 2. Organometallic Compounds and Co-ordination Complexes of the d- and f-block Metals. *J. Chem. Soc., Dalton Trans.* **1989**, S1-S83.
27. Martín, A.; Orpen, A.G. Structural Systematics. 6.1 Apparent Flexibility of Metal Complexes in Crystals. *J. Amer. Chem. Soc.* **1996**, *118*, 1464-1470.

Chapter 3: $[(MeCN)_3Co(C_2F_5)_3]$: A Versatile Precursor to Cobalt(III) Perfluoroethyl Complexes

The following chapter has been adapted and reproduced with permission from: Shreiber, S. T.; Scudder, J. J.; Vicic, D. A. *Organometallics* **2019**, *38*, 3169-3173.

3.1 Abstract: The air-stable [*fac*-$(MeCN)_3Co(C_2F_5)_3$] (**3a**) was prepared through the reaction of cobalt(II) bromide with [Me_3Si-C_2F_5] and AgF. Upon reaction of **3a** with wet pyridine, the unexpected product [*fac*-$(H_2O)_3Co(C_2F_5)_3 \cdot 6$ pyridine] (**3b**) was formed in which water coordinates to cobalt instead of pyridine, and the pyridines form short contacts with each of the hydrogen atoms in the bound water molecules. Facile exchange of the bound acetonitrile ligands in **3a** with terpyridine (tpy) and bipyridine (bpy) did occur, however, affording [$(tpy)Co(C_2F_5)_3$] (**3e**) and [$(bpy)Co(C_2F_5)_3(MeCN)$] (**3f**) in high yields.

3.2 Introduction: There is a continuous demand to develop better ways to incorporate fluoroalkyl groups into organic molecules. Such groups can modulate the stability, reactivity, and conformation of the parent molecule, and thus fluoroalkylations are commonly employed reactions in the materials and life-science fields.[1-4] A critical component for the development of new fluoroalkylation methods is a fundamental understanding of how the reactivity of fluoroalkyl complexes is influenced by both the metal center and the ancillary ligand(s) of choice.[5] The metal identity will influence factors such as M-C(fluoroalkyl) bond strength, accessibility to different redox states, and functional group tolerances. Ligands offer the potential to tune vacant site control, steric environment, light absorption abilities, etc. In order to fully map out the reactivity patterns of metal fluoroalkyl complexes across the periodic table, protocols for preparing new and well-defined compounds are needed so that stoichiometric and catalytic reactions can be better studied.

Cobalt is a promising metal to develop for trifluoromethylation and fluoroalkylation reactions, as well-defined cobalt fluoroalkyl complexes have been demonstrated to participate in photolytic Co-R_f homolysis reactions leading to CF_3 and R_f radicals.[6-7] Additionally, cobalt has been shown to support the Co=CF_2 moiety, which could participate in unique bond-forming reactions.[8-12] Since strong M-CF_3 and M-R_f bonds can prohibit commonly employed two electron processes like reductive eliminations, developing first-row metal methodologies that invoke alternate ways to introduce perfluoroalkyl groups into organic substrates is of high value. Given the potential for the use of cobalt in future methods development involving fluoroalkyl groups, we sought to design a cobalt precursor bearing not only fluoroalkyl ligands but also readily exchangeable co-ligands to enable access to a series of derivatives in order to identify, compare, and contrast basic reactivity patterns.

3.3 Results and Discussion

3.3.1. Synthesis of the Cobalt(III) Perfluoroethyl Precursor: Cobalt(II) bromide reacts with an excess amount of [Me_3Si-C_2F_5] in the presence of three equivalents AgF in acetonitrile to afford [$(MeCN)_3Co(C_2F_5)_3$] (**3a**, Scheme 3a) in 61% isolated yield. The silver(I) salts serve the dual role of forming a stable silver-based perfluoroethyl transfer reagent as well as a one electron oxidant to oxidize Co(II) to Co(III).[13] Me_3Si-F was detected as a byproduct by ^{19}F NMR spectroscopy, and a silver mirror on the reaction vessel could be observed upon completion of the reaction. The acetonitrile complex **3a** is an air-stable solid that, once isolated, shows air-stability even in solution (see below). X-ray quality crystals can be grown from acetonitrile/ether, and an ORTEP diagram of **3a** is provided in Figure 3a. The X-ray and ^{19}F NMR data confirm that both in the solid state

and in solution the *facial* isomer, in which all of the perfluoroethyl groups are *trans* to acetonitrile ligands, is formed exclusively. The cobalt-carbon bond lengths in **3a** are 1.971(9), 1.947(10), and 1.975(9) Å, with the shortest cobalt-carbon bond located *trans* to the longest cobalt-nitrogen bond of 2.005(8) Å.

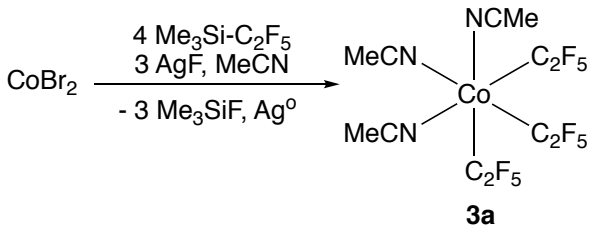

Scheme 3a. Synthesis of the air-stable perfluoroethyl cobalt (III) precursor (**3a**).

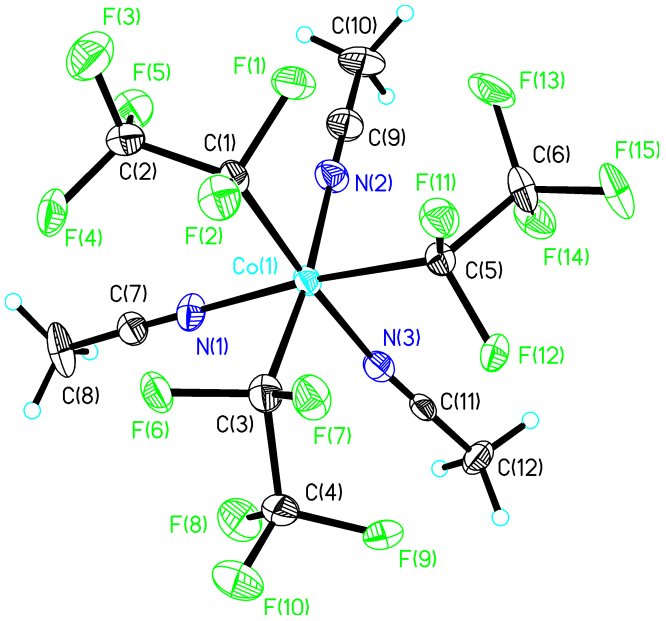

Figure 3a. ORTEP diagram of **3a**. Selected bond lengths (Å): Co1-C1 1.971(9); Co1-C3 1.947(10); Co1-C5 1.975(9); Co1-N1 1.974(8); Co1-N2 2.005(8); Co1-N3 1.969(8). Selected bond angles (°): C3-Co1-N3 94.8(4); C3-Co1-C1 90.0(4); N3-Co1-C1 175.1(4); C3-Co1-N1 87.7(4); N3-Co1-N1 86.1(3); C1-Co1-N1 94.6(3); C3-Co1-C5 91.5(3); N3-Co1-C5 88.0(3); C1-Co1-C5 91.3(4); N1-Co1-C5 174.0(4); C3-Co1-N2 173.6(4); N3-Co1-N2 86.2(3); C1-Co1-N2 89.1(4); N1-Co1-N2 86.0(3); C5-Co1-N2 94.9(3).

3.3.2. Synthesis of an Aquo Cobalt(III) Fluoroalkyl Complex: With compound **3a** in hand, the lability of the bound acetonitriles to undergo ligand substitution reactions was explored. Crystallizing a solution of **3a** in pyridine under aerobic conditions at -5 °C

surprisingly did not afford the expected [$(pyr)_3Co(C_2F_5)_3$], but instead led to [*fac*-$(H_2O)_3Co(C_2F_5)_3 \cdot 6$ pyridine] (**3b**, Scheme 3b). The structure of **3b** was confirmed by X-ray crystallography (Figure 3b), which indicates that water coordinates to cobalt instead of pyridine and that all hydrogens from the cobalt-bound water ligands display short contacts to outer-sphere pyridine molecules ranging from 1.94(2) to 2.10(2) Å. The cobalt-carbon bond lengths in **3b** were 1.9365(14), 1.9407(15), and Co1-C5 1.9436(15) Å, which on average were shorter than those found for **3a**. The preparation of **3b** can be standardized by crystallizing a solution of **3a** from 1% water in pyridine. In contrast, the crystallization of **3a** from a 1% water in acetonitrile mixture did not lead to the generation of a related aquo complex, but instead led simply to the recrystallization of **3a** as determined by X-ray crystallography. Thus, water coordination is observed in pyridine solvent but not in acetonitrile. Water coordination to **3a** to form **3b** is reproducible, and an X-ray crystallographic analysis on crystals from a second batch of synthesized material reproduces the original structure of **3b**. Moreover, dissolution of **3b** in anhydrous pyridine leads to broad and multiple signals in the ^{19}F NMR spectrum (see Appendix B) which are distinct from those of **3b**. Addition of a drop of water to a solution containing the products of **3a** with anhydrous pyridine quantitatively converts the mixture to **3b** by ^{19}F NMR (see Appendix B).

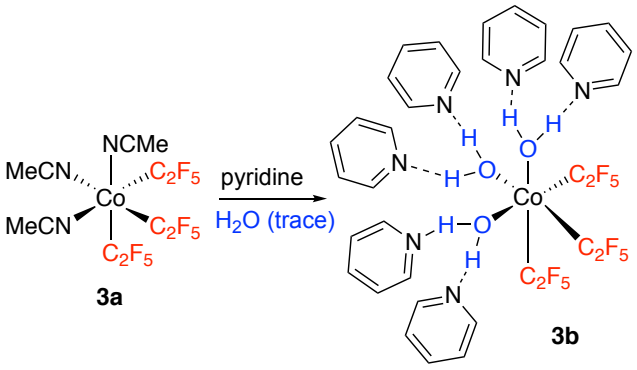

Scheme 3b. Synthesis of the aquo complex **3b**.

Compound **3b** is remarkable considering that formation constants for pyridine substitutions at octahedral metal hexaaquo complexes typically favor a bound pyridine.[14] Moreover, pyridine is typically considered to be a stronger ligand than water in the spectrochemical series.[15-16] In line with such known spectrochemical data, Forniés and co-workers show that the platinum aquo complex **3c** can be used to prepare the pyridine complex **3d** (Scheme 3c) under mild, room temperature conditions.[17] It is unclear whether the basicity (from the pyridine and water coordination) or the sterics of the pyridines plays a role in the selective generation of the aquo complex **3b** from the perfluoroethyl complex **3a**.

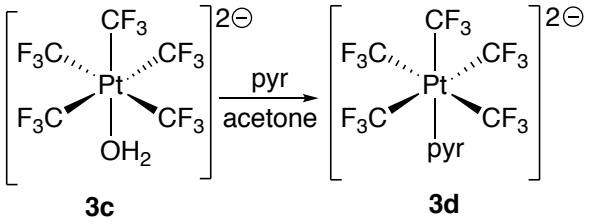

Scheme 3c. Generation of pyridine complex **3d** from aquo complex **3c**.

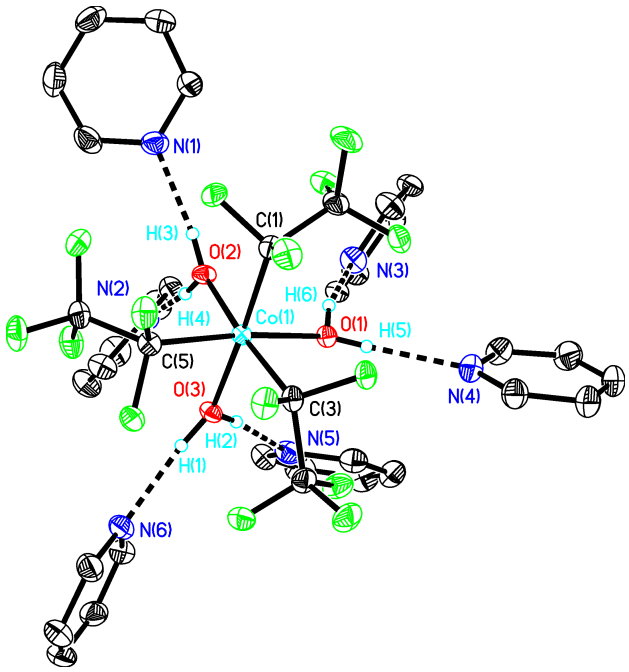

Figure 3b. ORTEP diagram of **3b**. A co-crystallized pyridine molecule is removed for clarity. Selected bond lengths (Å): Co1-C1 1.9365(14); Co1-C3 1.9407(15); Co1-C5 1.9436(15); Co1-O2 1.9871(11); Co1-O1 2.0013(10); Co1-O3 2.0056(11); O1-H5 0.80(2); H5-N4 2.04(2); O1-H6 0.87(2); H6-N3 1.95(2); O2-H3 0.81(2); H3-N1 1.96(2); O2-H4 0.81(2); H4-N2 2.01(2); O3-H2 0.80(2); H2-N5 2.10(2); O3-H1 0.85(2); H1-N6 1.94(2). Selected bond angles (°): C1 Co1 C3 91.26(6); C1-Co1-C5 92.07(6); C3-Co1-C5 91.17(6); C1-Co1-O2 89.63(6); C3-Co1-O2 172.66(5); C5-Co1-O2 96.08(5); C1-Co1-O1 95.28(5); C3-Co1-O1 89.57(5); C5-Co1-O1 172.60(5); O2-Co1-O1 83.09(5); C1-Co1-O3 172.55(5); C3-Co1-O3 95.84(5); C5-Co1-O3 90.05(6); O2-Co1-O3 83.05(5); O1-Co1-O3 82.55(5).

3.3.3. Coordination of bpy and tpy to Cobalt(III) Perfluoroethyl Precursor: Complex **3a** reacts with the chelating ligands terpyridine and bipyridine, however, to cleanly afford the ligand substitution products [(tpy)Co(C_2F_5)$_3$] (**3e**) and [(bpy)Co(C_2F_5)$_3$(MeCN)] (**3f**), as described in Scheme 3d. X-ray crystallographic data of **3e** (Figure 3c) revealed some asymmetry in the cobalt-nitrogen bond lengths of 1.890(5), 1.978(5), and 1.983(5) Å, with the central pyridyl ring displaying the shortest bond to cobalt. The cobalt-carbon bond lengths in **3e** were on average longer than those seen in **3a** and **3b**, at 2.009(6), 2.037(6), and 2.078(6) Å. The X-ray and NMR analyses of **3f** confirmed that, upon addition of

bipyridine to **3a**, the *meridional* isomer is exclusively formed that has two perfluoroethyl groups in the axial positions and the remaining acetonitrile ligand in the plane of the bipyridine. The X-ray crystal structure of **3f** is shown in Figure 3d, and the data shows that complex **3f** displays cobalt-nitrogen and cobalt-carbon bond lengths comparable to **3e**. The experimentally determined cobalt-nitrogen bond lengths in **3f** are 1.879(3), 1.954(3), and 1.990(3) and the cobalt-carbon bond lengths are 2.035(4), 2.047(4), and 1.982(4).

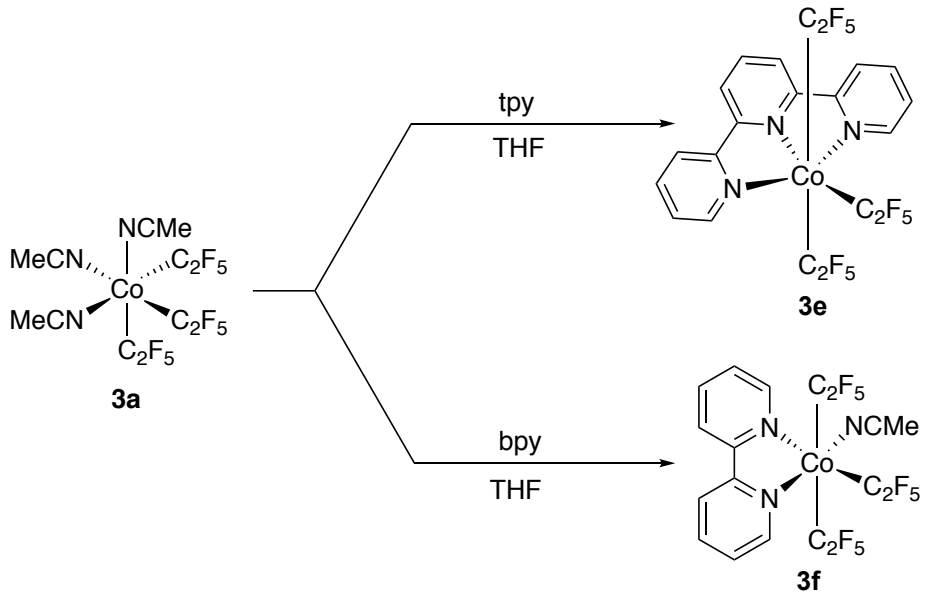

Scheme 3d. Synthetic route to tpy and bpy complexes of **3a**.

The ^{19}F NMR spectrum of **3e** warrants some discussion. It is known, but rarely discussed, that NMR resonances of isolated perfluoroethyl groups commonly appear as two singlets and exhibit little to no vicinal coupling.[18] The absence or low values for $^{3}J_{FF}$ for perfluoroalkyl groups has been suggested to arise in part from rotational averaging of coupling constants of opposite sign between the vicinal CF_2 and CF_3 groups.[19-21] Complex **3e** is an interesting case study because the *meridional* geometry imposed by the terpyridine ligands affords two different types of isolated perfluoroethyl groups in a 2:1 ratio with the ability of the distinct perfluoroethyl groups to exhibit long-range couplings to one another

despite displaying no vicinal couplings within an individual perfluoroethyl group. Thus, in complex **3e**, the CF_3 resonance of the axial perfluoroethyl groups appears as a triplet since it couples to the sole CF_2 group of the other perfluoroethyl situated *trans* to a nitrogen. Likewise, the resonance of the CF_3 group of the perfluoroethyl that is in the plane of the terpyridine ligand appears as a quintet since it couples to the CF_2 groups of the two axial perfluoroethyls. ^{19}F-COSY NMR confirms these assignments (see Appendix B).

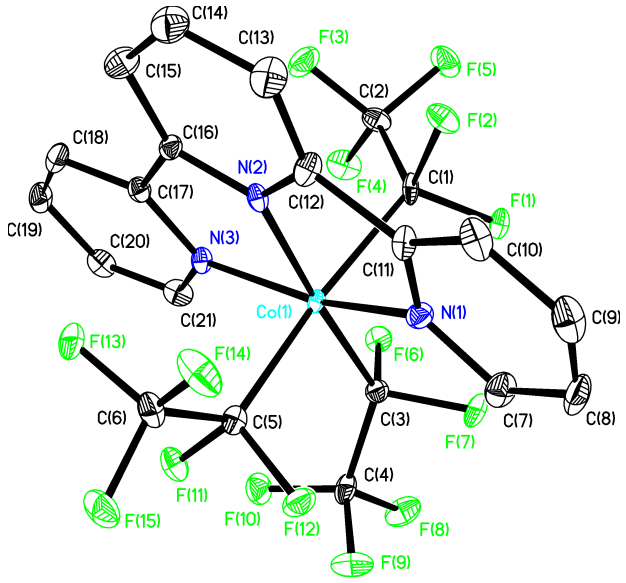

Figure 3c. ORTEP diagram of **3e**. Hydrogen atoms are omitted for clarity. Selected bond lengths (Å): Co1-N2 1.890(5); Co1-N1 1.978(5); Co1-N3 1.983(5); Co1-C5 2.009(6); Co1-C3 2.037(6); Co1-C1 2.078(6); C11-C12 1.470(9); C16-C17 1.464(8). Selected bond angles (°): N2-Co1-N1 81.1(2); N2-Co1-N3 80.8(2); N1-Co1-N3 161.9(2); N2-Co1-C5 93.7(2); N1-Co1-C5 87.5(2); N3-Co1-C5 91.7(2); N2-Co1-C3 173.9(2); N1-Co1-C3 101.6(2); N3-Co1-C3 96.6(2); C5-Co1-C3 91.9(2); N2-Co1-C1 86.5(2); N1-Co1-C1 85.6(2); N3-Co1-C1 95.3(2); C5-Co1-C1 173.0(2); C3-Co1-C1 88.2(2).

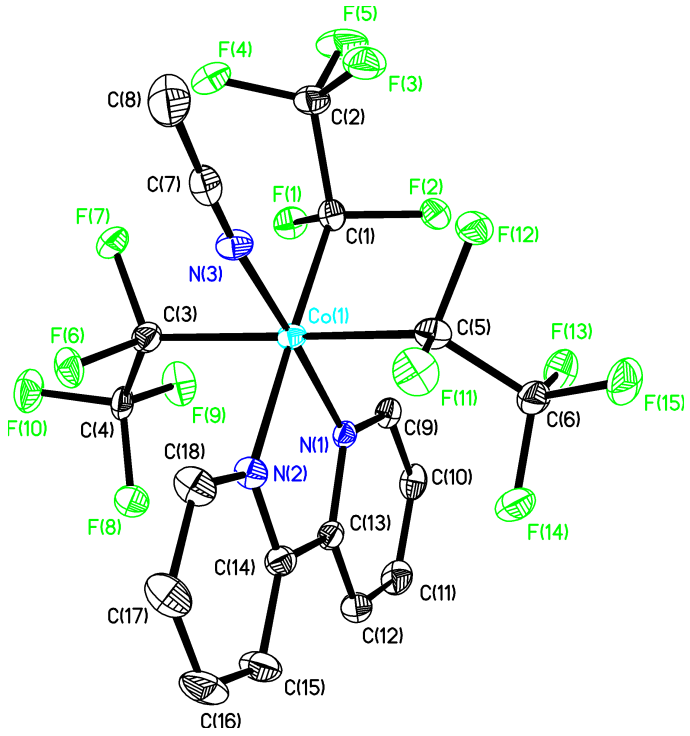

Figure 3d. ORTEP diagram of **3f**. Hydrogen atoms are omitted for clarity. Selected bond lengths (Å): Co1-N3 1.879(3); Co1-N1 1.954(3); Co1-C1 1.982(4); Co1-N2 1.990(3); Co1-C5 2.035(4); Co1-C3 2.047(4); C13-C14 1.466(5). Selected bond angles (°): N3-Co1-N1 174.55(12); N3-Co1-C1 90.66(14); N1-Co1-C1 94.65(13); N3-Co1-N2 92.89(12); N1-Co1-N2 81.80(12); C1-Co1-N2 176.42(13); N3-Co1-C5 84.99(14); N1-Co1-C5 93.54(13); C1-Co1-C5 92.77(15); N2-Co1-C5 87.98(13); N3-Co1-C3 87.29(14); N1-Co1-C3 93.70(13); C1-Co1-C3 92.12(14); N2-Co1-C3 87.62(13); C5-Co1-C3 170.91(14).

3.4. Conclusions: A synthetic protocol to the new cobalt trifluoroethyl complex [*fac*-$(MeCN)_3Co(C_2F_5)_3$] has been developed. The acetonitrile ligands in this precursor are labile and can be replaced by other ligands such as water, bipyridine, and terpyridine. The coordination of water to cobalt in the presence of a large excess of pyridine is remarkable, considering pyridine is typically considered to be a stronger ligand than water in the spectrochemical series. Thus, the aquo complex **3b** exhibits an unusual combination of air-stability, affinity for water over a basic solvent like pyridine, and a resistance to undergo hydrolysis of the perfluoroethyls, making it an interesting platform for exploring the

reactivity of the metal-bound water ligands in a variety of applications, including water-oxidation.

3.5. Experimental

3.5.1. General Information: All manipulations were performed using standard Schlenk and high vacuum techniques or in a nitrogen-filled glovebox, unless otherwise stated.[22] Solvents were purified by passing through activated alumina and/or copper in a solvent purification system supplied by Pure Process Technology. Solution ^{1}H NMR spectra were recorded at ambient temperature on a Bruker 400 MHz spectrometer and referenced to residual proton solvent signals. ^{19}F spectra were recorded on the Bruker NMR spectrometer operating at 376 MHz and referenced to α,α,α-trifluorotoluene as an internal standard (δ = -63.7). A Bruker D8 Quest diffractometer was used for X-ray crystal structure determinations. The CCDC 1936218-1936220, and 1942398 contain the supplementary crystallographic data for this paper. These data can be obtained free of charge via www.ccdc.cam.ac.uk/data_request/cif, or by e-mailing data_request@ccdc.cam.ac.uk, or by contacting The Cambridge Crystallographic Data Centre, 12 Union Road, Cambridge CB2 1EZ, UK; fax: +44 1223 336033.

3.5.2. Preparation of [*fac*-$(MeCN)_3Co(C_2F_5)_3$] (3a): $TMSC_2F_5$ (0.70 mL, 4.0 mmol), AgF (410 mg, 3.2 mmol) were stirred for 2 hours in 5 mL of dry acetonitrile. $CoBr_2$ (218 mg, 1.00 mmol in 5 mL of acetonitrile) was added, and the green slurry was stirred for 3 days. The resulting yellow – brown slurry was filtered over a pad of activated alumina, and then the solvents were removed under vacuum. The precipitate was collected by filtration and washed with ether to yield 330 mg (61%) of a yellow solid. The solid can be recrystallized by dissolving product in acetonitrile, layering with ether, and placing in

freezer to give yellow needle crystals. ^{19}F NMR (CD_3CN, 376 MHz): δ -81.1 (s, 3F), -95.6 (s, 2F). Anal. Calcd (found) for $C_{12}H_9CoF_{15}N_3$: C, 26.73 (26.41); H, 1.68 (1.34).

3.5.3. Preparation of [*fac*-$(H_2O)_3Co(C_2F_5)_3 \cdot$ 6 pyridine] (3b): In a vial in air, compound **3a** (45 mg, 0.083 mmol) was dissolved in 2 mL of a 1% solution of water in pyridine. Pentane (15 mL) was then added to the vial. The vial was placed in freezer, and yellow block crystals (55 mg, 70% yield) were obtained. ^{19}F NMR (C_5D_5N, 376 MHz): δ -78.9 (br s, 3F), -96.9 (br s, 2F). The crystal structure contained one additional molecule of pyridine in the asymmetric unit. Elemental analysis suggested partial desolvation of pyridines (two to three pyridines) upon drying under vacuum. Anal. Calcd (found) for $C_{26}H_{26}CoF_{15}N_4O_3$ (**2** minus two pyridines): C, 39.71 (39.28); H, 3.33 (2.88).

3.5.4. Preparation of [(terpyridine)$Co(C_2F_5)_3$] (3e): Compound **1** (89 mg, 0.16 mmol) was dissolved in 4 mL of THF. A solution of terpyridine (36 mg, 0.16 mmol) in 4 mL of THF was then added, and the resulting solution was stirred for 8 hours. The volatiles were reduced, and the resulting orange solid was collected by filtration (80 mg, 80% yield). The compound is thermally stable to 200 °C under vacuum, and does not sublime under these conditions. ^1H NMR (DMSO-d_6, 400 MHz): δ – 8.76 (d, J = 8.0 Hz, 2H), 8.64-8.55 (m, 3H), 8.35 (d, J = 5.9 Hz, 2H), 8.24 (td, J = 7.7, 1.3 Hz, 2H), 7.68 (td, 7.6, 1.6 Hz, 2H). ^{19}F NMR (CD_2Cl_2, 376 MHz): δ -79.07 (p, J = 14.8 Hz, 3F), -80.78 (t, J = 8.5 Hz, 6F), -95.08 (m, 2F), -103.81 (m, 4F). Anal. Calcd (found) for $C_{21}H_{11}CoF_{15}N_3$: C, 38.85 (38.92); H, 1.71 (2.05).

3.5.5. Preparation of [*mer*-(MeCN)(bipyridine)$Co(C_2F_5)_3$] (3f): A solution of 2,2'-bipyridine (48 mg, 0.30 mmol) in 6 mL of THF was added to a stirring solution of [*fac*-$(MeCN)_3Co(C_2F_5)_3$ (164 mg, 0.304 mmol) in 4 mL of THF. The resulting mixture was

stirred under an inert atmosphere for 1 day. The volatiles were then removed under vacuum, and the solid was collected by filtration. The solid was washed with pentane and dried to yield 144 mg (78%) of yellow solid. ^{1}H NMR (CD_3CN, 400 MHz): δ: 8.92 (d, J = 5.7 Hz, 1H), 8.81 (d, J = 5.8 Hz, 1H), 8.24 – 8.16 (m, 3H), 8.04 (td, J = 7.8, 1.4 Hz, 1H), 7.71 – 7.67 (m, 1H), 7.53 – 7.49 (m, 1H), 2.50 (s, 3H). ^{19}F NMR (CD_3CN, 376 MHz): δ : -79.63 (app sept, J = 12.1 Hz, 3F), -81.72 (t, J= 5.5 Hz, 3F), -93.79 to -93.94 (m, 2F), -99.81 to -100.06 (m, 1F), -100.57 to -100.85 (m, 1F), -104.64 to -104.97 (m, 1F), -105.37 to -105.7 (m, 1F). Anal. Calcd (found) for $C_{18}H_{11}CoF_{15}N_3$: C, 35.26 (35.16); H, 1.81 (1.90).

3.6 References

1. Lemos, A.; Lemaire, C.; Luxen, A. Progress in Difluoroalkylation of Organic Substrates by Visible Light Photoredox Catalysis. *Adv. Synth. Cat.* **2019,** *361*, 1500-1537.
2. Feng, Z.; Xiao, Y.-L.; Zhang, X. Transition-Metal (Cu, Pd, Ni)-Catalyzed Difluoroalkylation via Cross-Coupling with Difluoroalkyl Halides. *Acc. Chem. Res.* **2018,** *51*, 2264-2278.
3. Barata-Vallejo, S.; Cooke, M. V.; Postigo, A. Radical Fluoroalkylation Reactions. *ACS Catal.* **2018,** *8*, 7287-7307.
4. Ni, C.; Hu, J. The Unique Fluorine Effects in Organic Reactions: Recent Facts and Insights Into Fluoroalkylations. *Chem. Soc. Rev.* **2016,** *45*, 5441-5454.
5. Wang, H.; Vicic, D. A. Organometallic aspects of fluoroalkylation reactions with copper and nickel. *Synlett* **2013,** *24*, 1887-1898.
6. Liebing, P.; Oehler, F.; Wagner, M.; Tripet, P. F.; Togni, A. Perfluoroalkyl Cobaloximes: Preparation Using Hypervalent Iodine Reagents, Molecular Structures, Thermal and Photochemical Reactivity. *Organometallics* **2018,** *37*, 570-583.
7. Harris, C. F.; Kuehner, C. S.; Bacsa, J.; Soper, J. D. Photoinduced Cobalt(III)-Trifluoromethyl Bond Activation Enables Arene C-H Trifluoromethylation. *Angew. Chem., Int. Ed.* **2018,** *57*, 1311-1315.
8. Harrison, D. J.; Lee, G. M.; Leclerc, M. C.; Korobkov, I.; Baker, R. T. Cobalt Fluorocarbenes: Cycloaddition Reactions with Tetrafluoroethylene and Reactivity of the Perfluorometallacyclic Products. *J. Am. Chem. Soc.* **2013,** *135*, 18296-18299.
9. Harrison, D. J.; Gorelsky, S. I.; Lee, G. M.; Korobkov, I.; Baker, R. T. Cobalt Fluorocarbene Complexes. *Organometallics* **2013,** *32*, 12-15.

10. Lee, G. M.; Harrison, D. J.; Korobkov, I.; Baker, R. T. Stepwise Addition of Difluorocarbene to a Transition Metal Centre. *Chem. Commun.* **2014,** *50*, 1128-1130.
11. Leclerc, M. C.; Bayne, J. M.; Lee, G. M.; Gorelsky, S. I.; Vasiliu, M.; Korobkov, I.; Harrison, D. J.; Dixon, D. A.; Baker, R. T. Perfluoroalkyl Cobalt(III) Fluoride and Bis(perfluoroalkyl) Complexes: Catalytic Fluorination and Selective Difluorocarbene Formation. *J. Am. Chem. Soc.* **2015,** *137*, 16064-16073.
12. Harrison, D. J.; Daniels, A. L.; Korobkov, I.; Baker, R. T. Tetracarbonyl(trifluoromethyl)cobalt(I) [$Co(CO)_4(CF_3)$] as a Precursor to New Cobalt Trifluoromethyl and Difluorocarbene Complexes. *Organometallics* **2015,** *34*, 4598-4604.
13. Yu, S.; Dudkina, Y.; Wang, H.; Kholin, K. V.; Kadirov, M. K.; Budnikova, Y. H.; Vicic, D. A. Accessing Perfluoroalkyl Nickel(II), (III), and (IV) Complexes Bearing a Readily Attached [C_4F_8] Ligand. *Dalton Trans.* **2015,** *44*, 19443-19446.
14. Atkins, P.; Overton, T.; Rourke, J.; Weller, M.; Armstrong, F.; Hagerman, M. *Shriver & Atkins' Inorganic Chemistry 5th Edition*. W. H. Freeman and Company: NY, 2010.
15. Shimura, Y. A Quantitative Scale of the Spectrochemical Series for the Mixed Ligand Complexes of d6 Metals. *Bull. Chem. Soc. Jpn.* **1988,** *61*, 693-698.
16. Ishii, T.; Tsuboi, S.; Sakane, G.; Yamashita, M.; Breedlove, B. K. Universal Spectrochemical Series of Six-Coordinate Octahedral Metal Complexes for Modifying the Ligand Field Splitting. *Dalton Trans.* **2009**, 680-687.
17. Martínez-Salvador, S.; Forniés, J.; Martín, A.; Menjón, B. Highly Trifluoromethylated Platinum Compounds. *Chem.– Eur. J.* **2011,** *17*, 8085-8097.
18. Dolbier, W. R., Jr. *Guide to Fluorine NMR for Organic Chemists, 2nd Edition.* John Wiley & Sons, Inc., NJ, 2016.
19. Newmark, R. A. Vicinal Fluorine–Fluorine Coupling Constants in Perfluoropropyl Groups. *J. Fluorine Chem.* **2009,** *130*, 389-393.
20. Graves, R. E.; Newmark, R. A. Fluorine Coupling in Hexalfuoroethane. *J. Chem. Phys.* **1967,** *47*, 3681-2.
21. Harris, R. K.; Woodman, C. M. N.M.R. Spectra of Molecules Containing CF_2 Groups. II. Perfluorobutane. *J. Mol. Spectrosc.* **1968,** *26*, 432-43.
22. Vicic, D. A.; Jones, G. D. In *Comprehensive Organometallic Chemistry III: Experimental Methods and Techniques: Basic Techniques*, Elsevier Ltd., **2007**; 197-218.

Chapter 4: Synthesis and Oxidative Stability of an Anionic Perfluoroethyl Cobalt(III) Complex

The following chapter has been adapted with permission from: Shreiber, S. T.; Vicic, D. A. *Helv. Chim. Acta* **2020**, *103*, e20000149.

4.1 Abstract: Upon reaction of the versatile tris(perfluoroethyl) cobalt(III) precursor [*fac*-$(MeCN)_3Co(C_2F_5)_3$] with potassium tris(pyrazolyl)borate (KTp) in the presence of a tetraphenylphosphonium salt, κ^2- and κ^3- adducts of the scorpionate ligand with cobalt were observed. Heating this mixture to 50 °C induced complete κ^3-coordination of the Tp ligand to cobalt to afford the anionic complex $[PPh_4][(\kappa^3\text{–Tp})Co(C_2F_5)_3]$ in 81% isolated yield. This new fluoroalkyl cobalt complex was characterized by NMR and UV-Vis spectroscopies, X-ray crystallography, and cyclic voltammetry. The oxidation of $[PPh_4][(\kappa^3\text{–Tp})Co(C_2F_5)_3]$ occurs at much less positive potentials relative to the related $[(MeCN)_3Co(C_2F_5)_3]$ and $[(tpy)Co(C_2F_5)_3]$ derivatives.

4.2 Introduction: Fluoroalkyl groups are known to alter the chemical stability, reactivity, and conformational bias of parent organic molecules, and great effort has been invested to incorporate such functionalities in molecules and materials in a variety of fields.[1-4] One approach to methods development is to first prepare well-defined transition-metal fluoroalkyl complexes and then develop an understanding of the chemical transformations that are possible with such species. In such a way, one can obtain an intimate understanding of how ligand environments affect structure, reactivity, and electronics of the metal-fluoroalkyl moieties.[5] First-row metals, due to their abundance in nature and more accessible redox states, have been investigated as agents that could mediate difficult bond forming reactions such as reductive eliminations involving fluoroalkyl groups.[6-8] In

particular, high-valent copper- and nickel-fluoroalkyl complexes have shown reactivities that bode well for the successful development of new fluoroalkylation methodologies.

For example, heteroleptic anionic copper(III) complexes such as **4a** were observed to reductively eliminate trifluoromethylated products in up to 99% yields (Scheme 4a(a)).[8-10] Shen has found the charge neutral high valent complex [(bpy)Cu(CF_3)$_2$(CH_3)] **(4b)** quantitatively forms trifluoroethane through a difficult methyl-trifluoromethyl reductive elimination process (Scheme 4a(b)).[11] High-valent nickel has also shown promise for use in fluoroalkylation chemistries. Sanford showed that the tris(pyrazolyl)borate complex **4c** (Scheme 4a(c)) undergoes two-electron oxidation with Umemoto's Reagent to form the organonickel(IV) complex **4d**, which upon heating to 55 °C in acetonitrile reductively eliminates trifluorotoluene in 76% yield.[12] Later, the same group disclosed the use of a related tris(pyrazolyl)borate nickel(IV) complex as a catalyst for C-H trifluoromethylations of (hetero)arenes.[13] Our group has recently reported that nickel can mediate trifluoromethylations without the need for additional ligands other than solvent. For example, complex **4e** reacts with the two-electron oxidant bis(4-*tert*-butylphenyl)iodonium hexafluorophosphate to afford trifluoromethylated arene in 54% yield through a proposed high-valent [Ar-Ni^{IV}(CF_3)$_3$($MeCN$)$_2$] intermediate (Scheme 4a(d)).[14]

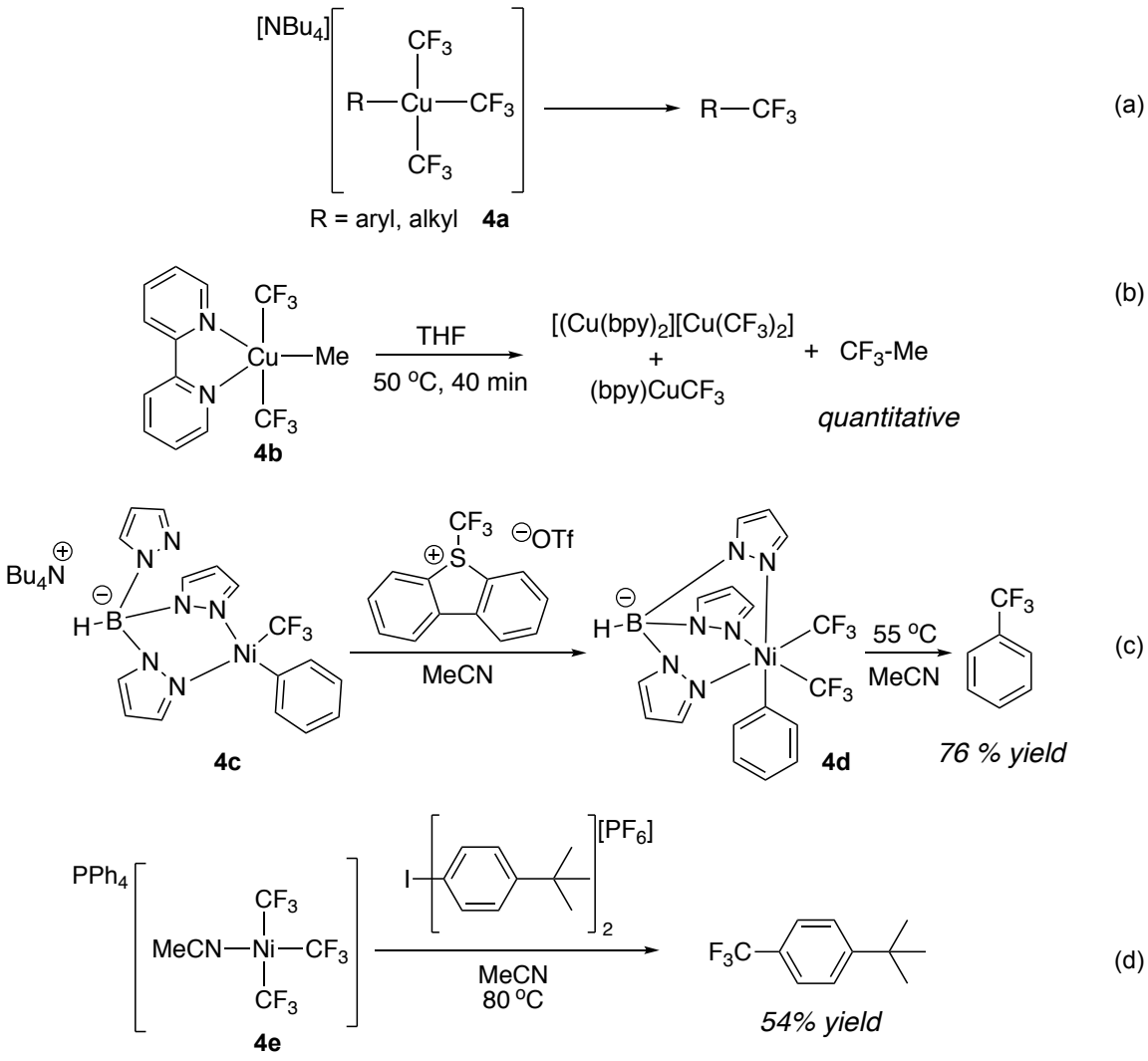

Scheme 4a. Examples of new reactivity enabled by high-valent fluoroalkyl copper and nickel complexes.

Electrochemical analysis of the anionic $[(MeCN)Ni(CF_3)_3]^-$ complex described in Scheme 4a(d) revealed that oxidation of **4e** occurs at a readily accessible onset potential of ca. +0.02 V vs the ferrocene/ferrocenium couple, with peak potentials at +0.38 V and +0.76 V.[14] We were curious as to whether anation could make fluoroalkyl complexes of cobalt(III) similarly accessible to further oxidation, as fluoroalkylations involving the formally cobalt(IV) state are to our knowledge unreported. Cobalt, like copper and nickel, is also a first-row metal with relatively low-cost and high natural abundance, and as such is a

promising platform to develop new fluoroalkylation methodologies. To date, well-defined fluoroalkyl cobalt complexes in oxidation states less than +4 have been used as models of cobalamins and to generate fluoroalkyl radicals and fluorocarbenes for small molecule functionalization reactions.[15-21] Less is known about direct reductive eliminations at cobalt involving trifluoromethyl or perfluoroalkyl groups. Such reductive eliminations are expected to be promoted by the higher valent states of cobalt. Herein we describe the synthesis of an anionic tris(pyrazolyl)borate cobalt fluoroalkyl complex and determine the redox properties of this compound through cyclic voltammetry experiments.

4.3 Results and Discussion

4.3.1. Synthesis of the Anionic Perfluoroethyl Cobalt(III) Complex: The preparation of the air-stable perfluoroethyl cobalt(III) precursor [*fac*-$(MeCN)_3Co(C_2F_5)_3$] (**4f**, Scheme 4b) has been previously described,[22] and the lability of the coordinated acetonitrile ligands render this complex attractive for ligand substitution studies. Reaction of **4f** with KTp in THF followed by the addition of tetraphenylphosphonium chloride at room temperature led to a mixture of two products as suggested by ^{19}F NMR spectroscopy. However, dissolving the resulting solids in acetonitrile and heating the mixture to 50 °C for one hour led to the formation of a single product by ^{19}F NMR spectroscopy (CD_3CN, δ-78.7 (br s, 3F) and -90.3 (br s, 2F)).

The structure of the new product was confirmed by X-ray crystallography to be the desired $[PPh_4][(\kappa^3\text{–Tp})Co(C_2F_5)_3]$ (**4h**, Scheme 4b)**.** The ORTEP diagram of **4h** is shown in Figure 4a. Complex **4h** exhibits an octahedral geometry in the solid-state with the cobalt-carbon bond lengths averaging to 1.984(5) Å and the cobalt-nitrogen bond lengths averaging

2.10(5) Å. For comparison, the cobalt-carbon and cobalt-nitrogen bond lengths in **4f** averaged to 1.964(16) Å and 1.982(14) Å, respectively.

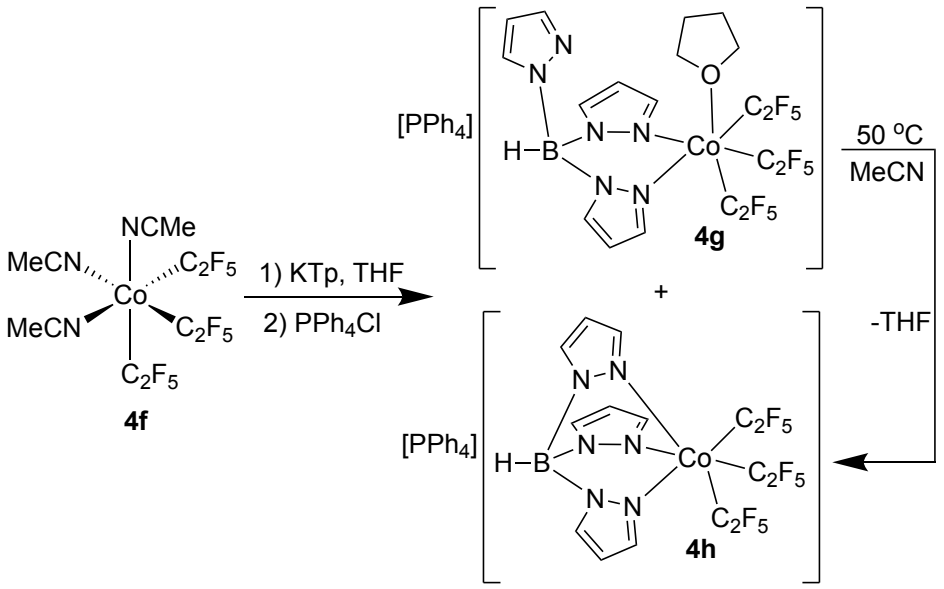

Scheme 4b. Synthetic route to anionic tris(perfluoroethyl) cobalt(III) complex **4h**.

Isolated yields of 81% were obtained for the air-stable κ^3 - tris(perfluoroethyl) cobalt(III) anion **4h**. Based on the ^{19}F NMR data (see Appendix C) we propose that at room temperature a mixture of products derived from κ^2– and κ^3-coordination of the Tp ligand is formed, and upon heating **4g** converts fully to **4h** (Scheme 2). Complex **4g** exhibits four ^{19}F NMR signals in a 3:6:4:2 ratio, indicating the perfluoroethyl groups are in a 2:1 symmetrical arrangement, similar to the ^{19}F NMR spectra observed for [(tpy)Co(C_2F_5)$_3$] (tpy = terpyridine) and [*mer* - (MeCN)(bpy)Co(C_2F_5)$_3$] (bpy = bipyridine) complexes.[22] The ^{19}F NMR spectrum of **4h**, in contrast, exhibits two signals in a 3:2 ratio, consistent with the octahedral structure determined by X-ray crystallography.

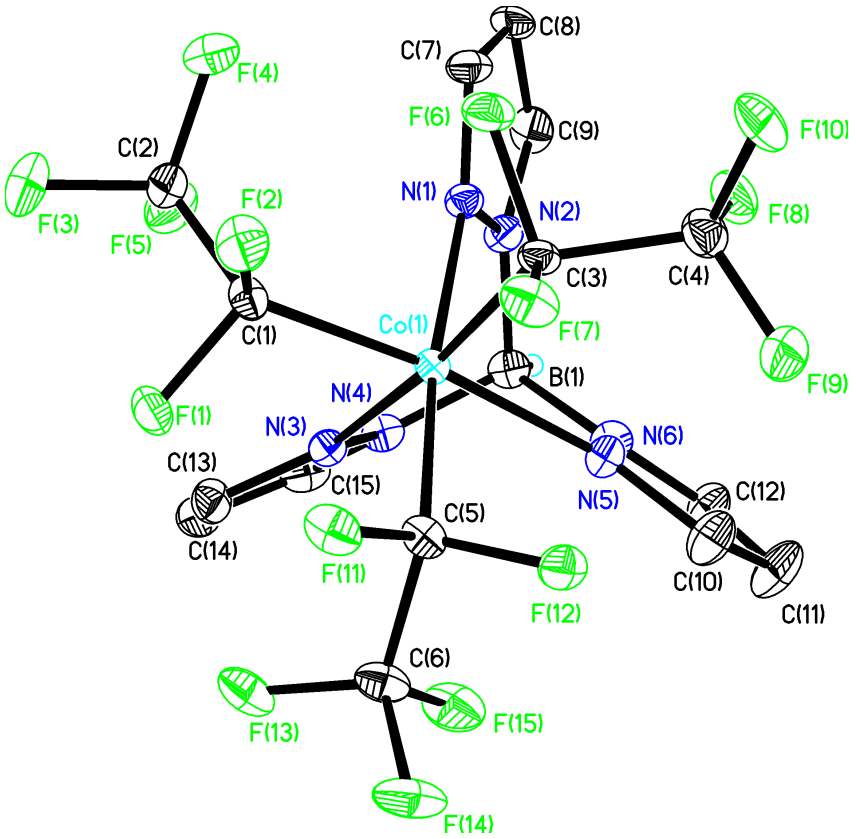

Figure 4a. ORTEP Diagram of **4h**·THF. The $[PPh_4]^+$ counter-ion and co-crystallized THF solvent are omitted for clarity. Selected bond lengths (Å): Co1-C3 1.979(3); Co1-C5 1.986(3); Co1-C1 1.986(3); Co1-N3 2.085(3); Co1-N1 2.100(3); Co1-N5 2.119(3). Selected bond angles (°): C3-Co1-C5 88.79(13); C3-Co1-C1 89.82(13); C5-Co1-C1 89.35(14); C3-Co1-N3 173.25(12); C5-Co1-N3 97.64(12); C1-Co1-N3 88.22(12); C3-Co1-N1 87.26(12); C5-Co1-N1 173.55(12); C1-Co1-N1 95.73(12); N3-Co1-N1 86.51(10); C3-Co1-N5 96.37(12); C5-Co1-N5 87.37(12); C1-Co1-N5 172.92(12); N3-Co1-N5 86.00(10); N1-Co1-N5 88.00(10).

4.3.2. Evaluation of Electrochemical Properties of Cobalt(III) Fluoroalkyl Complexes: With the new air-stable anionic perfluoroalkyl cobalt(III) complex **4h** in hand, we evaluated its electrochemical properties by cyclic voltammetry (Figure 4b). In MeCN solvent, the oxidation of **4h** is irreversible and occurs with an onset potential of +0.83 V and a peak potential of +1.16 V vs. the ferrocene/ferrocenium couple. The charge neutral and (tris)acetonitrile complex **4f**, on the other hand, undergoes oxidation at much more positive potentials, with an onset value of +1.72 V and a peak potential of +2.00 V (Figure

4b). Moreover, the known[22] tris(perfluoroethyl)cobalt terpyridine complex [(tpy)Co(C_2F_5)$_3$] exhibits an oxidation wave with an onset potential of +1.53 V and a peak potential of +1.97 V (Figure 4b). These results show, for the family of [Co(C_2F_5)] complexes, that the anionic tris(pyrazolyl)borate ligand better enables oxidation of the resulting coordination complex than do simple charge-neutral nitrogen donor ligands. For comparison, however, oxidation of **4h** occurs at much more positive values than non-fluorinated organometallic complexes of cobalt(III). For example, oxidation of charge neutral [(N^C)$_3$Co] (N^C = 2-(p-tolyl)pyridine) in MeCN occurs at a half-wave potential of +0.15 V in MeCN[23,24] and the oxidation of [Co(1-norbornyl)$_4$]$^-$ in THF occurs at a half-wave potential of -2.02 V[25]. Fluorocarbon ligands are well-known to stabilize the HOMO of the metal complexes relative to their nonfluorinated congeners.[26,27] Within the series of complexes investigated here, the electron donating character of the Tp ligand coupled with the increased negative charge, makes **4h** much easier to oxidize than **4f** and [(tpy)Co(C_2F_5)$_3$]. Similar redox trends have been observed for Tp and tpy complexes of osmium.[28] Trends between [PPN][(Tp)OsCl$_3$] (PPN = bis-(triphenylphosphoranylidene) ammonium cation) and [(tpy)OsCl$_3$] and **4h** and [(tpy)Co(C_2F_5)$_3$] are also evident in the UV-Vis spectra (see Appendix C), where the terpyridine complexes are dominated by broad and intense charge transfer bands throughout the visible region while the Tp complexes have finer structured bands with moderate intensities. Despite the more positive oxidation potential observed for **4h** relative to hydrocarbyl complexes of cobalt, the redox couple is still in the window of commonly used oxidants,[29] which facilitates future studies pertaining to the generation of fluoroalkylated and formally cobalt(IV) intermediates.[30]

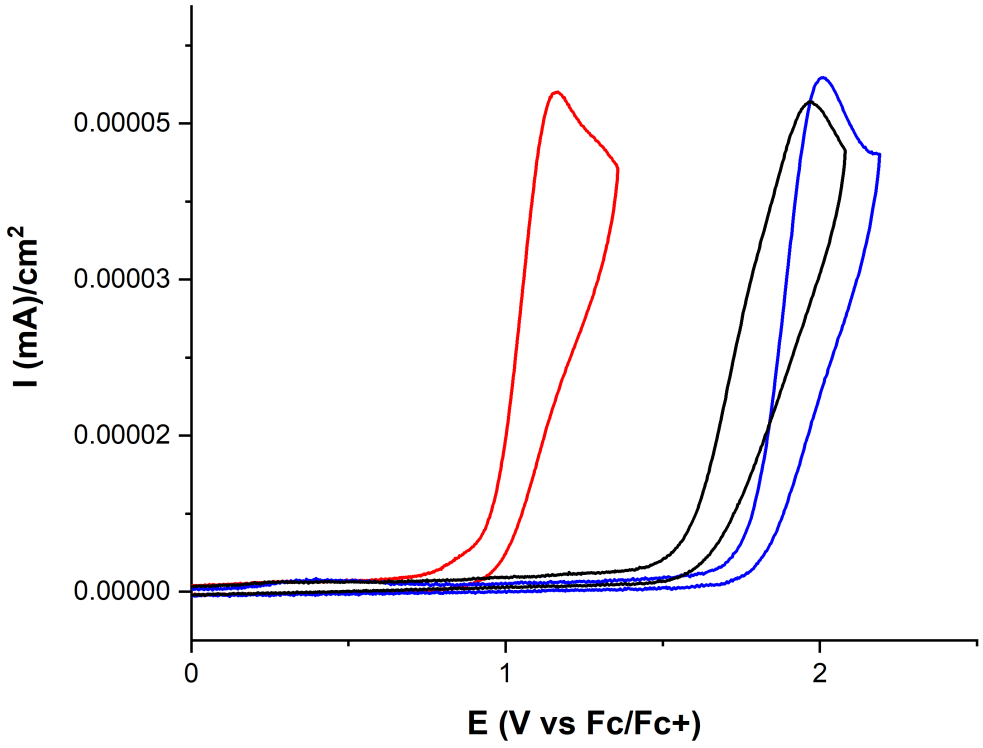

Figure 4b. Cyclic voltammograms of **4f** (blue), **4h** (red), and [(tpy)Co(C_2F_5)$_3$] (black) in MeCN. See Appendix C for conditions.

4.4. Conclusion: Reaction of [*fac*-(MeCN)$_3$Co(C_2F_5)$_3$] (**4f**) with potassium tris(pyrazolyl)borate in the presence of a tetraphenylphosphonium salt led to the formation [PPh$_4$][(κ^3–Tp)Co(C_2F_5)$_3$] (**4h**) in 81% isolated yield upon mild heating. Electrochemical measurements were performed on **4f**, **4h**, and [(tpy)Co(C_2F_5)$_3$] in order to fill voids in knowledge about the redox potentials of cobalt(III) perfluoroalkyl complexes. The data suggest that the redox potentials are highly tunable based on ligand identity, which bodes well for exploring the oxidatively-induced reactivity of high-valent cobalt complexes in fluoroalkylation methodology development.

4.5. Experimental

4.5.1. General Information: All manipulations were performed using standard Schlenk and high vacuum techniques or in a nitrogen filled glovebox, unless otherwise stated. Solvents were purified by passing through activated alumina and/or copper in a solvent purification system supplied by Pure Process Technology. Solution ^{1}H NMR spectra were recorded at ambient temperature on a Bruker 400 MHz spectrometer and referenced to residual proton solvent signals. ^{19}F spectra were recorded on a Bruker NMR spectrometer operating at 376 MHz and referenced to α, α, α,-trifluorotoluene as an internal standard (δ = -63.7). $^{31}P\{^{1}H\}$ spectra were recorded on a Bruker NMR spectrometer operating at 162 MHz and referenced to phosphoric acid as an external standard (δ = 0.00). A Bruker D8 Quest diffractometer was used for X-ray crystal structure determinations. Cyclic voltammetry data was collected in a nitrogen filled glovebox at room temperature on a PARSTAT 4000A potentiostat. The UV-vis spectra were recorded on a Varian Cary 5000 spectrophotometer, with a path length of 1 cm. The CCDC 2019505 contains the supplementary crystallographic data for this paper. These data can be obtained free of charge via www.ccdc.cam.ac.uk/data_request/cif, or by e-mailing data_request@ccdc.cam.ac.uk, or by contacting The Cambridge Crystallographic Data Centre, 12 Union Road, Cambridge CB1 1EZ, UK; fax: +44 1223 336033.

4.5.2. Synthesis of $[PPh_4][(\kappa^3\text{–Tp})Co(C_2F_5)_3]$ (4h): In a nitrogen-filled glovebox, a solution of KTp (48 mg, 0.19 mmol) in 4 mL of THF was added to a stirred solution of **4f** (0.10 g, 0.19 mmol) in 4 mL of THF. The resulting mixture was stirred for 2 hours. Tetraphenylphosphonium chloride (72 mg, 0.19 mmol) and 1 mL of THF was then added, and the mixture was stirred for an additional hour. The insoluble were filtered off and the

volatiles were removed under high vacuum. The resulting crude mixture was dissolved in 4 mL of acetonitrile and heated to 50 °C for one hour, or until complete conversion to **4h** is observed by ^{19}F NMR spectroscopy. The solution was filtered again, and the solution was pumped dry. The residue was dissolved in a minimal amount of THF, and pentane was added to precipitate the product. The product is collected by filtration, washed with ether, and dried to yield 149 mg of yellow solid (81%). X-ray quality crystals were grown from THF/Pentane. ^{1}H NMR (CD_3CN, 400 MHz): δ 8.03 (br s, 3H), 7.97 – 7.86 (m, 4H), 7.78 – 7.61 (m, 19H), 6.08 (t, *J*=2.2 Hz, 3H), 4.50 (bq, J = 107.7 Hz, B-H). ^{19}F NMR (CD_3CN, 376 MHz): δ –78.7 (br s, 3F), –90.3 (br s, 2F). $^{31}P\{^{1}H\}$ NMR (CD_3CN, 162 MHz): δ 23.9 (s). Anal. Calcd (found) for $C_{39}H_{30}CoF_{15}N_6PB$: C, 48.37 (48.57); H, 3.12 (3.24).

4.6 References

1. Ni, C.; Hu, J. The Unique Fluorine Effects in Organic Reactions: Recent Facts and Insights Into Fluoroalkylations. *Chem. Rev.* **2016**, *45*, 5441-5454.
2. Purser, S.; Moore, P. R.; Swallow, S.; Gouverneur, V. Fluorine in Medicinal Chemistry. *Chem. Soc. Rev.* **2008**, *37*, 320-330.
3. Barata-Vellejo, S.; Cooke, M. V.; Postigo, A. Radical Fluoroalkylation Reactions. *ACS Catal.* **2018**, *8*, 7287-7307.
4. Wang, J.; Sánchez-Roselló, M.; Aceña, J. L.; del Pozo, C.; Sorochinsky, A. E.; Fustero, S.; Soloshonok, V. A.; Liu, H. Fluorine in Pharmaceutical Industry: Fluorine-Containing Drugs Introduced to the Market in the Last Decade (2001-2011). *Chem. Rev.* **2014**, *114*, 2432-2506.
5. Wang, H.; Vicic, D. A. Organometallic Aspects of Fluoroalkylation Reactions with Copper and Nickel. *Synlett* **2013**, *24*, 1887-1898.
6. Nebra, N. High-Valent Ni^{III} and Ni^{IV} Species Relevant to C-C and C-Heteroatom Cross-Coupling Reactions: State of the Art. *Molecules* **2020**, *25*, 1141.
7. D'Accriscio, F.; Borja, P.; Saffon-Merceron, N.; Fustier-Boutignon, M.; Mézailles, N.; Nebra, N. C-H Bond Trifluoromethylation of Arenes Enabled by a Robust, High-Valent Nickel(IV) Complex. *Angew. Chem. Int. Ed.* **2017**, *56*, 12898-12902.
8. Lu, Z.; Liu, H.; Liu, S.; Leng, X.; Lan, Y.; Shen, Q. A key Intermediate in Copper-Mediated Arene Trifluoromethylation, $[nBu_4N][Cu(Ar)(CF_3)_3]$: Synthesis, Characterization and $C(sp^2)$-CF_3 Reductive Elimination. *Angew. Chem. Int. Ed.* **2019**, *58*, 8510-8514.
9. Tan, X.; Liu, Z.; Shen, H.; Zhang, P.; Zhang, Z.; Li, C. Silver-Catalyzed Decarboxylative Trifluoromethylation of Aliphatic Carboxylic Acids. *J. Am. Chem. Soc.* **2017**, *139*, 12430-12433.

10. Paeth, M.; Tyndall, S. B.; Chen, L.-Y.; Hong, J.-C.; Carson, W. P.; Liu, X.; Sun, X.; Liu, J.; Yang, K.; Hale, E. M.; Tierney, D. L.; Liu, B.; Cao, Z.; Cheng, M.-J.; Goddard III, W. A.; Liu, W. Csp^3-Csp^3 Bond-Forming Reductive Elimination from Well-Defined Copper(III) Complexes. *J. Am. Chem. Soc.* **2019**, *141*, 3153-3159.
11. Liu, S.; Liu, H.; Lu, Z.; Lu, C.; Leng, X.; Lan, Y.; Shen, Q. C(sp^3)-CF_3 Reductive Elimination from a Five-Coordinate Neutral Copper(III) Complex. *J. Am. Chem. Soc.* **2020**, *142*, 9785-9791.
12. Bour, J. R.; Camasso, N. M.; Sanford, M. S. Oxidation of Ni(II) to Ni(IV) with Aryl Electrophiles Enables Ni-Mediated Aryl-CF_3 Coupling. *J. Am. Chem. Soc.* **2015**, *137*, 8034-8037.
13. Meucci, E. A.; Nguyen, S. N.; Camasso, N. M.; Chong, E.; Ariafard, A.; Canty, A. J.; Sanford, M. S. Nickel(IV)-Catalyzed C-H Trifluoromethylation of (Hetero)arenes. *J. Am. Chem. Soc.* **2019**, *141*, 12872-12879.
14. Shreiber, S. T.; DiMucci, I. M.; Khrizanforov, M. N.; Titus, C. J.; Nordlund, D.; Dudkina, Y.; Cramer, R. E.; Budnikova, Y.; Lancaster, K. M.; Vicic, D. A. $[(MeCN)Ni(CF_3)_3]^-$ and $[Ni(CF_3)_4]^{2-}$: Foundations Towards the Development of Trifluoromethylations at Unsupported Nickel. *Inorg. Chem.* **2020**, *59*, 9143-9151.
15. Harris, C. F.; Kuehner, C. S.; Soper, J. D. Photoinduced Cobalt(III)-Trifluoromethyl Bond Activation Enables Arene C-H Trifluoromethylation. *Angew. Chem. Int. Ed.* **2018**, *57*, 1311-1315.
16. Liebing, P.; Oehler, F.; Wagner, M.; Tripet, P. F.; Togni, A. Perfluoroalkyl Cobaloximes: Preparation Using Hypervalent Iodine Reagents, Molecular Structures, Thermal and Photochemical Reactivity. *Organometallics* **2018**, *37*, 570-583.
17 Harrison, D. J.; Gorelsky, S. I.; Lee, G. M.; Korobkov, I.; Baker, R. T. Cobalt Fluorocarbene Complexes. *Organometallics* **2013**, *32*, 12-15.
18. Harrison, D. J.; Lee, G. M.; Leclerc, M. C.; Korobkov, I.; Baker, R. T. Cobalt Fluorocarbenes: Cycloaddition Reactions with Tetrafluoroethylene and Reactivity of the Perfluorometallacyclic Products. *J. Am. Chem. Soc.* **2013**, *135*, 18296-18299.
19. Lee, G. M.; Harrison, D. J.; Korobkov, I.; Baker, R. T. Stepwise Addition of Difluorocarbene to a Transition Metal Centre. *Chem. Commun.* **2014**, *50*, 1128-1130.
20. Leclerc, M. C.; Bayne, J. M.; Lee, G. M.; Gorelsky, S. I.; Vasiliu, M.; Korobkov, I.; Harrison, D. J.; Dixon, D. A.; Baker, R. T. Perfluoroalkyl Cobalt(III) Fluoride and Bis(perfluoroalkyl) Complexes: Catalytic Fluorination and Selective Difluorocarbene Formation. *J. Am. Chem. Soc.* **2015**, *137*, 16064-16073.
21. Harrison, D. J.; Daniels, A. L.; Korobkov, I.; Baker, R. T. Tetracarbonyl(trifluoromethyl)cobalt(I) $[Co(CO)_4(CF_3)]$ as a Precursor to New Cobalt Trifluoromethyl and Difluorocarbene Complexes. *Organometallics* **2015**, *34*, 4598-4604.
22. Shreiber, S. T.; Scudder, J. J.; Vicic, D. A.; $[(MeCN)_3Co(C_2F_5)_3]$: A Versatile Precursor to Cobalt(III) Perfluoroethyl Complexes. *Organometallics* **2019**, *38*, 3169-3173.

23. Baillargeon, J.; Xie, Y.; Hamann, T. W. Bifurcation of Regeneration and Recombination in Dye-Sensitized Solar Cells via Electronic Manipulation of Tandem Cobalt Redox Shuttles. *ACS Appl. Mater. Interfaces* **2017**, *9*, 33544-33548.
24. The values cited in references 23 and 25 were approximated to the ferrocene/ferrocenium couple.
25. Byrne, E. K.; Theopold, K. H. Redox Chemistry of Tetrakis(1-norbornyl)cobalt. Synthesis and Characterization of a Cobalt(V) Alkyl and Self-Exchange Rate of a Co(III)/Co(IV) Couple. *J. Am. Chem. Soc.* **1987**, *109*, 1282-1283.
26. Yamaguchi, Y.; Ichioka, H.; Klein, A.; Brennessel, W. W.; Vicic, D. A. Linear Bis(perfluoroalkyl) Complexes of Nickel Bipyridine. *Organometallics* **2012**, *31*, 1477-1483.
27. Algarra, A. G.; Grushin, V. V.; MacGregor, S. A. Natural Bond Orbital Analysis of the Electronic Structure of [LnM(CH_3)] and [LnM(CF_3)] Complexes. *Organometallics* **2012**, *31*, 1467-1476.
28 Demadis, K. D.; El-Samanody, E.-S.; Meyer, T. J.; White, P. S. Structural and Redox Chemistry of Osmium(III) Chloro Complexes Containing 2,2′:6′,2″-Terpyridyl and Tris-Pyrazolyl Borate Ligands. *Polyhedron* **1999**, *18*, 1587-1594.
29. Connelly, N. G.; Geiger, W. E. Chemical Redox Agents for Organometallic Chemistry. *Chem. Rev.* **1996**, *96*, 877-910.
30. We are aware that oxidation of higher valent cobalt fluoroalkyl complexes likely oxidizes the ligand and not the metal, as is observed for nickel[14] and copper.[31]
31. DiMucci, I. M.; Lukens, J. T.; Chatterjee, S.; Carsch, K. M.; Titus, C. J.; Lee, S. J.; Nordlund, D.; Betley, T. A; MacMillan, S. N.; Lancaster, K. M. The Myth of d^8 Copper(III). *J. Amer. Chem. Soc.* **2019**, *141*, 18508-18520.

Chapter 5: Synthesis and Characterization of the Dinuclear Cobalt(III) Complex: $[(C_2F_5)_3Co(\mu\text{-}F)]_2^{2-}$

The following chapter has been adapted (reprinted) with permission from: Shreiber, S. T.; Vicic, D. A. *J. Organomet. Chem.* **2021**, *949*, 121974.

5.1 Abstract: Reaction of the versatile tris(perfluoroethyl) cobalt(III) precursor [*fac*-$(MeCN)_3Co(C_2F_5)_3$] with $[NMe_4]F$ and $[PPh_4]Cl$ in THF formed the unexpected fluorinated dinuclear bridging cobalt(III) dimer $[(C_2F_5)_3Co(\mu\text{-}F)]_2^{2-}$. The new organometallic cobalt(III) fluoride complex was characterized by NMR, and UV-vis spectroscopies, X-ray crystallography, cyclic voltammetry, and by computational methods. In the strongly coordinating solvent MeCN, $[(C_2F_5)_3Co(\mu\text{-}F)]_2^{2-}$ exhibited dynamic processes on the NMR timescale which were consistent with solvent coordination. However, in the weakly coordinating solvent CH_2Cl_2, a more static structure is observed suggesting that the dimer retains its structure in solution state. An electrochemical analysis of $[(C_2F_5)_3Co(\mu\text{-}F)]_2^{2-}$ was performed, and the data compared to previously reported cobalt(III) perfluoroethyl complexes.

5.2 Introduction:

There has been significant interest over the past decade in developing new methodologies for the incorporation of fluorine and fluoroalkyl groups into organic substrates due to the advantageous properties these groups can confer.[1-4] Methods for fluorination and fluoroalkylation involving first-row metals are particularly attractive due the abundance of these metals in nature and their ability to access a wider range of formal oxidation states. Accessing the high-valent states of these metals has been important for triggering the difficult bond forming reactions often associated with fluorinated groups.[5,6] The synthesis, isolation, and characterization of new fluoroalkylated transition metal complexes allow for

critical understanding of the fundamental chemical transformations that are possible and is an important aspect of methods development.

Cobalt(II) fluoride in the +2 oxidation state is known to be rather inert, especially compared to cobalt(III) fluoride, which is capable of fluorinating hydrocarbons.[7,8] Cobalt(III) fluoride played an integral role as an effective fluorination reagent during the Manhattan Project, where it was used to prepare perfluorinated lubricants that were needed for the separation of uranium isotopes.[7,8] The CoF_3 is recyclable and can be regenerated by passing elemental fluorine through the reactor at elevated temperatures.[7] While effective for total fluorination of organic molecules, CoF_3 has poor selectivity and is not a viable reagent for fine chemical production. Furthermore, CoF_3 has poor solubility in organic solvents, and fluorination reactions are typically performed in solid/vapor phase set-ups of well-over 100 ^oC.[7-9]

Derivatives of cobalt(III) fluoride complexes bearing novel skeletons could serve as a milder reagent that allow for more selective fluorinations. Replacement of one or more of the fluorines of CoF_3 could increase solubility, allow for reactions to occur under milder conditions, and enable more selectivity in organic transformations. A recent review paper has summarized the transformations involving cobalt fluorides to date.[8] Although well-defined organometallic cobalt(III) fluorides exist, organic transformations mediated by these species is limited to the transformation of acyl chlorides to acyl fluorides.[10,11]

Recently, we have prepared the air-stable perfluoroethyl cobalt precursor, [*fac*-$(MeCN)_3Co(C_2F_5)_3$] (**5a**), and found the acetonitrile ligands are labile towards ligand substitution reactions.[12,13] For instance, complex **5a** reacts with an anionic tris(pyrazolyl)borate (Tp) ligand in the presence of $[PPh_4]Cl$ to afford $[PPh_4][(\kappa^3\text{-}Tp)Co(C_2F_5)_3]$, whose oxidation occurs at a much more negative redox potential than **5a**.[13]

In this chapter, we investigate whether reaction of **5a** with a fluoride salt would lead to a simple anionic cobalt(III) fluoride complex with excellent solubility and an accessible oxidation which could trigger homolyses reactions.

5.3 Results and Discussion

5.3.1. Synthesis of the Cobalt Fluoride Dimer: Reaction of **5a** with $[NMe_4]F$ in THF solvent at room temperature for one hour produces a new species that, upon counter-ion exchange with $[PPh_4]Cl$, produces **5b** (Scheme 5a) as an isolable solid that was characterized by X-ray diffractometry (Figure 5a). Attempts to cleanly isolate **5b** as an NMe_4 salt in the absence of any $[PPh_4]Cl$ proved unsuccessful. Complex **5b** adopts a square pyramidal structure in the solid state with bridging fluorides that occupy positions at the base of the pyramid along with two other perfluoroethyl groups, with apical perfluoroethyls completing the pyramid. The solid-state structure reveals that the cobalt-carbon bonds trans to the bridging fluorides are significantly longer (1.943(2) and 1.944(2) Å) than the apical cobalt-carbon bond (1.898(2) Å), consistent with the trans influencing properties of fluoride.

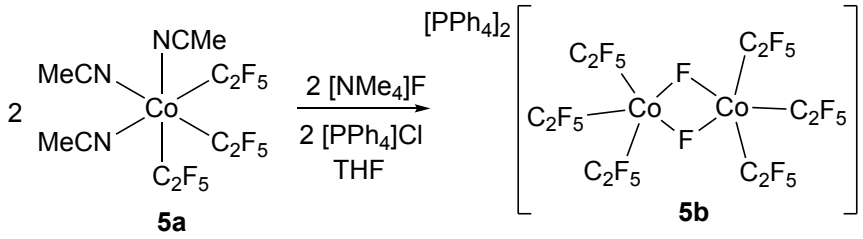

5a **5b**

Scheme 5a. Synthesis of dimer **5b**.

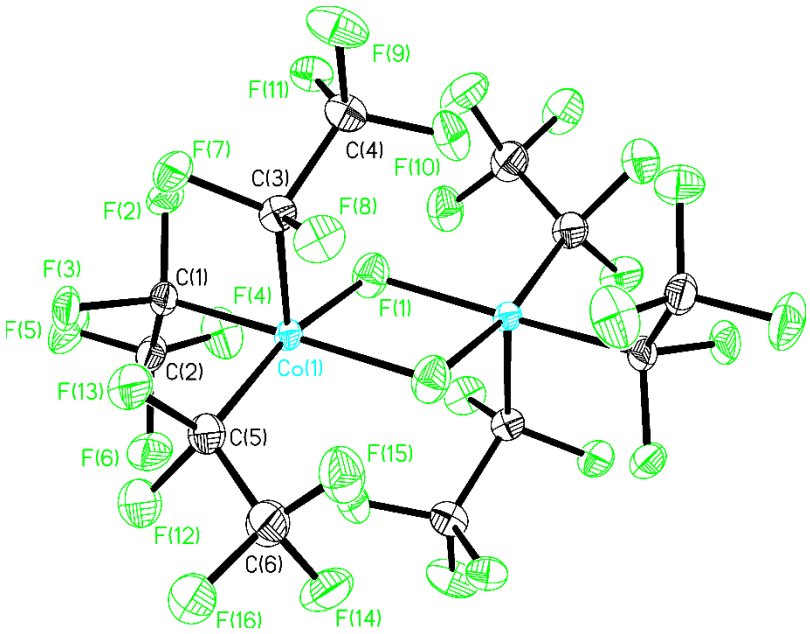

Figure 5a: ORTEP Diagram of **5b**. The $[PPh_4]^+$ counter-ions and a symmetry-related cobalt fragment in the asymmetric unit have been omitted for clarity. Selected distances (Å): Co1-C3 1.898(2); Co1-F1 1.9123(14); Co1A-F1 1.9233(15); Co1-C1 1.943(2); Co1-C5 1.944(2); Co1-Co1A 3.0107(5). Selected bond angles (°): C3-Co1-F1 99.64(8); C3-Co1-C1 93.73(9); F1-Co1-C1 91.83(8); C3-Co1-C5 93.19(10); F1-Co1-C5 166.58(9); C1-Co1-C5 91.19(10).

An absence of $^3J_{FF}$ coupling is observed in the ^{19}F NMR spectrum between the CF_2 and CF_3 groups. This absence may be due to line broadening from square pyramidal/trigonal bipyramidal interconversions in solution, but may also be due to rotational averaging of coupling constants of opposite sign between the vicinal CF_2 and CF_3 groups, as has been reported for isolated perfluoroethyl groups.[12,14-16]

5.3.2. Characterization of the Dimer's Solution Behavior: The NMR spectrum suggests that **5b** undergoes solvent-dependent dynamic processes in solution. The room temperature ^{19}F NMR spectrum of **5b** in MeCN-d_3 displays four broad signals in the region between –427 to –495 ppm for the bridging fluorides (see Appendix D). Recording the ^{19}F NMR at –30 °C provided a more static spectrum for **5b**, with signals at –80.7, –101.2 ppm, and a lone resonance at δ = –427.3. Compound **5b** appears to adopt a more static structure

in CD_2Cl_2, as the room temperature ^{19}F NMR spectrum in that solvent gave sharp signals at –81.4, –101.7, and –472.9 ppm. Cobalt(III) fluorides exhibit a wide range of ^{19}F NMR chemical shifts. Baker reported ^{19}F NMR chemical shifts for [(Cp)Co(L)(R_f)(F)] (L = PPh_3, PPh_2Me, $R_f = CF_3$, C_2F_5, Cp = cyclopentadienyl) derivatives appear in the range of –716 to –759 ppm in C_6D_6.[10] Cobalt(III) fluorides bearing nitrogen ligands such as [(Me_3-tacn)CoF_3]·H_2O (Me_3-tacn = 1,4,7-trimethyl-1,4,7-triazacyclononane) and [(tpy)CoF_3]·MeOH·H_2O (tpy = terpyridine) exhibit resonances for the Co-F moieties in the ^{19}F NMR spectra at –149 ppm and –116 ppm, respectively, in CH_3OD.[17]

The UV-Vis spectrum of **5b** in MeCN is shown in Figure 5b. Over various time points, slight differences in peak positions and intensities were observed. The initial spectrum has λ_{max} values of 363, 395, and 533 nm. During the course of 24 hours, the absorbance at 363 nm diminishes in intensity while the absorbance at 395 nm increases in intensity and red shifts to 401 nm, and the maxima at 533 nm decreases in intensity. The UV-Vis spectrum of **5b** in CH_2Cl_2 (Figure 5b), in contrast, showed no changes over time, exhibiting peaks with λ_{max} of 416 and 516 nm with molar absorptivities of 240 and 350 M^{-1} cm^{-1}, respectively, in line with previously reported cobalt(III) perfluoroethyl complexes.[13]

One possibility to account for the dynamic behavior of **5b** in acetonitrile solution is the presence of equilibria involving solvent coordination to form derivatives like $[(MeCN)_2Co(C_2F_5)_3(F)]^-$ (**5c**, Scheme 5b). Time-dependent density functional theory (TD-DFT) calculations (CAM-B3LYP/m6-31G*) were performed to qualitatively understand the appearance of the UV-Vis spectrum of **5c**, and the results are shown in Figure 5c. While the dimer **5b** exhibits two main peaks in the calculated spectrum (Figure 5c, black line) at 341 and 506 nm, complex **5c** is predicted to have one main absorption

peak centered at 411 nm (Figure 5c, red line). As the experimental spectrum of **5b** in acetonitrile (blue line, Figure 5c) does show peaks at 363 and 395 nm, it is plausible that both **5b** and **5c** (and/or other solvated derivatives) exist in solution, which is consistent with both the experimental UV-Vis and ^{19}F NMR data of **5b** in acetonitrile.

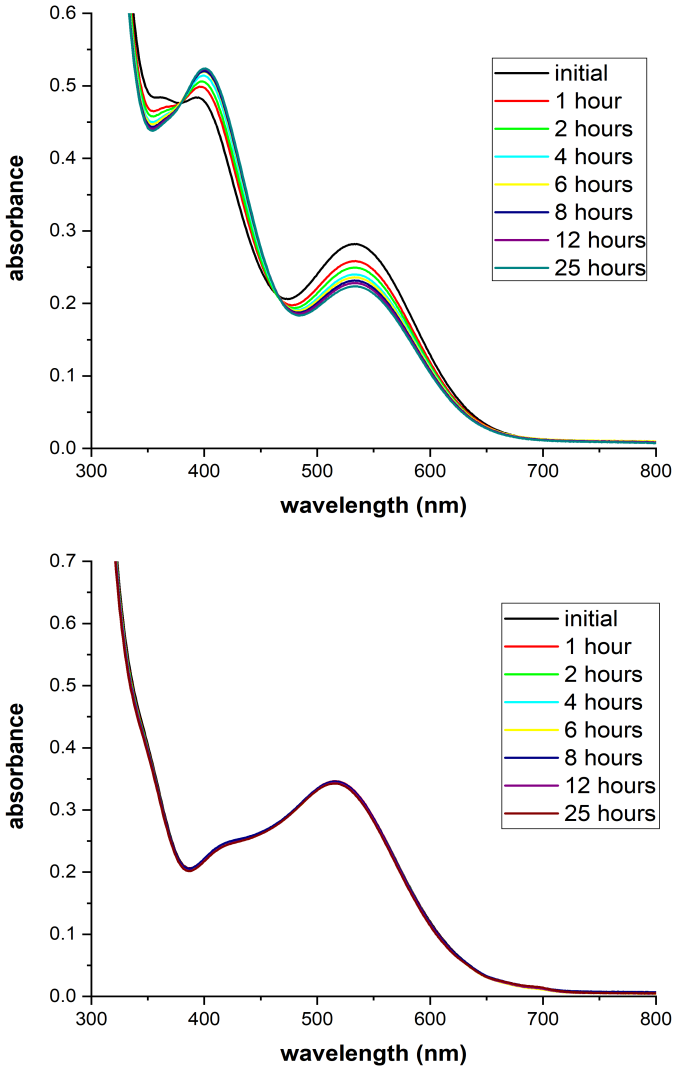

Figure 5b. UV-vis spectrum of **5b** recorded in acetonitrile (top) and dichloromethane (bottom).

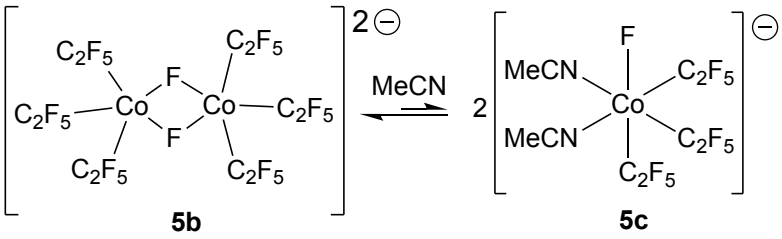

5b **5c**

Scheme 5b. Proposed equilibrium of **5b** in acetonitrile solution.

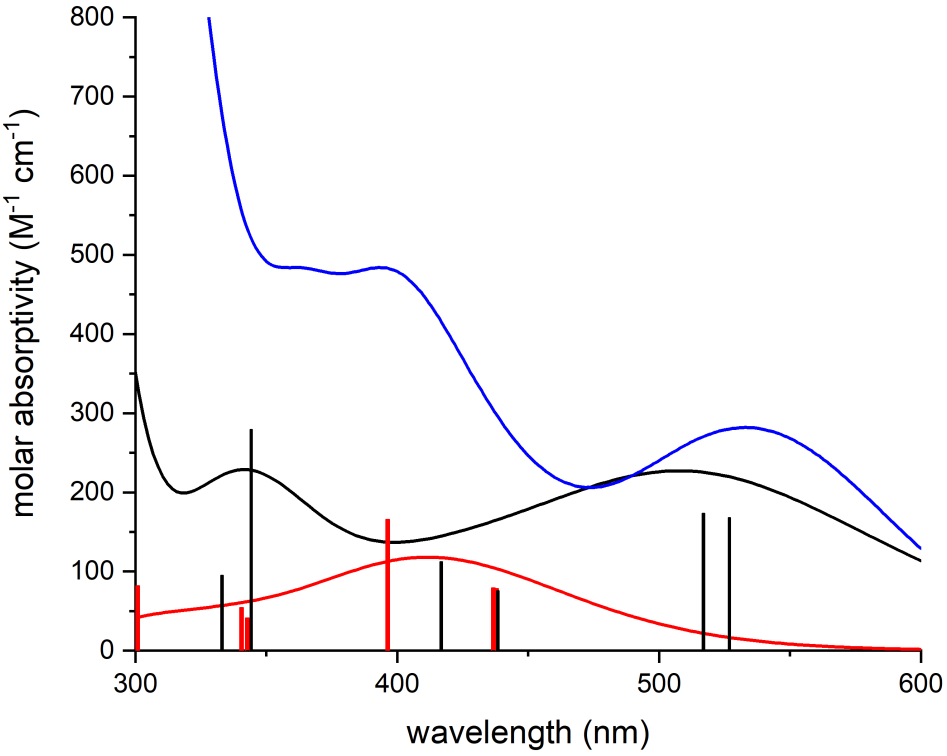

Figure 5c. Experimental UV-Vis spectrum of **5b** recorded in acetonitrile (blue) overlaid with calculated TD-DFT spectra of **5b** (black) and **5c** (red), with major transitions shown.

5.3.3. Evaluation of Electrochemical Properties: We next evaluated the electrochemical properties of **5b** by cyclic voltammetry in MeCN solvent (Figure 4, top). Oxidation of **5b** is irreversible, and the cyclic voltammogram shows a complex trace that is likely a reflection of equilibria processes occurring with acetonitrile solvent. Multiple waves appear at potentials below 1.0 V vs. the ferrocene/ferrocenium couple, which are relatively

low potentials for oxidation compared to that observed for the charge-neutral complexes **5a** and $[(tpy)Co(C_2F_5)_3]$[12] (Figure 5d, top, orange vs blue and black lines). The potential required for oxidation of **5b** better resembles that observed for the anionic $[(Tp)Co(C_2F_5)_3]^-$, which has a peak potential of +1.16 V vs the ferrocene/ferrocenium couple (also shown in Figure 5d, top, red line).[13] The CV data for complex **5b** in dichloromethane (Figure 5d, bottom) appears to be less complex than that in acetonitrile solvent, paralleling the trends observed for the experimental UV-Vis and ^{19}F NMR spectra. In dichloromethane, the oxidation of **5b** shifts to more positive potentials relative to $[(Tp)Co(C_2F_5)_3]^-$, with an initial onset potential of +0.82 V vs the ferrocene/ferrocenium couple. The well-defined complexes $[(Tp)Co(C_2F_5)_3]^-$, $[(tpy)Co(C_2F_5)_3]$, as well as **5a** however, did not see such significant shifts upon changing the solvent from acetonitrile to dichloromethane (Figure 5d). The data show that oxidation of **5b** occurs at lower potentials in strongly coordinating solvents, likely due to the electron donating ability of coordinated solvent. Oxidations of the cobalt(III) complexes, while formally producing cobalt(IV) species, likely involve oxidation of the non-innocent fluoroalkyl ligands.[18,19] Because the oxidations fall within redox potential windows of commonly used oxidants,[20] the generation of a more stable and isolable oxidized species may be possible given the appropriate set of ligands.

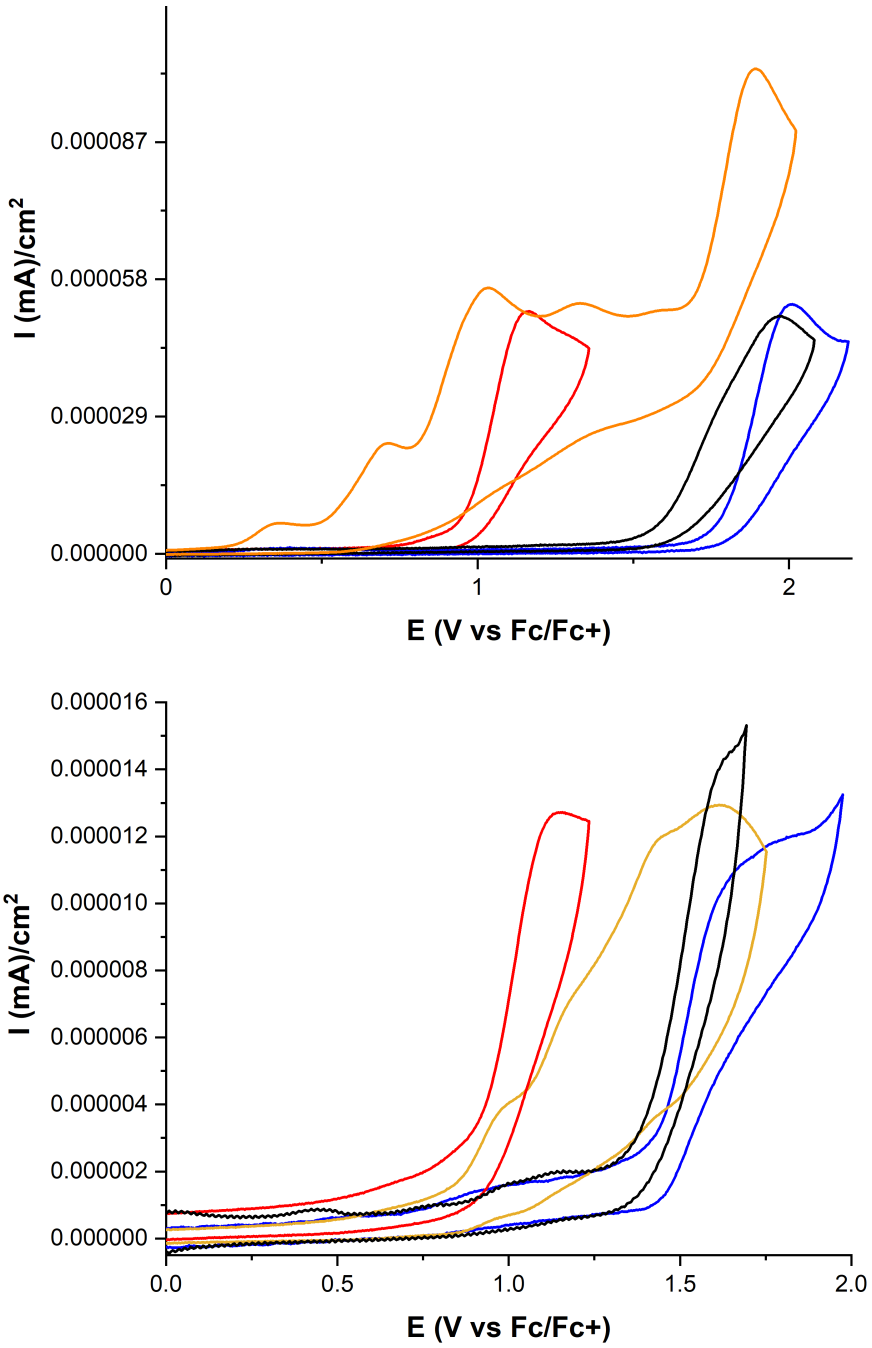

Figure 5d. Cyclic voltammograms of **1** (blue), **2** (orange), $[(Tp)Co(C_2F_5)_3]^-$ (red), and $[(tpy)Co(C_2F_5)_3]$ (black) in acetonitrile (top) and dichloromethane (bottom). Metal complex, 10 mM; 100 mM $[NBu_4][PF_6]$; working and counter electrodes were platinum with a Ag pseudo reference; scan rate, 100 mV/s.

5.4 Conclusions: In this report, we show that the precursor $[MeCN)_3Co(C_2F_5)_3]$ reacts with NMe_4F in the presence of PPh_4Cl to form the unique anionic bridging fluoride dimer $[PPh_4]_2[(C_2F_5)_3Co(\mu\text{-}F)_2Co(C_2F_5)_3]$ (**5b**). Complex **5b** was characterized by NMR and UV-vis spectroscopies, X-ray crystallography, cyclic voltammetry, and was modeled with computational methods. Solution studies by NMR and UV-Vis spectroscopies revealed that **5b** undergoes dynamic processes in strongly coordinating acetonitrile solvent. In weakly coordinating dichloromethane solvent, a more static structure is observed. Electrochemical experiments show that the dianion **5b** is oxidized at much lower potentials than related perfluoroethyl cobalt(III) complexes. Overall, **5b** is an easily prepared cobalt(III) fluoride that has excellent solubility with potential binding sites for other ligands. As such, dimer **5b** offers an interesting platform for exploring applications in fluoroalkylation reactions and the chemistry of high-valent cobalt.

5.5. Experimental

5.5.1. General Information: All manipulations were performed using standard Schlenk and high vacuum techniques or in a nitrogen filled glovebox, unless otherwise stated. Solvents were purified by passing through activated alumina and/or copper in a solvent purification system supplied by Pure Process Technology. Solution ^1H NMR spectra were recorded at ambient temperature on a Bruker 400 MHz spectrometer and referenced to residual proton solvent signals. ^{19}F spectra were recorded on the Bruker NMR spectrometer operating at 376 MHz and referenced to α,α,α-trifluorotoluene as an internal standard (δ = –63.7). ^{31}P {H} spectra were recorded on a Bruker NMR spectrometer operating at 162 MHz and referenced to phosphoric acid as an external standard (δ = 0.00). A Bruker D8 Quest diffractometer was used for X-ray crystal structure determinations. Cyclic

voltammetry data was collected in a nitrogen filled glovebox at room temperature on a PARSTAT 4000A potentiostat. UV-Vis spectra were recorded on a Varian Cary 5000 spectrophotometer, with path length 1 cm. The CCDC 2059468 contains the supplementary crystallographic data for this paper. These data can be obtained free of charge via www.ccdc.cam.ac.uk/data_request/cif, or by e-mailing data_request@ccdc.cam.ac.uk, or by contacting The Cambridge Crystallographic Data Centre, 12 Union Road, Cambridge CB2 1EZ, UK; fax: +44 1223 336033.

5.5.2. Preparation of $[PPh_4]_2[(C_2F_5)_3Co(\mu\text{-}F)_2Co(C_2F_5)_3]$ (5b): In a nitrogen-filled glovebox, a vial was charged with $[(MeCN)_3Co(C_2F_5)_3]$ (0.10 g, 0.19 mmol), NMe_4F (18 mg, 0.19 mmol), and PPh_4Cl (72 mg, 0.19 mmol), and THF (5 mL) and stirred for one hour. The insolubles were filtered off and the filtrate was recrystallized by vapor diffusion of THF/pentane to yield 118 mg of a red/pink crystals (80%). ^{1}H NMR (CD_3CN, 400 MHz): δ 7.91 (t, *J*= 8.3 Hz, 8H), 7.81-7.59 (m, 32H). ^{31}P {H} NMR (CD_3CN, 162 MHz): δ 23.9 (s). ^{19}F NMR (CD_2Cl_2, 376 MHz, r.t.): δ -81.4 (s, 18F), -101.7 (s, 12F), -472.9 (s, 2F). ^{19}F NMR (CD_3CN, 376 MHz, -30^{o}C): δ -80.7 (s, 18F), -101.2 (s, 12F), -427.3 (s, 2F). Anal. Calcd (found) for $C_{60}H_{40}Co_2F_{32}P_2$: C, 46.53 (46.52); H, 2.60 (2.73).

5.5.3. Computational Details: Density functional theory (DFT) and time-dependent density functional theory (TD-DFT) calculations were done on **5b** and **5c** using Gaussian09.[21] Geometry optimization and frequency calculations were done using B3LYP functional[22,23] with the basis set m6-31G* for cobalt[24] and 6-31G** for all other atoms. The IEFPCM solvation model with acetonitrile was employed. The true minima were confirmed by the presence of no imaginary frequencies. TD-DFT was performed on the optimized geometries using the CAM-B3LYP functional with the split basis set m6-

31G* for Co and 6-31G** for all other atoms, with the IEFPCM solvation model (acetonitrile).

5.6 References

1. Barata-Vellejo, S.; Cooke, M. V.; Postigo, S. Radical Fluoroalkylation Reactions. *ACS Catal.* **2018**, *8,* 7287-7307.
2. Ni, C.; Hu, J. The Unique Fluorine Effects in Organic Reactions: Recent Facts and Insights into Fluoroalkylations. *Chem. Rev.* **2016**, *45*, 5441-5454.
3. Lantaño, B.; Torviso, M. R.; Bonesi, S. M.; Barata-Vellejo, S.; Postigo, A. Advances in Metal-Assisted Non-Electrophilic Fluoroalkylation Reactions of Organic Compounds. *Coord. Chem. Rev.* **2015**, *285*, 76-108.
4. Nobile, E.; Castanheiro, T.; Besset, T. Radical-Promoted Distal C-H Functionalization of C(sp3) Centers with Fluorinated Moieties. *Angew. Chem. Int. Ed.* **2021**, *60*, 12170-12191.
5. Nebra, N. High-Valent Ni(III) and Ni(IV) Species Relevant to C-C and C-Heteroatom Cross-Coupling Reactions: State of the Art. *Molecules* **2020,** *25*, 1141.
6. Hickman, A. J.; Sanford, M. S. High-valent Organometallic Copper and Palladium in Catalysis. *Nature* **2012**, *484*, 177-185.
7. Barbour, A. K.; Barlow, G. B.; Tatlow, J. C. The Fluorination of Hydrocarbons with Cobalt Trifluoride. *J. Appl. Chem.* **1952**, *2*, 127-133.
8. Zhang, X.-G.; Guo, P.; Han, J.-F.; Ye, K.-Y. Cobalt Fluorides: Preparation, Reactivity and Applications in Catalytic Fluorination and C-F Functionalization. *Chem. Commun.* **2020**, *56*, 8512-8523.
9. Goldwhite, H. The Manhattan Project. *J. Fluorine Chem.* **1986**, *33*, 109-132.
10. Leclerc, M. C.; Bayne, J. M.; Lee, G. M.; Gorelsky, S. I.; Vasiliu, M.; Korobkov, I.; Harrison, D. J.; Dixon, D. A.; Baker, R. T. Perfluoroalkyl Cobalt(III) Fluoride and Bis(perfluoroalkyl) Complexes: Catalytic Fluorination and Selective Difluorocarbene Formation. *J. Am. Chem. Soc*. **2015**, *137*, 16064-16073.
11. Lee, G. M.; Clément, R.; Baker, R. T. High-Throughput Evaluation of In Situ-Generated Cobalt(iii) Catalysts for Acyl Fluoride Synthesis. *Catal. Sci. Technol.* **2017**, *7*, 4996-5003.
12. Shreiber, S. T.; Scudder, J. J.; Vicic, D. A. $[(MeCN)_3Co(C_2F_5)_3]$: A Versatile Precursor to Cobalt(III) Perfluoroethyl Complexes. *Organometallics* **2019**, *38* 3169-3173.
13 Shreiber, S. T.; Vicic, D. A. Synthesis and Oxidative Stability of an Anionic Perfluoroethyl Cobalt(III) Complex. *Helv. Chim. Acta* **2020**, *103*, e2000149.
14. Newmark, R.A. Vicinal Fluorine-Fluorine Coupling Constants in Perfluoropropyl Groups. *J. Fluorine Chem.* **2009**, *130*, 389-393.
15. Graves, R. E.; Newmark, R. A. Fluorine Coupling in Hexafluoroethane. *J. Chem. Phys.* **1967**, *47*,3681-3682.
16. Harris, R. K.; Woodman, C. M. Spectra of Molecules Containing CF_2 groups, II Perfluorobutane. *J. Mol. Spectrosc.* **1968**, *26*, 432-443.
17. Blower, P. J.; Levason, W.; Luthra, S. K.; McRobbie, G.; Monzittu, F. M.; Mules, T. O.; Reid, G.; Subhan, M. N. Exploring Transition Metal Fluoride Chelates – Synthesis,

Properties and Prospects Towards Potential PET Probes. *Dalton Trans.* **2019**, *48*, 6767-6776.
18. Hoffmann, R.; Alvarez, S.; Mealli, C.; Falceto, A.; Cahill, T. J.; Zeng, T.; Manca, G. From Widely Accepted Concepts in Coordination Chemistry to Inverted Ligand Fields. *Chem. Rev.* **2016**, *116*, 8173-8192.
19. Shreiber, S. T.; DiMucci, I. M.; Khrizanforov, M. N.; Titus, C. J.; Nordlund, D.; Dudkina, Y.; Cramer, R. E.; Budnikova, Y.; Lancaster, K. M.; Vicic, D. A. $[(MeCN)Ni(CF_3)_3]^-$ and $[Ni(CF_3)_4]^{2-}$: Foundations toward the Development of Trifluoromethylations at Unsupported Nickel. *Inorg. Chem.* **2020**, *59*, 9143-9151.
20. Connelly, N. G.; Geiger, W. E. Chemical Redox Agents for Organometallic Chemistry. *Chem. Rev.* **1996**, *96*, 877-910.
21. Gaussian 09, Revision D.01, M. J. Frisch, G. W. Trucks, H. B. Schlegel, G. E. Scuseria, M. A. Robb, J. R. Cheeseman, G. Scalmani, V. Barone, B. Mennucci, G. A. Petersson, H. Nakatsuji, M. Caricato, X. Li, H. P. Hratchian, A. F. Izmaylov, J. Bloino, G. Zheng, J. L. Sonnenberg, M. Hada, M. Ehara, K. Toyota, R. Fukuda, J. Hasegawa, M. Ishida, T. Nakajima, Y. Honda, O. Kitao, H. Nakai, T. Vreven, J. A. Montgomery, Jr., J. E. Peralta, F. Ogliaro, M. Bearpark, J. J. Heyd, E. Brothers, K. N. Kudin, V. N. Staroverov, T. Keith, R. Kobayashi, J. Normand, K. Raghavachari, A. Rendell, J. C. Burant, S. S. Iyengar, J. Tomasi, M. Cossi, N. Rega, J. M. Millam, M. Klene, J. E. Knox, J. B. Cross, V. Bakken, C. Adamo, J. Jaramillo, R. Gomperts, R. E. Stratmann, O. Yazyev, A. J. Austin, R. Cammi, C. Pomelli, J. W. Ochterski, R. L. Martin, K. Morokuma, V. G. Zakrzewski, G. A. Voth, P. Salvador, J. J. Dannenberg, S. Dapprich, A. D. Daniels, O. Farkas, J. B. Foresman, J. V. Ortiz, J. Cioslowski, and D. J. Fox, Gaussian, Inc., Wallingford CT, **2013**.
22. Becke, A. D. Density-Functional Thermochemistry. III. The Role of Exact Exchange. *J. Chem. Phys.* **1993,** *98*, 5648-52.
23. Lee, C.; Yang, W.; Parr, R. G., Development of the Colle-Salvetti Correlation-Energy Formula into a Functional of the Electron Density. *Phys. Rev. B: Condens. Matter* **1988,** *37*, 785-9.
24. Mitin, A. V.; Baker, J.; Pulay, P. An Improved 6-31G* Basis Set for First-Row Transition Metals. *J. Chem. Phys.* **2003**, *118*, 7775-7782.

Chapter 6: $[(MeCN)Ni(CF_3)_3]^-$ and $[Ni(CF_3)_4]^{2-}$: Foundations toward the Development of Trifluoromethylations with Solvated Nickel

The following chapter has been adapted and reproduced with permission from: Shreiber, S. T.; DiMucci, I. M.; Khrizanforov, M. N.; Titus, C. J.; Nordlund, D.; Dudkina, Y.; Cramer, R. E.; Budnikova, Y.; Lancaster, K. M.; Vicic, D. A. *Inorg. Chem.* **2020**, *59*, 9143-9151.

6.1 Abstract: The nickel anions $[(MeCN)Ni(CF_3)_3]^-$ and $[Ni(CF_3)_4]^{2-}$ were prepared by formal addition of three and four equivalents, respectively, of "$AgCF_3$" to $[(dme)NiBr_2]$ in the presence of $[PPh_4]^+$ counter-ion. Detailed insights into the electronic properties of these new compounds were obtained through the use of density functional theory (DFT) calculations, spectroscopy-oriented configuration interaction (SORCI) calculations, X-ray absorption spectroscopy, and cyclic voltammetry. The data collectively show that trifluoromethyl complexes of nickel, even in the most common oxidation state of nickel(II), are highly covalent systems whereby a hole is distributed on the trifluoromethyl ligands and surprisingly rendering the metal to a physically more reduced state. In the cases of $[(MeCN)Ni(CF_3)_3]^-$ and $[Ni(CF_3)_4]^{2-}$, these complexes are better described as physically d^9 metal complexes. $[(MeCN)Ni(CF_3)_3]^-$ is electrophilic and reacts with other nucleophiles like phenoxide to yield the heterolyptic $[(PhO)Ni(CF_3)_3]^{2-}$ salt, revealing the broader potential of $[(MeCN)Ni(CF_3)_3]^-$ in the development of trifluoromethylations with solvated nickel. Proof-in-principle experiments show that reaction of $[(MeCN)Ni(CF_3)_3]^-$ with an aryl iodonium salt yields trifluoromethylated arene, presumably via a high valent formally organonickel(IV) intermediate. Evidence for the feasibility of such intermediates is provided with the structurally characterized $[PPh_4]_2[Ni(CF_3)_4(SO_4)]$, which was derived through the two-electron oxidation of $[Ni(CF_3)_4]^{2-}$.

6.2 Introduction: It was first reported (without full experimental disclosure)[1] that the complex ion $[Cu(CF_3)_4]^-$ (**6a**, Scheme 6a) could be generated by the oxidation of the cuprate salt $[Cu(CF_3)_2]^-$. Shortly thereafter, Naumann and co-workers reported the synthesis and isolation of $[PPh_4][Cu(CF_3)_4]$ as well as the X-ray structure of the related salt $[PPN][Cu(CF_3)_4]$.[2] The $[Cu(CF_3)_4]^-$ core was described as having "surprising"[2] stability as it possessed a rare and formally copper(III) center. Knowledge of the structure of **6a** stimulated studies of its electronic structure, and in 1995 Snyder put forth the provocative analysis that the trifluoromethyl ligands were oxidized rather than the copper center (a feature later referred to as "sigma non-innocence"[3-4]) and that the oxidation state of the copper ion in **6a** was actually copper(I) and not copper(III).[5] Such a description of the electronic state of **6a** has sparked debate and further theoretical studies,[3, 6-7] but recent experimental evidence for a $3d^{10}$ ground state electronic configuration and ligand field inversion in **6a**[8-10] supports Snyder's proposal of a copper(I) complex that displays sigma non-innocence of the trifluoromethyl ligands.

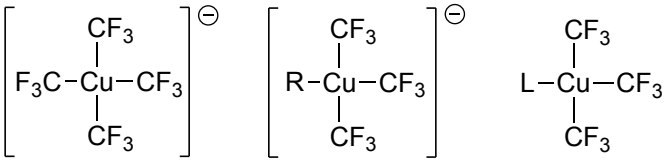

6a **6b** **6c**

Scheme 6a. High-valent copper trifluoromethyl complexes.

Salts of **6a** have not only been important for providing insights into the nature of bonding in metal-fluoroalkyl complexes, but have also demonstrated reactivity important to the development of trifluoromethylation methodologies. For example, Zhang and co-workers revealed that equilibria involving ion pairs of $[Cu(CF_3)_4]^-$ can be exploited in reactions with aryl boronic acids to afford high yields of trifluoromethylated arenes (Scheme 6b,a).[11]

Menjon and co-workers showed that **6a** can generate trifluoromethyl radicals under photolytic conditions, which could then be trapped by arenes and nitrones (Scheme 6b,b).[12] Importantly, the homoleptic tetra(trifluoromethyl)copper(III) functionality in **6a** can also be rendered into heteroleptic derivatives (**6b**) by addition of nucleophiles to charge-neutral tris(trifluoromethyl)copper complexes (**6c**, Scheme 6b,c). This derivatization is of high synthetic value as eliminations from **6b** can render cross-coupled and trifluoromethylated organic products.[13-14] Finally, the charge-neutral tris(trifluoromethyl)copper derivatives **6c** have also served as precursors of $[LCu(CF_3)_2(R)]$[15-18] intermediates *en route* to the generation of $[R\text{-}CF_3]$ products (Scheme 6b,d).

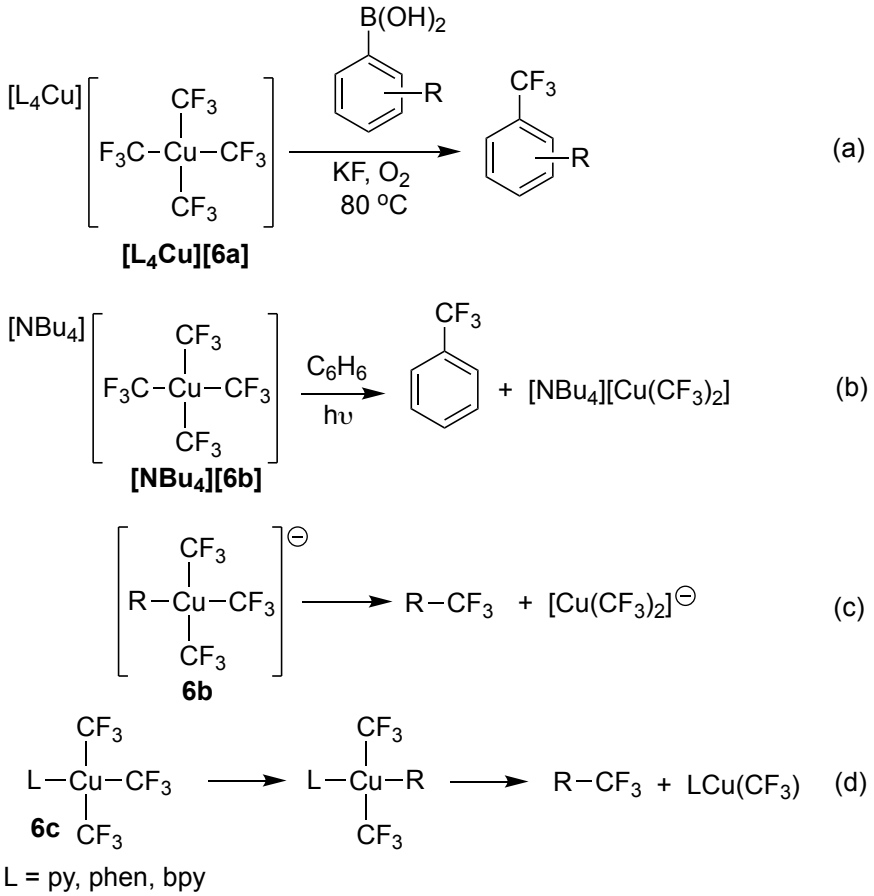

Scheme 6b. Known applications of formally copper(III) trifluoromethyl copper complexes.

We hypothesized that a homoleptic tetra(trifluoromethyl)metal complex bearing a bona fide d^8 ground state electronic configuration may be possible with nickel, as nickel in the +2 oxidation state is more commonly encountered than copper in its +3 oxidation state. Moreover, if $[Ni(CF_3)_4]^{2-}$ and $[Ni(R)(CF_3)_3]^{2-}$ complexes could be generated, then access to their higher oxidation states would be more facile than for $[Cu(CF_3)_4]^-$ and $[LCu(CF_3)_2(R)]$ derivatives, which are already highly oxidized molecular species. Nickel fluoroalkyl complexes often exhibit two additional oxidations beyond the formal nickel(II) state and show higher reactivity in their oxidized forms.[19-24] Access to higher oxidation states would provide the opportunity to explore whether difficult chemical bond forming reactions involving the trifluoromethyl group could be triggered by oxidative means with unsupported[25] architectures at nickel.

6.3 Results and Discussion

6.3.1. Synthesis of Trifluoromethyl Nickelates: A family of trifluoromethyl nickel complexes could be prepared by routes that all employ a common set of starting materials and reagents, as described in Scheme 6c. The reaction of $[(dme)NiBr_2]$ with two equivalents of $Me_3Si\text{-}CF_3$ and AgF leads to the charge neutral (bis)trifluoromethyl complex **6d**.[26] Here, we reveal that reaction of $[(dme)NiBr_2]$ with an extra equivalent of $Me_3Si–CF_3$ and AgF in the presence of $[PPh_4]Cl$ in acetonitrile cleanly leads to the formation of the new anionic tris trifluoromethyl complex **6e** in 93% isolated yield. Diagnostic ^{19}F NMR signals for **6e** arise from the two types of trifluoromethyl groups situated in a static and square planar arrangement (CD_3CN, δ –25.2 (septet, J = 4.5 Hz, 3F) and –31.1 (quartet, J = 4.5 Hz, 6F)). Gratifyingly, performing the trifluoromethylation of $[(dme)NiBr_2]$ with slightly over four equivalents of $Me_3Si\text{-}CF_3$ and AgF in the presence of $[PPh_4]Cl$ leads to

the appearance of a new singlet in the ^{19}F NMR at δ –26.2 that corresponds to the target dianionic complex **6f**. Complete conversion to **6f** was difficult to achieve and **6f** can only be generated in mixtures with **6e**, but the solubility properties of the dianion facilitated its isolation in analytically pure form in 19% yield by selective crystallization.

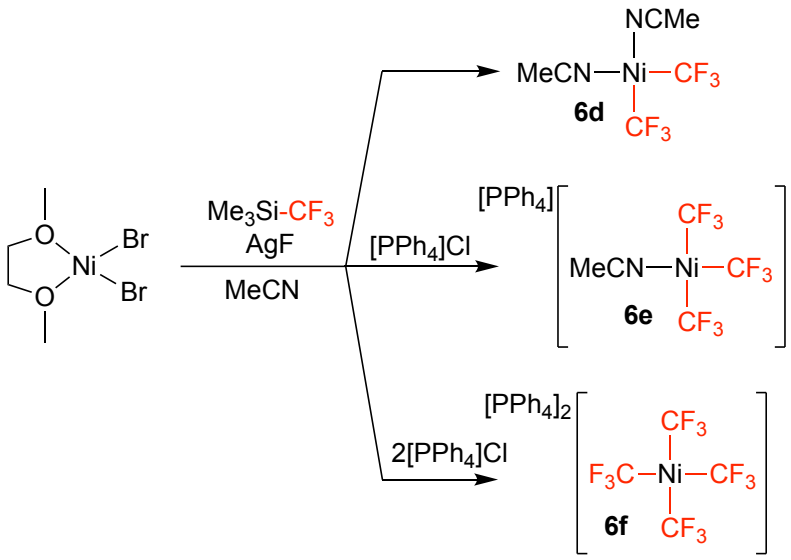

Scheme 6c. Generation of known **6d**[26] and new trifluoromethyl complexes of nickel from a common starting material. For the number of equivalents of all reagents used, see Appendix E.

The structures of the new complexes **6e** and **6f** were confirmed by X-ray crystallography, and ORTEP diagrams of both structures are shown in Figure 6a. Rotational disorder of the trifluoromethyl groups in **6e** prevented rigorous quantitative analysis of the crystallographic bond lengths and angles, but it is clear that the nickel centers of both structures adopt a distorted square planar geometry, with complex **6f** showing a slightly larger distortion which is highlighted in the side-on view of **6f** in Figure 6a. The *trans* trifluoromethyl groups in **6e** are situated at an angle (C-Ni-C) of 177.90(10)° while the *trans* trifluoromethyl groups at **6f** have angles of 168.10(17) and 166.49(17)°. For

reference, the angles for the *trans* trifluoromethyl ligands in $[Cu(CF_3)_4]^-$ were measured at 165.0(7) and 172.2(6)°.[2]

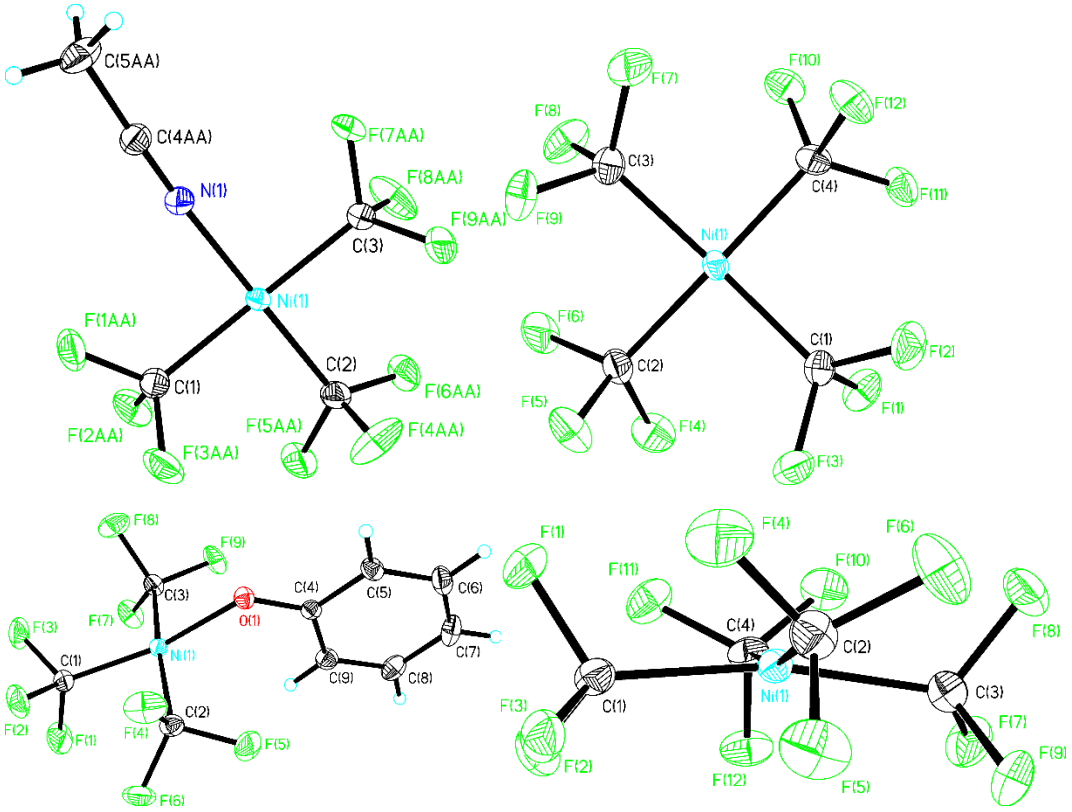

Figure 6a. ORTEP diagrams of the nickel centers of **6e** (top left), **6f** (top right and bottom right), and **6g** (bottom left). Ellipsoids shown at the 40% level. Selected bond lengths (Å) for **6e**: Ni1-N1 1.8816(18); Ni1-C2 1.885(2); Ni1-C3 1.938(2); Ni1-C1 1.953(2). Selected bond angles (°) for **6e**: N1-Ni1-C2 177.62(10); N1-Ni1-C3 89.43(8); C2-Ni1-C3 90.15(9); N1-Ni1-C1 90.28(8); C2-Ni1-C1 90.06(9); C3-Ni1-C1 177.90(10). Selected bond lengths (Å) for **6f**: Ni1-C4 1.924(4); Ni1-C3 1.927(4); Ni1-C1 1.930(4); Ni1-C2 1.939(4). Selected bond angles (°) for **6f**: C4-Ni1-C3 90.40(17); C4-Ni1-C1 91.82(17); C3-Ni1-C1 168.10(17); C4-Ni1-C2 166.49(17); C3-Ni1-C2 89.89(18); C1-Ni1-C2 90.66(17). Selected bond lengths (Å) for **6g**: Ni1 C1 1.8989(13); Ni1-O1 1.9056(9); Ni1-C2 1.9342(13); Ni1-C3 1.9448(13). Selected bond angles (°) for **6g**: C1-Ni1-O1 165.64(5); C1-Ni1-C2 90.16(6); O1-Ni1-C2 89.08(5); C1-Ni1-C3 91.62(6); O1-Ni1-C3 91.06(5); C2-Ni1-C3 172.23(6); C4-O1-Ni1 128.35(8).

6.3.2. Electrochemistry of Nickel Complexes: With complexes **6e** and **6f** in hand, we evaluated their electrochemical properties by cyclic voltammetry (Figure 6b). Oxidation of the monoanionic $[PPh_4][(MeCN)Ni(CF_3)_3]$ is irreversible and occurs at the onset potential of ca. +0.02 V vs the ferrocene/ferrocenium couple. Peak potentials for **6e** appear

at +0.38 V and +0.76 V. The oxidation of complex **6f** was more facile, with an onset potential of ca. -0.10 V and peak potentials at +0.10, +0.50 and +0.79 V. Interestingly, both **6e** and **6f** display peak potentials in the region where oxidation occurs for the bis-trifluoromethyl complex **6d** (Figure 6b), suggestive that upon oxidation **6e** and **6f** undergo chemical transformations leading to **6d**. However, because the waves in the CVs are all irreversible, more evidence will be required corroborate this speculation. The CVs are interesting to compare with that of the copper derivative $[NBu_4][Cu(CF_3)_4]$ ($[NBu_4][\mathbf{6a}]$). Because $[NBu_4][\mathbf{6a}]$ is already a highly oxidized species (irrespective of whether the holes lie predominantly on the metal or ligand), no oxidation peak was observed in the CV in the region spanning from 0 to +1.5 V vs the ferrocene/ferrocenium couple (see Appendix E). Thus, changing the metal identity from copper to nickel in the $[M(CF_3)_4]^{n-}$ (and formally d^8) platform provides exciting opportunities to explore redox triggered-reactions involving these solvated trifluoromethyl nickel sources using readily available and practical oxidants.

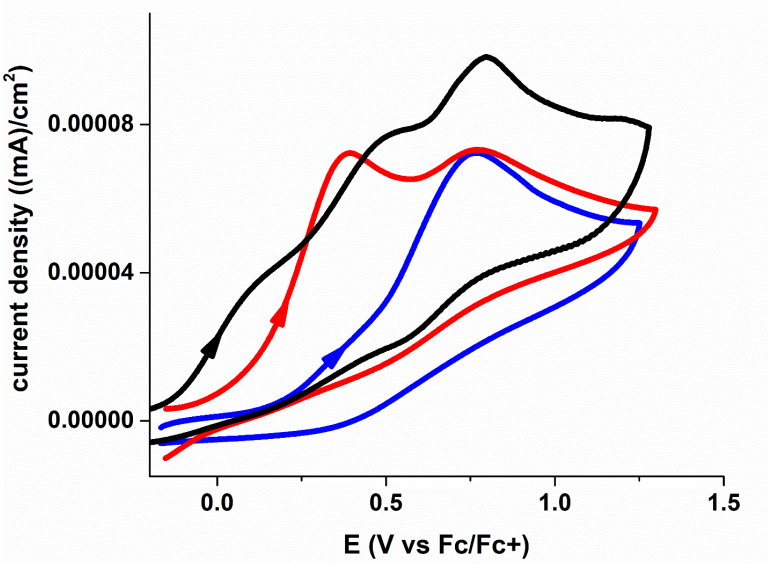

Figure 6b. Cyclic voltammograms of **6d** (blue), **6e** (red), and **6f** (black) in MeCN. Metal complex: 0.5 mM. Electrolyte: $[Bu_4N][PF_6]$: 100 mM; working electrode: glassy carbon; counter electrode: platinum; pseudo reference: silver. Scan rate: 100 mV/s.

6.3.3. Investigation of Physical Oxidation State of Anionic Nickelates: We collaborated with Kyle Lancaster's group at Cornell in order to examine the physical oxidation state of complexes **6e** and **6f** to look for evidence that the metal is in a physically reduced d electron count, similar to copper complex **6a**. This section highlights the key experimental details found by Lancaster's group and their interpretation. Full details of Lancaster's studies, including experimental details, can be found within the published report this chapter has been adapted from.

The Ni $L_{2,3}$-edge (2p $\rightarrow$ valence/continuum) XAS (x-ray absorption spectroscopy) data were obtained for **6e** and **6f** (Figure 6c). The Ni 2p $\rightarrow$ 3d excitations are dipole allowed and thus intense, but lose intensity commensurate with ligand-orbital admixture into 3d-containing frontier MOs. Consequently, total $L_{2,3}$-edge XAS areas afford a convenient means to quantify 3d participation in vacant MOs. The splitting between the L_3 and L_2 peaks arises due to 2p spin-orbit coupling. The L_3 peaks for **6e** and **6f** occur at 854.3 and 854.4 eV, respectively. The L_2 peaks for **6e** and **6f** occur at 871.1 and 871.3 eV, respectively. For comparison, typical low-spin Ni^{II} species show L_3 peaks at 853.3 ± 0.5 and L_2 at 870.4 ± 0.5 eV.[27,28] This shift in $L_{2,3}$-edge is consistent with what was seen when comparing **6a** to other Cu^{II} species in the literature, and not necessarily indicative of metal oxidation. Using $[^nBu_4N]_2$ $[Ni(mnt)_2]$[29] and $[Et_4N]_2[NiCl_4]$[30] as covalency calibrants and assuming that 16-electron **6e** and **6f** have a single Ni 3d-containing LUMO, the total $L_{2,3}$-edge intensities give 48.9 ± 6.9 and 51.1 ± 7.1 % Ni 3d/hole for **6e** and **6f**, respectively (Figure 6c). The data translates to Ni 3d vacancies of 1 electron— surprisingly, these complexes are more appropriately described as physically d^9 rather than d^8. Ni K-edge XAS data, hybrid DFT, and spectroscopy-oriented configuration interaction (SORCI)

calculations,[31] were also performed for compounds **6e** and **6f**, and collectively supported the Ni $L_{2,3}$-edge XAS data of a ground state d-count of 9 for both complexes.

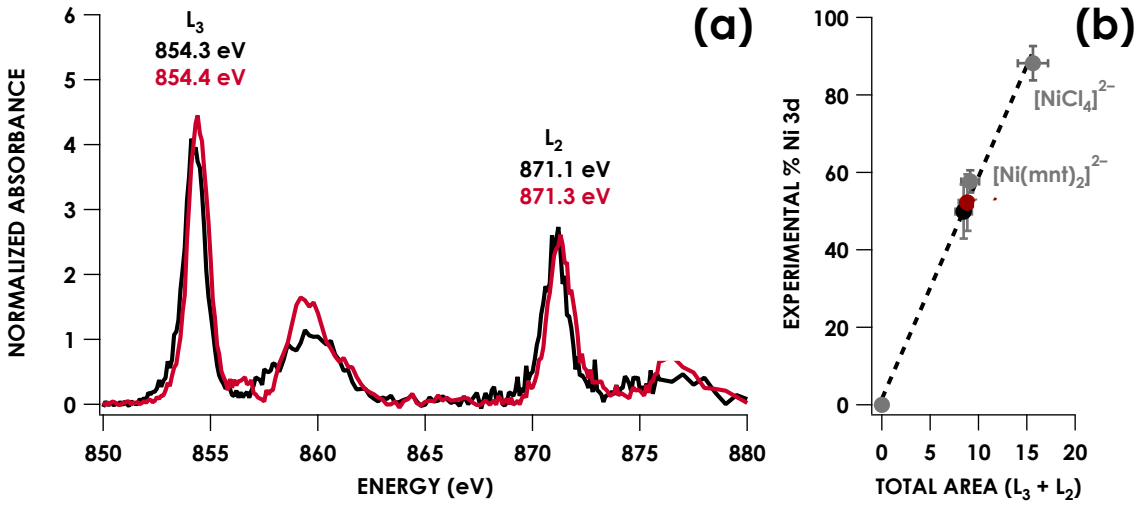

Figure 6c. (a) Ni $L_{2,3}$-edge XAS obtained at 298 K from neat solid samples of **6e** (black) and **6f** (red). Data were obtained via partial fluorescence yield detection windowed on Ni 3d → 2p X-ray emission. (b) Plot of Ni $L_{2,3}$ area vs. Ni 3d character. A line was fitted through zero (0,0 is included in the fit because zero d-character will yield zero intensity) and two calibrants with independently quantified Ni 3d covalencies yielding a line with slope = 5.69 ± 0.45 and y-intercept = 1.69 ± 4.71. The R^2 value is 0.994. The summed $L_{2,3}$ areas obtained for **6e** and **6f** are interpolated yielding 48.9 ± 6.9% and 51.1 ± 7.1% Ni 3d character per hole, respectively.

6.3.4. Reactivity of trifluoromethyl nickelates: The knowledge that monoanionic **6e** can accommodate an additional trifluoromethyl anion to afford **6f** prompted us to explore the reactivity of **6e** with a different nucleophile to determine if a heteroleptic dianionic complex could be prepared. If so, such structures could potentially be developed as intermediates in new nickel-mediated trifluoromethylations, akin to the emerging methodologies involving $[Cu(CF_3)_3(R)]^-$. Reaction of **6e** with $[NMe_4][OPh]$ indeed led to the production of the new dianionic nickel phenoxide complex **6g**. The solubility properties of **6g** bearing pure phosphonium counter-ions enable its selective precipitation (80% based on available $[PPh_4]^+$ counter-ion) as an analytically pure and crystalline solid, and the ORTEP diagram of **6g** is shown in Figure 6a. Interestingly, NMR data suggest that

when isolated crystals of **6g** are dissolved in MeCN, the phenolate moiety dissociates from nickel and reaffords monoanionic complex **6e** in solution (Scheme 6d). Benzene is generated in the process along with triphenylphosphine oxide, indicating a non-innocent interaction between phenoxide and the phosphonium counter-ion. Equilibrium processes between phosphonium salts and phenoxide-derived phosphoranes are known,[32] but to our knowledge these interactions leading to the irreversible generation of phosphine oxide is unknown. Control experiments show that simple reaction of $[NMe_4][OPh]$ with $[PPh_4]Cl$ in acetonitrile solvent in the absence of nickel indeed leasds to triphenylphosine oxide, plus benzene (see Appendix E). The source of the oxygen atom does not appear to be derived from the phenoxide moiety, as reaction of $[NMe_4]$[*p*-fluorophenoxide] with $[PPh_4]Cl$ in acetonitrile still yields triphenylphosphine oxide but does not produce any detectable fluorobenzene. Thus, we suspect that adventitious water may be the source of the oxygen atom in $[O{=}PPh_3]$. Changing the counter-ion and reacting $[NBu_4][(MeCN)Ni(CF_3)_3]$ with $[NMe_4][OPh]$ gratifyingly leads to a solution stable complex whose ^{19}F NMR signals (CD_3CN, δ –21.2 (septet, J = 4.1 Hz) and –31.3 (quartet, J = 4.1 Hz)) are consistent with the desired $[NR_4][(PhO)Ni(CF_3)_3]$ product. With knowledge of this noninnocent interaction of $[PPh_4]^+$ with phenoxide, it is clear that judicious choice of counter-ions will be a critical component to methods development with these heterolyptic complexes of nickel. Utilizing an ammonium counter ion (see Chapter 7 for synthetic details), we have found another heterolyptic nickel salt, **6h**, bearing deprotonated 7-azaindole could be prepared (Scheme 6e). Complex **6h** is solution stable and does not show equilibrium properties at room temperature with, ^{19}F NMR signals at (CD_3CN, δ –22.7 (septet, J = 4.1 Hz) and –29.5 (quartet, J = 4.1 Hz)). We are currently working to identify other

conditions and reagents that favor coordination of other organic nucleophiles to **6e** and identify redox agents that could ultimately trigger new trifluoromethyl cross-couplings at nickel.

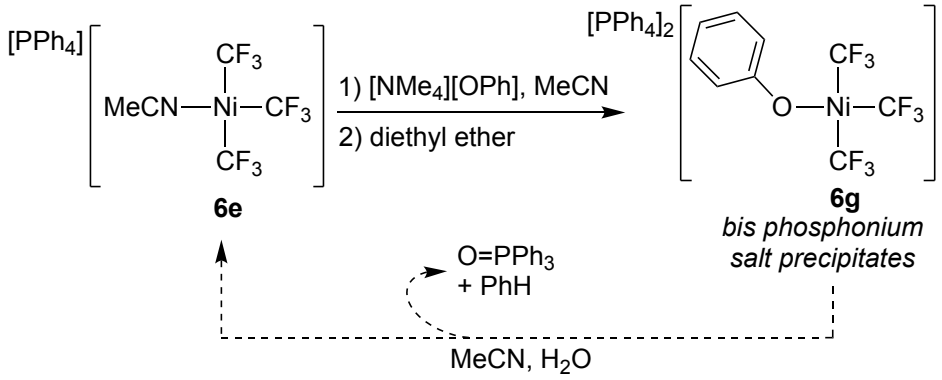

Scheme 6d. Synthesis of heterolyptic **6g** and resulting solution properties.

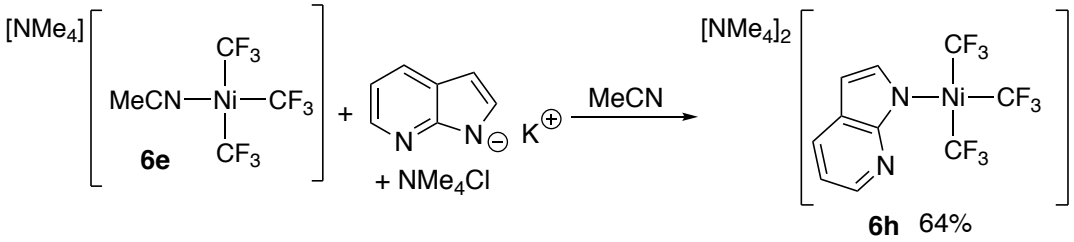

Scheme 6e. Synthesis of heterolyptic nickel salt **6h**.

Preliminary explorations of the reactivates of **6e** and **6f** are described in Scheme 6f and 6g. Complex **6e** reacts with the two electron oxidant bis(4-tert-butylphenyl)iodonium hexafluorophosphate to afford trifluoromethylated arene in 54% yield, producing $[(MeCN)_2Ni(CF_3)_2]$ (**6d**) in 75% yield as the only detectable nickel containing product (Scheme 6f). Hypervalent iodine reagents are known to oxidize both Pd(II) and Ni(II) to Pd(IV) and Ni(IV),[33] so we speculate that the intermediate in this trifluoromethylation reaction is the high valent $[Ar–Ni^{IV}(CF_3)_3(MeCN)_2]$. Such a species, upon reductive elimination or aryl–CF_3 product would afford **6d** as the nickel-containing byproduct.

Further experiments with **6f** shows that oxidation to formally nickel(IV) trifluoromethyl derivatives is indeed possible (Scheme 6g). We observed that a two electron oxidation of **6f** with potassium persulfate produced a new species detected by ^{19}F NMR spectroscopy (CD_3CN, δ -19.2 (sept, J = 7.3 Hz) and -30.6 (sept, J = 7.3 Hz) in 11% NMR yield along with other fluorine-containing nickel species consistent with $[(SO_4)Ni(CF_3)_2(MeCN)_2]$, $[(MeCN)_2Ni(CF_3)_4]$, and $[(MeCN)Ni(CF_3)_5]^-$ (see Appendix E), however, further insights into the identity of these higher valent nickel complexes was later provided (see Chapter 7). Fortuitous crystallization of one of the new species from MeCN/ether enabled its solid-state structure determination (Figure 6d) and confirms the identity of the crystallized compound as $[PPh_4]_2[Ni(CF_3)_4(SO_4)]$ (**6i**, Scheme 6g). To our knowledge, this is the first example of an unsupported[25] trifluoromethyl nickel(IV) complex, and the identification of such a structure lends credence to the proposal that a high-valent nickel(IV) species is a viable intermediate in the trifluoromethylation reaction described in Scheme 6e. Further efforts to develop trifluoromethylation chemistry with **6e** and **6f** are planned in our laboratories (see Chapter 7 and 9).

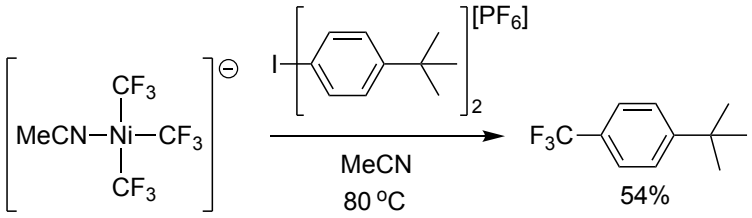

6e

Scheme 6f. Trifluoromethylation of aryl iodonium with **6e**.

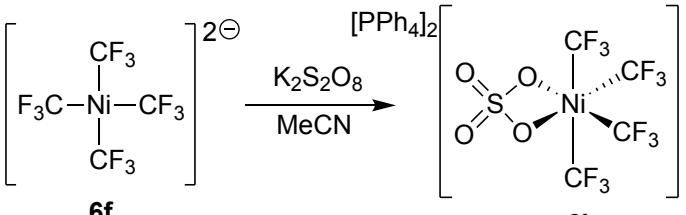

6f 6i

Scheme 6g. Oxidation of **6f** generating high-valent formally Ni(IV) **6i**.

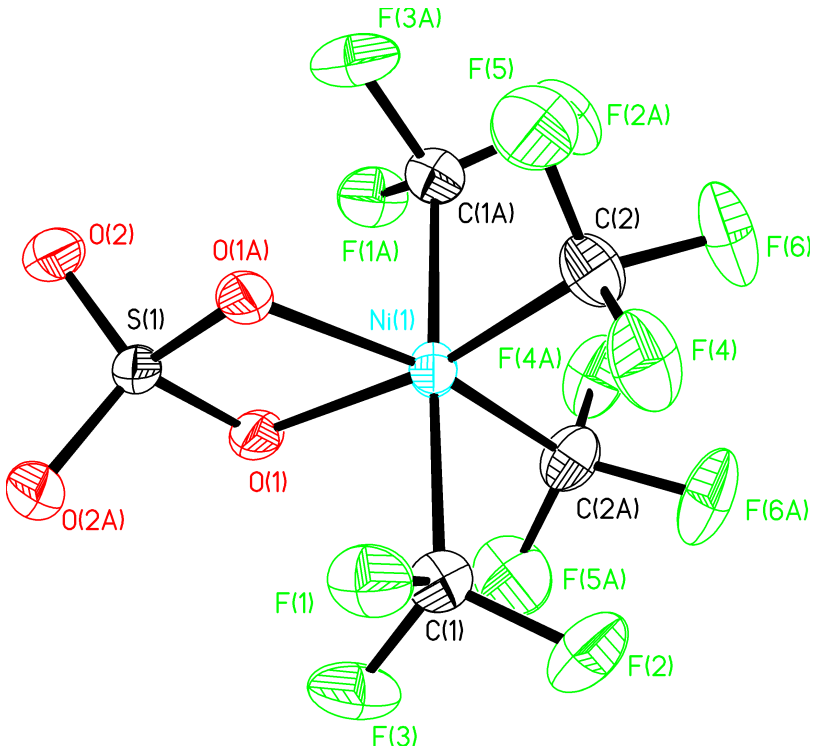

Figure 6d. ORTEP diagram of **6i**. Selected bond lengths (Å): Ni1-C1 2.021(6); Ni1-C2 1.942(6); Ni1-O1 1.964(4); Selected bond angles (°): C2-Ni1-C2A 97.7(4); C2-Ni1-O1 94.7(2); O1-Ni1-O1A 73.0(3); C2-Ni1-C1 92.0(3); C1-Ni1-C1A 177.9(3); O1-S1-O1A 99.5(3).

6.4 Conclusions: Herein we describe easy access to $[(MeCN)Ni(CF_3)_3]^-$ and $[Ni(CF_3)_4]^{2-}$ and provide full experimental and computational analyses of their electronic structures. The trifluoromethyl ligands, by virtue of their highly covalent interactions with nickel, render both **6e** and **6f** to physically more reduced states than their formal oxidation state implies. Spectroscopic data and electronic structure calculations support ground state d^9 electron counts for both $[(MeCN)Ni(CF_3)_3]^-$ and $[Ni(CF_3)_4]^{2-}$, and surprisingly show that holes can be distributed on trifluoromethyl ligands even in nickel complexes bearing formally common oxidation states. The cyclic voltammetry studies show that oxidations of $[(MeCN)Ni(CF_3)_3]^-$ and $[Ni(CF_3)_4]^{2-}$ are facile, which bodes well for the development of redox-triggered methodologies at nickel. As copper exhibits relatively weak backbonding towards pi-acceptors,[34,35] the nickel complexes **6e** and **6f** may show broader

applicability than **6a-6c** in emergent synthetic methods involving pi-systems of organic substrates. Finally, two important precedents regarding the reactivity of complexes **6e** and **6f** have been set in this report. We have shown that **6e** reacts with a bis(aryl)iodonium salt to afford a trifluoromethylated arene, indicating the viability of solvated trifluoromethyl nickel complexes in important C-C bond forming reactions. Moreover, the clean formation of **6d** as the byproduct of the trifluoromethylation reaction bodes well for future development of catalytic processes. We have also established that the homoleptic precursor **6f** can be used to directly prepare a formally Ni(IV) complex, showing for the first time that supporting ligands are not a requirement for accessing the higher valent states of trifluoromethyl nickel.

6.5. Experimental

6.5.1. General Information: All manipulations were performed using standard Schlenk and high vacuum techniques or in a nitrogen-filled glovebox, unless otherwise stated. Solvents were purified by passing through activated alumina and/or copper in a solvent purification system supplied by Pure Process Technology. Solution ^{1}H NMR spectra were recorded at ambient temperature on a Bruker 400 MHz spectrometer and referenced to residual proton solvent signals. ^{19}F NMR spectra were recorded on a Bruker NMR spectrometer operating at 376 MHz and referenced to α,α,α-trifluorotoluene as an internal standard ($\delta = -63.7$). $^{31}P\{^{1}H\}$ NMR spectra were recorded on a Bruker NMR spectrometer operating at 162 MHz and referenced to phosphoric acid as an external standard ($\delta = 0.00$). A Bruker D8 Quest diffractometer was used for X-ray crystal structure determinations. UV-Vis spectrum was recorded on a Varian Cary Spectrophotometer, with path length 1 cm. Cyclic Voltammetry data was collected in a nitrogen filled glovebox at room

temperature on a PARSTAT 4000A potentiostat. The CCDC 1981245-1981247 and 1988483 contains the supplementary crystallographic data for this paper. These data can be obtained free of charge via www.ccdc.cam.ac.uk/data_request/cif, or by e-mailing data_request@ccdc.cam.ac.uk, or by contacting The Cambridge Crystallographic Data Centre, 12 Union Road, Cambridge CB2 1EZ, UK; fax: +44 1223 336033.

6.5.2. Preparation of $[PPh_4][(MeCN)Ni(CF_3)_3]$ (6e): In a nitrogen-filled glovebox, AgF (195 mg, 1.54 mmol) and TMS-CF_3 (0.26 mL, 1.8 mmol) were stirred in 10 mL of MeCN for 1.5 hours. Then, 1 mL of MeCN, (dme)$NiBr_2$ (155 mg, 0.500 mmol) and PPh_4Cl (188 mg, 0.500 mmol) were added. The reaction mixture was stirred for 2 days and then filtered over Celite. The filtrate was pumped dry to yield 300 mg of yellow solid (93% Yield). X-Ray quality crystals were grown from a saturated solution of THF. ^{1}H NMR (CD_3CN, 400 MHz): δ 7.96 – 7.88 (m, 4H) , 7.80 – 7.62 (m, 16H). ^{19}F NMR (CD_3CN, 376 MHz): δ -25.23 (sept, J = 4.5 Hz, 3F), -31.06 (q, J = 4.5 Hz, 6F). ^{31}P{^{1}H} NMR (CD_3CN, 162 MHz): δ 23.88 (s). Anal. Calcd (found) for $C_{29}H_{23}F_9NiP$: C, 53.91 (54.21); H, 3.59 (3.99).

6.5.3. Preparation of $[PPh_4]_2[Ni(CF_3)_4]$ (6f): In a nitrogen-filled glovebox, AgF (293 mg, 2.25 mmol), and TMS-CF_3 (0.40 mL, 2.5 mmol) were stirred in 10 mL of MeCN for 2 hours. Then, 2 mL of MeCN, (dme)$NiBr_2$ (155 mg, 0.500 mmol), and PPh_4Cl (375 mg, 1.00 mmol) were added. The reaction mixture was stirred for 2 days and then filtered over Celite. The filtrate was pumped dry to yield a crude yellow solid mixture of **(6e)** and **(6f)**. Recrystallization in MeCN/ether yields 98 mg of light yellow solid (19% Yield). X-Ray quality crystals are also grown in MeCN/ether. ^{1}H NMR (CD_3CN, 400 MHz): δ 7.99 – 7.87 (m, 4H) , 7.82 – 7.62 (m, 16H). ^{19}F NMR (CD_3CN, 376 MHz): δ -26.2 (s). ^{31}P{^{1}H} NMR

(CD_3CN, 162 MHz): δ 23.85 (s). Anal. Calcd (found) for $C_{52}H_{40}F_{12}NiP_2$: C, 61.62 (61.70); H, 3.98 (4.01).

6.5.4. Preparation of $[PPh_4]_2[(PhO)Ni(CF_3)_3]$ (6g): In a nitrogen-filled glovebox, a solution of tetramethylammonium phenoxide (prepared from NMe_4OH and PhOH) (13mg, 0.077 mmol) in 0.5 mL of MeCN was added to a stirring solution of **5** (50 mg, 0.077 mmol) in 0.5 mL of MeCN. The solution was stirred for 30 minutes and ethyl ether (0.6 mL) was slowly added. The solution was placed in glovebox freezer (-30°C) were yellow crystals were obtained and washed with additional ether (33 mg, 80% yield based on $[PPh_4]$. Anal. Calcd (found) for $C_{57}H_{45}F_9NiOP_2$: C, 65.98 (65.73); H, 4.37 (4.48). Solution NMR data of **(6g)** were complicated as the decomposition of phosphonium counter-ion by phenoxide occurs in MeCN (see Appendix E). ^{19}F NMR of $[NBu_4]_2[(PhO)Ni(CF_3)_3]$ (CD_3CN, 25 °C) δ –21.2 (septet, J = 4.1 Hz) and –31.3 (quartet, J = 4.1 Hz). ^{19}F NMR of $[PPh_4]_2[(PhO)Ni(CF_3)_3]$ (CD_3CN, –30 °C) δ –21.8 (septet, J = 3.5 Hz) and –32.0 (quartet, J = 3.4 Hz).

6.5.5. Preparation of $[NMe_4]_2[(C_7H_5N_2)Ni(CF_3)_3]$ (6h): In a glovebox, to a stirring solution of $[NMe_4][(MeCN)Ni(CF_3)_3]$ (38 mg, 0.10 mmol) and NMe_4Cl (12 mg, 0.10 mmol) in 0.5 mL of MeCN, a solution of $KC_7H_5N_2$ (16 mg, 0.10 mmol) in 1.5 mL of MeCN was added and stirred for 15 minutes. The insoluble were removed, and ether was added to predicate the product. After placing in the glovebox freezer (-30 °C), the product was collected and washed with ether to yield 34 mg (64%) of a light yellow solid. ^1H NMR (CD_3CN, 376 MHz): δ 8.04 (dd, J = 4.6 Hz, 1.8 Hz, 1H), 7.53 (dd, J = 7.5 Hz, 1.8 Hz, 1H), 7.42 (d, J = 2.7 Hz, 1H), 6.58 (dd, J = 7.5 Hz, 4.6 Hz, 1H), 6.08 (d, J = 2.7 Hz, 1H), 3.12

(s, 12H). ^{19}F NMR (CD_3CN, 376 MHz): δ -22.7 (sept, J = 4.1 Hz, 3F), -29.5 (q, J = 4.1 Hz, 6F) . Anal. Calcd (found) for $C_{18}H_{29}NiF_9N_4$: C, 40.70 (41.42); H, 5.50 (5.90).

6.5.6. Generation of $[PPh_4]_2[(\kappa^2\text{-}SO_4)Ni^{IV}(CF_3)_4]$ (6i): In a nitrogen-filled glovebox, **6f** (20 mg, 0.02 mmol) and $K_2S_2O_8$ (8 mg, 0.03 mmol) were stirred in one mL of MeCN for one day. The insolubles were filtered and discarded, and then the volatiles were removed under vacuum. Fluorobenzene was then added as internal standard, and the ^{19}F NMR yield of **6i** was found to be 11 %. Fortuitous crystallization in MeCN/Ether provided X-Ray quality crystals. ^{19}F NMR (CD_3CN, 376 MHz): δ -19.15 (sept, J = 7.3 Hz, 6F), -30.60 (sept, J = 7.3 Hz, 6F).

6.5.7. Reaction of $[PPh_4][(MeCN)Ni(CF_3)_3]$ with bis(aryl)iodonium Reagent: In a nitrogen-filled glovebox, **6e** (15 mg, 0.023 mmol) and bis(4-tert-butylphenyl)iodonium hexafluorophosphate (24 mg, 0.046 mmol) were dissolved in CD_3CN/CH_3CN. Fluorobenzene was added as internal standard and the reaction was heated to 80˚ C. The reaction was monitored by ^{19}F NMR until **6e** was consumed. In this manner, 4-*t*-butylbenzotrifluoride was synthesized in 54 % yield. $[(MeCN)_2Ni(CF_3)_2]$ was also formed as the nickel-containing product in 75% yield. Analytical data of trifluomethylated product matched that previously reported in the literature.[36]

6.6 References

1. Willert-Porada, M. A.; Burton, D. J.; Baenziger, N. C. Synthesis and X-Ray Structure of Bis(trifluoromethyl)(N,N-diethyldithiocarbamato)copper; a Remarkably Stable Perfluoroalkylcopper(III) Complex. *J. Chem. Soc., Chem. Commun.* **1989,** (21), 1633-4.
2. Naumann, D.; Roy, T.; Tebbe, K. F.; Crump, W. Synthesis and Structure of a Surprisingly Stable Tetrakis(trifluoromethyl)cuprate(III) Salt. *Angew. Chem.* **1993,** *105*, 1555-6.
3. Hoffmann, R.; Alvarez, S.; Mealli, C.; Falceto, A.; Cahill, T. J.; Zeng, T.; Manca, G. From Widely Accepted Concepts in Coordination Chemistry to Inverted Ligand Fields. *Chem. Rev.* **2016,** *116*, 8173-8192.

4. Steen, J. S.; Knizia, G.; Klein, J. E. M. N. σ-Noninnocence: Masked Phenyl-Cation Transfer at Formal NiIV. *Angew. Chem., Int. Ed.* **2019,** *58*, 13133-13139.
5. Snyder, J. P. Elusiveness of CuIII Complexation; Preference for Trifluoromethyl Oxidation in the Formation of $[CuI(CF_3)_4]^-$ Salts. *Angew. Chem., Int. Ed. Engl.* **1995,** *34* (1), 80-1.
6. Kaupp, M.; von Schnering, H. G. Formal Oxidation State versus Partial Charge—A Comment. *Angew. Chem. Int. Ed.* **1995,** *34*, 986-986.
7. Alvarez, S.; Hoffmann, R.; Mealli, C. A Bonding Quandary—or—A Demonstration of the Fact That Scientists Are Not Born With Logic. *Chem. – Eur. J.* **2009,** *15*, 8358-8373.
8. Walroth, R. C.; Lukens, J. T.; MacMillan, S. N.; Finkelstein, K. D.; Lancaster, K. M. Spectroscopic Evidence for a $3d^{10}$ Ground State Electronic Configuration and Ligand Field Inversion in $[Cu(CF_3)_4]^{1-}$ *J. Am. Chem. Soc.* **2016,** *138*, 1922-1931.
9. Gao, C.; Macetti, G.; Overgaard, J. Experimental X-ray Electron Density Study of Atomic Charges, Oxidation States, and Inverted Ligand Field in $Cu(CF_3)_4^-$ *Inorg. Chem.* **2019,** *58*, 2133-2139.
10. DiMucci, I. M.; Lukens, J. T.; Chatterjee, S.; Carsch, K. M.; Titus, C. J.; Lee, S. J.; Nordlund, D.; Betley, T. A.; MacMillan, S. N.; Lancaster, K. M. The Myth of d^8 Copper(III). *J. Amer. Chem. Soc.* **2019,** *141*, 18508-18520.
11. Zhang, S.-L.; Bie, W.-F. Ligand-Dependent Formation of Ion-Pair CuI/CuIII Trifluoromethyl Complexes Containing Bisphosphines. *Dalton Trans.* **2016,** *45*, 17588-17592.
12. Baya, M.; Joven-Sancho, D.; Alonso, P. J.; Orduna, J.; Menjón, B. M−C Bond Homolysis in Coinage-Metal $[M(CF_3)_4]^-$ Derivatives. *Angew. Chem.* **2019,** *131*, 10059-10063.
13. Tan, X.; Liu, Z.; Shen, H.; Zhang, P.; Zhang, Z.; Li, C. Silver-Catalyzed Decarboxylative Trifluoromethylation of Aliphatic Carboxylic Acids. *J. Am. Chem. Soc.* **2017,** *139*, 12430-12433.
14. Lu, Z.; Liu, H.; Liu, S.; Leng, X.; Lan, Y.; Shen, Q. A Key Intermediate in Copper-Mediated Arene Trifluoromethylation, $[nBu_4N][Cu(Ar)(CF_3)_3]$: Synthesis, Characterization, and $C(sp^2)-CF_3$ Reductive Elimination. *Angew. Chem. Int. Ed.* **2019,** *58*, 8510-8514.
15. Paeth, M.; Carson, W.; Luo, J.-H.; Tierney, D.; Cao, Z.; Cheng, M.-J.; Liu, W. Copper-Mediated Trifluoromethylation of Benzylic Csp^3-H Bonds. *Chem. – Eur. J.* **2018,** *24*, 11559-11563.
16. Guo, S.; AbuSalim, D. I.; Cook, S. P. 1,2-(Bis)trifluoromethylation of Alkynes: A One-Step Reaction to Install an Underutilized Functional Group. *Angew.Chem. Int. Ed.* **2019,** *58*, 11704-11708.
17. Guo, S.; AbuSalim, D. I.; Cook, S. P. Aqueous Benzylic C-H Trifluoromethylation for Late-Stage Functionalization. *J. Am. Chem. Soc.* **2018,** *140*, 12378-12382.
18. Zhang, S.-L.; Bie, W.-F. Isolation and Characterization of Copper(III) Trifluoromethyl Complexes and Reactivity Studies of Aerobic Trifluoromethylation of Arylboronic Acids. *RSC Adv.* **2016,** *6*, 70902-70906.

19. Yu, S.; Dudkina, Y.; Wang, H.; Kholin, K. V.; Kadirov, M. K.; Budnikova, Y. H.; Vicic, D. A. Accessing Perfluoroalkyl Nickel(ii), (iii), and (iv) Complexes Bearing a Readily Attached [C_4F_8] Ligand. *Dalton Trans.* **2015,** *44*, 19443-19446.
20. Camasso, N. M.; Sanford, M. S. Design, synthesis, and carbon-heteroatom coupling reactions of organometallic nickel(IV) complexes. *Science* **2015,** *347*, 1218-1220.
21. Chong, E.; Kampf, J. W.; Ariafard, A.; Canty, A. J.; Sanford, M. S. Oxidatively Induced C–H Activation at High Valent Nickel. *J. Am. Chem. Soc.* **2017,** *139*, 6058-6061.
22. Bour, J. R.; Ferguson, D. M.; McClain, E. J.; Kampf, J. W.; Sanford, M. S. Connecting Organometallic Ni(III) and Ni(IV): Reactions of Carbon-Centered Radicals with High-Valent Organonickel Complexes. *J. Am. Chem. Soc.* **2019,** *141*, 8914-8920.
23. Mirica, L. M.; Smith, S. M.; Griego, L. Organometallic Chemistry of High-Valent Ni(III) and Ni(IV) Complexes. From: *Nickel Catalysis in Organic Synthesis* **2020**, 223-248.
24. D'Accriscio, F.; Borja, P.; Saffon-Merceron, N.; Fustier-Boutignon, M.; Mézailles, N.; Nebra, N. C−H Bond Trifluoromethylation of Arenes Enabled by a Robust, High-Valent Nickel(IV) Complex. *Angew. Chem. Int. Ed.* **2017,** *56*, 12898-12902.
25. Here the term “unsupported” is meant to indicate the absence of charge-neutral ligands datively bonding to a metal.
26. Zhang, C.-P.; Wang, H.; Klein, A.; Biewer, C.; Stirnat, K.; Yamaguchi, Y.; Xu, L.; Gomez-Benitez, V.; Vicic, D. A. A Five-Coordinate Nickel(II) Fluoroalkyl Complex as a Precursor to a Spectroscopically Detectable Ni(III) Species. *J. Am. Chem. Soc.* **2013,** *135*, 8141-8144.
27. Shearer, J.; Dehestani, A.; Abanda, F. Probing Variable Amine/Amide Ligation in $Ni^{II}N_2S_2$ Complexes Using Sulfur K-Edge and Nickel L-Edge X-ray Absorption Spectroscopies: Implications for the Active Site of Nickel Superoxide Dismutase. *Inorg. Chem.* **2008,** *47*, 2649-2660.
28. Koroidov, S.; Hong, K.; Kjaer, K. S.; Li, L.; Kunnus, K.; Reinhard, M.; Hartsock, R. W.; Amit, D.; Eisenberg, R.; Pemmaraju, C. D.; Gaffney, K. J.; Cordones, A. A. Probing the Electron Accepting Orbitals of Ni-Centered Hydrogen Evolution Catalysts with Noninnocent Ligands by Ni L-Edge and S K-Edge X-ray Absorption. *Inorg. Chem.* **2018,** *57*, 13167-13175.
29. Sarangi, R.; DeBeer George, S.; Rudd, D. J.; Szilagyi, R. K.; Ribas, X.; Rovira, C.; Almeida, M.; Hodgson, K. O.; Hedman, B.; Solomon, E. I. Sulfur K-Edge X-ray Absorption Spectroscopy as a Probe of Ligand−Metal Bond Covalency: Metal vs Ligand Oxidation in Copper and Nickel Dithiolene Complexes. *J. Am. Chem. Soc.* **2007,** *129*, 2316-2326.
30. Solomon, E. I.; Hedman, B.; Hodgson, K. O.; Dey, A.; Szilagyi, R. K. Ligand K-Edge X-Ray Absorption Spectroscopy: Covalency of Ligand–Metal Bonds. *Coord. Chem. Rev.* **2005,** *249*, 97-129.
31. Neese, F. A Spectroscopy Oriented Configuration Interaction Procedure. *J. Chem. Phys.* **2003,** *119*, 9428-9443.

32. Sigal, I. S.; Westheimer, F. H. Disproportionation Among Aryloxyphosphoranes. *J. Am. Chem. Soc.* **1979,** *101*, 5329-34.
33. Sousa e Silva, C. F.; Tierno, F. A.; Wengryniuk, E. S. Hypervalent Iodine Reagents in High Valent Transition Metal Chemistry. *Molecules* **2017,** *22*, 780.
34. Munakata, M.; Kitagawa, S.; Kosome, S.; Asahara, A. Studies of Copper(I) Olefin Complexes. Formation Constants of Copper Olefin Complexes with 2,2'-Bipyridine, 1,10-phenanthroline, and Their Derivatives. *Inorg. Chem.* **1986,** *25*, 2622-7.
35. Strauss, S. H. Copper(I) and Silver(I) Carbonyls. To Be or Not to Be Nonclassical. *Dalton* **2000,** 1-6.
36. Chang, B.; Shao, H.; Yan, P.; Qiu, W.; Weng, Z.; Yuan, R. Quinone-Mediated Trifluoromethylation of Arenes and Heteroarenes with Visible Light. *ACS Sustainable Chem. Eng.* **2017**, *5*, 334-341.

Chapter 7: Solvated Nickel Complexes as Stoichiometric and Catalytic Perfluoroalkylation Agents

The following chapter has been adapted with permission from: Shreiber, S. T.; Vicic, D. A. *Angew. Chem. Int. Ed.* **2021**, *60*, 18162-18167.

7.1 Abstract: The acetonitrile-solvated $[(MeCN)Ni(C_2F_5)_3]^-$ was prepared in order to compare and contrast its reactivity with the known $[(MeCN)Ni(CF_3)_3]^-$ towards organic electrophiles. Both $[(MeCN)Ni(CF_3)_3]^-$ and $[(MeCN)Ni(C_2F_5)_3]^-$ successfully react with aryl iodonium and diazonium salts as well as alkynyl iodonium salts to give fluoroalkylated organic products. Electrochemical analysis of $[(MeCN)Ni^{II}(C_2F_5)_3]^-$ suggests that, upon electro-oxidation to $[(MeCN)_nNi^{III}(C_2F_5)_3]$, reductive homolysis of a perfluoroethyl radical occurs, with the concomitant formation of $[(MeCN)Ni^{II}(C_2F_5)_2]$. Catalytic C-H trifluoromethylations of electron rich arenes were successfully achieved using either $[(MeCN)Ni(CF_3)_3]^-$ or the related $[Ni(CF_3)_4]^{2-}$. Stoichiometric reactions reveal that solvated nickel is exceptionally capable of serving as reservoir of CF_3 anions or radicals under catalytically relevant conditions.

7.2 Introduction: Nickel is a promising platform for developing practical fluoroalkylation methodologies as fundamental steps relevant to chemical bond forming reactions have been established. Reductive eliminations involving fluoroalkyl groups have been demonstrated at higher valent states of nickel,[1-4] the generation of fluoroalkyl radicals via electron transfer or atom abstraction reactions of fluoroalkyl electrophiles with nickel is known,[5-12] fluoroalkyl-based transmetalating reagents readily react with nickel,[13-15] and catalytic transformations involving select fluoroalkyl groups have been reported.[6, 10-13, 16-21] Nickel is also an earth-abundant metal with a reasonably low cost. However, most of the

aforementioned chemical transformations involving fluoroalkyl groups required nickel to bear stabilizing ligands other than solvent. While in many cases ligands can serve to tune and enable the reactivity of a nickel center, in other cases they can prevent catalysis through redistributions that affect the speciation of an active form of the nickel catalyst. Moreover, extraneous non-solvento ligands raise the cost of a chemical process and can even contribute to the air-sensitivity of the system. Given these considerations, we became interested in developing new fluoroalkylation methods with nickel that employed solvent as the only coordinating ligand other than the fluoroalkyl groups. Such reaction conditions have commonly been referred to as "ligandless" conditions in other systems.[22-28]

Previously, we found that $[PPh_4][$**7b**$]$ and $[PPh_4]_2[$**7c**$]$ (Scheme 7a) could be synthesized by the addition of one and two equivalents of "$AgCF_3$" to **7a** in the presence of $[PPh_4]Cl$.[29] The electronic properties of **7b** and **7c** were extensively studied through the use of density functional theory (DFT) calculations, spectroscopy-oriented configuration interaction (SORCI) calculations, X-ray absorption spectroscopy, and cyclic voltammetry.[29] Interestingly, the data collectively show that **7b** and **7c** are better described as physically d^9 metal complexes with the additional hole delocalized over the multiple trifluoromethyl ligands. Complexes **7b** and **7c** also displayed preliminary reactivities that warranted follow-up investigations. For example, **7b** was found to react with an aryl iodonium salt to yield trifluoromethylated arene, presumably through a high-valent, formally nickel(IV) intermediate.[29] Evidence that such architectures are accessible was provided by the synthesis and structural characterization of $[PPh_4]_2[Ni(CF_3)_4(SO_4)]$ (**7d**, Scheme 7a), the first example of a trifluoromethyl nickel(IV) complex that did not bear any charge-neutral datively bonded ligands.[29] The high-valent complex **7d**, while it could be crystallized,

proved to be unstable in solution. The instability of high-valent solvento complexes was also evident in electrochemical experiments, where **7b** and **7c** displayed irreversible oxidations on the timescale of the cyclic voltammogram.[29] We believed this redox instability could be beneficial in terms of catalysis, where high-valent intermediates would need to irreversibly form chemical bonds or release perfluoroalkyl radicals for chemistries that turn over. Therefore, we sought to investigate further the oxidative chemistries of **7b** and **7c** and compare the reactivities to those of a perfluoroethyl analogue.

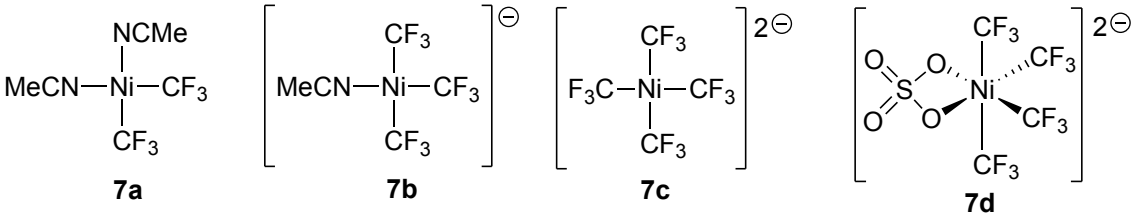

Scheme 7a. Trifluoromethyl nickel reagents previously characterized.

7.3 Results and Discussion

7.3.1. Synthesis of Ammonium Salts of Fluoroalkyl Nickelates: We have shown previously that [PPh_4] salts of **7b** and **7c** (Scheme 7a) were susceptible to side reactions involving organic nucleophiles and the phosphorus moiety,[29] so herein we describe the preparation of tetramethylammonium salts of **7b**, **7c**, and the new perfluoroethyl derivative **7e** (Scheme 7b). Such compounds were easily prepared by the addition of "Ag-R_f" to [(dme)$NiBr_2$] in acetonitrile solvent in the presence of [NMe_4]Cl. The ^{19}F NMR spectrum of **7e** displays four signals with integrations consistent with two perfluoroethyl groups cis to the acetonitrile group and one perfluoroethyl group that is trans to the acetonitrile. The CF_3 resonance that is *trans* to the coordinated acetonitrile appears as a quintet from the $^5J_{FF}$ coupling of the other two CF_2 groups, while the resonance for the CF_3 groups that are *cis* to the acetonitrile appear as a triplet. The absence of $^3J_{FF}$ coupling is common for

perfluoroalkyl groups and is suggested to arise from the rotational averaging of coupling constants of opposite sign between the vicinal CF_2 and CF_3 groups.[30-33]

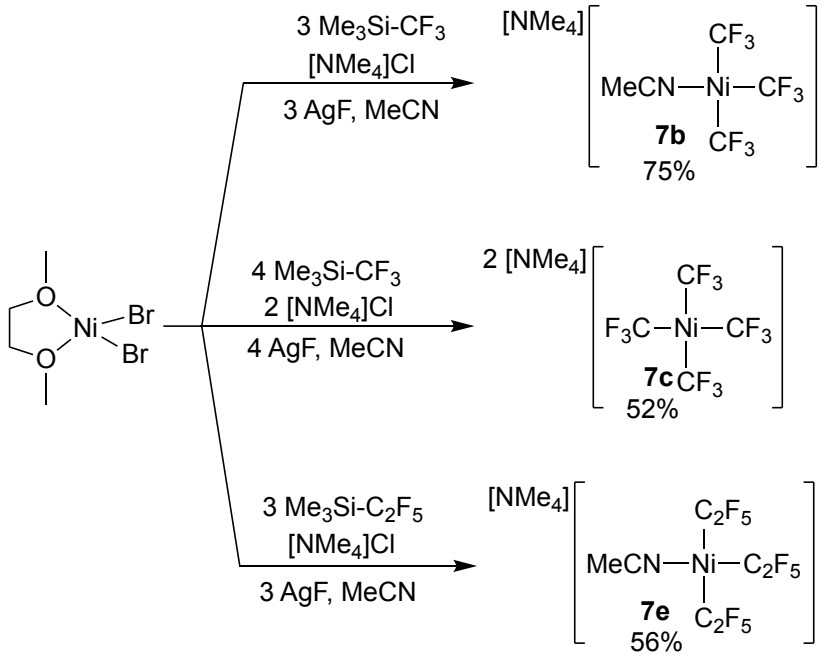

Scheme 7b. Synthesis of tetramethylammonium salts of **7b**, **7c**, and **7e**.

7.3.2. Electrochemistry of Solvated Perfluoroethyl Nickel: The electrochemical properties of the newly prepared anionic complex **7e** were evaluated by cyclic voltammetry (Figure 7a). The oxidation of **7e** is irreversible and occurs at an onset potential of +0.21 V vs the ferrocene/ferrocenium couple. Peak potentials for **7e** appear at +0.60 V and +1.26 V, which are slightly more positive than peaks observed for the trifluoromethyl derivative **7b**.[29] Interestingly, the peak potential for the second redox event occurs at the same potential as the oxidation for the charge neutral bisperfluoroethyl complex **7g** (Figure 7a), consistent with the notion that upon oxidation to the nickel(III) species **7f**, a perfluoroethyl radical is lost which generates **7g** during the timescale of the experiment (Scheme 7c). Similar redox trends were found for the trifluoromethyl derivatives $[(MeCN)Ni(CF_3)_3]^-$

(**7b**) and $[(MeCN)_2Ni(CF_3)_2]$ (**7a**),[29] suggesting that while the higher oxidation states of solvated nickel fluoroalkyl complexes can be easily accessed via oxidation of anionic complexes such as **7b** and **7e**, the higher valent complexes, especially in the nickel(III) state have limited stabilities.

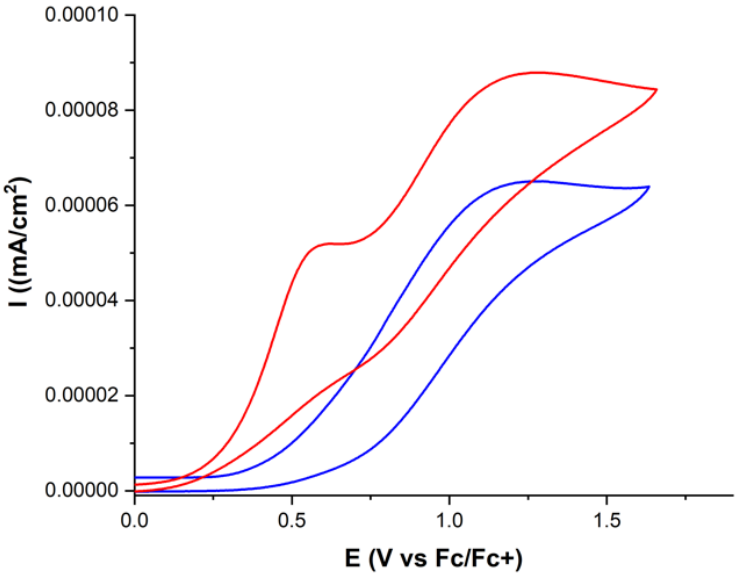

Figure 7a. Cyclic voltammograms of $[(MeCN)Ni(C_2F_5)_3]^-$ (**7e**, red) and $[(MeCN)_2Ni(C_2F_5)_2]$ (**7g**, blue) in MeCN. Complex, 10 mM; electrolye, 100 mM $[NBu_4][PF_6]$; working and counter electrode, platinum; silver psuedoreference; scan rate, 100mV/s.

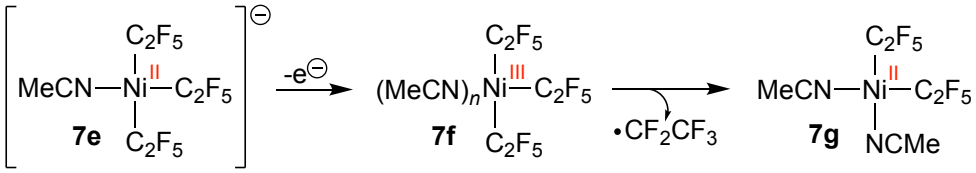

Scheme 7c. Proposed formation of **7g** from **7e** upon oxidation.

7.3.3. Stoichiometric Fluoroalkylations: Given the accessible oxidations available to the solvated nickel fluoroalkyl complexes, we explored their reactivity with various oxidizing

electrophiles. The reactivity of the tris-perfluoroalkyl nickelates with iodonium salts is summarized in Scheme 7d. Quite different reactivities were observed depending on the iodonium salt used. Reaction with the alkynyl benziodoxolone reagent **7h** (Scheme 7d, eq a) led to fluoroalkylated products (56% for CF_3 and 54% for C_2F_5). In the case of trifluoromethyl, $[(MeCN)_2Ni(CF_3)_2]$ was determined to be the major identifiable nickel species after reaction was complete. Reactions that occurred with bis(4-tert-butylphenyl) iodonium hexafluorophosphate are shown in Scheme 7d, eq b. Interestingly, even though more elevated temperatures were required, the byproducts $[(MeCN)_2Ni(CF_3)_2]$ and $[(MeCN)_2Ni(C_2F_5)_2]$ could be observed in higher quantities than the reactions described in Scheme 7d, eq 2. Control experiments revealed that reactions with reagent **7h** were more sensitive to the addition of TEMPO than reactions with the aryl iodonium salts (see Appendix F).

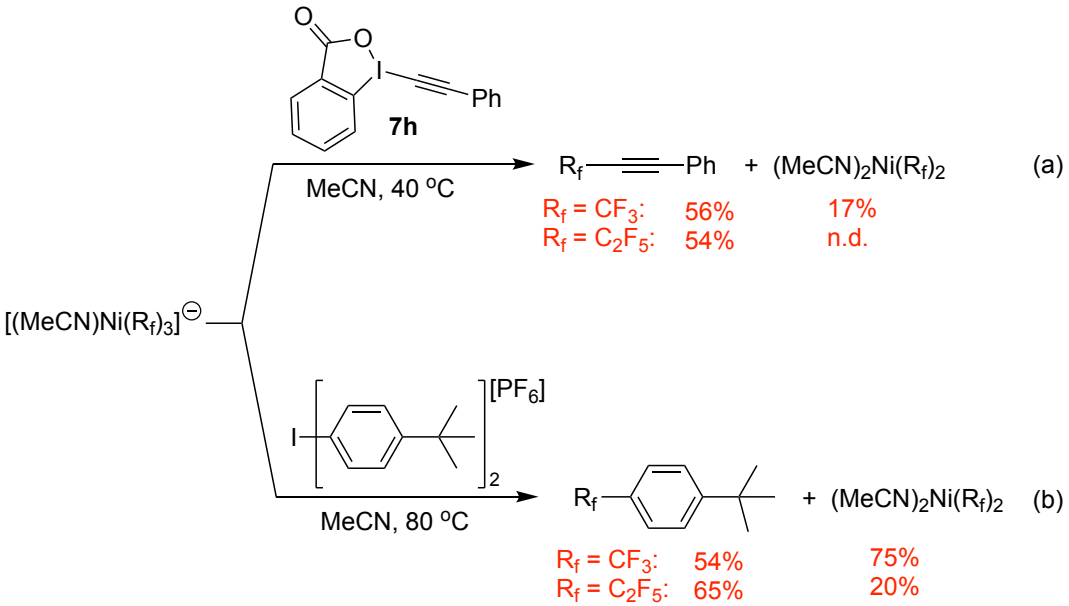

Scheme 7d. Reaction of $[MeCN)Ni(R_f)_3]^-$ with select iodonium salts. Yields determined by ^{19}F NMR spectroscopy. See reference 29 for eq b, $R_f = CF_3$.

Next, we explored reactions of the tris-perfluoroalkyl nickelates with diazonium salts, and the results are provided in Scheme 7e. Reactions with the diazonium salts occurred more rapidly than the iodonium salts, and starting material was consumed after 15 minutes. Fluoroalkylated arenes were formed in fair to good yields (41-70%), and similar reactivities were observed for both electron donating and withdrawing substituents (Scheme 7e). Along with the fluorinated arenes, the bis(perfluoroalkyl)nickel byproducts were also observed in yields ranging from 30-58%. A control reaction of 3,5-dichlorophenyl diazonium with **7b** in the presence of TEMPO revealed that trifluoromethyl arene was produced in only 19% yield, while TEMPO-CF_3 was formed in 76% yield (see Appendix F).

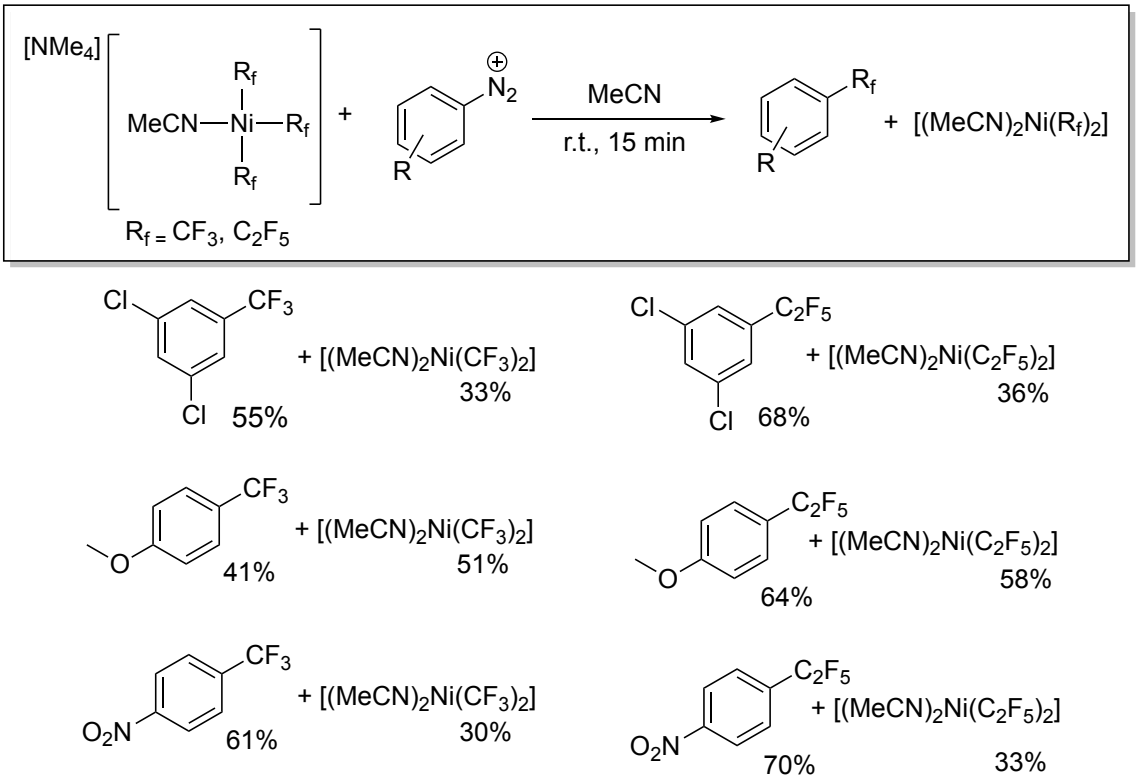

Scheme 7e. Reaction of $[NMe_4][(MeCN)Ni(R_f)_3]$ with select diazonium salts. Yields were determined by ^{19}F NMR spectroscopy.

7.3.4. Synthesis of a Solvated Isolable Charge Neutral Formally Ni(IV) Trifluoromethyl Complex: Diazonium compounds, like iodonium salts, are known to act as two-electron oxidants, and it is plausible that, in both systems explored in Schemes 7d and 7e, a high-valent species like [Ar-Ni(R_f)$_3$(MeCN)$_2$] is involved in reductive eliminations that produces both fluoroalkylated arene and [(MeCN)$_2$Ni(R_f)$_2$] co-products. While we were unable to identify a charge-neutral and high valent [Ar-Ni(R_f)$_3$(MeCN)$_2$] species, we show here that we can identify the related solvated species [Ni(CF_3)$_4$(MeCN)$_2$] (**7i**) upon chemical oxidation of [Ni(CF_3)$_4$]$^{2-}$. Reaction of [Ni(CF_3)$_4$]$^{2-}$ with two equivalents of Magic Blue (tris(4-bromophenyl)ammoniumyl hexachloro antimonate) oxidant led to **7i** in 53% yield by ^{19}F NMR spectroscopy (Scheme 7f) and in 30% isolated yield. As there are two types of trifluoromethyl groups in complex **7i** (*trans* to a MeCN and *trans* to another CF_3), complex **7i** exhibited two septets in the ^{19}F NMR spectrum in acetonitrile (δ –19.2 (sept, J = 7.2 Hz) and –30.7 (sept, J = 7.2 Hz). X-ray quality crystals could be grown from ether/pentane at low temperature, and an ORTEP diagram of **7i** is shown in Figure 7b. The trifluoromethyl groups that are trans to each other exhibit nickel-carbon distances of 2.0298(19) Å, while the trifluoromethyl groups that are trans to acetonitrile ligands were shorter at 1.9569(17) Å. This result is consistent with the known trans influencing properties of the trifluoromethyl group.[34] The nickel-carbon bond lengths of octahedral **7i** in the formal +4 oxidation state were significantly longer than the average nickel(II)-carbon bond lengths in **3** (1.930(8) Å),[29] which adopts a distorted square planar arrangement in the formal +2 oxidation state and also possesses four trifluoromethyl ligands. To our knowledge, **7i** represents only the second formally nickel(IV) complex reported bearing four trifluoromethyl ligands.[29]

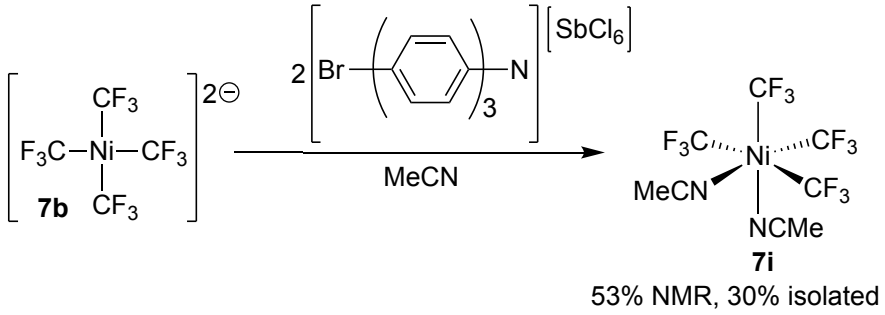

Scheme 7f. Oxidation of **7b** to generate isolable **7i**.

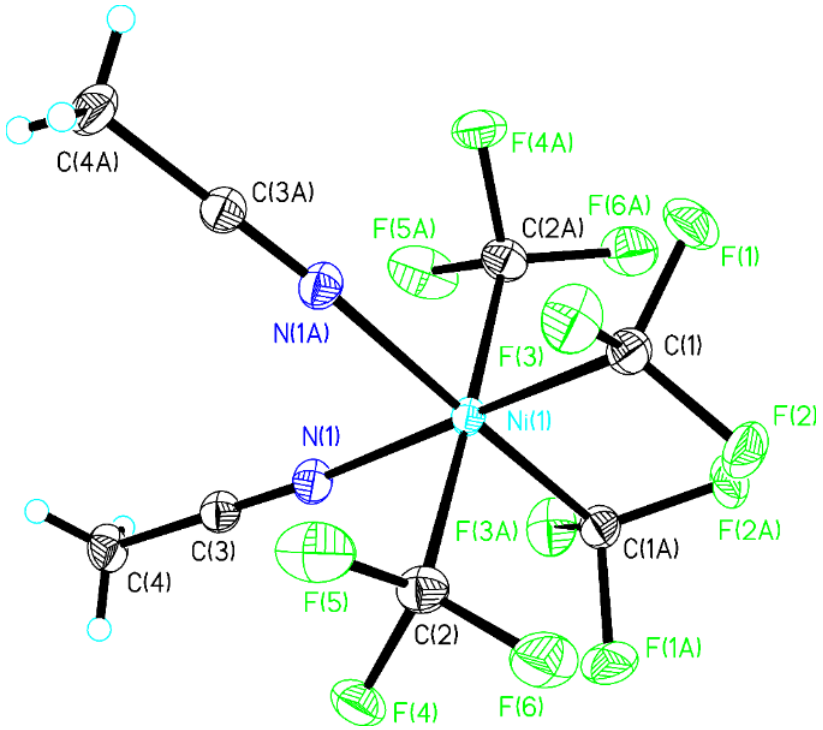

Figure 7b. ORTEP diagram of **7i**. Ellipsoids shown at the 40% level. Selected bond lengths (Å): Ni1-C1 1.9569(17); Ni1-C2 2.0298(19); Ni1-N1 1.9682(15). Selected bond angles (°): C1-Ni1-N1 174.35(7); C1-Ni1-N1A 91.62(7); N1-Ni1-N1A 85.54(8); C1-Ni1-C2 93.32(8); Ni-Ni1C2A 87.55(7).

7.3.5. Catalytic Trifluoromethylation of (hetero)arenes: Because the cyclic voltammograms of the anionic fluoroalkyl complexes of nickel revealed evidence of nickel-carbon bond homolyses reactions, we also examined the ability of solvated nickel complexes to perform Minisci-like C-H bond trifluoromethylations. In 2016, Wang reported the first example of a nickel-catalyzed C–H trifluoromethylation of electron-rich

heteroarenes using iodotrifluoromethane as the CF_3 source and [(dppp)$NiCl_2$] as the nickel source (dppp = 1,3-bis(diphenylphosphino)propane).[6] In 2019, Sanford reported that the high-valent [TpNi$(CF_3)_3$] (**7j**, Tp = tris(pyrazolyl)borate) could also mediate catalytic C-H trifluoromethylations of (hetero)arenes in the presence of Umemoto's Reagent II (**7k**).[17] Mechanistic investigations of this process, both experimental and computational, suggested that the reactions proceeded through radical chain pathways involving nickel in variable oxidation states.[17] Since our solvated nickel system could shuttle between the formally +2 to +4 oxidation states, we explored the possibility of using these complexes in similar C-H trifluoromethylations, as eliminating the need for extraneous supporting ligands would represent a significant advance in practicality. Table 7a summarizes the catalyst screens for the C-H trifluoromethylation reaction outlined and are based on the conditions identified by Sanford.[17] Gratifyingly, the solvated complex **7b** and the homolyptic complex **7c** catalyzed the trifluoromethylation of 1,3,5-trimethoxybenzene by Umemoto II reagent in 78% and 96% yields, respectively, providing the first proof-in-principle that the solvated nickel complexes can perform catalytic trifluoromethylations. Notably, $[NMe_4]_2[Ni(CF_3)_4]$ (**7c**) performed just as well as [(Tp)Ni$(CF_3)_3$] (**7j**) under these conditions, which was previously reported to afford product in 93% yield.[17] To test the effect of metal identity on the C-H trifluoromethylations, a reaction with the recently prepared [$(MeCN)_3Co(CF_3)_3$] (**7l**)[35] was examined (entry 5). Complex **7l**, while displaying catalytic turnover, afforded yields that were lower than nickel. Utilizing the homoleptic trifluoromethyl copper complex $[NBu_4][Cu(CF_3)_4]$ was found to achieve yields similar to that of the control (Table 7a, entry 2 vs. 6). With the optimal catalyst identified as $[NMe_4]_2[Ni(CF_3)_4]$ in Table 7a, we then determined the scope of the catalytic C-H

trifluoromethylations (Scheme 7g). Trifluoromethylations of electron rich arenes **7ma-7mc** proceeded smoothly, however introduction of an aldehyde into the aromatic scaffold (**7md**) lowered the yield of trifluoromethylated product significantly. Nitrogen- and sulfur-heterocycles (**7me-7mg**) were also successfully trifluoromethylated.

Table 7a. Screening of fluoroalkyl transition metal catalysts for trifluoromethylation of arenes.[a]

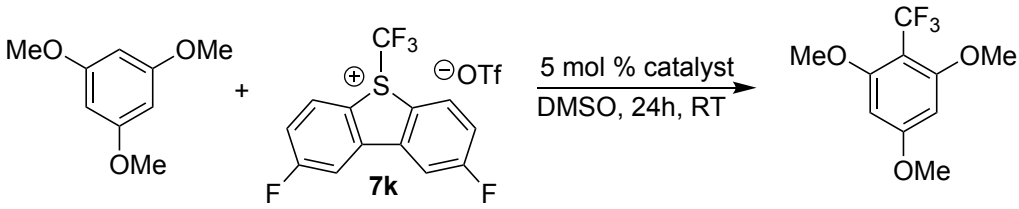

entry	catalyst	yield
1	$[(Tp)Ni(CF_3)_3]$ (**7j**)	96
2	None	16
3	$[NMe_4][(MeCN)Ni(CF_3)_3]$ (**7b**)	78
4	$[NMe_4]_2[Ni(CF_3)_4]$ (**7c**)	96
5	$[(MeCN)_3Co(CF_3)_3]$ (**7l**)	59
6	$[NBu_4][Cu(CF_3)_4]$	18

[a] All reactions were run on 0.05 mmol scale with Umemoto Reagent II as the limiting reagent, and 5 equiv. of arene. The yields were determined by ^{19}F NMR spectroscopy.

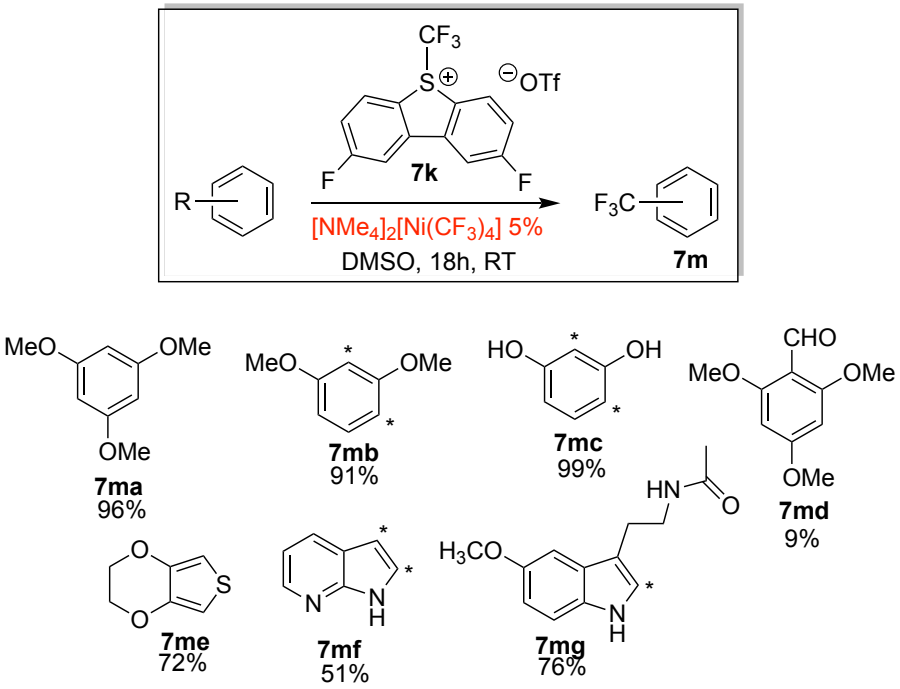

Scheme 7g. Scope of catalytic C-H functionalizations. The * reveals site(s) of selectivity for molecules with more than one type of aromatic C-H bond. Combined yields of trifluoromethylations at all possible sites are provided. Yields were determined by ^{19}F NMR spectroscopy.

As evident from Table 7a and reference 17, **7c** and **7j** provide similar yields in the catalytic C-H functionalization reactions. The advantage of using **7c** is that it can be prepared in one step, starting from [(dme)$NiBr_2$]. The preparation of complex **7j**, on the other hand, involves the synthesis of [$(MeCN)_2Ni(CF_3)_2$] from [(dme)$NiBr_2$], followed by ligation with pre-made [NMe_4][Tp] to produce [NMe_4][(Tp)$Ni(CF_3)_2$], followed by reaction with Umemoto II reagent to produce **7k**. Moreover, solvated **7b** and **7c** can serve as precatalysts for rapid ligand screening reactions. A disadvantage of using the anionic **7b** and **7c** relative to **7j** is that they are air-sensitive, though we have seen no issues storing large quantities in a glovebox at -30 °C.

7.3.6. Investigation of Nickel Catalyst with Umemoto II Reagent: To better understand the reactivity of [NMe_4]$_2$[$Ni(CF_3)_4$] (**7c**) with the Umemoto II reagent (**7k**), a

stoichiometric reaction was performed and monitored by ^{19}F NMR spectroscopy (Scheme 7h, a). Upon mixing **7c** with **7k** in CD_3CN, the ^{19}F NMR spectrum revealed a transformation that was consistent with the formation of compounds **7n** and **7o** (Scheme 7h). Putative compound **7n** exhibits a singlet in the ^{19}F NMR spectrum in CD_3CN at δ –25.1. The ^{19}F NMR spectrum of compound **7o** is more complicated and consists of an apparent undecet at δ –19.6 (J = 8.2 Hz) and a quartet at δ –28.8 (J = 8.2 Hz). Compound **7o** displays similarities in the ^{19}F NMR spectrum to the $NCCH_2$– (carbon bound) complex $[(NCCH_2)Ni(CF_3)_5]^{2-}$ (**7p**), a compound that was formed in trace amounts during the synthesis **7c**, fortuitously crystallized, and was structurally characterized (see Appendix F). The dianionic compound **7p** displays resonances at δ –24.3 (apparent septet, J = 7.5 Hz) and –27.4 (quartet, J = 7.5 Hz) in CD_3CN. In the absence of arene substrate (Scheme 7h), we propose that **7o** is formed via a sequential two electron oxidation of **7c** by Umemoto II reagent as outlined in Scheme 7h, eqs b and c. In catalytic reactions where arene trapping agents are present, CF_3 radicals sources may originate both by the reaction described in eq 7 and by reductive homolysis of **7q**, which would produce **7b** as a byproduct. Control reactions reveal that the catalysis described in Table 1 is completely shut down in the presence of TEMPO. We speculate that the formation of **7n** may arise through redistribution reactions involving trifluoromethyl anion (Scheme 7h, eq d). The reactions described in Scheme 7h, eq b-d, highlight the ability of solvated nickel to form trifluoromethyl complexes with a variety of coordination numbers, formal oxidation states, and formal overall charges. This flexible accommodation of trifluoromethyl groups may

prove to be useful in future methodologies where nickel is required to serve as a reservoir of CF_3 anions or radicals.

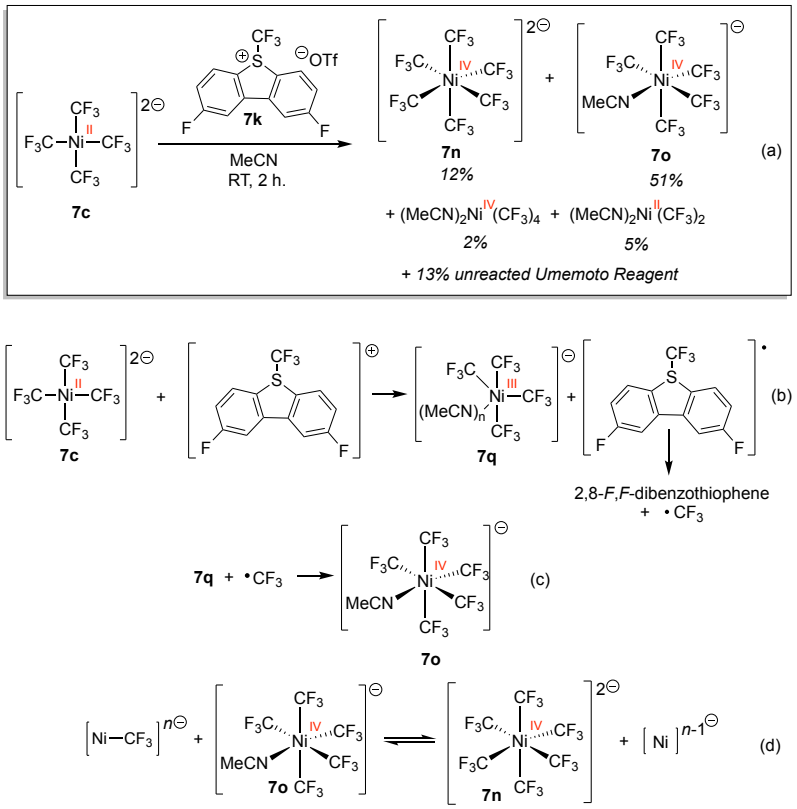

Scheme 7h. Possible mechanistic pathways in the reaction of Umemoto II reagent with **7c**.

In the reactions that are described in Scheme 7g, it is plausible that the trifluoromethyl group could be originating from Umemoto Reagent II or the nickel complex. To explore this possibility, a cross-over reaction of 1,3,5-trimethoxybenzene and Umemoto Reagent II with varying amounts of the solvated perfluoroethyl nickelate **7e** was performed, and the amount of trifluoromethyl to perfluoroethyl product was analyzed (Table 7b). With 5 mol% of **7**e, 84% yield of trifluoromethylated product, and 10% yield of perfluoroethylated product were observed. Further, increasing the nickel complex to 20 mol%, yielded 69% of trifluoromethylated product, and 43% of perfluoroethylated. Stoichiometric amounts found almost entirely perfluoroethylated product (Table 7b). Therefore, since significant

quantities of the cross-over product formation is occurring, the source of the perfluoroalkyl group in these reactions is most likely originating at the nickel complex.

Table 7b. Cross-over reaction, exploring the source of the fluoroalkyl group in aromatic C-H bond perfluoroalkylation with solvated nickel.[a]

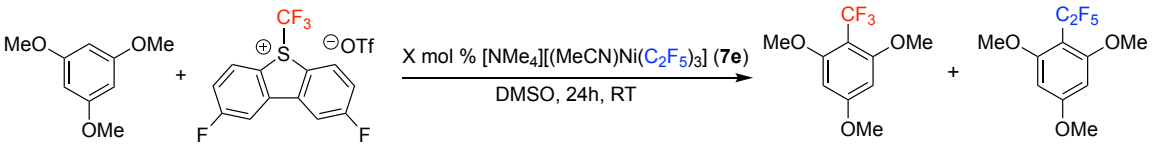

X mol% **7e**	-CF_3 yield	-C_2F_5 yield
5	84	10
20	69	43
100	3	135

[a] All reactions were run on 0.05 mmol scale with Umemoto Reagent II as the limiting reagent, and 5 equiv. of arene. The yields were determined by ^{19}F NMR spectroscopy.

7.4 Conclusions: A number of important precedents with regard to fluoroalkylations with solvated nickel have been described. First, we show that both $[(MeCN)Ni(CF_3)_3]^-$ and $[(MeCN)Ni(C_2F_5)_3]^-$ successfully react with aryl iodonium and diazonium salts as well as alkynyl iodonium salts to give fluoroalkylated organic products. These results clearly show that upon oxidation of acetonitrile-supported nickel fluoroalkyl complexes, the fluoroalkyl groups can be transferred to organic substrates. Secondly, the electrochemical analysis of $[(MeCN)Ni^{II}(C_2F_5)_3]^-$ suggests that, upon electro-oxidation to $[(MeCN)_nNi^{III}(C_2F_5)_3]$, reductive homolysis of a perfluoroethyl radical occurs, with the concomitant formation of $[(MeCN)Ni^{II}(C_2F_5)_2]$. This electrochemical behavior shows generality with trifluoromethyl derivatives.[29] Lastly, catalytic C-H trifluoromethylations of electron rich arenes were successfully achieved using either $[(MeCN)Ni(CF_3)_3]^-$ or the related

$[Ni(CF_3)_4]^{2-}$. From a broad perspective, the stoichiometric reactions of the solvated nickel complexes reveal that solvated nickel is exceptionally capable of serving as reservoir of CF_3 anions or radicals under catalytically relevant conditions, which bodes well for their use in future methods development.

7.5. Experimental

7.5.1. General Information: All manipulations were performed using standard Schlenk and high vacuum techniques or in a nitrogen filled glovebox, unless otherwise stated. Solvents were purified by passing through activated alumina and/or copper in a solvent purification system supplied by Pure Process Technology. Solution ^1H NMR spectra were recorded at ambient temperature on a Bruker 400 MHz spectrometer and referenced to residual proton solvent signals. ^{19}F spectra were recorded on the Bruker NMR spectrometer operating at 376 MHz and referenced to α,α,α-trifluorotoluene as an internal standard (δ = -63.7). A Bruker D8 Quest diffractometer was used for X-ray crystal structure determinations. Cyclic voltammetry data was collected in a nitrogen filled glovebox at room temperature on a PARSTAT 4000A potentiostat. The CCDC 2074356 and 2074357 contain the supplementary crystallographic data for this paper. These data can be obtained free of charge via www.ccdc.cam.ac.uk/data_request/cif, or by e-mailing data_request@ccdc.cam.ac.uk, or by contacting The Cambridge Crystallographic Data Centre, 12 Union Road, Cambridge CB2 1EZ, UK; fax: +44 1223 336033.

7.5.2. Preparation of $[NMe_4][(MeCN)Ni(CF_3)_3]$ (7b): In a nitrogen filled glovebox, AgF (390 mg, 3.1 mmol) and TMS-CF_3 (0.52 mL, 3.5 mmol) were stirred in 20 mL of MeCN for 1.5 hours. Then, (dme)$NiBr_2$ (310 mg, 1.0 mmol), NMe_4Cl (110 mg, 1.0 mmol), and 7 mL of MeCN were added. The reaction was stirred for 2 days and then filtered over Celite.

The filtrate was pumped dry, and the solid was collected by filtration and washed with diethyl ether to yield 287 mg of yellow solid (75% yield). ^{1}H NMR (CD_3CN, 400 MHz): δ 3.07 (s, 12 H). ^{19}F NMR (CD_3CN, 376 MHz): δ -25.2 (sept, J = 4.4 Hz, 3 F), -31.04 (quartet, J = 4.4 Hz, 6F). Anal. Calcd (found) for $C_9H_{15}F_9NiN_2$: C, 28.38 (28.23); H, 3.97 (3.99).

7.5.3. Preparation of $[NMe_4]_2[Ni(CF_3)_4]$ (7c): In a nitrogen filled glovebox, AgF (586 mg, 4.5 mmol) and TMS-CF_3 (0.74 mL, 5.0 mmol) were stirred in 20 mL of MeCN for 1.5 hours. Then, (dme)$NiBr_2$ (310 mg, 1.0 mmol), NMe_4Cl (220 mg, 1.0 mmol), and 7 mL of MeCN were added. The reaction was stirred for 2 days and then filtered over Celite. The filtrate was pumped dry and the solid was collected by filtration and washed with diethyl ether. The crude solid was recrystallized by dissolving in 10 mL of MeCN, filtering off any insolubles, adding 10 mL of diethyl ether, followed by placing in glovebox freezer (-30 ^{o}C) overnight. The precipitate is collected by filtration and washed with diethyl ether to yield 250 mg of yellow solid (52% yield) ^{1}H NMR (CD_3CN, 400 MHz): δ 3.12 (s, 24 H). ^{19}F NMR (CD_3CN, 376 MHz): δ -26.1 (s, 12 F). Anal. Calcd (found) for $C_{12}H_{24}F_{12}NiN_2$: C, 29.84 (29.63); H, 5.01 (4.97).

7.5.4. Preparation of $[NMe_4][(MeCN)Ni(C_2F_5)_3]$ (7e): In a nitrogen filled glovebox, AgF (390 mg, 3.1 mmol) and TMS-C_2F_5 (0.61 mL, 3.5 mmol) were stirred in 10 mL of MeCN for 1.5 hours. Then, (dme)$NiBr_2$ (310 mg, 1.0 mmol), NMe_4Cl (110 mg, 1.0 mmol), and 10 mL of MeCN were added. The reaction was stirred for 4 days and then filtered over Celite. The filtrate was pumped dry, and the solid was collected by filtration and washed with diethyl ether to yield 300 mg of yellow solid (56% yield). ^{1}H NMR (CD_3CN, 400 MHz): δ 3.12 (s, 12 H). ^{19}F NMR (CD_3CN, 376 MHz): δ -79.0 (quin, J = 8.6 Hz, 3 F), -

81.2 (t, 5.6 Hz, 6 F), -97.0 to -97.4 (m, 2 F), -108.3 to -108.6 (m, 4 F). Anal. Calcd (found) for $C_{12}H_{15}F_{15}NiN_2$: C, 27.15 (26.76); H, 2.85 (2.88).

7.5.5. Preparation of $[Ni(CF_3)_4(MeCN)_2]$ (7i): In a nitrogen-filled glovebox, a vial was charged with $[NMe_4]_2[Ni(CF_3)_4]$ (96 mg, 0.20 mmol), tris(4-bromophenyl)ammoniumyl hexachloroantimonate ('Magic Blue') (328 mg, 0.402 mmol) and 5 mL of MeCN. The reaction was stirred for 30 minutes. The insoluble were filtered off and the solution was pumped dry. Diethyl ether was added and the insolubles were filtered off. Pentane was added and the mixture was placed in the glovebox freezer (-30°C). Yellow crystals were collected, 25 mg (30 % yield). ^{19}F NMR (CD_3CN, 376 MHz): δ -19.2 (sept, J = 7.2 Hz, 6 F), -30.7 (sept, J = 7.2 Hz, 6 F). Anal. Calcd (found) for $C_8H_6F_{12}NiN_2$: C, 23.05 (22.91); H, 1.45 (1.46).

7.5.6. General Procedure for Perfuoroalkylation of Alkynyl Iodonium Reagent as Described in Scheme 7d, eq a: In a nitrogen-filled glovebox, nickel complex (0.023 mmol) and 1-(2-phenylethynyl)-1,2-benziodoxol-3(1H)-one (**7h**) (16 mg, 0.046 mmol) were dissolved in CD_3CN/CH_3CN. Either fluorobenzene or trifluorotoluene was added as internal standard and the reaction was heated to 40° C and monitored by ^{19}F NMR spectroscopy until all starting material was consumed.

7.5.7. Reaction of $[NMe_4][(MeCN)Ni(C_2F_5)_3]$ with bis(aryl)iodonium Reagent as Described in Scheme 7d, eq b: In a nitrogen-filled glovebox, $[NMe_4][(MeCN)Ni(C_2F_5)_3]$ (12 mg, 0.023 mmol) and bis(4-tert-butylphenyl)iodonium hexafluorophosphate (24 mg, 0.046 mmol) were dissolved in CD_3CN/CH_3CN. Trifluorotoluene was added as internal standard and the reaction was heated to 80° C and monitored by ^{19}F NMR spectroscopy until all starting material was consumed. In this manner, 4-*t*-butylpentafluoroethylbenzene

was synthesized in 65 % yield. $[(MeCN)_2Ni(C_2F_5)_2]$ was also formed as the nickel-containing product in 20% yield.

7.5.8. General Procedure for Perfluoroalkylation of Diazonium Salts as Described in Scheme 7e: In a nitrogen-filled glovebox, nickel complex (0.05 mmol) and diazonium salt (0.05 mmol) were dissolved in CD_3CN/CH_3CN and stirred for 15 minutes. Trifluorotoluene was added as an internal standard and the yield was determined by ^{19}F NMR spectroscopy.

7.5.9. General Procedure for Trifluoromethylation of (hetero)arenes: In a nitrogen-filled glovebox, (hetero)arene substrate (0.25 mmol, 5 equiv), and Umemoto Reagent II (**7k**) (22 mg, 0.05 mmol) were dissolved in DMSO (0.9 mL). The catalyst was added as 100 μL of a 0.025 M stock solution in DMSO. The reaction was stirred for 18 hours at room temperature and trifluorotoluene was added as an internal standard and the yield was determined by ^{19}F NMR spectroscopy.

7.5.10. Oxidation of $[NMe_4]_2[Ni(CF_3)_4]$ with Umemoto's Reagent II: In a nitrogen-filled glovebox, a vial was charged with $[NMe_4]_2[Ni(CF_3)_4]$ (24 mg, 0.050 mmol), Umemoto's Reagent II (**7k**) (22 mg, 0.050 mmol) and CD_3CN/CH_3CN. The reaction was stirred for 2 hours and trifluorotoluene was added as an internal standard and the nickel containing products were identified by ^{19}F NMR spectroscopy.

$[(MeCN)_2Ni(CF_3)_4]$ (**7i**) (2%): ^{19}F NMR (CD_3CN, 376 MHz): δ –19.2 (sept, J = 7.2 Hz, 6 F), –30.7 (sept, J = 7.2 Hz, 6 F).

$[(MeCN)Ni(CF_3)_5]^-$ (**7o**) (51%): ^{19}F NMR (CD_3CN, 376 MHz): δ –19.6 (app. undecet, J = 8.2 Hz, 3 F), –28.8 (quartet, J = 8.2 Hz, 12 F).

$[Ni(CF_3)_6]^{2-}$ (**7n**) (12%): ^{19}F NMR (CD_3CN, 376 MHz): δ –25.1 (s, 18 F).

$[(MeCN)_2Ni(CF_3)_2]$ (**7a**) (5%): ^{19}F NMR (CD_3CN, 376 MHz): δ –27.8 (s, 6 F).

^{19}F NMR data for $[(NCCH_2)Ni(CF_3)_5]^{2-}$ (**7p**) : ^{19}F NMR (CD_3CN, 376 MHz): δ –24.3 (app. septet, J = 7.5 Hz, 3 F), –27.4 (quartet, J = 7.5 Hz, 12 F).

7.5.11. Radical Trapping Experiments with TEMPO

7.5.11.1 Trifluoromethylation of an Alkynyl Iodonium (conditions similar to Scheme 7d, eq a but in the presence of TEMPO): In a nitrogen-filled glovebox, $[NMe_4][(MeCN)Ni(CF_3)_3]$ (9 mg, 0.02 mmol), 1-(2-phenylethynyl)-1,2-benziodoxol-3(1H)-one (**7h**) (16 mg, 0.046 mmol) and TEMPO (4 mg, 0.02 mmol) were dissolved in CD_3CN/CH_3CN. Trifluorotoluene was added as internal standard and the reaction was heated to 40˚ C and monitored by ^{19}F NMR spectroscopy until all starting material was consumed. In this manner, (3,3,3-trifluoro-1-propyn-1-yl)benzene was identified in 12 % NMR yield. TEMPO–CF_3 was detected in 51% yield.

7.5.11.2 Trifluoromethylation of an Aryl Iodonium Salt (conditions similar to Scheme 7d, eq b but in the presence of TEMPO): In a nitrogen-filled glovebox, $[NMe_4][(MeCN)Ni(CF_3)_3]$ (9 mg, 0.02 mmol), bis(4-tert-butylphenyl)iodonium hexafluorophosphate (24 mg, 0.046 mmol), and TEMPO (4 mg, 0.02 mmol) were dissolved in CD_3CN/CH_3CN. Trifluorotoluene was added as internal standard and the reaction was heated to 80˚ C and monitored by ^{19}F NMR spectroscopy until all starting material was consumed. In this manner, 4-*t*-butyltrifluoromethylbenzene was synthesized in 40 % yield. TEMPO–CF_3 was not detected.

7.5.11.3 Trifluoromethylation of a Diazonium Salt (conditions similar to Scheme 7e but in the presence of TEMPO): In a nitrogen-filled glovebox, $[NMe_4][(MeCN)Ni(CF_3)_3]$ (19 mg, 0.050 mmol), 3,5-dichlorophenyldiazonium tetrafluoroborate (13 mg, 0.050 mmol) and TEMPO (8 mg, 0.05 mmol) were dissolved in CD_3CN/CH_3CN and stirred for 15 minutes. Trifluorotoluene was added as an internal standard and the yield was determined by ^{19}F NMR spectroscopy. In this manner, 1,3-dichloro-5-(trifluoromethyl)benzene was synthesized in 19 % yield. TEMPO–CF_3 was detected in 76% yield.

7.5.11.4 Oxidation of $[NMe_4]_2[Ni(CF_3)_4]$ with "magic blue" in the Presence of TEMPO: In a nitrogen-filled glovebox, a vial was charged with $[NMe_4]_2[Ni(CF_3)_4]$ (24 mg, 0.050 mmol), tris(4-bromophenyl)ammoniumyl hexachloroantimonate ('Magic Blue') (82 mg, 0.10 mmol), TEMPO (8 mg, 0.05 mmol) and CD_3CN/CH_3CN. The reaction was stirred for 30 minutes and trifluorotoluene was added as an internal standard. The insoluble were filtered off and the yields were determined by ^{19}F NMR spectroscopy. In this manner, $[(MeCN)_2Ni(CF_3)_4]$ (**9**) was synthesized in 59% yield, and TEMPO–CF_3 was detected in 14% yield.

7.5.11.5 Catalytic Trifluoromethylation in the Presence of TEMPO: In a nitrogen-filled glovebox, 1,3,5 - trimethoxybenzene (40 mg, 0.25 mmol, 5 equiv), Umemoto Reagent II (**7k**) (22 mg, 0.050 mmol), and TEMPO (8 mg, 0.05 mmol) were dissolved in DMSO (0.9 mL). 100 μL of a 0.025 M stock solution of $[NMe_4]_2[Ni(CF_3)_4]$ in DMSO was added. The reaction was stirred for 18 hours at room temperature and trifluorotoluene was added as an internal standard and the yield of 1,3,5-trimethoxy-2-(trifluoromethyl)benzene was 1% and TEMPO–CF_3 was detected in 9% yield.

In the absence of nickel catalyst, 1,3,5-trimethoxy-2-(trifluoromethyl)benzene was not detected, and TEMPO–CF_3 was detected in trace amounts.

In the absence of nickel catalyst and 1,3,5-trimethoxybenzene, TEMPO–CF_3 was detected in trace amounts.

7.5.12. Cross-over perfluoroalkylation of 1,3,5-trimethoxybenzene: In a nitrogen-filled glovebox, to three vials 1,3,5-trimethoxybezene (0.25 mmol, 5 equiv), and Umemoto Reagent II (**7k**) (0.05 mmol, 1 equiv) were added to each. To the first (5 mol% reaction), DMSO (0.9 mL) and 100 μL of a 0.025 M stock solution in DMSO of **7e** was added. To the second (20 mol% reaction), DMSO (0.6 mL) and 400 μL of a 0.025 M stock solution in DMSO of **7e** was added. To the third (100 mol% reaction), **7e** (0.05 mmol, 1 equiv.) was added and 1 mL of DMSO. All three reactions were stirred for 24 hours at room temperature trifluorotoluene was added as an internal standard and the yield was determined by ^{19}F NMR spectroscopy.

7.6 References

1. Bour, J. R.; Camasso, N. M.; Sanford, M. S. Oxidation of Ni(II) to Ni(IV) with Aryl Electrophiles Enables Ni-Mediated Aryl-CF_3 Coupling. *J. Am. Chem. Soc.* **2015,** *137*, 8034-8037.
2. Bour, J. R.; Roy, P.; Canty, A. J.; Kampf, J. W.; Sanford, M. S. Oxidatively Induced Aryl–CF_3 Coupling at Diphosphine Nickel Complexes. *Organometallics* **2020,** *39*, 3-7.
3. Jongbloed, L. S.; Vogt, N.; Sandleben, A.; de Bruin, B.; Klein, A.; van der Vlugt, J. I. Nickel-Alkyl Complexes with a Reactive PNC-Pincer Ligand. *Eur. J. Inorg. Chem.* **2018,** 2408-2418.
4. Bour, J. R.; Camasso, N. M.; Meucci, E. A.; Kampf, J. W.; Canty, A. J.; Sanford, M. S. Carbon–Carbon Bond-Forming Reductive Elimination from Isolated Nickel(III) Complexes. *J. Amer. Chem. Soc.* **2016,** *138*, 16105-16111.
5. Mikhaylov, D. Y.; Budnikova, Y. H.; Gryaznova, T. V.; Krivolapov, D. V.; Litvinov, I. A.; Vicic, D. A.; Sinyashin, O. G. Electrocatalytic Fluoroalkylation of Olefins. *J. Organomet. Chem.* **2009,** *694*, 3840-3843.
6. Wu, Y.; Zhang, H.-R.; Jin, R.-X.; Lan, Q.; Wang, X.-S. Nickel-Catalyzed C-H Trifluoromethylation of Electron-Rich Heteroarenes. *Adv. Syn. Cat.* **2016,** *358*, 3528-3533.

7. Xu, C.; Cheng, R.; Luo, Y.-C.; Wang, M.-K.; Zhang, X. Trans-Selective Aryldifluoroalkylation of Endocyclic Enecarbamates and Enamides by Nickel Catalysis. *Angew. Chem., Int. Ed.* **2020,** *59*, 18741-18747.
8. Fu, X.-P.; Xiao, Y.-L.; Zhang, X. Nickel-Catalyzed Difluoromethylation of Arylboronic Acids with Bromodifluoromethane. *Chinese J. Chem.* **2018,** *36*, 143-146.
9. Xing, G. H.; X. Z. X. Nickel-Catalyzed Difluoromethylation of (Hetero)aryl Bromides with $BrCF_2H$. *Chinese J. Org. Chem.* **2019,** *39*, 215-222.
10. Zhang, S.; Weniger, F.; Ye, F.; Rabeah, J.; Ellinger, S.; Zaragoza, F.; Taeschler, C.; Neumann, H.; Brueckner, A.; Beller, M. Selective Nickel-Catalyzed Fluoroalkylations of Olefins. *Chem. Commun.* **2020,** *56*, 15157-15160.
11. Xu, C.; Guo, W.-H.; He, X.; Guo, Y.-L.; Zhang, X.-Y.; Zhang, X. Difluoromethylation of (Hetero)aryl Chlorides with Chlorodifluoromethane Catalyzed by Nickel. *Nat. Commun.* **2018,** *9*, 1-10.
12. An, L.; Xu, C.; Zhang, X. Highly Selective Nickel-Catalyzed Gem-Difluoropropargylation of Unactivated Alkylzinc Reagents. *Nat. Commun.* **2017,** *8*, 1460.
13. Xu, L.; Vicic, D. A. Direct Difluoromethylation of Aryl Halides via Base Metal Catalysis at Room Temperature. *J. Amer. Chem. Soc.* **2016,** *138*, 2536-2539.
14. Kaplan, P. T.; Xu, L.; Chen, B.; McGarry, K. R.; Yu, S.; Wang, H.; Vicic, D. A. Mild, Safe, and Versatile Reagents for $(CF_2)_n$ Transfer and the Construction of Fluoroalkyl-Containing Rings. *Organometallics* **2013,** *32*, 7552-7558.
15. Zhang, C.-P.; Wang, H.; Klein, A.; Biewer, C.; Stirnat, K.; Yamaguchi, Y.; Xu, L.; Gomez-Benitez, V.; Vicic, D. A. A Five-Coordinate Nickel(II) Fluoroalkyl Complex as a Precursor to a Spectroscopically Detectable Ni(III) Species. *J. Am. Chem. Soc.* **2013,** *135*, 8141-8144.
16. Feng, Z.; Xiao, Y.-L.; Zhang, X. Transition-Metal (Cu, Pd, Ni)-Catalyzed Difluoroalkylation via Cross-Coupling with Difluoroalkyl Halides. *Acc. Chem. Res.* **2018,** *51*, 2264-2278.
17. Meucci, E. A.; Nguyen, S. N.; Camasso, N. M.; Chong, E.; Ariafard, A.; Canty, A. J.; Sanford, M. S. Nickel(IV)-Catalyzed C-H Trifluoromethylation of (Hetero)arenes. *J. Am. Chem. Soc.* **2019,** *141*, 12872-12879.
18. Zhou, M.; Zhao, H.-Y.; Zhang, S.; Zhang, Y.; Zhang, X. Nickel-Catalyzed Four-Component Carbocarbonylation of Alkenes under 1 atm of CO. *J. Am. Chem. Soc.* **2020,** *142*, 18191-18199.
19. Zhao, H.-Y.; Gao, X.; Zhang, S.; Zhang, X. Nickel-Catalyzed Carbonylation of Difluoroalkyl Bromides with Arylboronic Acids. *Org. Lett.* **2019,** *21*, 1031-1036.
20. Mikhaylov, D. Y.; Budnikova, Y. H.; Gryaznova, T. V.; Sinyashin, O. G. Electrocatalytic fluoroalkylation of olefins. *ECS Trans.* **2010,** *25*, 67-77.
21. An, L.; Tong, F.-F.; Zhang, S.; Zhang, X. Stereoselective Functionalization of Racemic Cyclopropylzinc Reagents via Enantiodivergent Relay Coupling. *J. Am. Chem. Soc.* **2020,** *142*, 11884-11892.
22. Carrow, B. P.; Hartwig, J. F. Ligandless, Anionic, Arylpalladium Halide Intermediates in the Heck Reaction. *J. Amer. Chem. Soc.* **2010,** *132*, 79-81.
23. Fantasia, S.; Windisch, J.; Scalone, M. Ligandless Copper-Catalyzed Coupling of Heteroaryl Bromides with Gaseous Ammonia. *Adv. Syn. Cat.* **2013,** *355*, 627-631.

24. Schroeter, F.; Lerch, S.; Strassner, T. Oxidative and Reductive Cross-Coupling Reactions Catalyzed by an Anionic "Ligandless" Palladium Complex. *Org. Process Res. Dev.* **2018,** *22*, 1614-1621.
25. Williams, D. R.; Bawel, S. A. General Methodology for the Preparation of Unsymmetrical α-Linked Bisenones via Ligandless Cross-Coupling Reactions. *Org. Lett.* **2017,** *19*, 1730-1733.
26. Yin, J. X.; Hyland, C. J. T. Ring-Opening of Vinylcyclopropane-1,1-dicarboxylates by Boronic Acids under Ligandless Palladium Catalysis in Neat Water. *J. Org. Chem.* **2015,** *80*, 6529-6536.
27. Wiskur, S. L.; Korte, A.; Fu, G. C. Cross-Couplings of Alkyl Electrophiles Under "Ligandless" Conditions: Negishi Reactions of Organozirconium Reagents. *J. Am. Chem. Soc.* **2004,** *126*, 82-83.
28. Madin, A.; Overman, L. E. Controlling Stereoselection in Intramolecular Heck Reactions by Tailoring the Palladium Catalyst. *Tet. Lett.* **1992,** *33*, 4859-62.
29. Shreiber, S. T.; DiMucci, I. M.; Khrizanforov, M. N.; Titus, C. J.; Nordlund, D.; Dudkina, Y.; Cramer, R. E.; Budnikova, Y.; Lancaster, K. M.; Vicic, D. A. $[(MeCN)Ni(CF_3)_3]^-$ and $[Ni(CF_3)_4]^{2-}$: Foundations toward the Development of Trifluoromethylations at Unsupported Nickel. *Inorg. Chem.* **2020,** *59*, 9143-9151.
30. Graves, R. E.; Newmark, R. A. Fluorine Coupling in Hexalfuoroethane. *J. Chem. Phys.* **1967,** *47*, 3681-2.
31. Newmark, R. A. Vicinal Fluorine–Fluorine Coupling Constants in Perfluoropropyl Groups. *J. Fluorine Chem.* **2009,** *130*, 389-393.
32. Harris, R. K.; Woodman, C. M. N.M.R. Spectra of Molecules Containing CF2 Groups. II. Perfluorobutane. *J. Mol. Spectrosc.* **1968,** *26*, 432-43.
33. Shreiber, S. T.; Scudder, J. J.; Vicic, D. A. $[(MeCN)_3Co(C_2F_5)_3]$: A Versatile Precursor to Cobalt(III) Perfluoroethyl Complexes. *Organometallics* **2019,** *38*, 3169-3173.
34. O. A. Tomashenko, V. V. Grushin. Aromatic Trifluoromethylation with Metal Complexes. *Chem. Rev.* **2011**, *111*, 4475-4521.
35. Xue, T.; Vicic, D. A. Routes to Acetonitrile-Supported Trifluoromethyl and Perfluorometallacyclopentane Complexes of Cobalt. *Organometallics* **2020,** *39*, 3715-3720.

Chapter 8: Synthesis, Structure, and Electrochemical Properties of $[LNi(R_f)(C_4F_8)]^-$ Complexes

The following chapter has been adapted and reproduced with permission from: Shreiber, S.T.; Amin, F.; Schäfer, S.A.; Cramer, R. E.; Klein, A.; Vicic, D.A. Synthesis, Strucure, and Electrochemical Properties of $[LNi(R_f)(C_4F_8)]^-$ and $[LNi(R_f)_3]^-$ Complexes. *Dalton Trans.* **2022**, *advance article* (doi.org/10.1039/D2DT00511E).

8.1 Abstract: The new anionic nickelate complexes $[(MeCN)Ni(C_4F_8)(CF_3)]^-$, $[(MeCN)Ni(C_4F_8)(C_2F_5)]^-$, $[(IMes)Ni(C_4F_8)(CF_3)]^-$, and $[(IMes)Ni(CF_3)_3]^-$ (IMes = 1,3-bis(2,4,6-trimethylphenyl)imidazol-2-ylidene) were synthesized and structurally characterized. The electrochemical properties of all new compounds were revealed by cyclic voltammetry studies and compared to the known CF_3 analogue $[(MeCN)Ni(CF_3)_3]^-$. The IMes-coordinated complexes exhibited initial oxidation events that were well-separated from any other oxidations in the cyclic voltammograms, suggesting that the NHC ligand environment (NHC = *N*-heterocyclic carbene) is an interesting platform for the development of new redox-triggered reactions that release trifluoromethyl and perfluoroalkyl radicals upon oxidation.

8.2 Introduction: Nickel is a promising platform for the development of new synthetic methodologies involving fluoroalkyl groups. Two fundamentally different ways for nickel to mediate carbon-carbon(fluoroalkyl) bond forming reactions are shown in Scheme 8a. It is known that low valent nickel can react with perfluoroalkyl electrophiles to generate perfluoroalkyl radicals (Scheme 8a, eq 1), which can in turn undergo additions to a variety of organic substrates like alkenes. Catalytic fluoroalkylations of this type have been demonstrated with nickel for both the trifluoromethyl[1-4] and fluoroalkyl[4-7] groups. Another mechanistic pathway for carbon-carbon(fluoroalkyl) bond forming reactions involves a

discrete reductive elimination event as described in Scheme 8a, eq 2. Catalysis involving putative reductive eliminations at nickel are only known for fluoroalkyl[8-11] and difluoromethyl,[12-14] but not for trifluoromethyl. Stoichiometric reductive eliminations involving trifluoromethyl groups have been demonstrated for high-valent [Ni(R)(CF_3)] complexes,[15-19] but to our knowledge these elimination reactions have not been included in catalytic transformations at nickel.

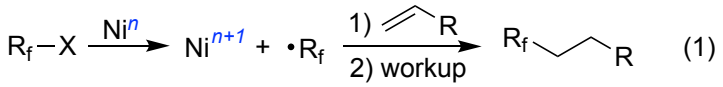

catalysis observed for $R_f = CF_3$ and fluoroalkyl

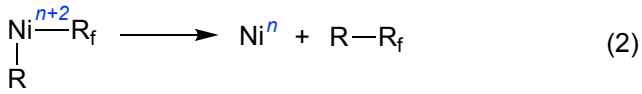

catalysis observed for R_f = fluoroalkyl only

Scheme 8a. Routes for enabling fluoroalkylation of organic molecules with nickel.

Our group has been developing the use of solvento complexes of nickel as reagents for the trifluoromethylation of organic electrophiles, and we have recently shown that $[(MeCN)Ni(R_f)_3]^-$ (R_f = CF_3, C_2F_5) reacts with aryl iodonium, alkynyl iodonium, and diazonium salts to afford fluoroalkylated arenes in moderate to good yields.[16, 20] Further studies have shown that the homoleptic $[Ni(CF_3)_4]^{2-}$ can catalyze C-H bond trifluoromethylations of electron-rich (hetero)arenes in up to 99% yield (Scheme 8b, also see Chapter 7).[20] One modification to this system that we sought to explore was the replacement of two of the spectator trifluoromethyl groups with a chelating C_4F_8 ligand. The motivation behind this change is that we[21-22] and others[23] have demonstrated that high-valent [Ni(C_4F_8)] complexes are oxidatively more stable than [Ni(CF_3)$_2$] derivatives and do not readily suffer from reductive homolyses reactions that often occurs with the [Ni(CF_3)$_2$] counterparts. The C_4F_8 ligand also appears to be less sensitive to α-fluoride

abstraction processes with trace amounts of Lewis acids relative to trifluoromethyl derivatives, which in turn renders the C_4F_8 complexes more stable towards adventitious water.[24-25] Only when very strong Lewis acids are used, such as BCl_3, BF_3, and Me_3SiOTf, have fluoride abstractions at the C_4F_8-containing metallacycle been reported.[26-27] Well-defined nickel(III) and nickel(IV) species with the C_4F_8 ligand have now been reported to be robust enough to be isolated and stored on the benchtop.[22-23] Given the aforementioned qualities of the C_4F_8 ligand, we targeted the synthesis of $[(L)Ni(R_f)(C_4F_8)]^-$ in order to characterize their chemical and electrochemical properties with their non-chelating fluoroalkyl counterparts.

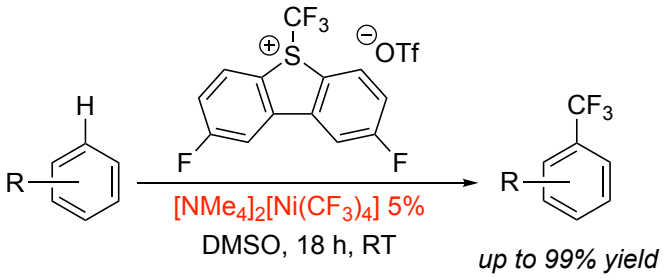

Scheme 8b. Catalytic trifluoromethylation of heteroarenes using a homoleptic trifluoromethyl nickel catalyst

8.3 Results and Discussion

8.3.1. Synthesis of C_4F_8 Derivatives: Complexes of the type $[(MeCN)Ni(C_4F_8)(R_f)]^-$ (**8b** and **8c** (Scheme 8c)). were successfully prepared by reacting the known[28] $[(MeCN)_2Ni(C_4F_8)]$ (**8a**) with $Me_3Si\text{-}R_f$ (R_f = CF_3 or C_2F_5) in the presence of AgF and NMe_4Cl. Complex **8b** displays a diagnostic ^{19}F NMR signal for the Ni-CF_3 resonance at δ = –31.4 (quintet, J = 3.5 Hz) in acetonitrile solvent, whereas the CF_3 resonance of the perfluoroethyl ligand in complex **8c** occurred at δ = –82.5 (t, J = 3.8 Hz, 3F). The structures of complexes **8b** and **8c** were further confirmed by X-ray crystallography, and ORTEP diagrams are provided in Figure 8a. Both complexes adopt a square-planar geometry in

the solid state, with the carbon-nickel-carbon angles of the perfluoro-metallacyclopentane units slightly smaller than any other angles in the square planes involving the nickel centers. The acetonitrile ligands in **8b** and **8c** are clearly less trans influencing than the fluoroalkyl ligands, and the CF_2 groups that are spatially opposing the acetonitriles in both structures bear the shortest nickel-carbon bonds. Note: The synthesis of **8b** and **8c** was originally done by Fatema Amin.

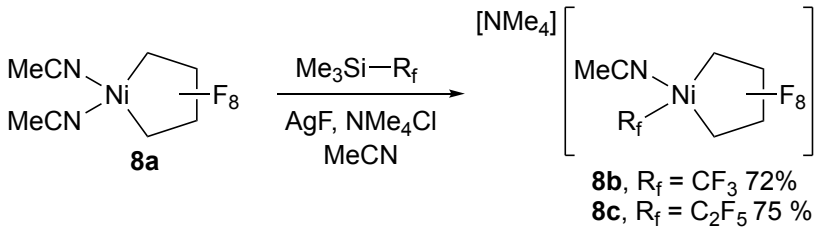

Scheme 8c. Synthesis of R_f derivatives of Ni(II)-C_4F_8.

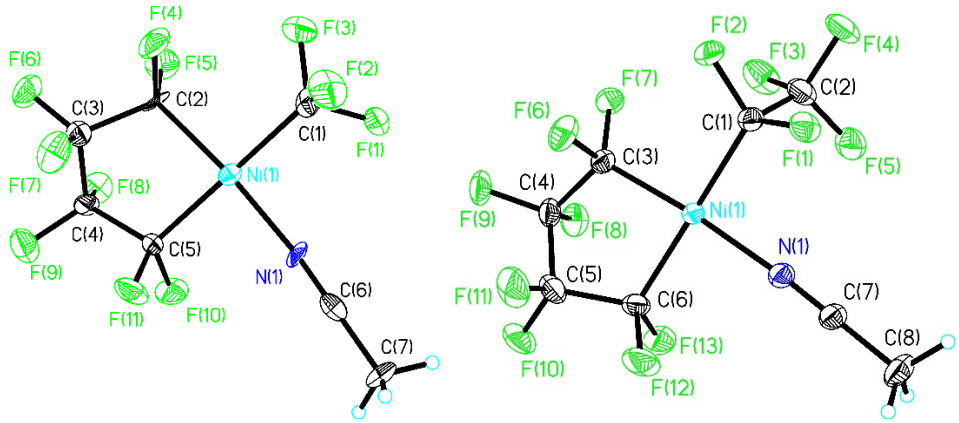

Figure 8a. ORTEP diagram of **8b** (left) and **8c** (right). Ellipsoids shown at the 40% level. **2:** Counter-ions and co-crystallized solvents are omitted for clarity. Selected bond lengths (Å) for **8b**: Ni1-N1 1.895(3); Ni1-C2 1.897(4); Ni1-C5 1.934(4); Ni1-C1 1.957(4); N1-C6 1.137(5). Selected bond angles (°) for **8b**: N1-Ni1-C2 170.67(15); N1-Ni1-C5 89.31(15); C2-Ni1-C5 86.91(16); N1-Ni1-C1 92.09(14); C2-Ni1-C1 92.38(15); C5-Ni1-C1 175.10(17); C6-N1-Ni1 173.3(4). Selected bond lengths (Å) for **8c**: Ni1-N1 1.8938(15); Ni1-C3 1.8967(18); Ni1-C6 1.9330(19); Ni1-C1 1.9556(18); N1-C7 1.136(2). Selected bond angles (°) for **8c**: N1-Ni1-C3 174.49(7); N1-Ni1-C6 88.14(7); C3-Ni1-C6 86.69(8); N1-Ni1-C1 91.65(7); C3-Ni1-C1 93.64(8); C6-Ni1-C1 176.16(8); C7-N1-Ni1 176.16(8).

8.3.2. Electrochemistry of Ni-C_4F_8 Complexes: The electrochemical properties of complexes **8a**, **8b** and **8c** were investigated by cyclic voltammetry, and the results are

shown in Figure 8b. Oxidation of **8a** is quasi-reversible, with a peak potential for oxidation at +0.39 V vs the Fc/Fc^+ couple (Figure 8b, black line). The oxidation of **8a** occurs at a peak potential much less positive than for the related trifluoromethyl derivative $[(MeCN)_2Ni(CF_3)_2]$, which occurs at +0.76 V, indicating that the trifluoromethyl group is more globally stabilizing in this family of complexes. Similar trends in the redox properties of C_4F_8 vs CF_3 complexes of nickel bipyridine[21, 29] and terpyridine[22, 30] have been reported. The large differences in these baseline values for the C_4F_8 and CF_3 parent nickel complexes appear to play a role in the degree to which anation affects the oxidation potentials of derivatives bearing an additional trifluoromethyl or perfluoroalkyl group. For instance, we show here that the oxidation peak potentials of the C_4F_8-bearing anionic complexes **8b** and **8c** display only minor differences (+0.53 V and +0.63 V, Figure 8b, red and blue lines, respectively), and that anation confers a slight stabilization relative to the parent $[(MeCN)_2Ni(C_4F_8)]$ complex with respect to oxidation. Addition of formally anionic trifluoromethyl ligands to the parent $[(MeCN)_2Ni(CF_3)_2]$ complex, however, is known to result in complexes that are easier to oxidize. For instance, $[(MeCN)Ni(CF_3)_3]^-$ and $[Ni(CF_3)_4]^{2-}$ display peak potentials at +0.38 and +0.10 V, respectively, far removed from the potential needed to oxidize $[(MeCN)_2Ni(CF_3)_2]$ (+0.76 V).[16] The irreversibility of the waves for **8b** and **8c** in Figure 8b is believed to be a result of fast reductive homolysis of CF_3 and C_2F_5 radicals from electrogenerated nickel(III) intermediates.[16, 20]

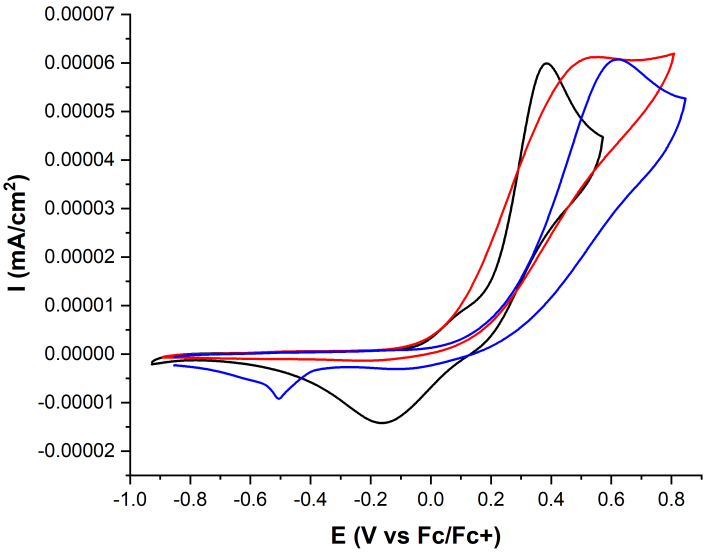

Figure 8b. Cyclic voltammograms of **8a** (black), **8b** (red), and **8c** (blue) in MeCN. Metal complex, 10 mM; electrolyte, 100 mM $[NBu_4][PF_6]$; working and counter electrode, platinum; silver psuedoreference; scan rate, 100 mV/s.

8.3.3. Catalysis with Solvated Ni-C_4F_8 Complex: Because the oxidation of complex **8b** is within the window of common oxidants,[31] we examined if **8b** could also serve as a catalyst for the C-H bond trifluoromethylation of arenes as described in Scheme 8d. Indeed, reaction of 1,3,5-trimethoxybenzene with Umemoto Reagent II in DMSO solvent with 5 mol% **8b**, yielded trifluoromethylated product in 83 % yield (Scheme 8d). For comparison, the non-chelated $[(MeCN)Ni(CF_3)_3]^-$ gave a 78 % yield of product in a prior report, and the dianionic $[Ni(CF_3)_4]^{2-}$ afforded product in 96 % yield (See Chapter 7).[20]

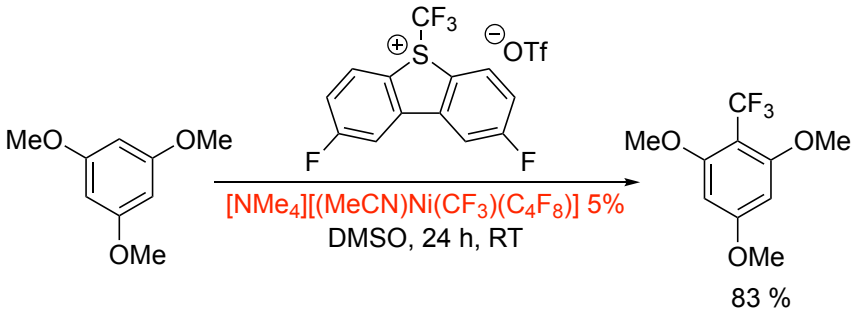

Scheme 8d. Catalytic trifluoromethylation with **8b**.

8.3.4. Synthesis of Ligated Nickel Fluoroalkyl Complexes and the Effect on Electrochemical Properties: The effect of ligands on the electronic properties of the nickelates was then explored in order to understand how the redox properties of the nickelates may be further tuned. Reaction of **8b** with the *N*-heterocyclic carbene IMes in acetonitrile solution led to the formation of the ligated $[(IMes)Ni(CF_3)(C_4F_8)]^-$ (**8d**) in 69 % yield (Scheme 8e). The ^{19}F NMR spectrum of **8d** in CD_3CN reveals the diagnostic Ni-CF_3 resonance at $\delta = -23.2$ (br s, 3F). A preliminary X-ray structure confirming the connectivity of compound **8d** was also obtained and is provided in Appendix G. The electrochemical properties of **8d** were examined, and the cyclic voltammogram data is shown in Figure 8c (orange line). Complex **8d** has a first peak potential at +0.30 V vs the Fc/Fc+ couple, which is 0.23 V easier to oxidize than the solvento complex $[(MeCN)Ni(C_4F_8)(CF_3)]^-$ (**8b)**. Thus, the greater electron donating ability of the NHC ligand relative to the acetonitrile is readily observable for these nickelate species by cyclic voltammetry. More interesting, however, is the result that complex **8d** exhibits a well-formed oxidation peak at +1.13 V, whereas complexes **8a-8c** do not (Figure 8c, orange line vs. black and red). We suggest that upon electrooxidation of **8d**, the resulting $[(IMes)Ni^{III}(C_4F_8)(CF_3)]$ eliminates a CF_3 radical to afford the three-coordinate[27]and charge neutral $[(IMes)Ni^{II}(C_4F_8)]$, and the oxidation wave at +1.13 V corresponds to the oxidation of the $[(IMes)Ni^{II}(C_4F_8)]$. We speculate that the differences in coordination numbers between $[(IMes)Ni(C_4F_8)]$ and $[(IMes)Ni(CF_3)(C_4F_8)]^-$ contributes to the separation of the oxidation peaks.

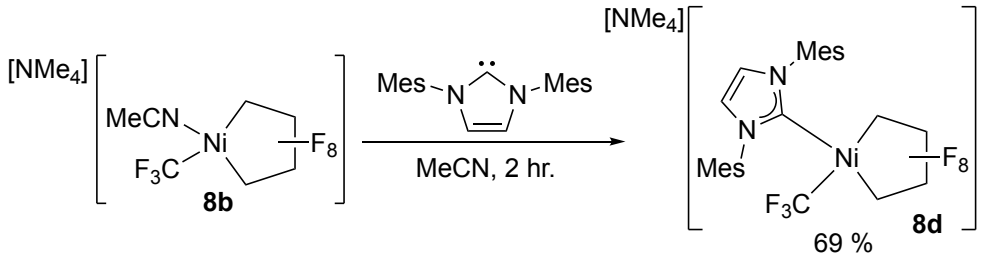

Scheme 8e. Synthesis of NHC ligated **8d**.

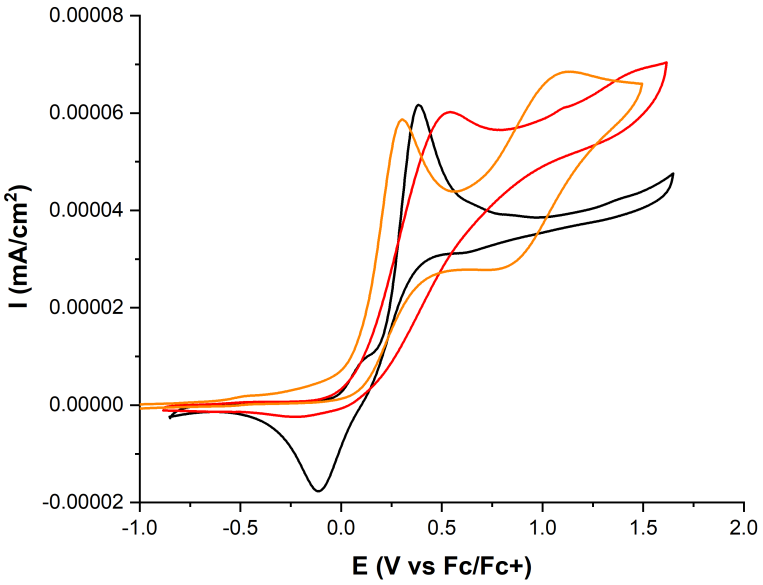

Figure 8c. Cyclic voltammograms of **8a** (black), **8b** (red), and **8d** (orange) in MeCN. Metal complex, 10 mM; electrolyte, 100 mM $[NBu_4][PF_6]$; working and counter electrode, platinum; silver psuedoreference; scan rate, 100 mV/s.

For comparison with $[(IMes)Ni(CF_3)(C_4F_8)]^-$, we have also prepared the non-C_4F_8 analogue $[(IMes)Ni(CF_3)_3]^-$ (**8f**). Reaction of the solvento complex **8e** with IMes in acetonitrile solvent cleanly led to the formation of **8f** in 66% yield (Scheme 8f). The ^{19}F NMR of **8f** displayed a reversal in the relative positions of the different trifluoromethyl groups with respect to **8e**, with the equivalent trans CF_3 groups resonating at higher frequencies (δ –22.9 (q, J = 5.3 Hz, 6F) and –26.8 (sept, J = 5.3 Hz, 3F). Complex **8f** was also structurally characterized, and the ORTEP diagram is shown in Figure 8d. The X-ray data show that the strongly donating NHC ligand of **8f** exhibits much more of a trans effect

than the acetonitriles in complexes **8b** and **8c**, as the CF_3 group that is trans to the NHC bears a nickel-carbon distance that is more on par with the two symmetrically equivalent CF_3 groups that are trans to each other.

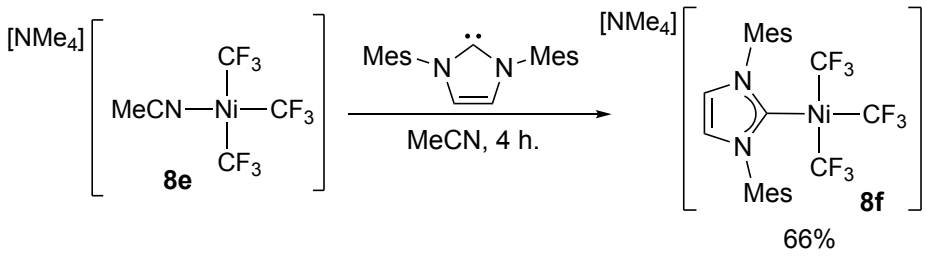

Scheme 8f. Synthesis of NHC ligated **8f**.

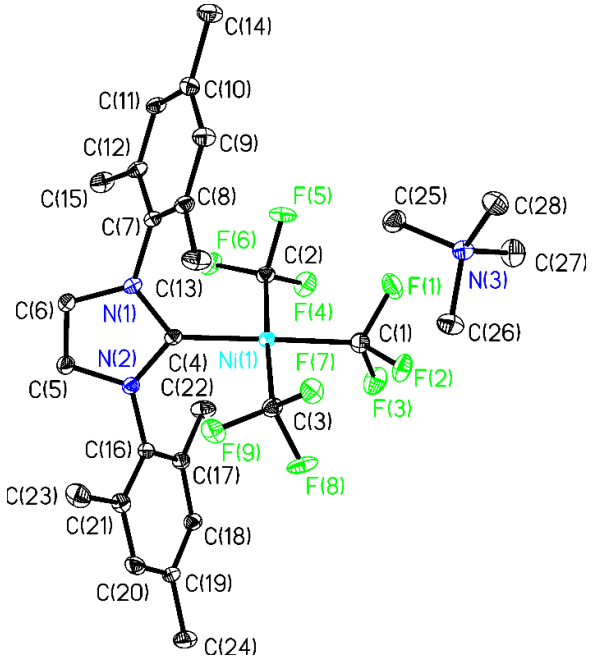

Figure 8d. ORTEP diagram of **8f.** Ellipsoids shown at the 40% level. Selected bond lengths (Å): Ni1-C4 1.923(5); Ni1-C1 1.939(5); Ni1-C2 1.949(5); Ni-C3 1.959(5); N1-C4 1.369(6); N2-C4 1.378(6). Selected bond angles (°) for **6**: C4-Ni1-C1 176.6(2); C4-Ni1-C2 90.6(2); C1-Ni1-C2 87.7(2); C4-Ni1-C3 91.8(2); C1-Ni1-C3 90.0(2); C2-Ni1-C3 177.5(2); N1-C4-N2 102.9(4).

The cyclic voltammogram of **8f** is shown in Figure 8e (blue line). The first peak potential was found to be +0.28 V vs the Fc/Fc+ couple, a value very similar to the solvento complex $[(MeCN)Ni(CF_3)_3]^-$ (**8e**) (Figure 8e, black line). Thus, a comparison of Figures 8c and 8e reveals that the C_4F_8 ligand had more of an effect on the potential of the first oxidation of

the anionic nickelates than the NHC ligand relative to the parent complex **8e**. The known **8e** displays two closely spaced oxidation peaks,[16] and Figure 8e highlights the changes in the redox profiles that ensue upon coordination of the NHC ligand to afford **8f**. The second oxidation peak for **8f** is widely separated from the first peak and occurs at +1.16 V, which is similar to **8d** but in contrast to **8e**. Therefore, the peak separations are inherently related to the NHC ligand, and not the nature of the perfluoroalkyl substituents. This ability to significantly separate the two oxidation events by the addition of ancillary ligands like NHCs bodes well for preventing over-oxidation pathways during the optimization of new electrochemical methods that rely on one electron oxidations of $[LNi(R_f)_3]^-$ derivatives in order to release R_f radicals.

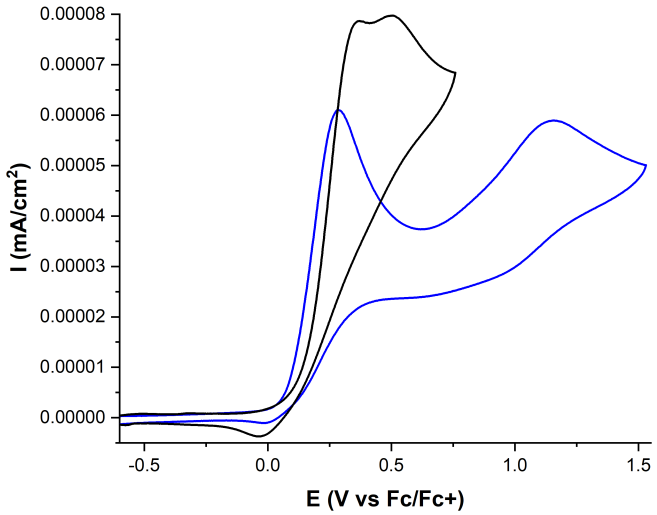

Figure 8e. Cyclic voltammograms of **8e** (black), and **8f** (blue) in MeCN. Metal complex, 10 mM; electrolyte, 100 mM $[NBu_4][PF_6]$; working and counter electrode, platinum; silver psuedoreference; scan rate, 100 mV/s.

8.4 Conclusions: The modularity of the $[L_2Ni(R_f)_2]$ and $[LNi(R_f)_3]^-$ system was exploited in order to reveal the electrochemical properties of derivatives that bear different perfluoroalkyl substituents as well as different dative ligands. Significant differences in

oxidation potentials were observed for the charge neutral $[(MeCN)_2Ni(C_4F_8)]$ versus $[(MeCN)_2Ni(CF_3)_2]$, with the former being much easier to oxidize. Anation to afford $[(MeCN)Ni(C_4F_8)(R_f)]^-$ (R_f = CF_3 or C_2F_5) and $[(MeCN)Ni(CF_3)_3]^-$ however, showed somewhat of a leveling effect where the different anionic complexes displayed similar oxidation potentials. In terms of reactivity, both $[(MeCN)Ni(CF_3)_3]^-$ and $[(MeCN)Ni(C_4F_8)(CF_3)]^-$ catalyze the trifluoromethylation of an electron rich arene with similar yields using Umemoto Reagent II as the electrophile. The cyclic voltammograms of the anionic derivatives can be significantly tuned by the replacement of the acetonitrile ligands with the NHC ligand IMes. The first oxidation potentials of $[(IMes)Ni(CF_3)_3]^-$ and $[(IMes)Ni(C_4F_8)(CF_3)]^-$ complexes were similar to that seen for $[(MeCN)Ni(CF_3)_3]^-$, but an oxidation wave occurring at more positive potentials was well-separated only for the NHC-containing derivatives. This identification of a ligand environment that better separates oxidation potentials in the anionic nickel perfluoroalkyl complexes is expected to aid in the development of new (electro)catalytic methods that target single electron oxidations in order to release trifluoromethyl and perfluoroalkyl radicals.

8.5. Experimental

8.5.1. General Information: All manipulations were performed using standard Schlenk and high vacuum techniques or in a nitrogen filled glovebox, unless otherwise stated. Solvents were purified by passing through activated alumina and/or copper in a solvent purification system supplied by Pure Process Technology. Solution ^1H NMR spectra were recorded at ambient temperature on a Bruker 400 MHz spectrometer and referenced to residual proton solvent signals. ^{19}F spectra were recorded on the Bruker NMR spectrometer operating at 376 MHz and referenced to α,α,α-trifluorotoluene as an internal standard (δ =

-63.7). A Bruker D8 Quest diffractometer was used for X-ray crystal structure determinations. Cyclic voltammetry data was collected in a nitrogen filled glovebox at room temperature on a PARSTAT 4000A potentiostat. The CCDC 2124819, 2124820, and 2124821 contain the supplementary crystallographic data for this paper. These data can be obtained free of charge via www.ccdc.cam.ac.uk/data_request/cif, or by e-mailing data_request@ccdc.cam.ac.uk, or by contacting The Cambridge Crystallographic Data Centre, 12 Union Road, Cambridge CB2 1EZ, UK; fax: +44 1223 336033.

8.5.2. Preparation of [NMe_4][$(MeCN)(CF_3)Ni(C_4F_8)$] (8b): In a nitrogen filled glovebox, AgF (111 mg, 0.875 mmol, 1 equiv.) and TMS-CF_3 (0.20 mL, 1.3 mmol, 1.5 equiv.) were stirred in 10 mL of anhydrous MeCN for 2 h. A solution of [$(MeCN)_2Ni(C_4F_8)$] (298 mg, 0.874 mmol, 1 equiv.) in 1 mL of anhydrous MeCN was added dropwise to the reaction mixture followed by addition of NMe_4Cl (91 mg, 0.87 mmol, 1 equiv). The reaction was stirred for one day at room temperature and filtered through a pad of celite. The resulting black-red solution was dried in vacuo to a dark brown paste. The paste was dissolved in a minimal amount of THF followed by the addition of pentane and cooling to -30 °C. The resulting black/brown solid was washed with pentane and dried under vacuum. Yield: 278 mg (72%). X-ray quality crystals were grown by cooling a saturated solution of THF. ^{1}H NMR (CD_3CN, 400 MHz): δ 3.07 (s, 12H). ^{19}F NMR (CD_3CN, 376 MHz): δ –31.4 (quintet, J = 3.5 Hz, 3F), –109.3 (app decet, J = 4.1 Hz, 2F), –117.3 (apparent octet, J = 3.6 Hz, 2F), –139.0 to –139.3 (m, 2F), –141.0 to –141.1 (m, 2F). Anal. Calcd (found) for $C_{11}H_{15}NiF_{11}N_2$: C, 29.83 (29.60); H, 3.41 (3.69). (Originally prepared by Fatema Amin)

8.5.3. Preparation of [NMe_4][$(MeCN)(CF_3CF_2)Ni(C_4F_8)$] (8c): In a nitrogen filled glovebox, AgF (106 mg, 0.835 mmol, 1.05 equiv.) and TMS-C_2F_5 (0.21 mL, 1.2 mmol,

1.5 equiv) were stirred in 10 mL of anhydrous MeCN for 2 h. A solution of the [(MeCN)$_2$Ni(C$_4$F$_8$)] (271 mg, 0.795 mmol, 1 equiv) in 1 mL of anhydrous MeCN was added dropwise to the reaction mixture followed by addition of NMe$_4$Cl (88 mg, 0.795 mmol, 1 equiv.). The reaction was stirred for 2 days at room temperature and filtered through a pad of celite. The resulting brown solution was dried in vacuo. The paste was dissolved in a minimal amount of THF followed by the addition of pentane and cooling to -30°C. The black/brown solid was washed with pentane and dried under vacuum. Yield: 293 mg (75%). ^{1}H NMR (CD$_3$CN, 400 MHz): δ 3.07 (s, 12H) ^{19}F NMR (CD$_3$CN, 376 MHz): δ −82.5 (t, *J* = 3.8 Hz, 3F), –110.2 (app tetradecet, *J* = 3.7 Hz, 2F), –112.1 (app t, *J* = 6.8 Hz, 2F), –116.6 (app sextet, *J* = 3.9 Hz, 2F), –139.2 to –139.4 (m, 2F), –140.9 to –141.1 (m, 2F). Anal. Calcd (found) for C$_{12}$H$_{15}$NiF$_{13}$N$_2$: C, 29.24 (29.10); H, 3.07 (3.21). (Originally prepared by Fatema Amin)

8.5.4. Preparation of [NMe$_4$][(IMes)(CF$_3$)Ni(C$_4$F$_8$)] (8d): In a nitrogen filled glovebox, to a stirring solution of [NMe$_4$][(MeCN)(CF$_3$)Ni(C$_4$F$_8$)] (81 mg, 0.18 mmol, 1 equiv.) in 0.5 mL of MeCN, a solution of IMes (69 mg, 0.23 mmol, 1.3 equiv.) in 1.5 mL of MeCN was added and stirred for 2 hours. The reaction was filtered over a pad of celite and the solvents were removed under vacuum. The resulting solid was collected and washed with ether to yield 88 mg of black solid (69%). ^{1}H NMR (CD$_3$CN, 400 MHz): δ 7.11 (br s, 1H), 7.06 (br s, 2H), 7.00 (br s, 2H), 3.06 (br s, 12H), 2.37 – 2.33 (br m, 6H), 2.26 (br s, 6H), 2.17 (br s, 6H). ^{19}F NMR (CD$_3$CN, 376 MHz): δ -23.2 (br s, 3F), -109.5 (s, 2F), -113.0 to - 113.1 (m, 2F), –138.5 to –138.8 (m, 2F), –139.3 to –139.6 (m, 2F). Anal. Calcd (found) for C$_{30}$H$_{36}$NiF$_{11}$N$_3$: C: 51.02 (53.55); H 5.14 (5.69). A better elemental analysis of this

compound could not be obtained, likely due to co-crystallized solvent, as was found in the preliminary X-ray data set (see Supporting Information).

8.5.5. Preparation of [NMe_4][(IMes)Ni(CF_3)$_3$] (8f): In a glovebox, to a stirring solution of [NMe_4][(MeCN)Ni(CF_3)$_3$] (60 mg, 0.16 mmol, 1 equiv.) in 0.5 mL of MeCN, a solution of IMes (58 mg, 0.19 mmol, 1.2 equiv.) in 1.5 mL of MeCN was added and stirred for 4 hours. The insoluble were removed, and the volatiles were removed under vacuum. The precipitate was collected and washed with ether to yield 68 mg (66%) of light yellow solid. ^{1}H NMR (CD_3CN, 376 MHz): δ 7.05 (s, 2H), 7.03 (br s, 4H), 3.07 (br s, 12H), 2.36 (s, 6H), 2.28 (s, 12H). ^{19}F NMR (CD_3CN, 376 MHz): δ -22.9 (q, J = 5.3 Hz, 6F), -26.8 (sept, J = 5.3 Hz, 3F). Anal. Calcd (found) for $C_{28}H_{36}NiF_9N_3$: C, 52.20 (52.07); H, 5.63 (5.55).

8.5.6. Catalytic Trifluoromethylation of 1,3,5-trimethoxybenzene: In a nitrogen filled glovebox, a vial was charged with 1,3,5-trimethoxybenzene (42 mg, 0.25 mmol, 5 equiv.), Umemoto Reagent II (22 mg, 0.050 mmol, 1 equiv.), and 0.9 mL of DMSO. While stirring, 100 μL of a 0.025 M stock solution of [NMe_4][(MeCN)(CF_3)Ni(C_4F_8)] in DMSO was added, and the reaction was continued to stir for 24 hours. Trifluorotoluene (6.14 μL, 0.0500 mmol, 1 equiv.) was added as an internal standard and the ^{19}F NMR was recorded. The NMR yield of the trifluoromethylated arene was determined to be 83%.

8.6 References

1. Mikhaylov, D. Y.; Budnikova, Y. H.; Gryaznova, T. V.; Krivolapov, D. V.; Litvinov, I. A.; Vicic, D. A.; Sinyashin, O. G. Electrocatalytic Fluoroalkylation of Olefins. *J. Organomet. Chem.* **2009,** *694*, 3840-3843.
2. Meucci, E. A.; Nguyen, S. N.; Camasso, N. M.; Chong, E.; Ariafard, A.; Canty, A. J.; Sanford, M. S. Nickel(IV)-Catalyzed C-H Trifluoromethylation of (Hetero)arenes. *J. Am. Chem. Soc.* **2019,** *141*, 12872-12879.
3. Wu, Y.; Zhang, H.-R.; Jin, R.-X.; Lan, Q.; Wang, X.-S. Nickel-Catalyzed C-H Trifluoromethylation of Electron-Rich Heteroarenes. *Advanced Synthesis & Catalysis* **2016,** *358*, 3528-3533.

4. Zhang, S.; Weniger, F.; Ye, F.; Rabeah, J.; Ellinger, S.; Zaragoza, F.; Taeschler, C.; Neumann, H.; Brueckner, A.; Beller, M. Selective Nickel-Catalyzed Fluoroalkylations of Olefins. *Chem. Commun.* **2020,** *56*, 15157-15160.
5. Xu, C.; Yang, Z.-F.; An, L.; Zhang, X. Nickel-Catalyzed Difluoroalkylation-Alkylation of Enamides. *ACS Catal.* **2019,** *9*, 8224-8229.
6. Xu, C.; Cheng, R.; Luo, Y.-C.; Wang, M.-K.; Zhang, X. Trans-Selective Aryldifluoroalkylation of Endocyclic Enecarbamates and Enamides by Nickel Catalysis. *Angew. Chem. Int. Ed.* **2020,** *59* , 18741-18747.
7. Zhou, M.; Zhao, H.-Y.; Zhang, S.; Zhang, Y.; Zhang, X. Nickel-Catalyzed Four-Component Carbocarbonylation of Alkenes under 1 atm of CO. *J. Am. Chem. Soc.* **2020,** *142*, 18191-18199.
8. Xiao, Y.-L.; Guo, W.-H.; He, G.-Z.; Pan, Q.; Zhang, X. Nickel-Catalyzed Cross-Coupling of Functionalized Difluoromethyl Bromides and Chlorides with Aryl Boronic Acids: A General Method for Difluoroalkylated Arenes. *Angew. Chem. Int. Ed.* **2014,** *53*, 9909-9913.
9. An, L.; Xu, C.; Zhang, X. Highly Selective Nickel-Catalyzed Gem-Difluoropropargylation of Unactivated Alkylzinc Reagents. *Nature Communications* **2017,** *8*, 1460.
10. He, X.; Gao, X.; Zhang, X. Nickel-Catalyzed Difluoroalkylation of (Hetero)aryl Bromides with Unactivated 1-Bromo-1,1-difluoroalkanes. *Chin. J. Chem.* **2018,** *36*, 1059-1062.
11. Zhao, H.-Y.; Gao, X.; Zhang, S.; Zhang, X. Nickel-Catalyzed Carbonylation of Difluoroalkyl Bromides with Arylboronic Acids. *Org. Lett.* **2019,** *21*, 1031-1036.
12. Fu, X.-P.; Xiao, Y.-L.; Zhang, X. Nickel-Catalyzed Difluoromethylation of Arylboronic Acids with Bromodifluoromethane. *Chinese Journal of Chemistry* **2018,** *36*, 143-146.
13. Xu, C.; Guo, W.-H.; He, X.; Guo, Y.-L.; Zhang, X.-Y.; Zhang, X. Difluoromethylation of (Hetero)aryl Chlorides with Chlorodifluoromethane Catalyzed by Nickel. *Nat. Commun.* **2018,** *9*, 1-10.
14. Gao Xing, H. X. Z. X. Nickel-Catalyzed Difluoromethylation of (Hetero)aryl Bromides with $BrCF_2H$. *Chinese Journal of Organic Chemistry* **2019,** *39*, 215-222.
15. Hu, W.-Q.; Pan, S.; Xu, X.-H.; Vicic, D. A.; Qing, F.-L. Nickel-Mediated Trifluoromethylation of Phenol Derivatives by Aryl C-O Bond Activation. *Angew. Chem., Int. Ed.* **2020,** *59*, 16076-16082.
16. Shreiber, S. T.; DiMucci, I. M.; Khrizanforov, M. N.; Titus, C. J.; Nordlund, D.; Dudkina, Y.; Cramer, R. E.; Budnikova, Y.; Lancaster, K. M.; Vicic, D. A. $[(MeCN)Ni(CF_3)_3]^-$ and $[Ni(CF_3)_4]^{2-}$: Foundations toward the Development of Trifluoromethylations at Unsupported Nickel. *Inorg. Chem.* **2020,** *59*, 9143-9151.
17. Ferguson, D. M.; Bour, J. R.; Canty, A. J.; Kampf, J. W.; Sanford, M. S. Aryl–CF_3 Coupling from Phosphinoferrocene-Ligated Palladium(II) Complexes. *Organometallics* **2019,** *38*, 519-526.
18. Bour, J. R.; Camasso, N. M.; Sanford, M. S. Oxidation of Ni(II) to Ni(IV) with Aryl Electrophiles Enables Ni-Mediated Aryl-CF_3 Coupling. *J. Am. Chem. Soc.* **2015,** *137*, 8034-8037.

19. Bour, J. R.; Camasso, N. M.; Meucci, E. A.; Kampf, J. W.; Canty, A. J.; Sanford, M. S. Carbon–Carbon Bond-Forming Reductive Elimination from Isolated Nickel(III) Complexes. *J. Amer. Chem. Soc.* **2016,** *138*, 16105-16111.
20. Shreiber, S. T.; Vicic, D. A. Solvated Nickel Complexes as Stoichiometric and Catalytic Perfluoroalkylation Agents**. *Angewandte Chemie International Edition* **2021,** *60*, 18162-18167.
21. Kosobokov, M. D.; Sandleben, A.; Vogt, N.; Klein, A.; Vicic, D. A. Nitrogen–Nitrogen Bond Formation via a Substrate-Bound Anion at a Mononuclear Nickel Platform. *Organometallics* **2018,** *37*, 521-525.
22. Yu, S.; Dudkina, Y.; Wang, H.; Kholin, K. V.; Kadirov, M. K.; Budnikova, Y. H.; Vicic, D. A. Accessing Perfluoroalkyl Nickel(ii), (iii), and (iv) Complexes Bearing a Readily Attached [C_4F_8] Ligand. *Dalton Trans.* **2015,** *44*, 19443-19446.
23. Bour, J. R.; Ferguson, D. M.; McClain, E. J.; Kampf, J. W.; Sanford, M. S. Connecting Organometallic Ni(III) and Ni(IV): Reactions of Carbon-Centered Radicals with High-Valent Organonickel Complexes. *J. Amer. Chem. Soc.* **2019,** *141*, 8914-8920.
24. Lee, G. M.; Korobkov, I.; Baker, R. T. d8 Nickel and Palladium Difluorocarbenes Derived from Trifluoromethyl POCOP-type Pincer Complexes. *J. Organomet. Chem.***2017,** *847*, 270-277.
25. Xue, T.; Vicic, D. A. Routes to Acetonitrile-Supported Trifluoromethyl and Perfluorometallacyclopentane Complexes of Cobalt. *Organometallics* **2020,** *39*, 3715-3720.
26. Burch, R. R.; Calabrese, J. C.; Ittel, S. D. Fluoroorganometallic Chemistry: Carbon-Fluorine Bond Activation in Perfluorometallacyclopentane Complexes. *Organometallics* **1988,** *7*, 1642-8.
27. Andrella, N. O.; Sicard, A. J.; Gorelsky, S. I.; Korobkov, I.; Baker, R. T. A T-Shaped Ni[κ2-$(CF2)_4$-] NHC Complex: Unusual Csp3-F and M-CF Bond Functionalization Reactions. *Chem. Sci.* **2015,** *6*, 6392-6397.
28. Kaplan, P. T.; Xu, L.; Chen, B.; McGarry, K. R.; Yu, S.; Wang, H.; Vicic, D. A. Mild, Safe, and Versatile Reagents for $(CF_2)_n$ Transfer and the Construction of Fluoroalkyl-Containing Rings. *Organometallics* **2013,** *32*, 7552-7558.
29. Yamaguchi, Y.; Ichioka, H.; Klein, A.; Brennessel, W. W.; Vicic, D. A. Linear Bis(perfluoroalkyl) Complexes of Nickel Bipyridine. *Organometallics* **2012,** *31*, 1477-1483.
30. Zhang, C.-P.; Wang, H.; Klein, A.; Biewer, C.; Stirnat, K.; Yamaguchi, Y.; Xu, L.; Gomez-Benitez, V.; Vicic, D. A. A Five-Coordinate Nickel(II) Fluoroalkyl Complex as a Precursor to a Spectroscopically Detectable Ni(III) Species. *J. Am. Chem. Soc.* **2013,** *135*, 8141-8144.
31. Connelly, N. G.; Geiger, W. E. Chemical Redox Agents for Organometallic Chemistry. *Chemical Reviews* **1996,** *96*, 877-910.

Chapter 9: Transformation of Brucine into Trifluoromethyl Neobrucine Using the Homoleptic Nickel Catalyst $[Ni(CF_3)_4]^{2-}$

9.1 Abstract: The homoleptic trifluoromethyl nickel complex $[Ni(CF_3)_4]^{2-}$ catalyzes a stereoselective trifluoromethylation of brucine with Umemoto II reagent. The trifluoromethylation process proceeds with concomitant isomerization of its alkenyl double bond leading to a trifluoromethylated neobrucine-like derivative. A minor difunctionalization product was also detected from the reaction mixture, consistent with a radical addition process that is occurring in parallel. Stoichiometric reactions between the nickel(II) catalyst precursor and brucine led to no reaction. However, a stochiometric reaction with a high-valent nickel(IV) complex formed trifluoromethylated neobrucine, implicating its intermediacy.

9.2 Introduction: Brucine (**9a**) and strychnine (**9b**) are two of the major pharmacologically-active constituents of the evergreen tree *Strychnos nux vomica*. Therapeutic activity of these alkaloids towards a variety of ailments have been reported in both traditional and modern medicines,[1-3] but despite the broad pharmacological activities of brucine and strychnine, narrow therapeutic windows and central nervous system toxicities limit their uses in clinical applications.[4] Thus, the development of methods to derivatize **9a** and **9b** with various functionalities in order to find more active biologics remains an active area of research.[5] One locus of interest in terms of reactivity is the C_{20}-C_{22} region of **9a** and **9b**. It has long been known that the double bond at the C_{21}-C_{22} position of **9a** and **9b** can be rearranged with Raney nickel to provide **9c** and **9d** as described in Scheme 9a, eq a.[6] Other conditions can also mediate this isomerization.[2,7] While this double bond isomerization can proceed with high yields, to our knowledge a concomitant allylic

functionalization at the C_{22} position has never been reported. A metal-catalyzed process to difunctionalize the C_{21}-C_{22} double bond has been reported by Hartwig (Scheme 9a, eq b),[8] and we wondered if a complementary method to install a trifluoromethyl group at the C_{22} position with migration of the double bond to the C_{20}-C_{21} position as described in Scheme 9a, eq c would be possible.

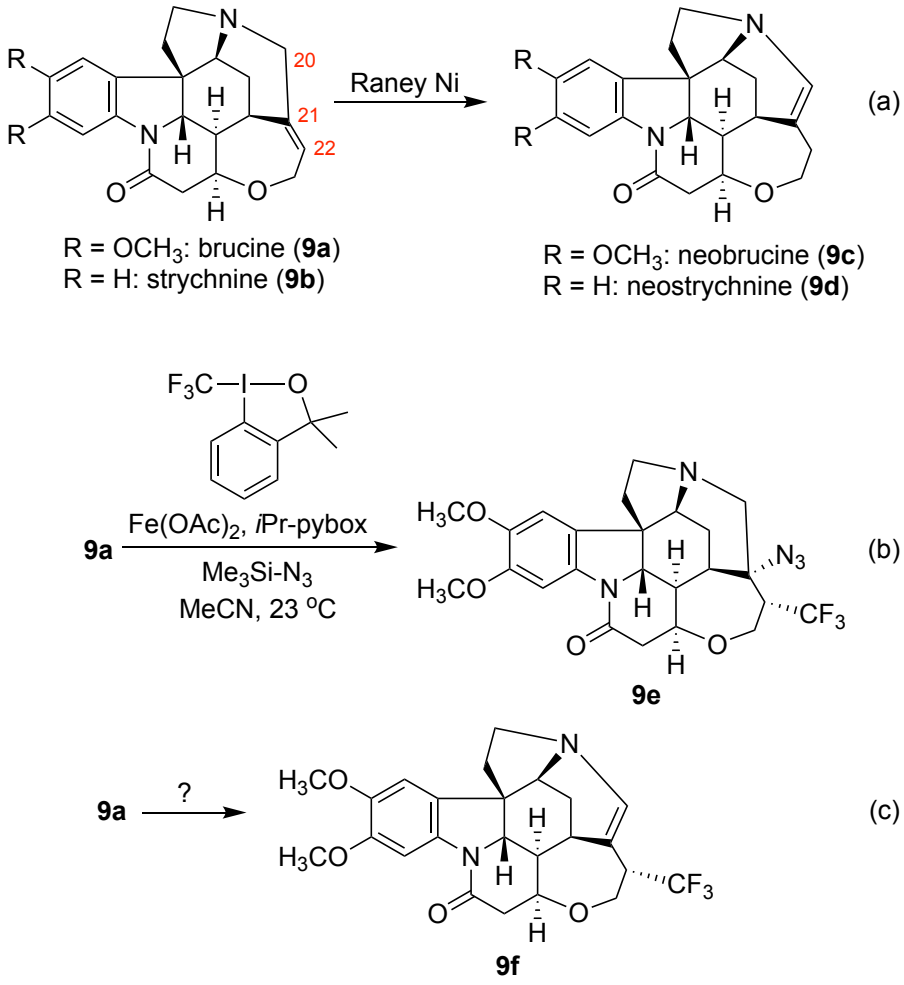

Scheme 9a. a) Transformation of brucine and strychnine into neo isomers b) Known difunctionalization of the olefin to generate trifluoromethyl brucine c) Unknown conditions to generate neo trifluoromethyl brucine.

Because of the success in using Raney nickel to mediate the olefin isomerization in Scheme 9a, eq a, we turned our attention to the use of nickel trifluoromethyl complexes to mediate

the transformation outlined in Scheme 9a, eq c. Recently, we reported the synthesis of the homoleptic $[NMe_4]_2[Ni(CF_3)_4]$ (**9g**), and showed that this simple trifluoromethyl nickel salt can catalytically trifluoromethylate electron rich arenes in the presence of the Umemoto II Reagent (**9h**) as described in Scheme 9b.[9,10] The substrates of that prior study did not possess any other alkene functionalities, and thus the reactivity of **9g** was selective for arene C-H trifluoromethylations. The presence of the C_{21}-C_{22} alkene in brucine, however, not only provides an opportunity to test the selectivity of **9g** towards arene verses alkene functionalizations, but also to evaluate the possibility of performing an olefin migration leading to net allylic functionalization as described in Scheme 9a, eq c.

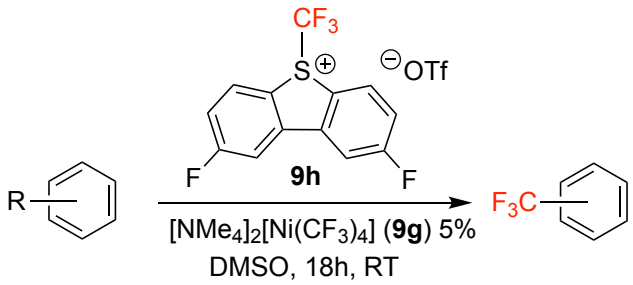

Scheme 9b. Catalytic trifluoromethylation of arene C-H bond using catalyst **9g**.

9.3 Results and Discussion

9.3.1. Initial Discovery and Optimizations for the Trifluoromethylation of Brucine: Reaction of various ratios of brucine (**9a**) with Umemoto II Reagent in the presence of nickel catalyst **9g** (Table 9a) did not lead to arene C-H functionalization when monitored by ^{19}F NMR spectroscopy. However, two unique doublets were evident in the ^{19}F NMR spectrum of the reaction mixture at δ -71.3 (d, J = 9.4 Hz) and δ -72.2 (d, J = 11.2 Hz), which were ultimately assigned to **9f** and **9i** (see below). Table 9a shows our efforts for optimizing this reaction based on using Umemoto II as the limiting reagent. The yields

reflect a proposed need for two equivalents of trifluoromethyl source to generate **9f** (one CF_3 to perform an addition reaction and another to perform a C-H abstraction) and one equivalent to generate **9i** through a simple radical addition reaction. Higher amounts of brucine relative to Umemoto II led to increased amounts of **9f** relative to **9i**, and the yields of **9f** can ultimately be raised to 81% with a brucine:Umemoto II of 2.5:1. Heating the reaction or use of excess **9h**, however, did not signifigantly increase yields (see Appendix H for full optimization tables).

Table 9a. Optimization for the trifluoromethylation of brucine[a]

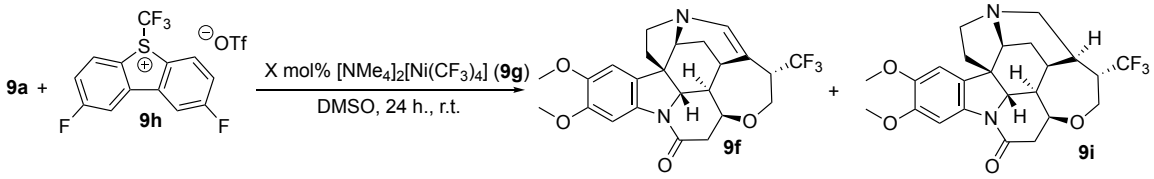

Entry	equiv brucine	Ni Catalyst	Yield **9f**	Yield **9i**
1	0.5	5 mol%	29%	7%
2	0.5	0 mol%	8%	3%
3	1	5 mol%	38%	9%
4	2.5	5 mol%	58%	10%
5	1	10 mol%	59%	10%
6	**2.5**	**10 mol%**	**81%**	**12%**

[a] Reactions were run in 1 mL of DMSO with Umemoto Reagent II (0.10 mmol) as the limiting reagent. Yields were determined by ^{19}F NMR with trifluorotoluene as an internal standard.

9.3.2. Exploration of Different Bases on Trifluoromethylating Brucine: Next, we evaluated if the reaction could be performed under basic and/or metal-free conditions, and the results are summarized in Table 9b. The nitrogen based DIPEA or Hünig's base (N, N

– diisopropylethylamine) provided **9f** in yields that were less than the base free-conditions (Table 9b, entry 1 vs 2). The use of NaH provided yields similar to those seen for base-free conditions (entry 1 vs 3); however, when the reaction was run with higher brucine loadings or elevated temperatures, yields did not further improve with NaH (see Appendix H). Interestingly, the reaction described in Table 9b could be run under metal free conditions (entry 4), but low yields of product are obtained (15%). Potassium or sodium *tert*-butoxide bases were not fruitful and provided low yields (entries 5 and 6).

Table 9b. Exploration of different bases on trifluoromethylation of brucine[a]

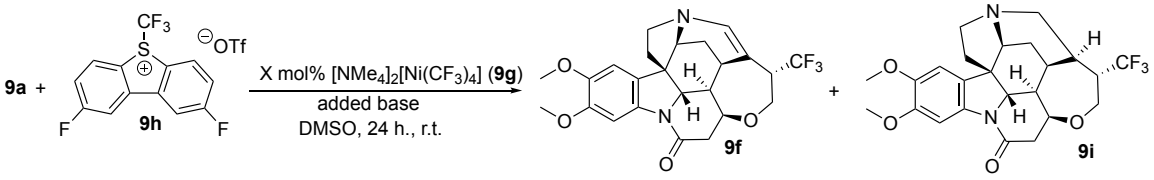

Entry	Base	Ni Catalyst	Yield **9f**	Yield **9i**
1	none	5%	38%	9%
2	DIPEA	5%	31%	5%
3	NaH[b]	5%	38%	4%
4	NaH[b]	0%	15%	4%
5	KO^{t}Bu	5%	9%	n.d.
6	NaO^{t}Bu	5%	7%	n.d.

[a] Reactions were run in 1 mL of DMSO with Umemoto Reagent II (0.05 mmol) and base (0.05 mmol) as the limiting reagent, and excess brucine (**9a** 0.10 mmol, 2 equiv.). Yields were determined by ^{19}F NMR with trifluorotoluene as an internal standard. [b] NaH used was in the form of 60% dispersion in mineral oil.

9.3.3. Scale-up and Isolation of 9f: Based on highest optimized yield (Table 9a, entry 6), the reaction was scaled up to 2 mmol for isolation of the major product **9f** (Scheme 9c). Performing the reaction for 24 hours yielded **9f** in 33% isolated yield, and increasing the

reaction time to 48 hours only slightly increased the yield to 37%. The ^{13}C NMR spectrum displayed two diagnostic quartets from the trifluoromethyl group and the adjacent carbon at δ 126.8 (q, $^{1}J_{CF}$ = 280 Hz) and 49.0 (q, $^{3}J_{CF}$ = 24.5 Hz) respectively. X-ray quality crystals of **9f** were grown by vapor diffusion of pentane into chloroform, and an ORTEP diagram is shown in Figure 9a. The X-ray structure confirms the stereoselective addition of CF_3 to the less sterically hindered face of brucine, and also confirms the double bond migration to the C_{20}-C_{21} position. While we were unable to isolate large amounts of minor product **9i** (Table 9a), the ^{1}H and ^{19}F NMR spectra of the trace material were consistent with the proposed structure as there was an absence of any vinylic hydrogens (see Appendix H), indicating it is not simply another isomer of **9f**. Moreover, HRMS data of the crude reaction mixture from Table 9a revealed a mass of the minor species consistent with that of **9i** (see Appendix H). We speculate that the origin of the hydrogen is derived either from solvent or trace amounts of water. In prior studies focused on the oxidation of catalyst **9g**, we have identified the C-bound acetonitrile complex $[(NCCH_2)Ni(CF_3)_5]^{2-}$, indicating a propensity of trifluoromethyl nickel complexes to react with solvent under oxidizing conditions. DFT calculations indicate that **9i** is the lowest energy isomer possible (see Appendix H).

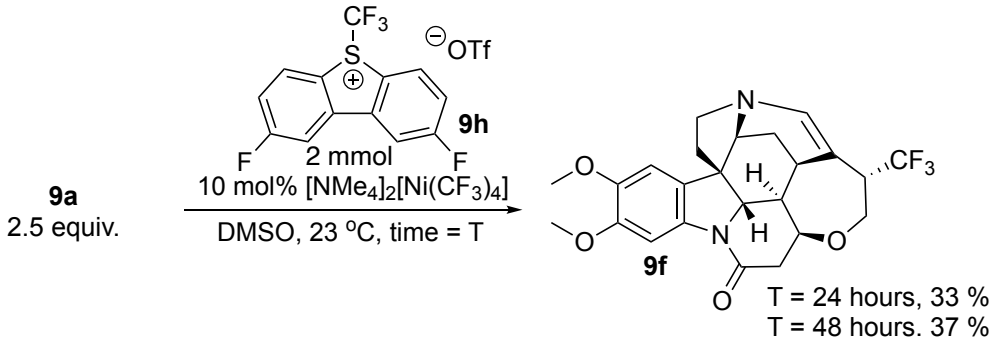

Scheme 9c. Scaled-up synthesis for the isolation of trifluoromethyl neobrucine.

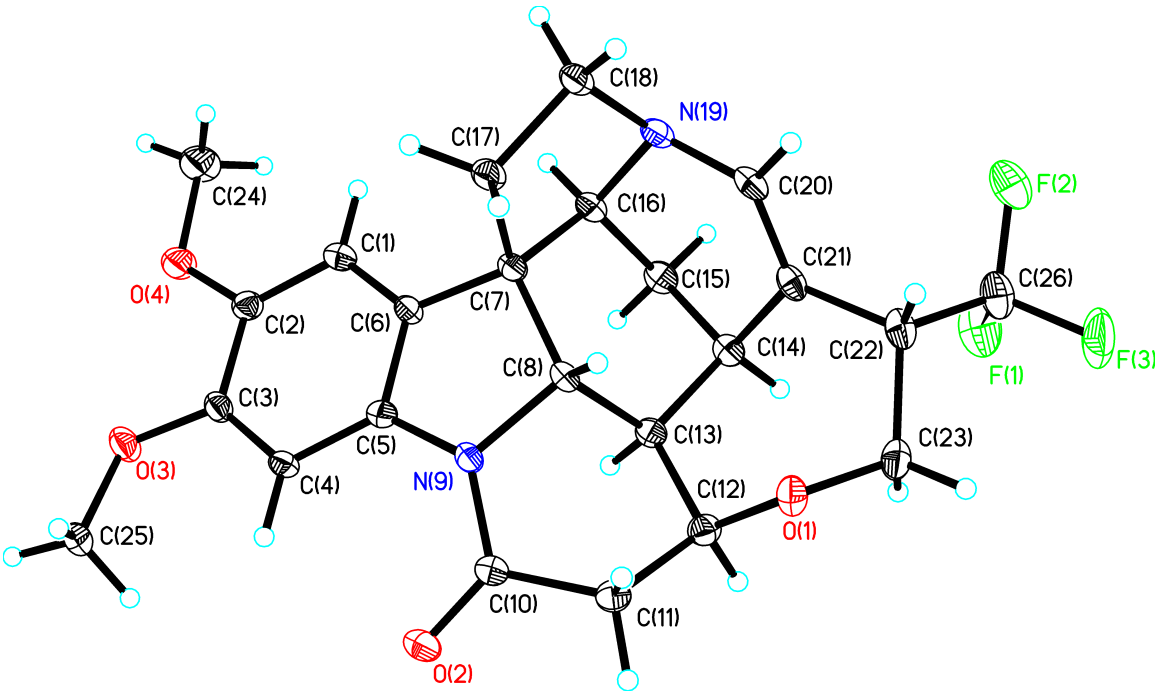

Figure 9a. ORTEP diagram of **9f**. Ellipsoids shown at the 40% level. Selected bond lengths (Å): C22-C26 1.519(5); C20-C21 1.338(4); Selected bond angles (°): C26-C22-C23 110.8(3); C20-C21-C22 120.4(3).

9.3.4. Investigating the Role of Nickel: In order to gain insights into the role of nickel in the trifluoromethylation reactions, stoichiometric reactions were performed with brucine and nickel precursors in different oxidation states. Our group has previously shown that nickel catalyst **9g** reacts with Umemoto Reagent II (**9h**) in acetonitrile to form a variety of highly trifluoromethylated and formally nickel(IV) complexes.[9] Therefore, acetonitrile was used as a solvent in the stoichiometric reactions in order to facilitate the identification of any trifluoromethylnickel products. No reaction was observed upon reaction of a 1:1 ratio of the nickel(II) catalyst **9g** and brucine (**9a**) in MeCN for 1 hour at room temperature. An additional five equivalents of brucine were added and the reaction was stirred for an additional 23 hours (Scheme 9d, top) with no product formation, indicating that **9g** does not directly react with brucine to afford **9f** or **9i**.

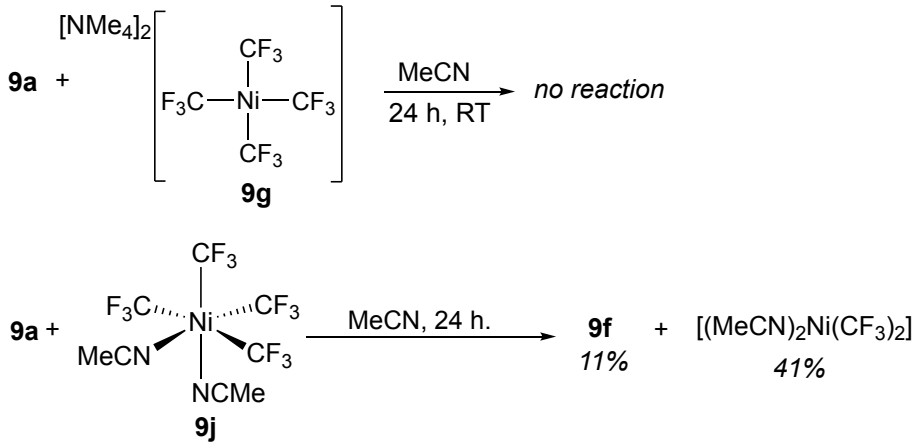

Scheme 9d. Stoichiometric reactions of brucine with nickel(II) and (IV) trifluoromethyl complexes.

The known[9] charge-neutral and formally nickel(IV) trifluoromethyl complex **9j** (Scheme 9d, bottom) was then allowed to react with brucine, and analyzed the products by ^{19}F NMR spectroscopy. The trifluoromethylated brucine product **9f** was detected in 11% yield, with the formation of $[(MeCN)_2Ni(CF_3)_2]$ as the main nickel-containing product in 41% yield (See Appendix H for full product analysis). The nickel(IV) complex likely undergoes decomposition to form sources of CF_3 radicals, as electrochemical measurements indicate that **9j**, although formally high valent, is still rather difficult to be reduced by external reagents, as it displays a peak potential of -0.66 V vs Fc/Fc^+ in MeCN solvent (see Appendix H). We have previously reported that the stoichiometric reaction of Umemoto II reagent with **9g** in MeCN produces mixtures of high valent $[(MeCN)Ni^{IV}(CF_3)_5]^-$, $[Ni^{IV}(CF_3)_6]^{2-}$, and $[(MeCN)_2Ni^{IV}(CF_3)_4]$.[9] Moreover, crossover experiments with the perfluoroethyl nickel(II) precatalyst $[(MeCN)Ni(C_2F_5)_3]^-$ in the presence of Umemoto II reagent and arene substrate show that the source of fluoroalkyl groups under these oxidizing conditions are derived from the nickel, rather than the Umemoto reagent (see

Chapter 7). We believe that similar pathways are operative using brucine as the substrate. Further experiments to probe the mechanistic details of this unique reaction are underway in our lab. One plausible mechanistic pathway is radical addition of a trifluoromethyl group to the olefin, generating a tertiary radical. Sequential proton abstraction could then lead to the reformation of the olefin. However, this mechanism does not account for the exact role of nickel, and therefore further research is required.

9.4 Conclusions: The homoleptic nickel complex $[Ni(CF_3)_4]^{2-}$ (**9g**) catalyzes a stereoselective trifluoromethylation of the complex molecule brucine in the presence of Umemoto II reagent to afford the isolable neobrucine-CF_3 derivative **9f**, which has been fully characterized. Control reactions show that the nickel precatalyst **9g** is not capable of transferring the trifluoromethyl groups in the absence of Umemoto II reagent, which supports the involvement of high-valent nickel in the trifluoromethylation reactions. We also identify a minor product resulting from the difunctionalization of the brucine double bond with hydrogen and CF_3. This new reaction provides a proof-in-principle demonstration that simple homoleptic trifluoromethyl nickel complexes can perform stereoselective catalytic trifluoromethylation reactions of complex molecules.

9.5. Experimental

9.5.1. General Information: All manipulations were performed using standard Schlenk and high vacuum techniques or in a nitrogen filled glovebox, unless otherwise stated. Solvents were purified by passing through activated alumina and/or copper in a solvent purification system supplied by Pure Process Technology. ^{1}H NMR spectra were recorded at ambient temperature on a Bruker 500 MHz spectrometer and referenced to residual proton solvent signals. ^{13}C {^{1}H} NMR spectra were recorded on a Bruker NMR

spectrometer operating at 126 MHz. ^{19}F NMR spectra were recorded on a Bruker NMR spectrometer operating at 376 MHz and referenced to α,α,α-trifluorotoluene as an internal standard (δ = -63.7). A Bruker D8 Quest diffractometer was used for X-ray crystal structure determinations. High-resolution mass spectrometry (HRMS) using electrospray ionization (ESI) was completed at the Notre Dame Mass Spectrometry Facility. Reaction optimizations and computational details can be found within Appendix H. The CCDC 2153715 contains the supplementary crystallographic data for compound **9f**. These data can be obtained free of charge via www.ccdc.cam.ac.uk/data_request/cif, or by e-mailing data_request@ccdc.cam.ac.uk, or by contacting The Cambridge Crystallographic Data Centre, 12 Union Road, Cambridge CB2 1EZ, UK; fax: +44 1223 336033.

9.5.2. Preparation of 9f: In a nitrogen filled glovebox, a round bottom flask was charged with Brucine (2.0 g, 5.0 mmol, 2.5 equiv.), Umemoto Reagent II (880 mg, 2.0 mmol, 1 equiv.), and 16 mL of DMSO. While stirring, 4 mL of a 0.025 M solution of $[NMe_4]_2[Ni(CF_3)_4]$ in DMSO was added, and continued to stir for 24 hours at room temperature. The reaction was removed from the glovebox and added to a seperatory funnel with diethyl ether (100 mL), followed by extraction with water (3 x 100 mL). The water layers were combined and re-extracted with diethyl ether (100 mL). The organic layers were combined, washed with brine (100 mL), dried over $MgSO_4$ and concentrated by rotary evaporation. The product was purified via flash column chromatography, yielding 152 mg of a white solid (33%). Reaction stirred for 48 hours, furnished 171 mg of product (37%). X-ray quality crystals were grown by vapor diffusion of pentane into chloroform. ^1H NMR (500 MHz, C_6D_6): δ 8.32 (s, 1H), 6.55 (s, 1H), 5.52 (s, 1H), 4.00 (dd, *J* = 11.9 Hz, 6.7 Hz, 1H), 3.56-3.48 (m, 7H), 3.29 (br s, 1H), 3.26-3.17 (m, 2H), 3.04-2.92 (m, 2H), 2.81-2.69

(m, 1H), 2.65-2.58 (m, 1H), 2.54 (dd, J = 16.2 Hz, 4.6 Hz, 1H), 2.16 (br s, 1H), 2.10 (dt, J = 13.3 Hz, 3.6 Hz, 1H), 1.89-1.77 (m, 1H), 1.59- 1.50 (m, 1H), 1.43 (dt, J = 13.6 Hz, 2.5 Hz, 1H), 0.83-0.77 (m, 1H). $^{13}C\{^{1}H\}$ NMR (126 MHz, C_6D_6): δ 169.5, 151.1, 147.5, 141.7, 137.0, 126.8 (q, J = 280 Hz), 124.3, 107.5, 104.9, 102.0, 78.4, 66.1, 64.7, 58.7, 57.1, 55.8, 54.0, 53.7, 51.6, 49.0 (q, J = 24.5 Hz), 45.6, 41.4, 27.2, 27.0. ^{19}F NMR (376 MHz, C_6D_6): δ -71.1 (d, J = 9.6 Hz). HRMS (ESI, *m/z*) calcd. for $C_{24}H_{26}F_3N_2O_4$ $[M+H]^+$: 463.1839; found: 463.1848.

HRMS analysis of a crude reaction mixture identified a mass consistent with the minor product (**9i**). HRMS (ESI, *m/z*) calcd. for $C_{24}H_{28}F_3N_2O_4$ $[M+H]^+$: 465.1996; found: 465.1990.

9.5.3. Reaction of $[NMe_4]_2[Ni(CF_3)_4]$ with brucine: In a nitrogen filled glovebox, to a solution of $[NMe_4]_2[Ni(CF_3)_4]$ (24 mg, 0.050 mmol, 1 equiv.) in 0.5 mL of MeCN, a solution of brucine (20 mg, 0.051 mmol, 1 equiv.) in 1 mL of MeCN was added. The reaction was stirred for 1 hour and ^{19}F NMR was recorded. An additional 5 equiv. of brucine was added and the reaction was continued to stir for 23 hours. The ^{19}F NMR was recorded again.

9.5.4. Reaction of $[(MeCN)_2Ni(CF_3)_4]$ with brucine: In a nitrogen filled glovebox, a vial was charged with $[(MeCN)_2Ni(CF_3)_4]$ (21 mg, 0.050 mmol, 1 equiv.) and brucine (20 mg, 0.051 mmol, 1 equiv.). MeCN (1 mL) was added and the reaction was stirred for 24 hours. One equivalent of trifluorotoluene was added, and the ^{19}F NMR spectra was recorded.

9.6 References

1. Behera, M. C.; Mohanty, T. L.; Paramanik,B. K. Silvics, Silvics, Phytochemistry and Ethnopharmacy of Endangered Poison Nut Tree (*Strychnos nux-vomica* L.): A review. *J. Pharmacogn. Phytochem.* **2017**, *6*, 1207-1216.

2. Mohsen, A. M. Y.; Heller, E.; Holzgrabe, U.; Jensen, A. A.; Zlotos, D. P. Structure-Activity Relationships of Strychnine Analogs at Glycine Receptors. *Chem. Biodivers.* **2014**, *11*, 1256-1262.
3. Patel, K.; Laloo, D.; Singh, G. K.; Gadewar, M.; Patel, D. K. A Review on Medicinal Uses, Analytical Techniques and Pharmacological Activities of *Strychnos nux-vomica* Linn.: A Concise Report. *Chin. J. Integr. Med.* **2017**, https://doi.org/10.1007/s11655-016-2514-1.
4. Lu, L.; Huang, R.; Wu, Y.; Jin, J.-M.; Chen, H.-Z.; Zhang, L.-J.; Luan, X. Brucine: A Review of Phytochemistry, Pharmacology, and Toxicology. *Front. Pharmacol.* **2020**, *11*, 377.
5. Ziyang, D.; Zhanhui, Y.; Jiaxi, J. Structural Modifications and Chiral Applications of Brucine. *Chin. J. Org. Chem.* **2020**, *40*, 4101-4121.
6. Chakravarti, R. N.; Robinson, R. 16. Strychnine and Brucine. Part XLVI. The Preparation of neoStrychnine and neoBrucine. *J. Chem. Soc.* **1947**, 78-80.
7. Saito, Y.; Yamanoue, K.; Segawa, Y.; Itami, K. Selective Transformation of Strychnine and 1,2-Disubstituted Benzenes by C-H Borylation. *Chem.* **2020**, *6*, 985-993.
8. Karimov, R. R.; Sharma, A.; Hartwig, J. F. Late Stage Azidation of Complex Molecules. *ACS Cent. Sci.* **2016**, *2*, 715-724.
9. Shreiber, S. T.; Vicic, D. A. Solvated Nickel Complexes as Stoichiometric and Catalytic Perfluoroalkylation Agents**. *Angew. Chem. Int. Ed.* **2021**, *60*, 18162-18167.
10. Shreiber, S. T.; DiMucci, I. M.; Khrizanforov, M. N.; Titus, C. J.; Nordlund, D.; Dudkina, Y.; Cramer, R. E.; Budnikova, Y.; Lancaster, K. M.; Vicic, D. A. $[(MeCN)Ni(CF_3)_3]^-$ and $[Ni(CF_3)_4]^{2-}$: Foundations toward the Development of Trifluoromethylations at Unsupported Nickel. *Inorg. Chem.* **2020**, *59*, 9143-9151.

Chapter 10: Conclusion

The research described in this dissertation detailed a number of new advancements in the realm of fluoroorganometallic chemistry. Through the synthesis of well-defined fluoroalkyl copper, nickel, and cobalt complexes, new discoveries regarding key physical properties of organometallic complexes and new reactivities have been found. These new understandings will help develop novel approaches for further enabling fluoroalkylations using first-row transition metals.

Chapter 2 described a new method for accessing mixed fluoroalkyl cuprates. A variety of complexes of copper transformed into their cuprate forms, which resulted in the formation of new species that were rapidly detectable by ^{19}F NMR spectroscopy. The NHC ligand system allowed for the characterization of previously unknown cuprates, and offers a new method for studying and enabling dynamic reactivity with such fluoroalkyl complexes of copper.

Understanding that cobalt is a promising platform for developing new fluoroalkyl chemistries, Chapter 3 presented the synthesis of versatile precursor to cobalt perfluoroethyl complexes. Generally, the previously described complexes of fluoroalkyl cobalt in the literature had non-labile ligands. The precursor developed in these studies has labile acetonitrile ligands that were shown to undergo rapid ligand substitution affording a variety of different complexes.

Utilizing the versatile precursor described in Chapter 3, new anionic and dianionic cobalt complexes were described in Chapters 4 and 5. These chapters also describe the electrochemical properties of cobalt(III) fluoroalkyl complexes. We revealed that anation has a large effect on lowering oxidation potentials over the simple substation of charge

neutral datively bonded ligands. As noted in other parts of this dissertation, access to high-valent states of copper and nickel has helped develop new bond forming reactions, and the reactivity of formally high-valent cobalt(IV) fluoroalkyl complexes is currently unknown. It is hoped that the data obtained from these chapters will be critical in future developments involving high-valent cobalt.

The data in Chapter 6 provided the foundational groundwork for using highly trifluoromethylated nickel complexes as synthons for new fluoroalkylation methodologies. Fundamental studies showed that such nickel d^8 complexes exist in physically reduced states and are better described as d^9. Furthermore, such species are easily oxidizable to higher valent states of nickel. The electrochemical studies guided the chemical oxidization of nickel(II) derivatives to isolable nickel(IV) species, as well as new reactivities with organic substrates.

Chapter 7 further described the various reactions that solvato perfluoroalkyl nickel complexes can undergo with organic substrates. Stoichiometric reactivities of the nickel complexes with hypervalent iodine reagents and diazonium salts proved successful in generating perfluoroalkylated products. Furthermore, the first demonstration of catalysis was achieved with these solvated complexes, namely the C-H trifluoromethylation of (hetero)arenes.

Chapter 8 described efforts towards modifying the solvated nickel system. We successfully replaced the spectator fluoroalkyl groups with the more stabilizing C_4F_8 chelating ligand. Electrochemical properties of those new C_4F_8 complexes revealed stark differences in oxidation events with the non-chelating congeners. The second avenue for modification was the substitution of the coordinated acetonitriles with simple N-heterocyclic carbene

ligands. This modification revealed that oxidation events of NHC-ligated species were well-separated energetically, in comparison to the non-NHC species having redox couples similar in energies. We believe the identification of a ligand system that better separates oxidation events in terms of energies bodes well for future oxidative reactivities, since over oxidation can be avoided.

An unexpected stereoselective trifluoromethylation of brucine is described in Chapter 9. The solvated nickel complexes ultimately catalyze an allylic C-H functionalization process leading to trifluoromethylated neobrucine. A minor product was also observed, resulting from a difunctionalization of the olefin in brucine. This new reactivity demonstrated proof-in-principle demonstration that the solvated nickel complexes can perform late-stage functionalization of complex molecules, and are an interesting platform for reaction discovery.

Appendix A: Supporting Information and Spectral Data for Chapter 2

Figure A1. ^{19}F NMR of [(SIMes)Cu(C_2F_5)] and [(SIMes)$_2$Cu][Cu(C_2F_5)$_2$] in CD_2Cl_2

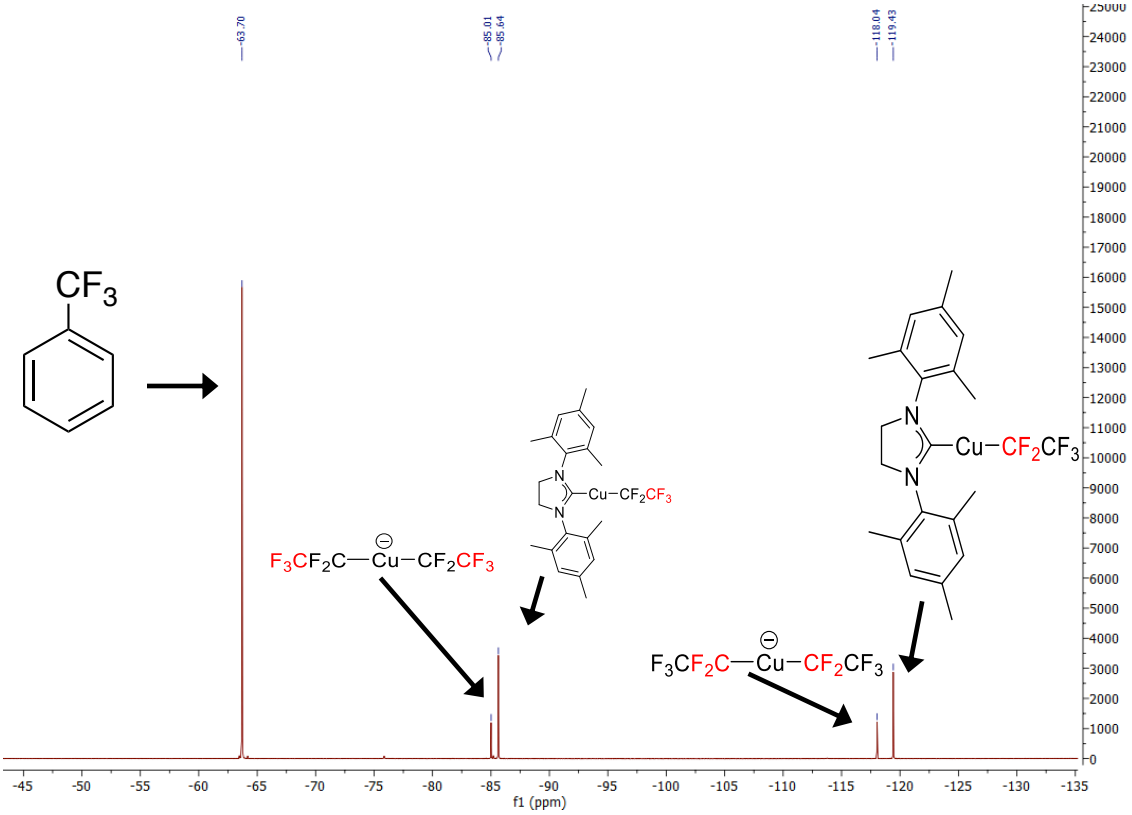

Figure A2. ^{1}H NMR of $[(SIMes)Cu(C_2F_5)]$ and $[(SIMes)_2Cu][Cu(C_2F_5)_2]$ in CD_2Cl_2

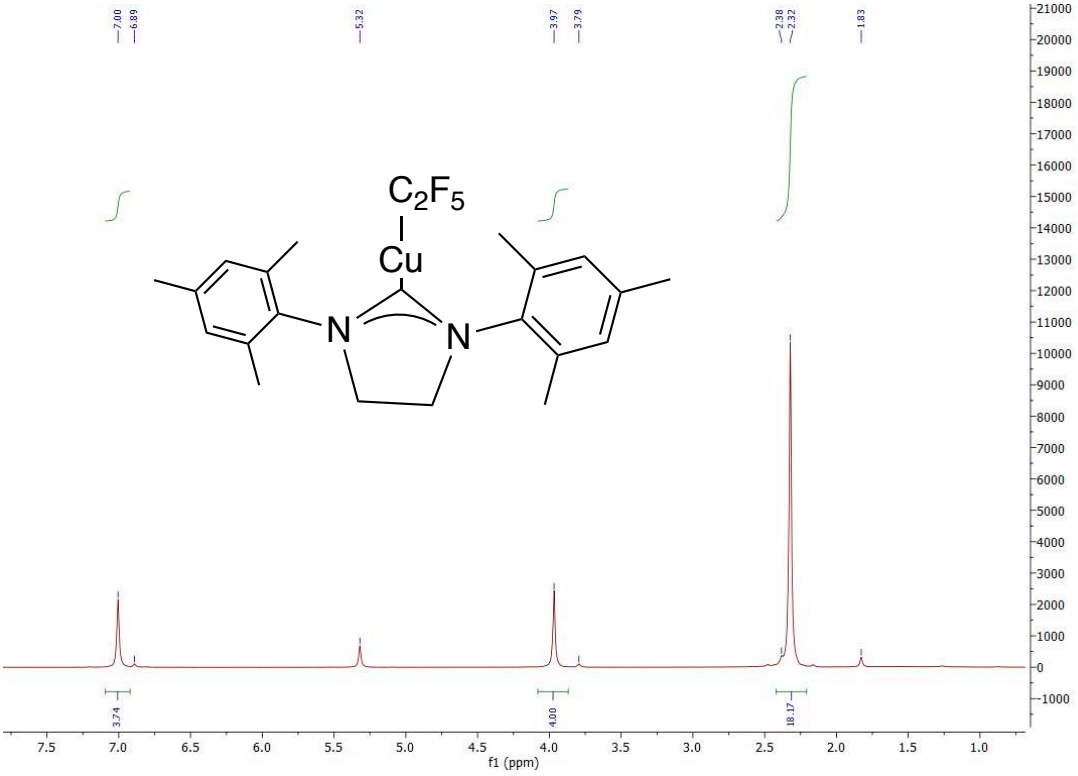

Figure A3. ^{19}F NMR of [(SIMes)Cu(C_2F_5)] mixed with [(SIMes)Cu(CF_3)] in CD_2Cl_2

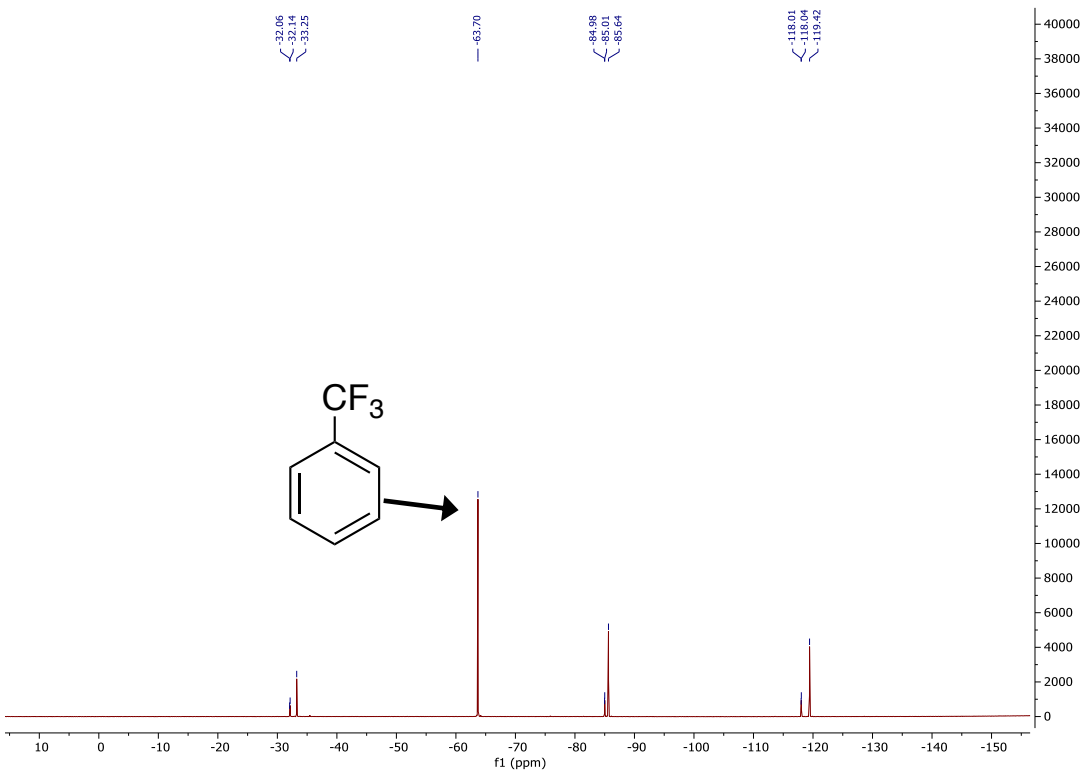

Figure A4. Zoomed image of Figure A3 of the Cu-CF_3 region

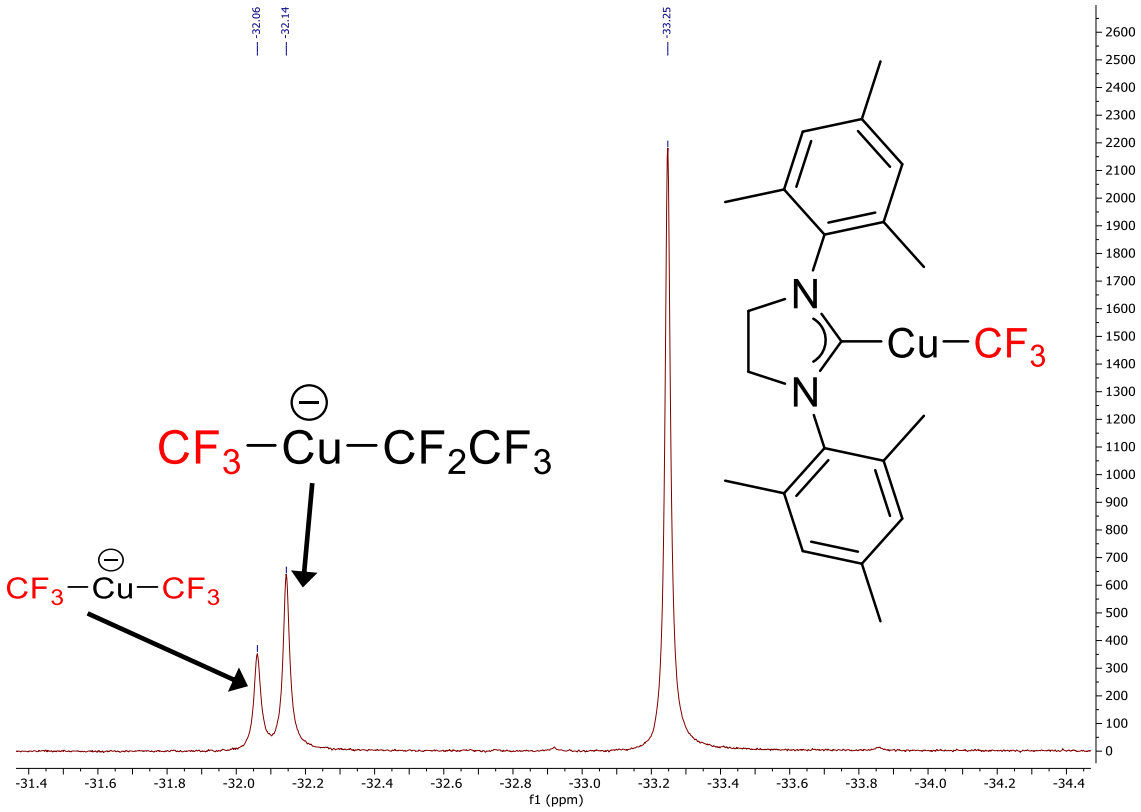

Figure A5. Zoomed image of Figure A3 the Cu-CF_2CF_3 region

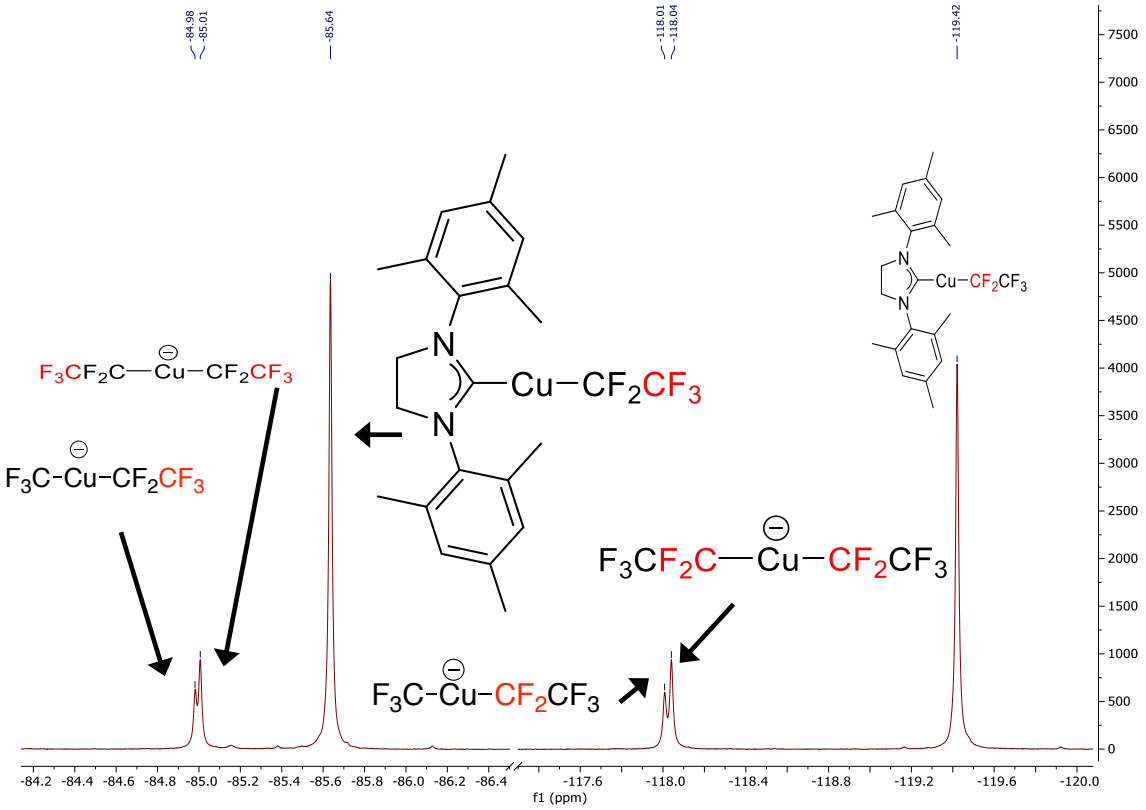

Figure A6. ^{19}F NMR of [(SIMes)Cu(C_2F_5)] mixed with [(SIMes)Cu(Cl)] in CD_2Cl_2

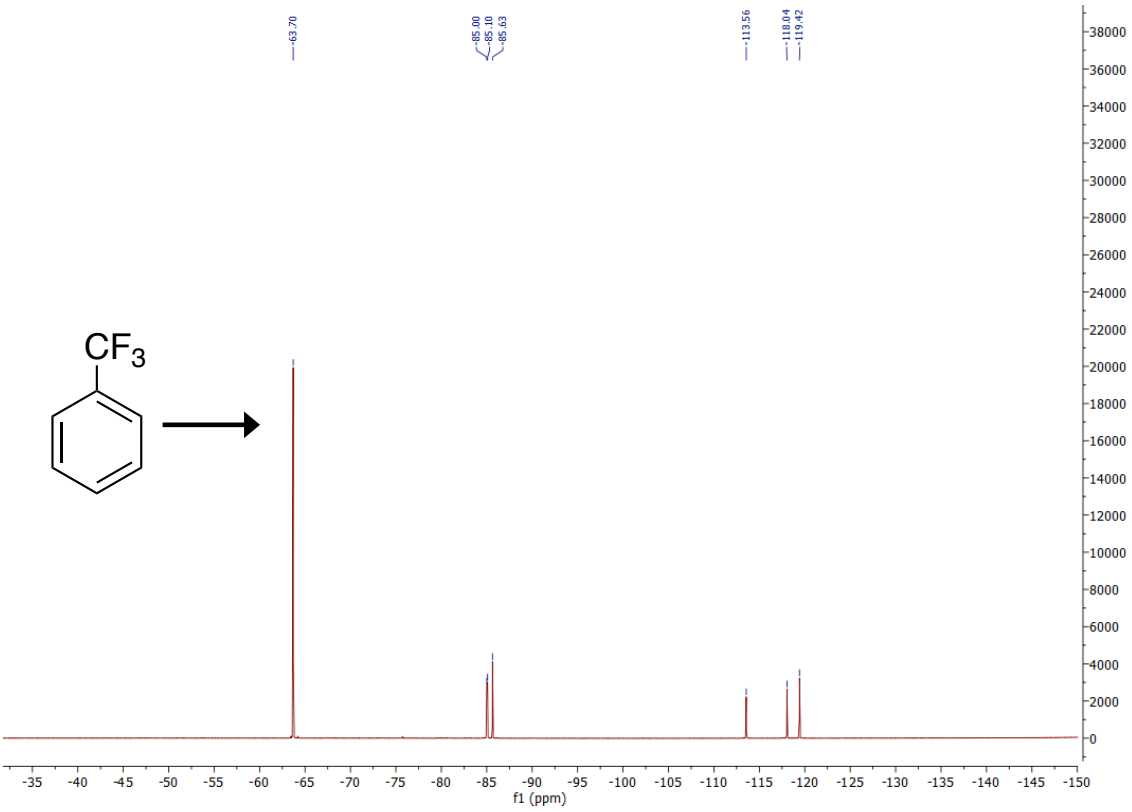

Figure A7. Zoomed image of Figure A6

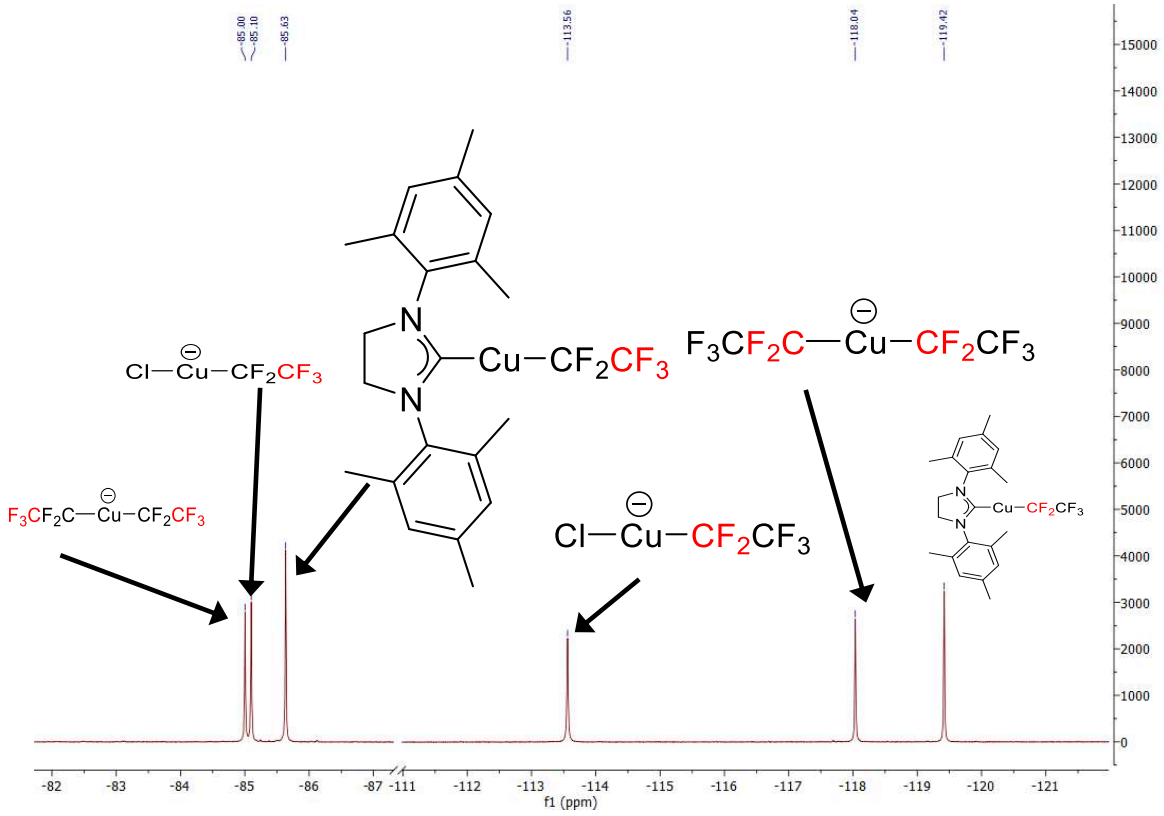

Figure A8. ^{19}F NMR of [(SIMes)Cu(CF_3)] mixed with [(SIMes)Cu(Cl)] in CD_2Cl_2

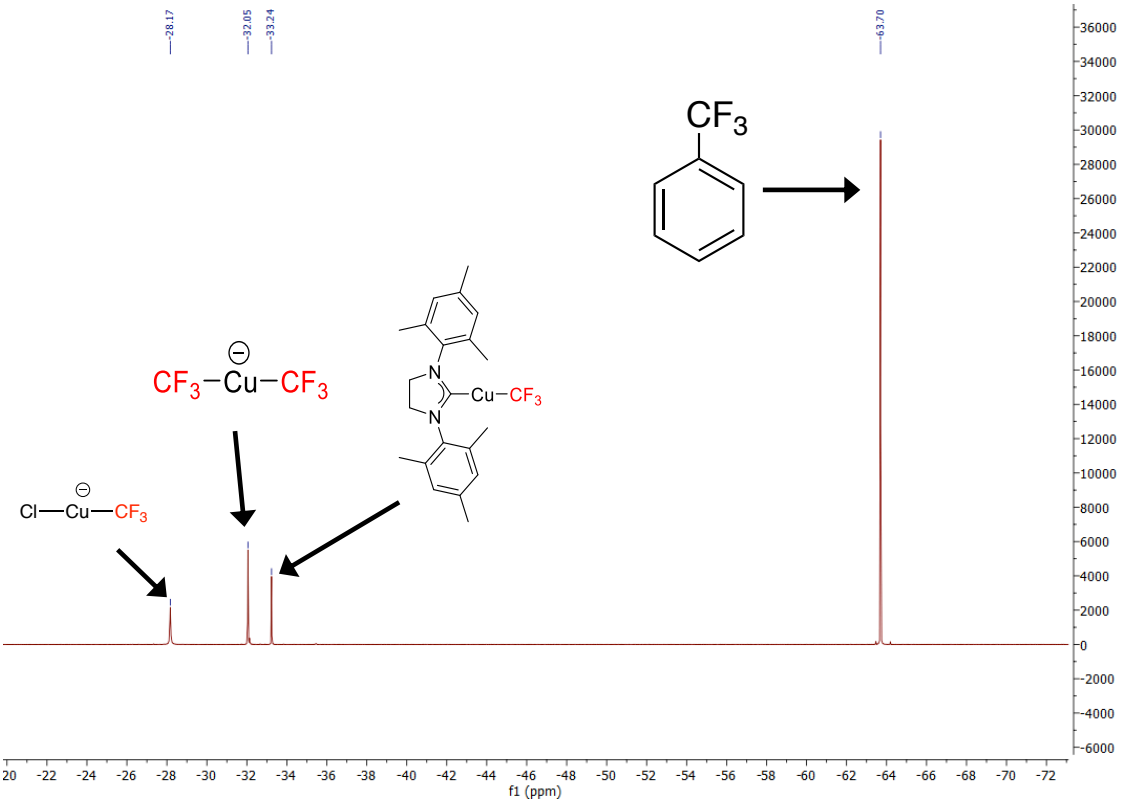

Figure A9. ORTEP Diagram of the crystal of **2j**

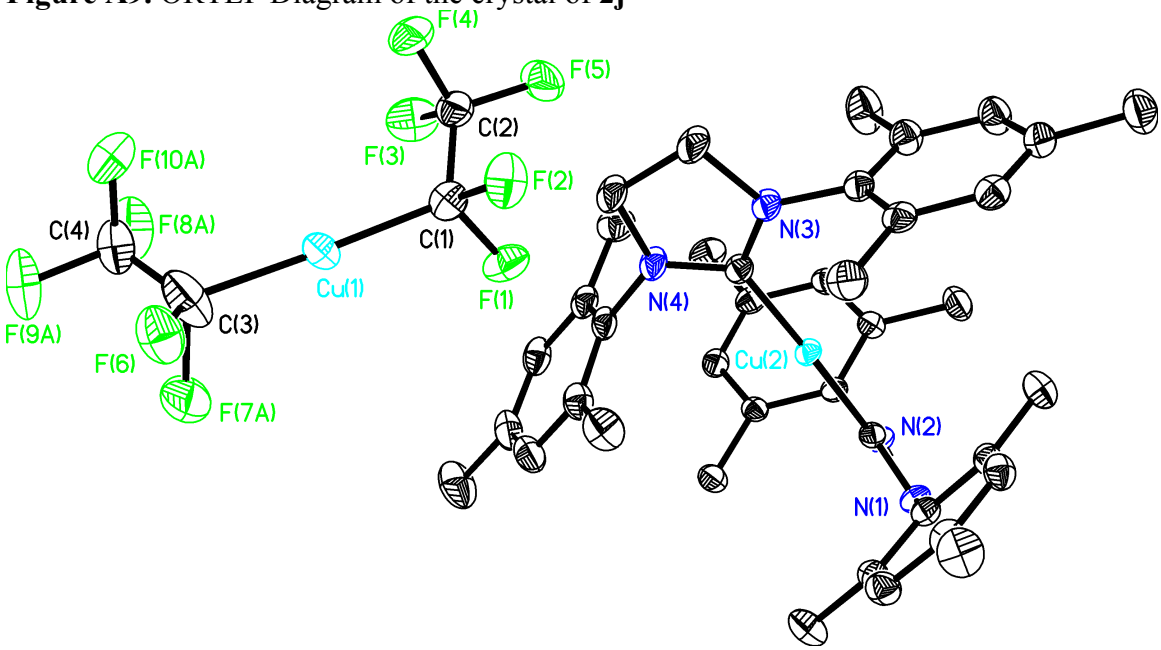

Appendix B: Supporting Information and Spectral Data for Chapter 3

Figure B1. ^{19}F NMR of **3a** in CD_3CN

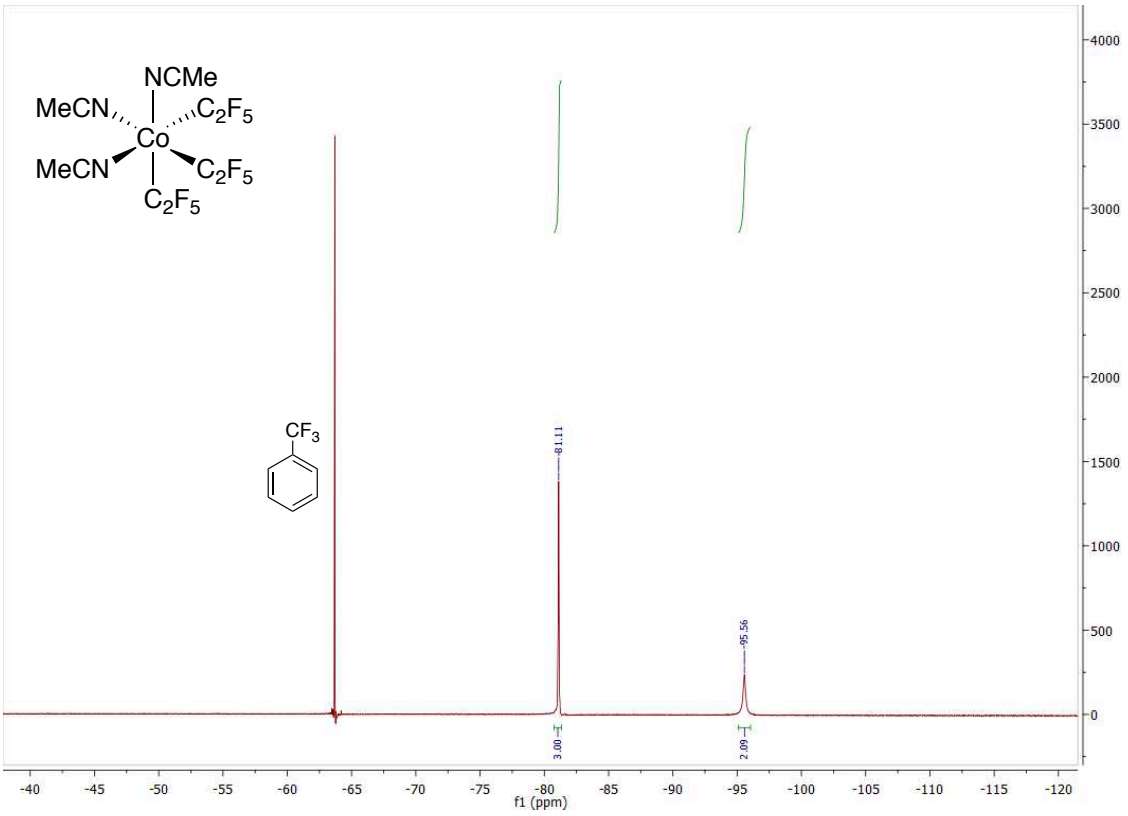

Figure B2. ^{19}F NMR of **3b** in C_5D_5N

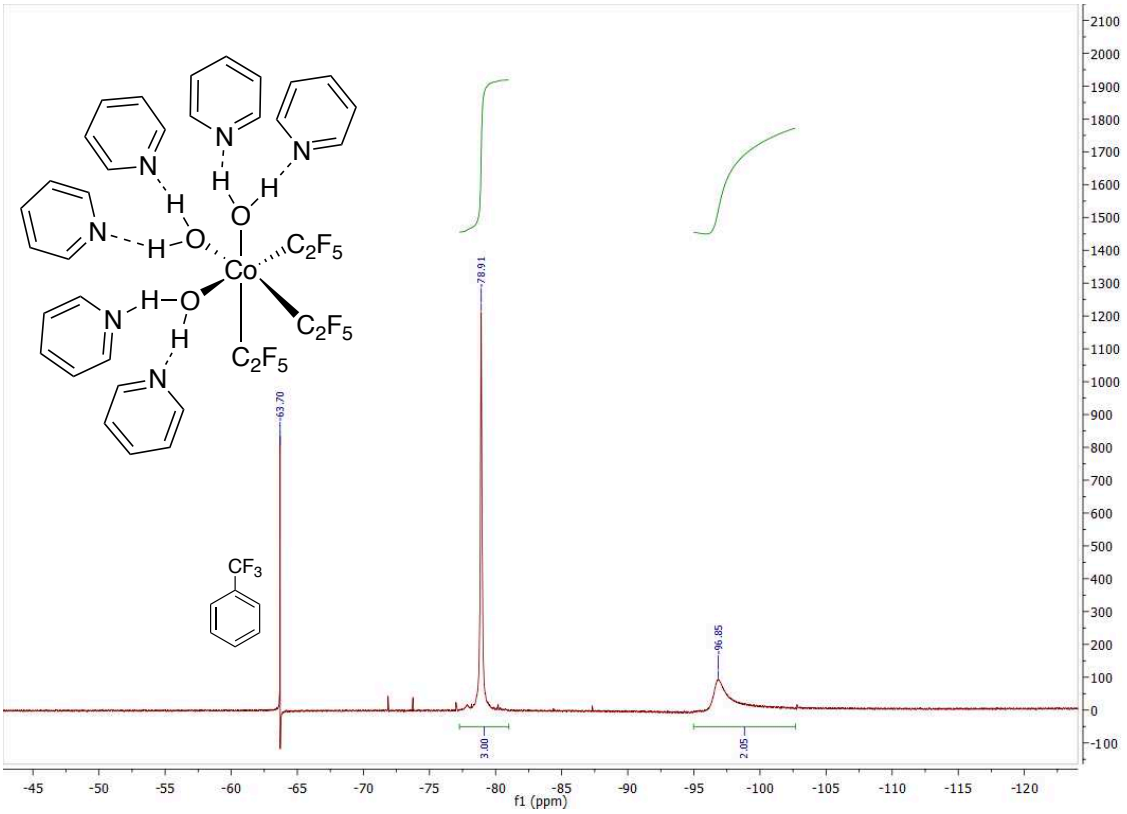

Figure B3. ^{1}H NMR of **3e** in DMSO – d_6

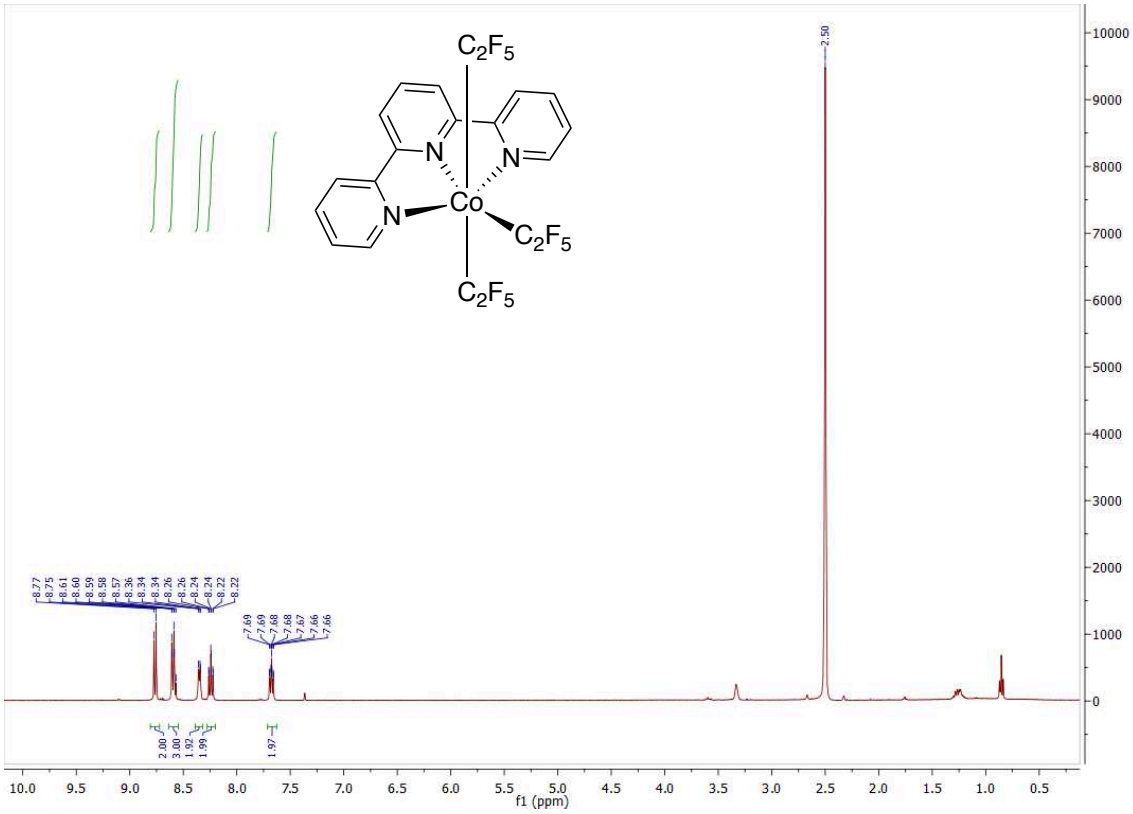

Figure B4. ^{19}F NMR of **3e** in CD_2Cl_2

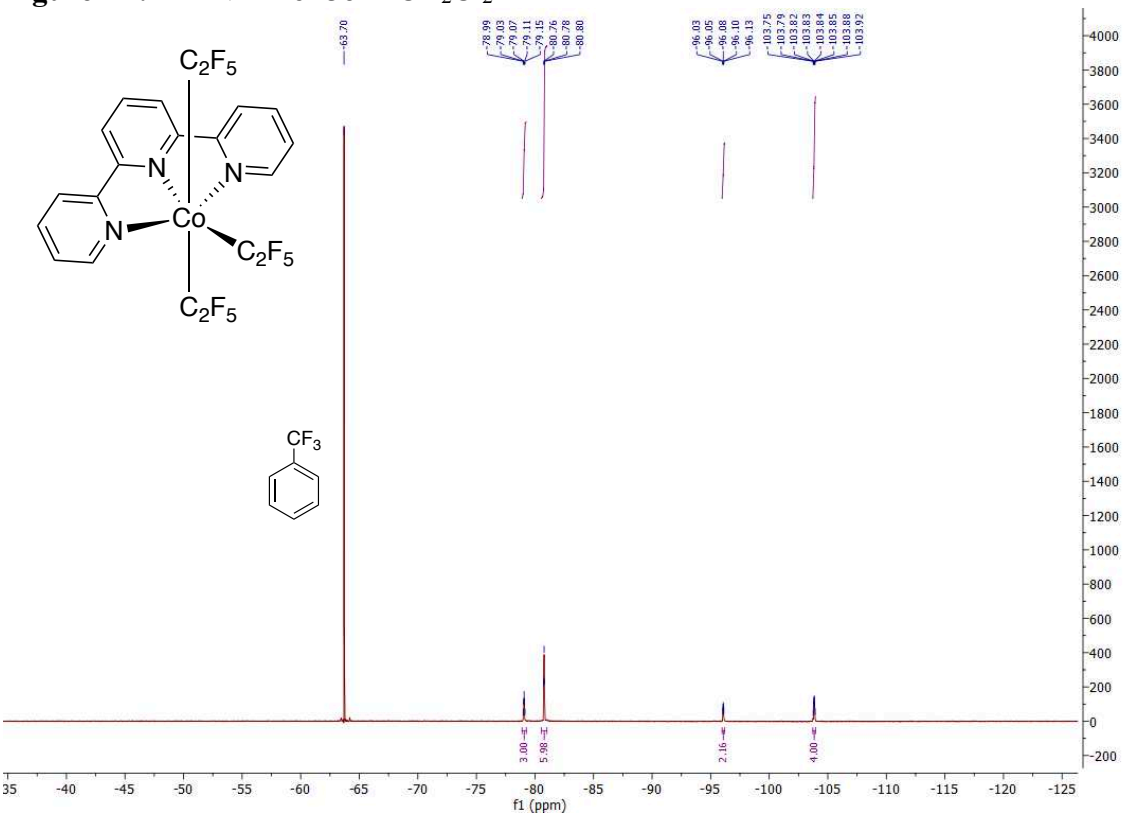

Figure B5. Magnified view of the downfield region of the ^{19}F NMR spectrum of **3e** in CD_2Cl_2

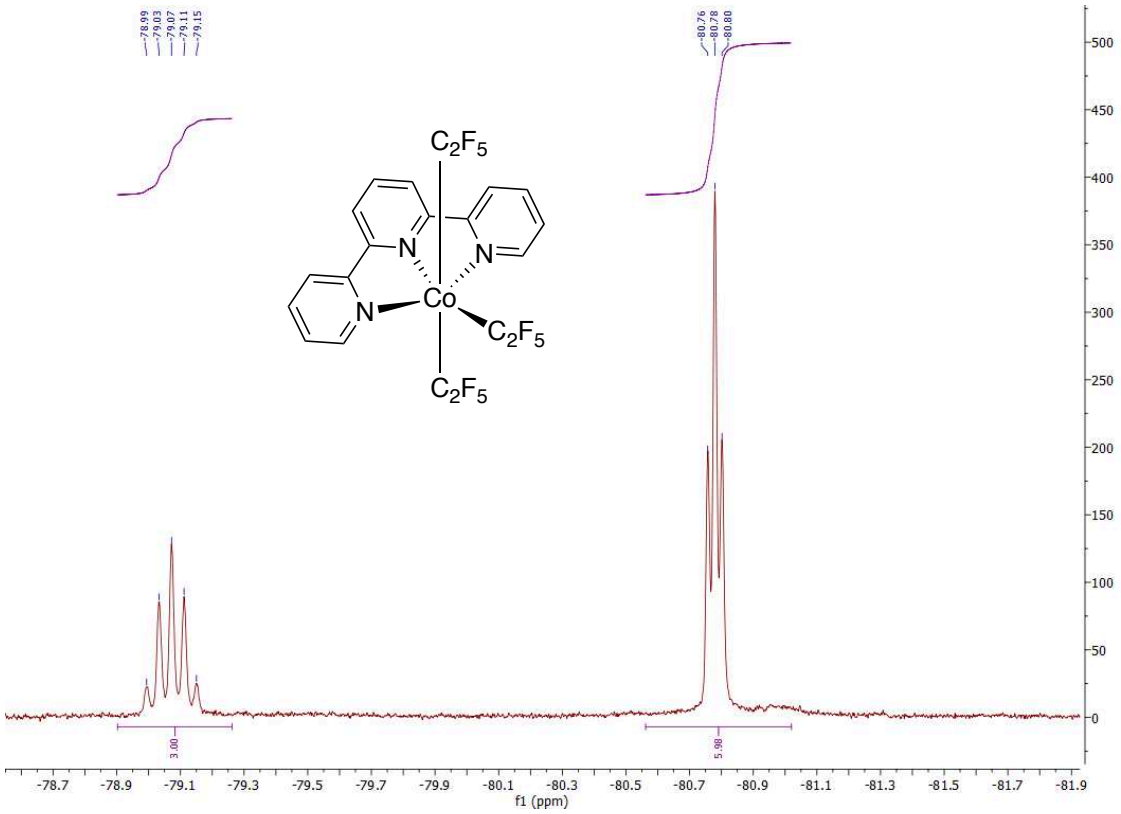

Figure B6. Magnified view of the upfield region of the ^{19}F NMR spectrum of **3e** in CD_2Cl_2

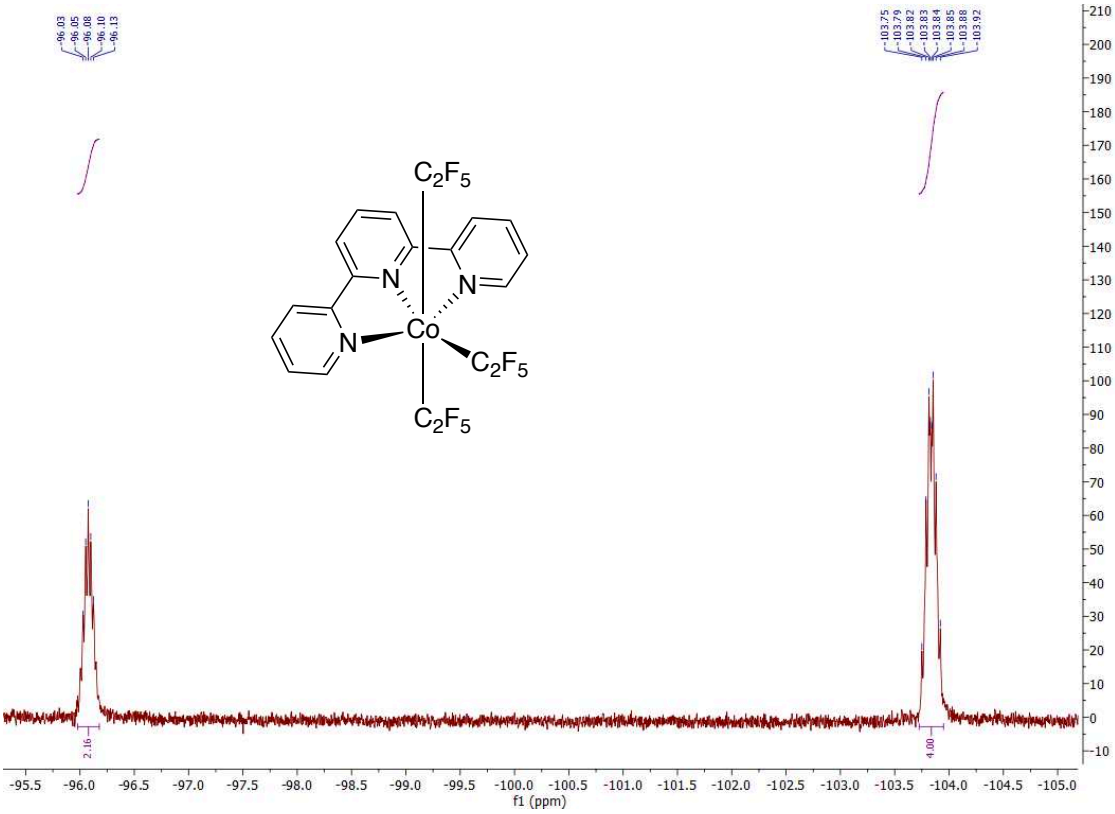

Figure B7. ^{19}F COSY of **3e** in CD_2Cl_2

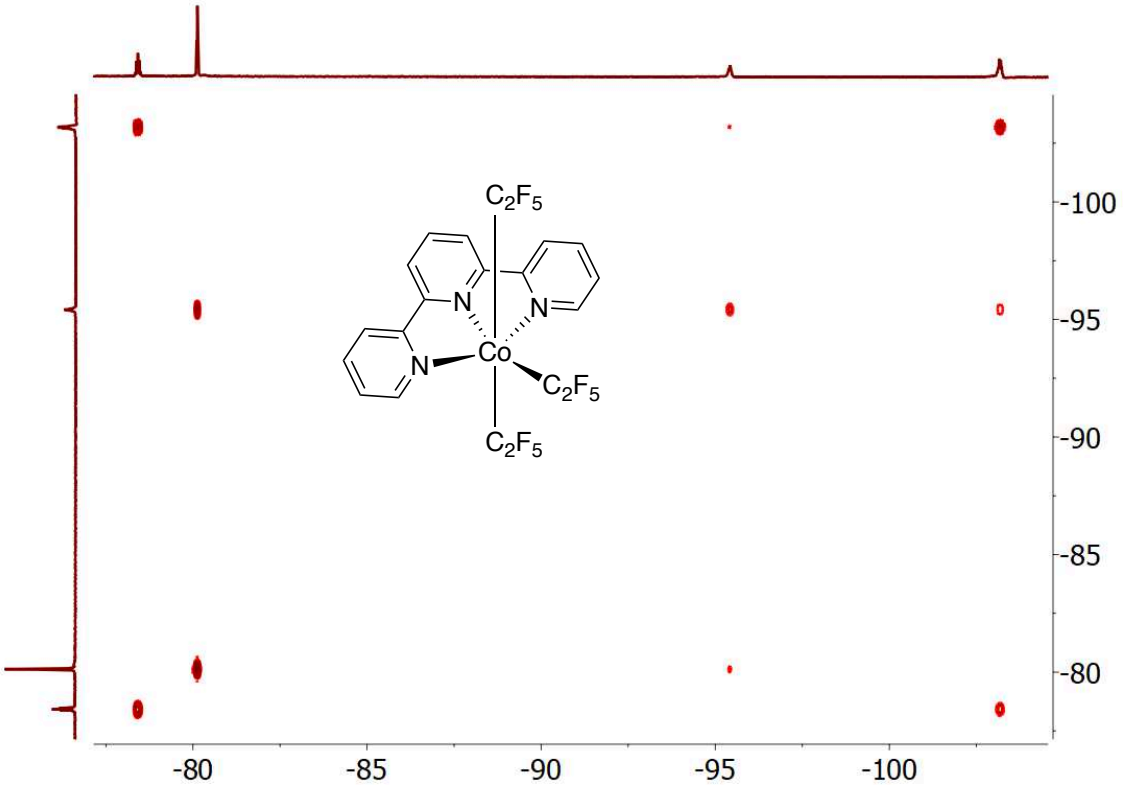

Figure B8. ^{1}H NMR of **3f** in CD_3CN

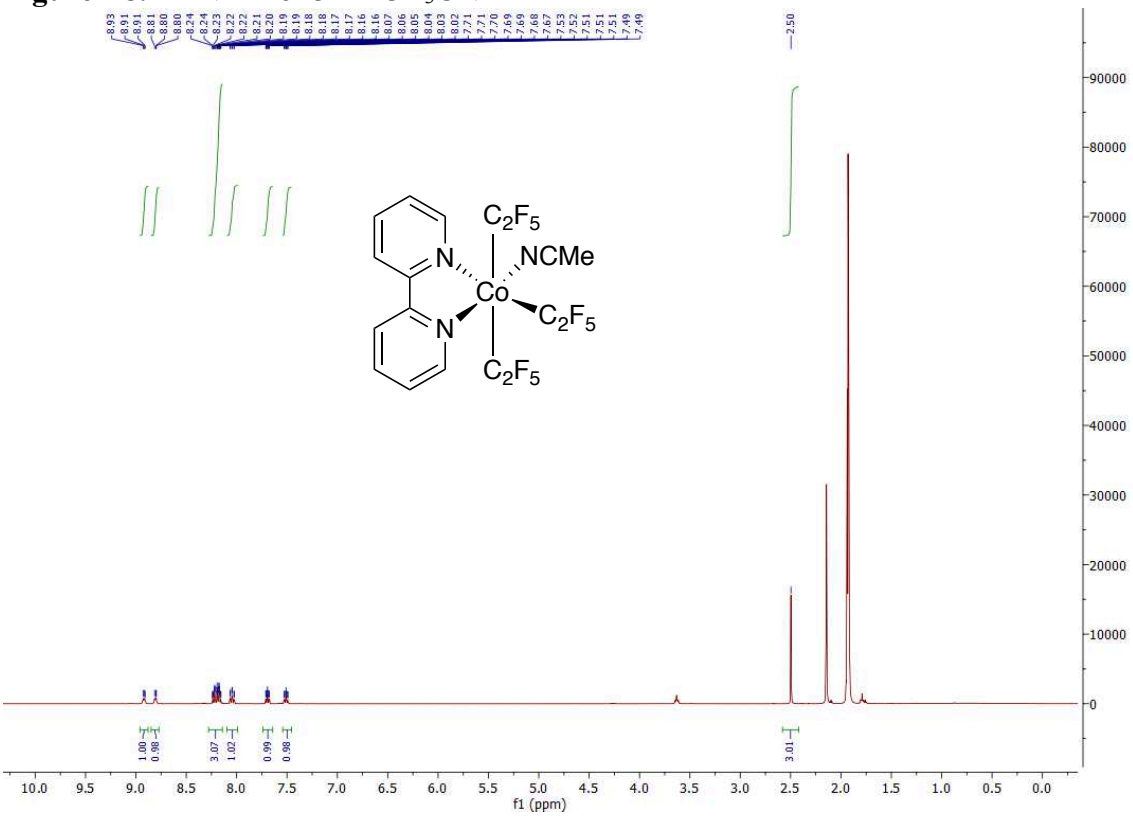

Figure B9. ^{19}F NMR of **3f** in CD_3CN

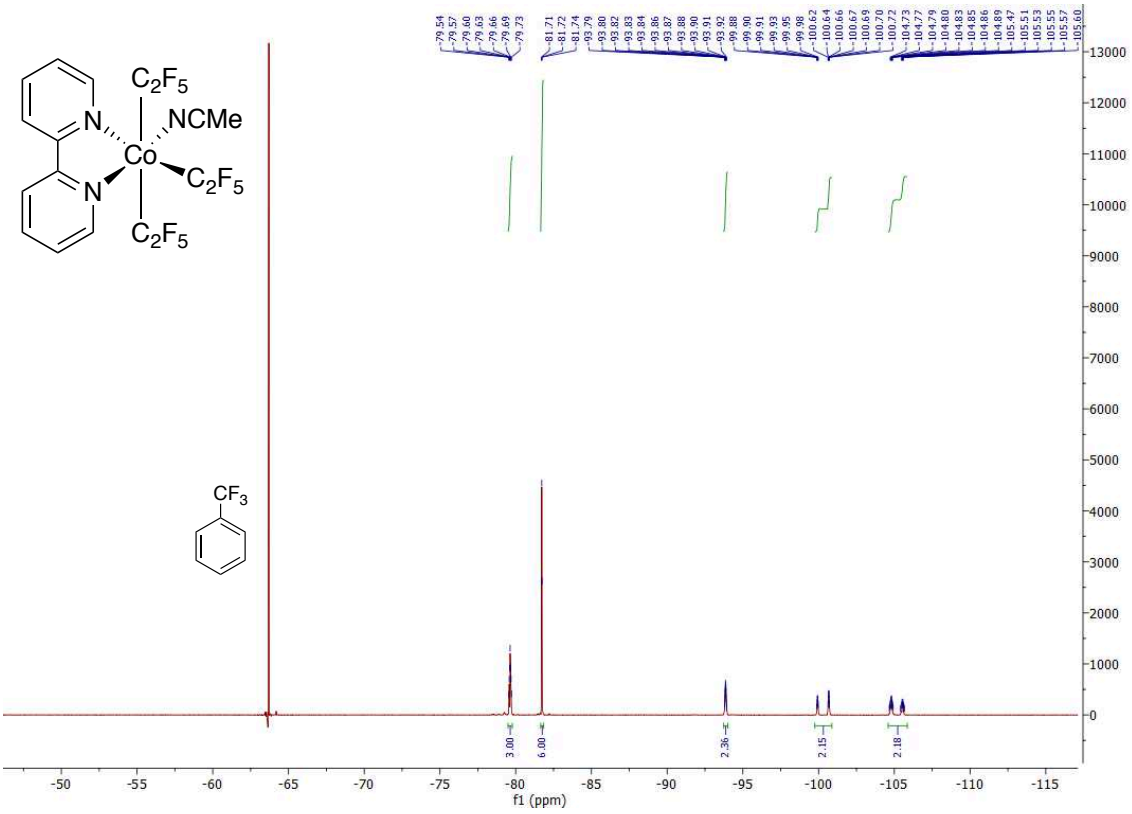

Figure B10. ^{19}F NMR spectrum that results upon dissolution of **3a** in anhydrous pyridine solvent.

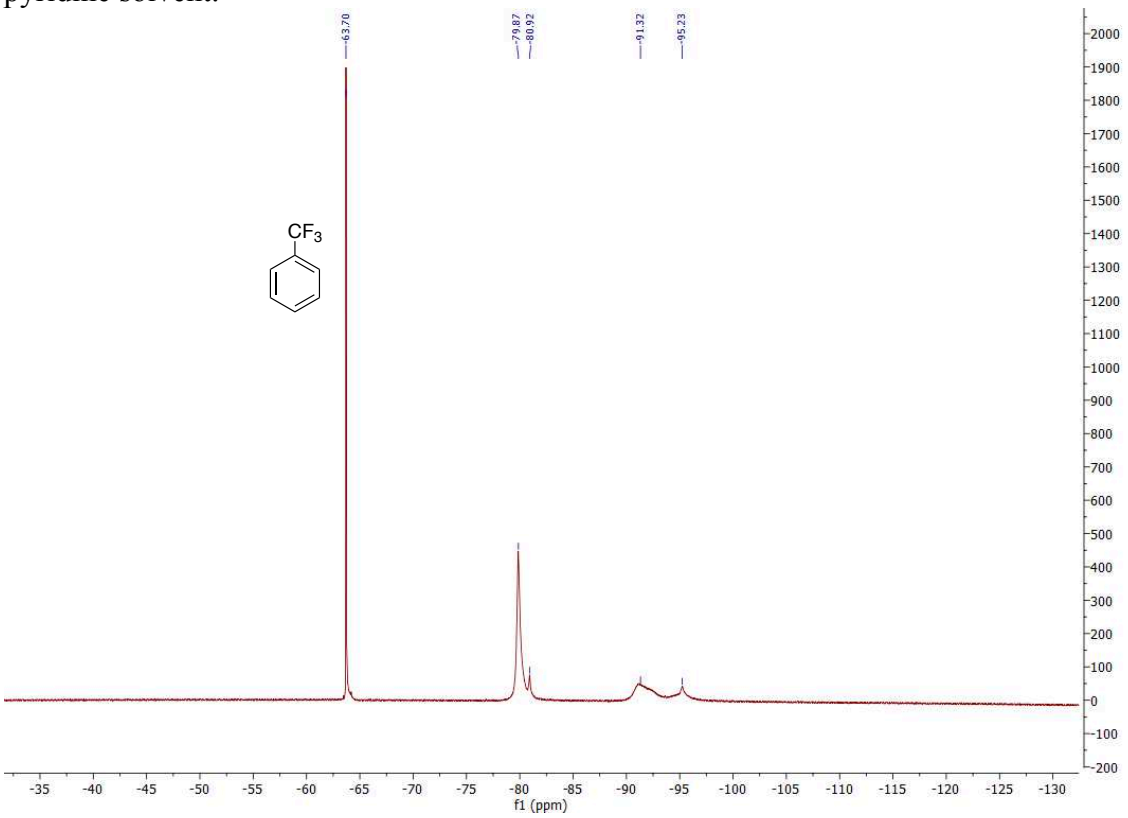

Figure B11. ^{19}F NMR spectrum of the sample described in Figure B10 after a drop of water added.

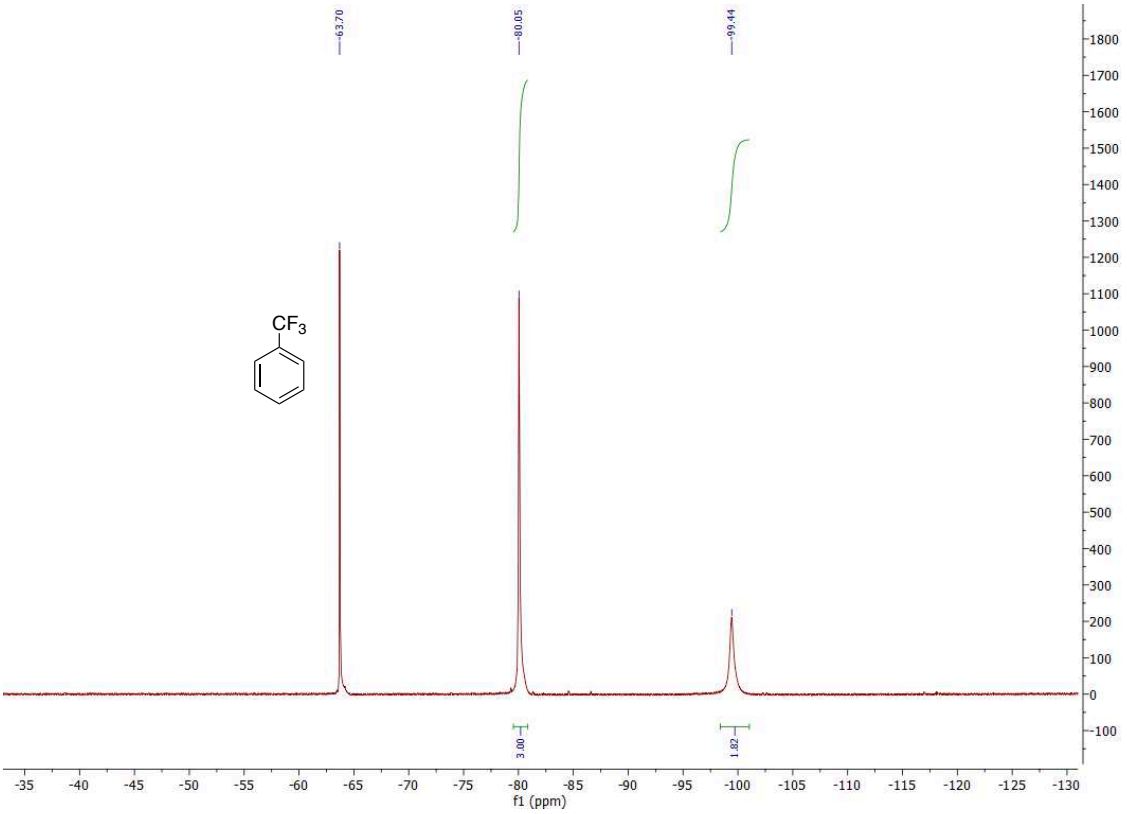

Appendix C: Supporting Information and Spectral Data for Chapter 4

Figure C1. ^{19}F NMR of $[PPh_4][(Tp)Co(C_2F_5)_3]$ **(4h)** in CD_3CN

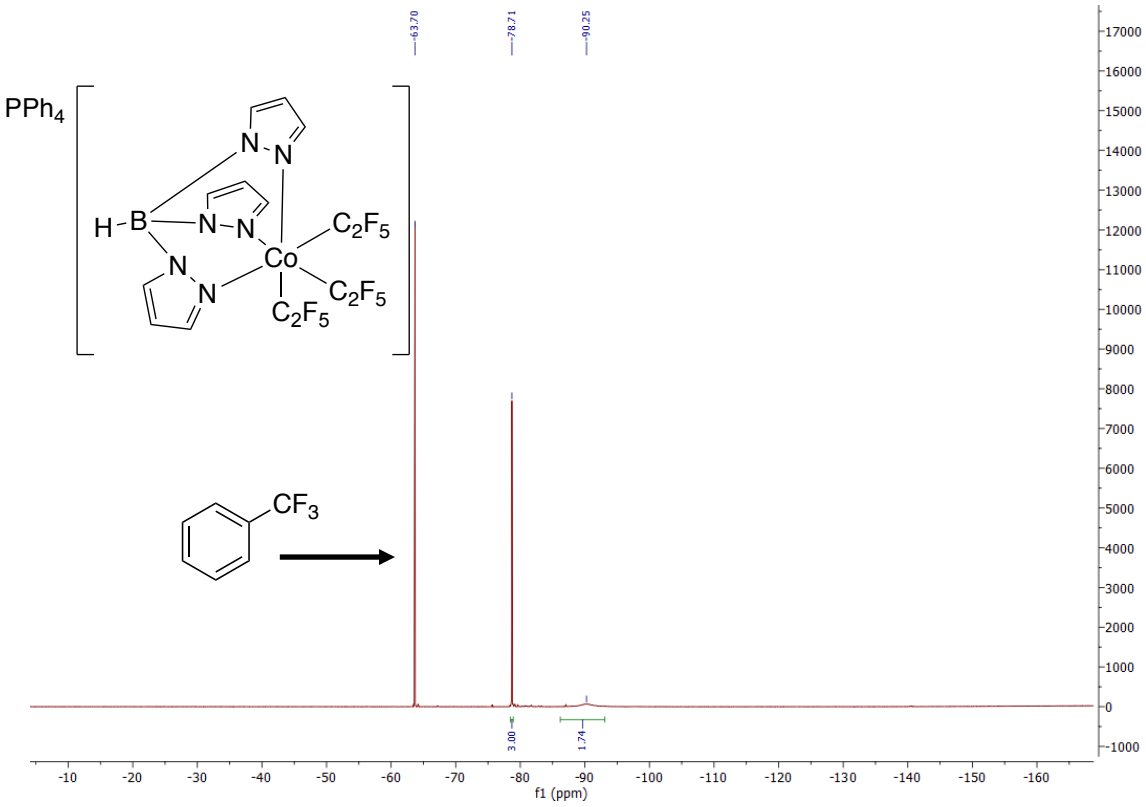

Figure C2. ^{1}H NMR of $[PPh_4][(Tp)Co(C_2F_5)_3]$ **(4h)** in CD_3CN

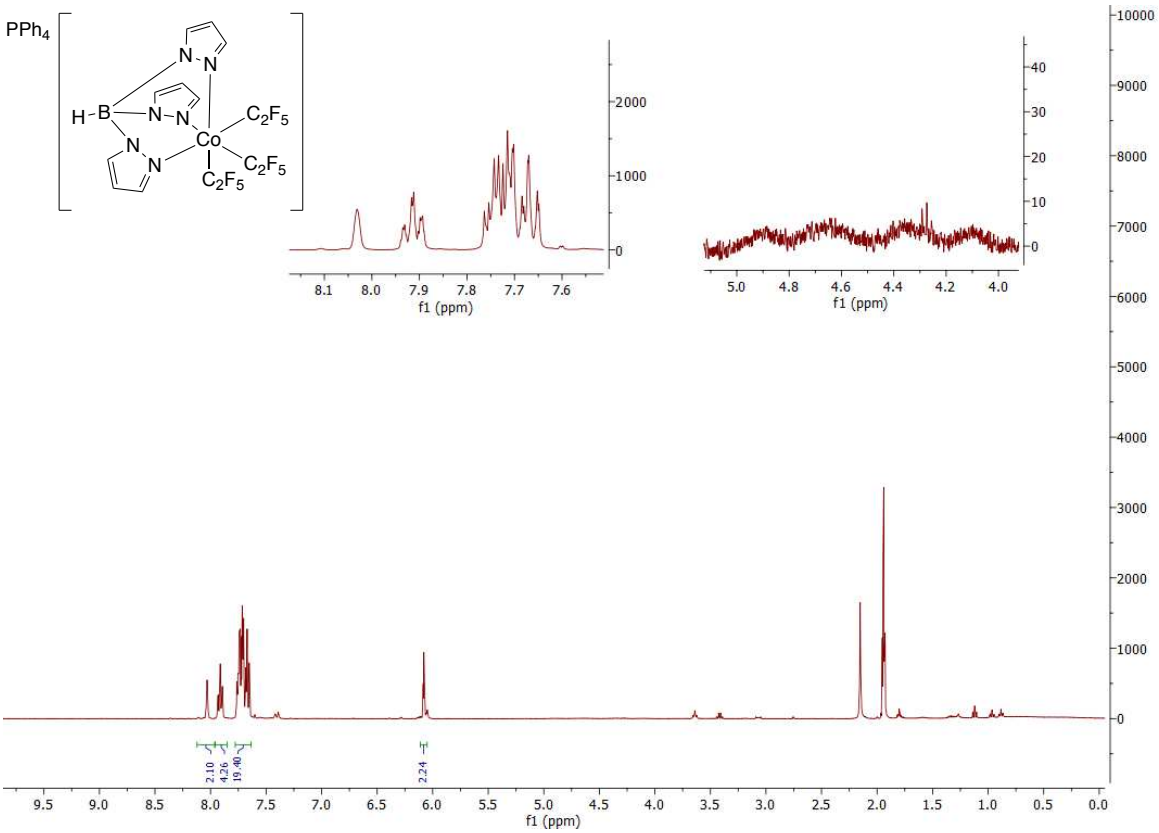

Figure C3. $^{31}P\{^{1}H\}$ NMR of $[PPh_4][(Tp)Co(C_2F_5)_3]$ **(4h)** in CD_3CN

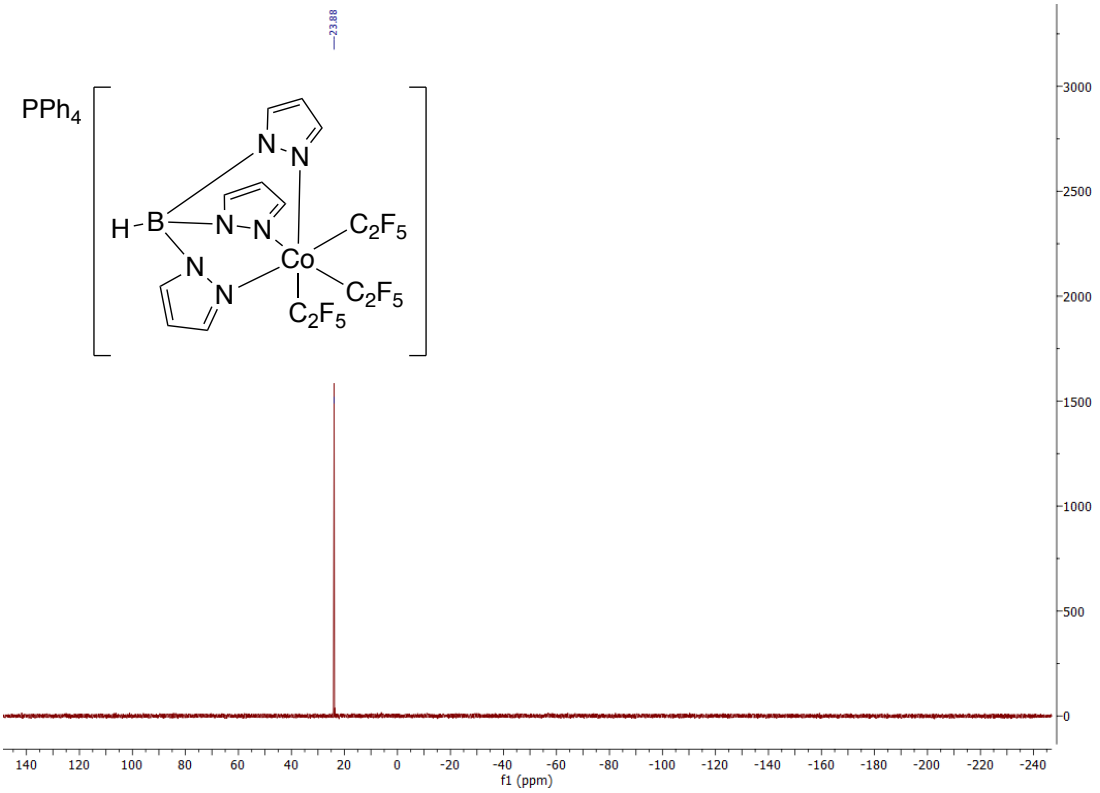

Figure C4. ^{19}F NMR of crude reaction mixture during synthesis of **4h** at room temperature before heating in CD_3CN

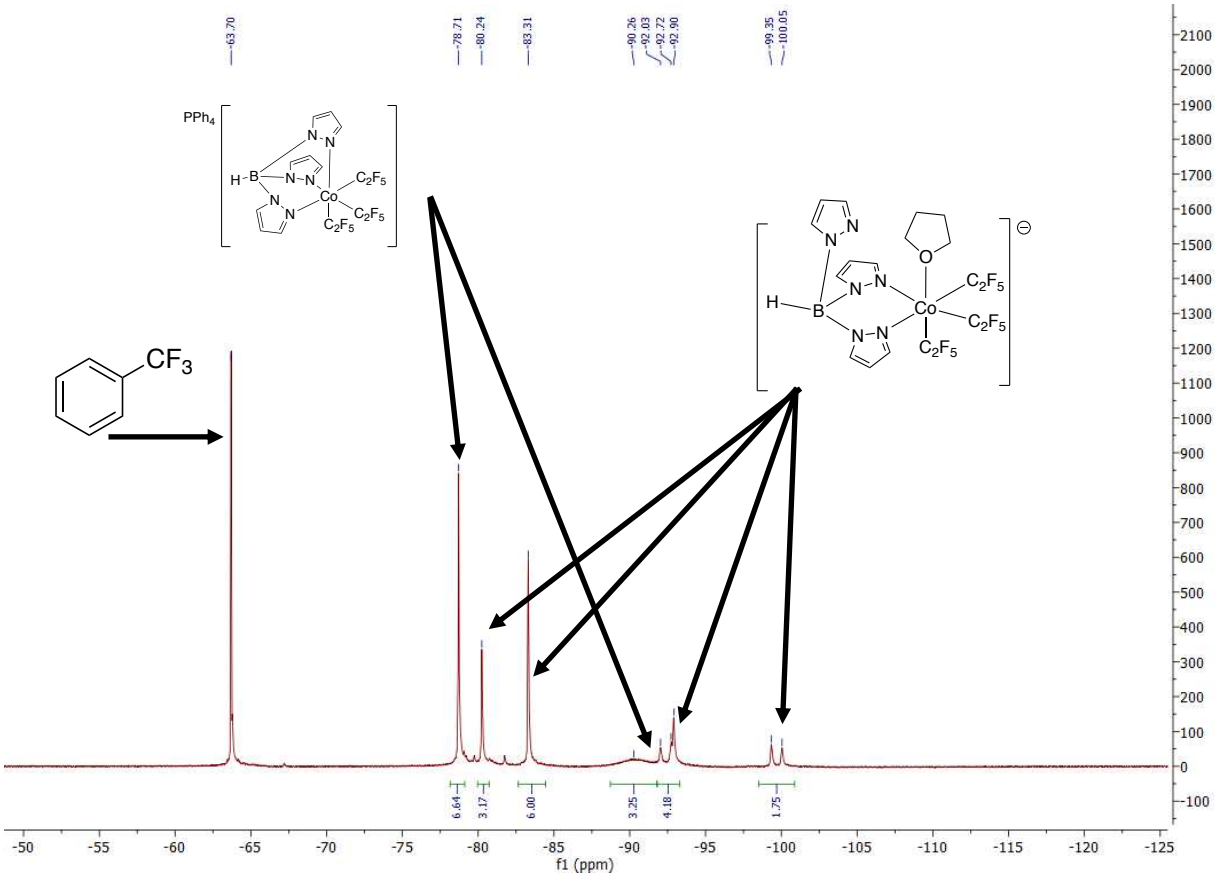

Figure C5. ^{1}H NMR of crude reaction mixture during synthesis of **4h** at room temperature before heating in CD_3CN

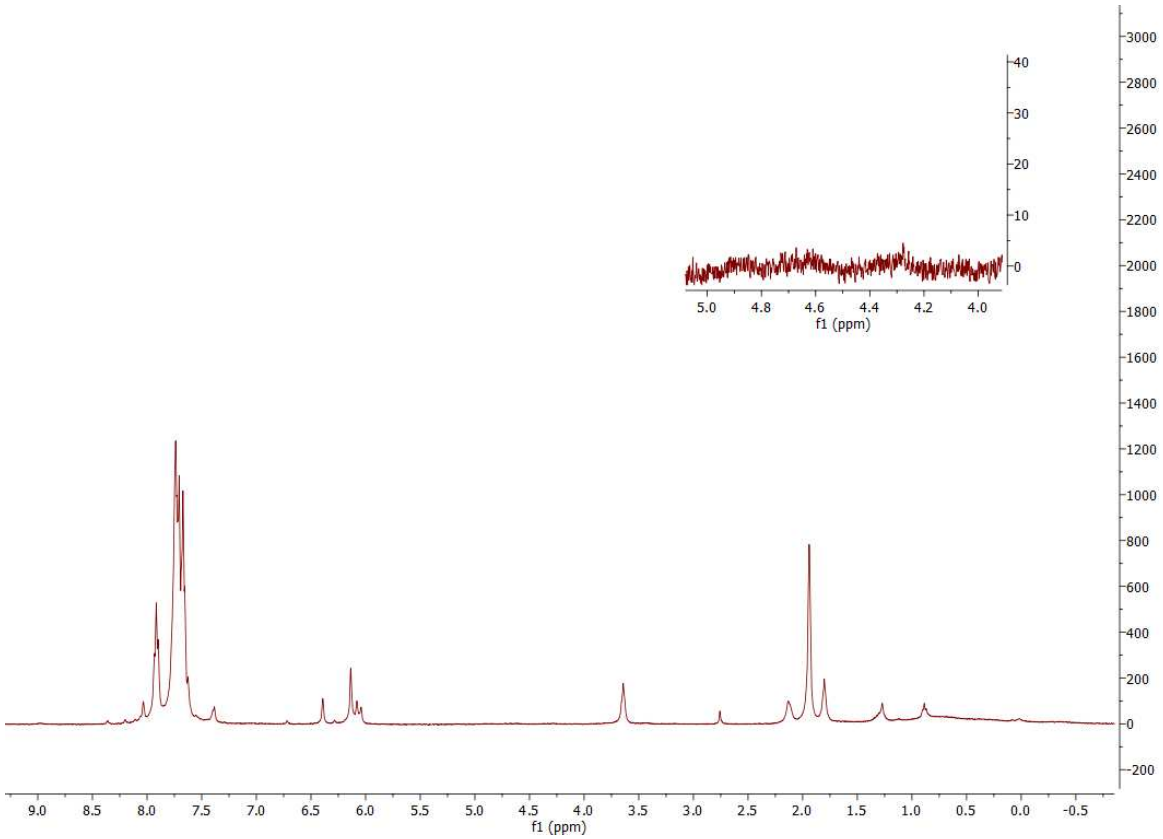

Figure C6. ^{19}F NMR of crude reaction mixture during the synthesis of **4h** at -78 ˚C in CD_3CN

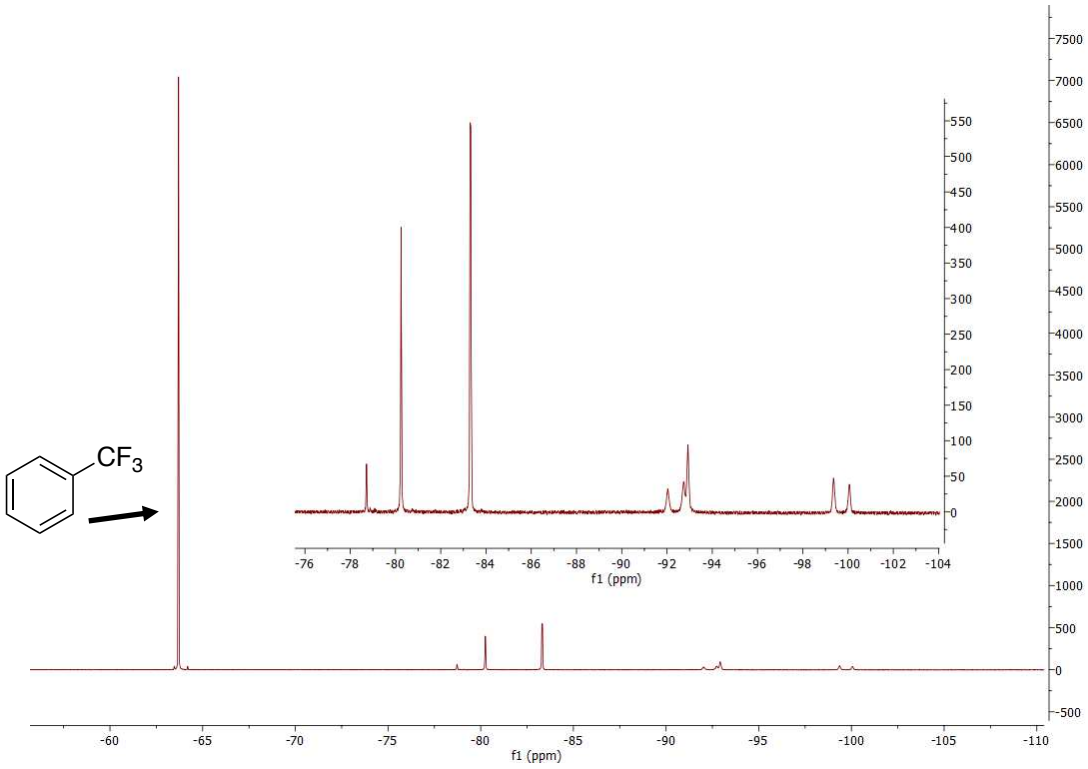

Figure C7. Cyclic voltammogram of **4f** (10 mM) in MeCN. Working and counter electrodes are platinum with a Ag pseudo reference. Electrolyte: $[NBu_4][PF_6]$ (100 mM). Scan rate: 100 mV s^{-1}.

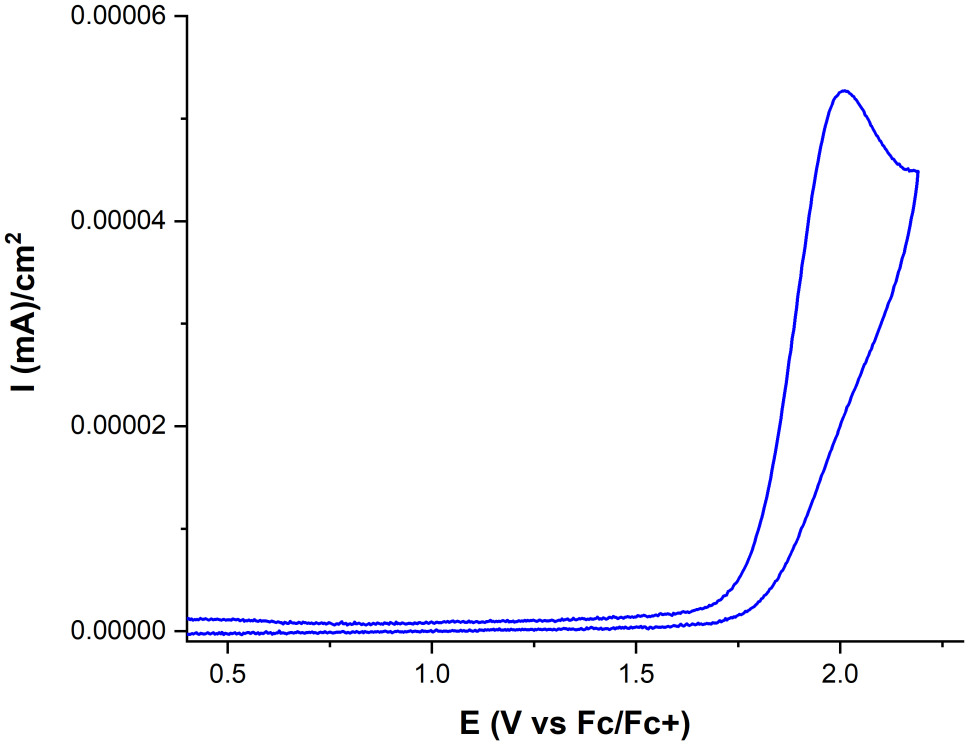

Figure C8. Cyclic voltammogram of **4h** (10 mM) in MeCN. Working and counter electrodes are platinum with a Ag pseudo reference. Electrolyte: $[NBu_4][PF_6]$ (100 mM). Scan rate: 100 mV s^{-1}.

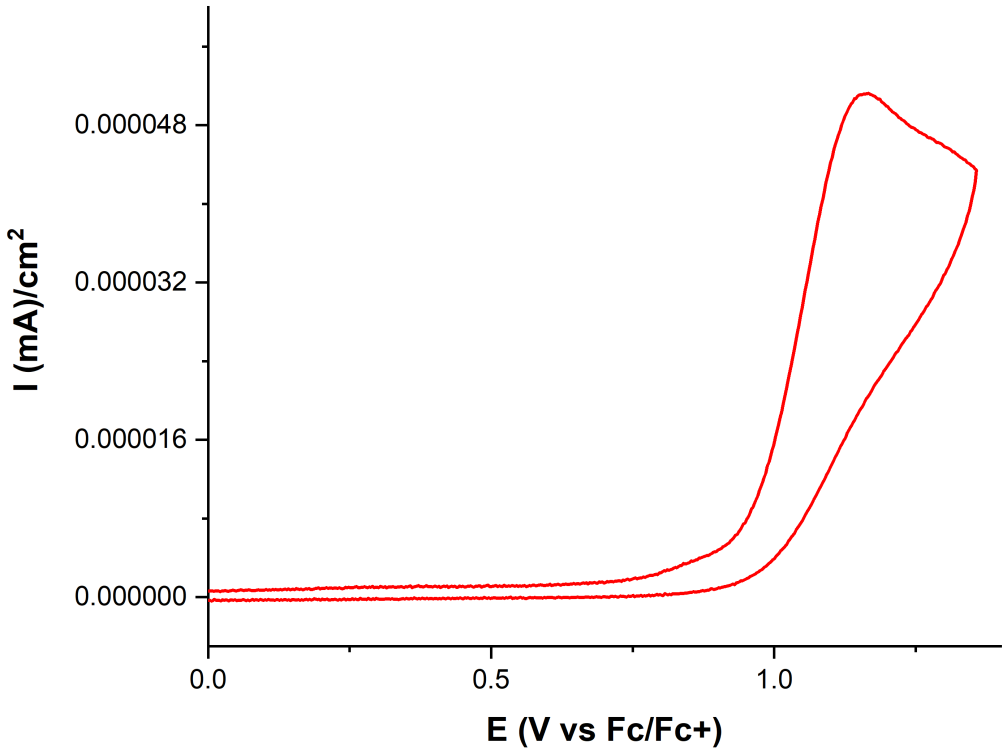

Figure C9. Cyclic voltammogram of **[(tpy)Co(C_2F_5)$_3$]** (10 mM) in MeCN. Working and counter electrodes are platinum with a Ag pseudo reference. Electrolyte: [NBu_4][PF_6] (100 mM). Scan rate: 100 mV s^{-1}.

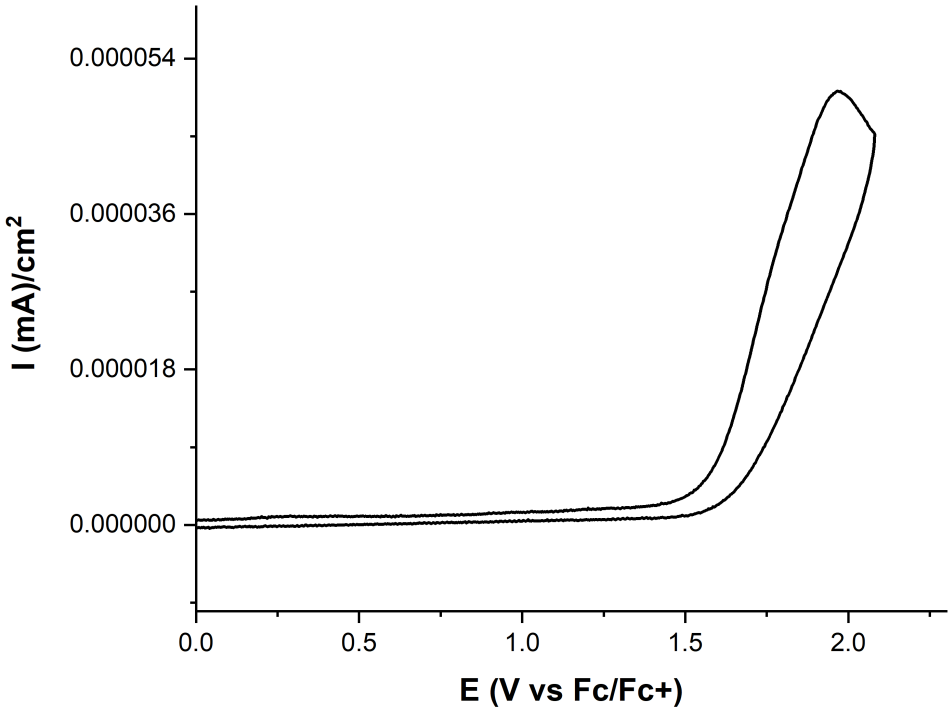

Figure C10. Experimental UV-vis spectra in MeCN: complex **4f** (blue, 1.1 mM), ε_{390} = 280 M^{-1} cm^{-1}, ε_{309} = 220 M^{-1} cm^{-1}; complex **4h** (red, 1.2 mM), ε_{434} = 280 M^{-1} cm^{-1}, ε_{328} = 200 M^{-1} cm^{-1}; [(tpy)Co(C_2F_5)$_3$] (black, 1.1 mM), ε_{480} = 63 M^{-1} cm^{-1}.

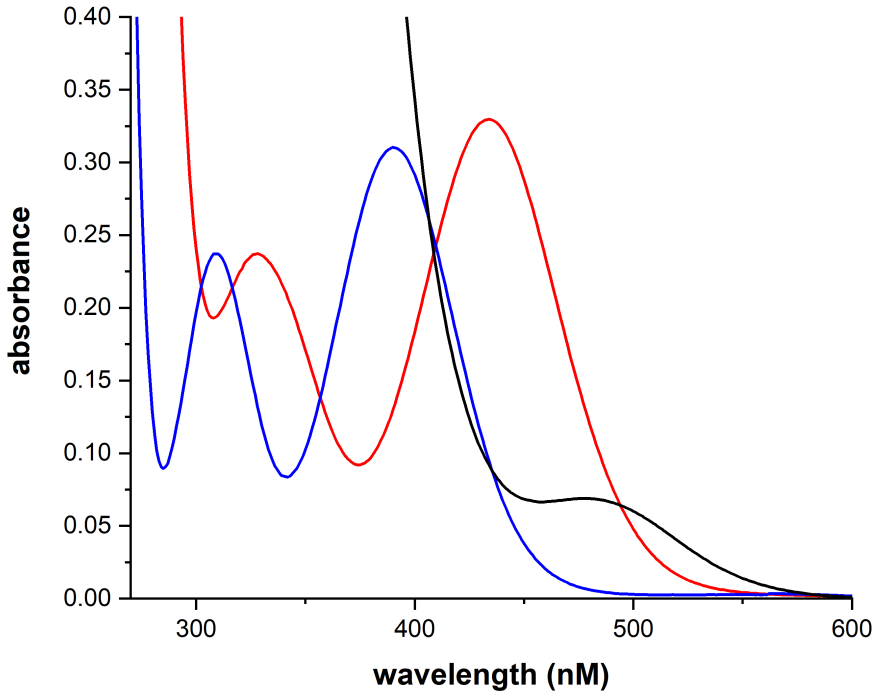

Figure C11. Experimental UV-vis spectra of diluted [(tpy)Co(C_2F_5)$_3$] in MeCN (0.093 mM). ε_{317} = 9700 M^{-1} cm^{-1}.

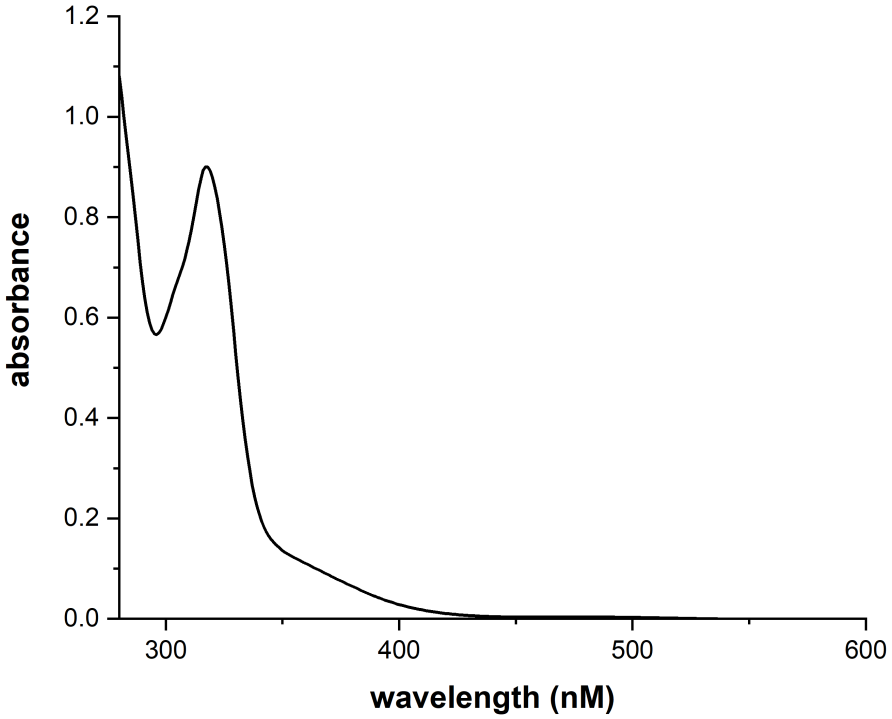

Appendix D: Supporting Information and Spectral Data for Chapter 5

Figure D1. ^{19}F NMR of $[PPh_4]_2[(C_2F_5)_3Co(\mu\text{-}F)_2Co(C_2F_5)_3]$ **(5b)** in CD_3CN at room temperature

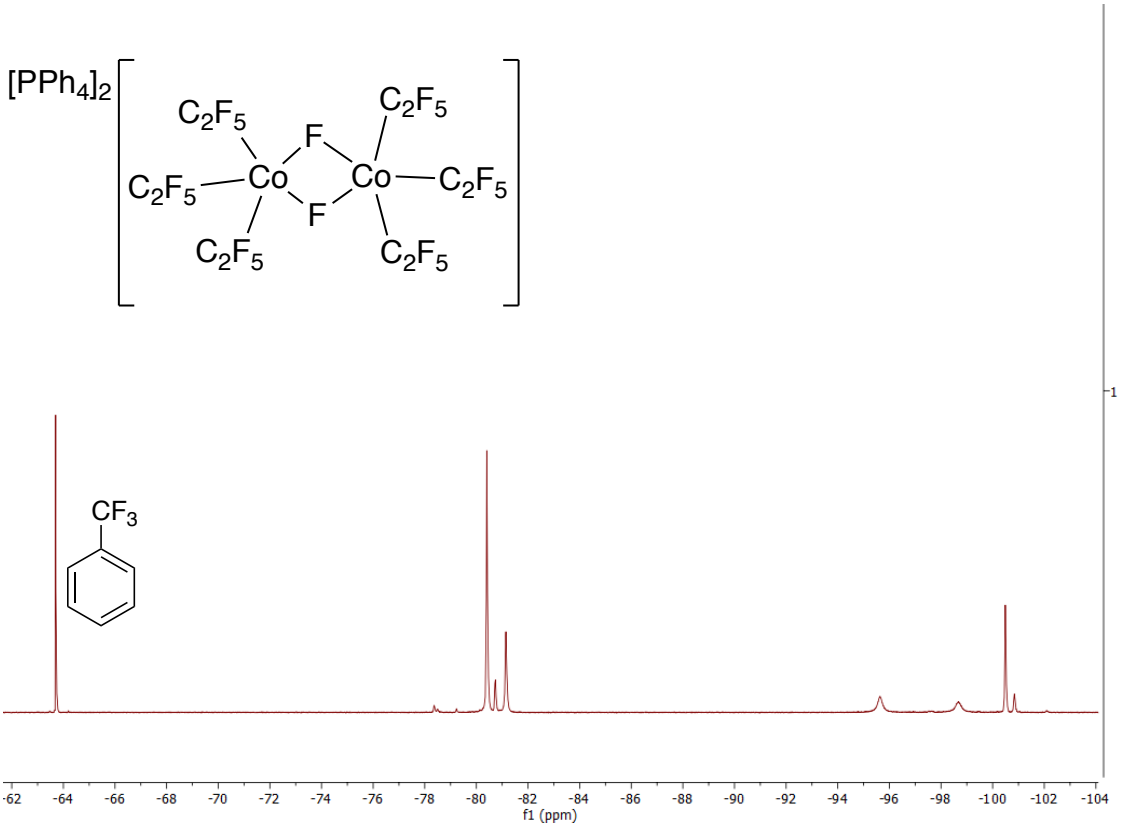

Figure D2. Expanded ^{19}F NMR of $[PPh_4]_2[(C_2F_5)_3Co(\mu\text{-}F)_2Co(C_2F_5)_3]$ **(5b)** in CD_3CN at room temperature

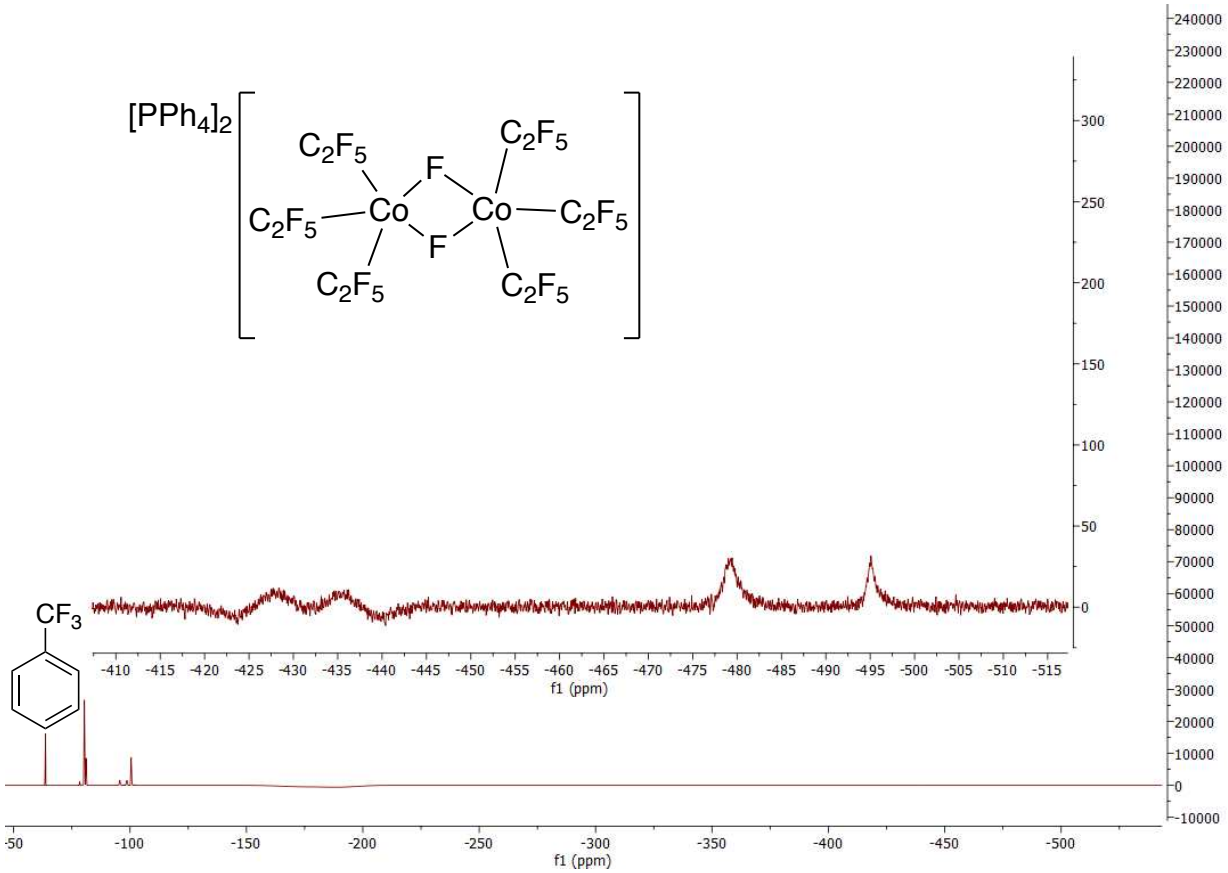

Figure D3. ^{19}F NMR of $[PPh_4]_2[(C_2F_5)_3Co(\mu\text{-}F)_2Co(C_2F_5)_3]$ **(5b)** in CD_3CN recorded at -30 °C

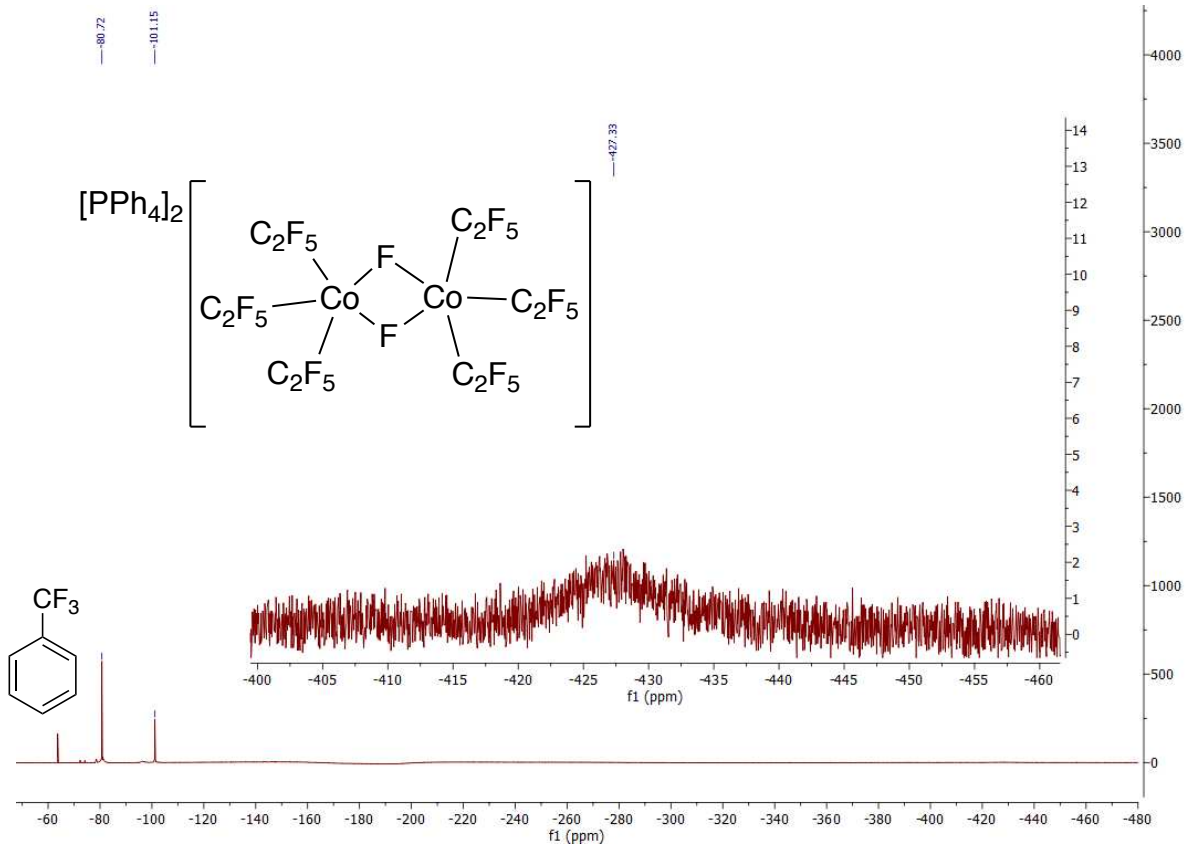

Figure D4. ^{19}F NMR of $[PPh_4]_2[(C_2F_5)_3Co(\mu\text{-}F)_2Co(C_2F_5)_3]$ **(5b)** in CD_2Cl_2 at room temperature

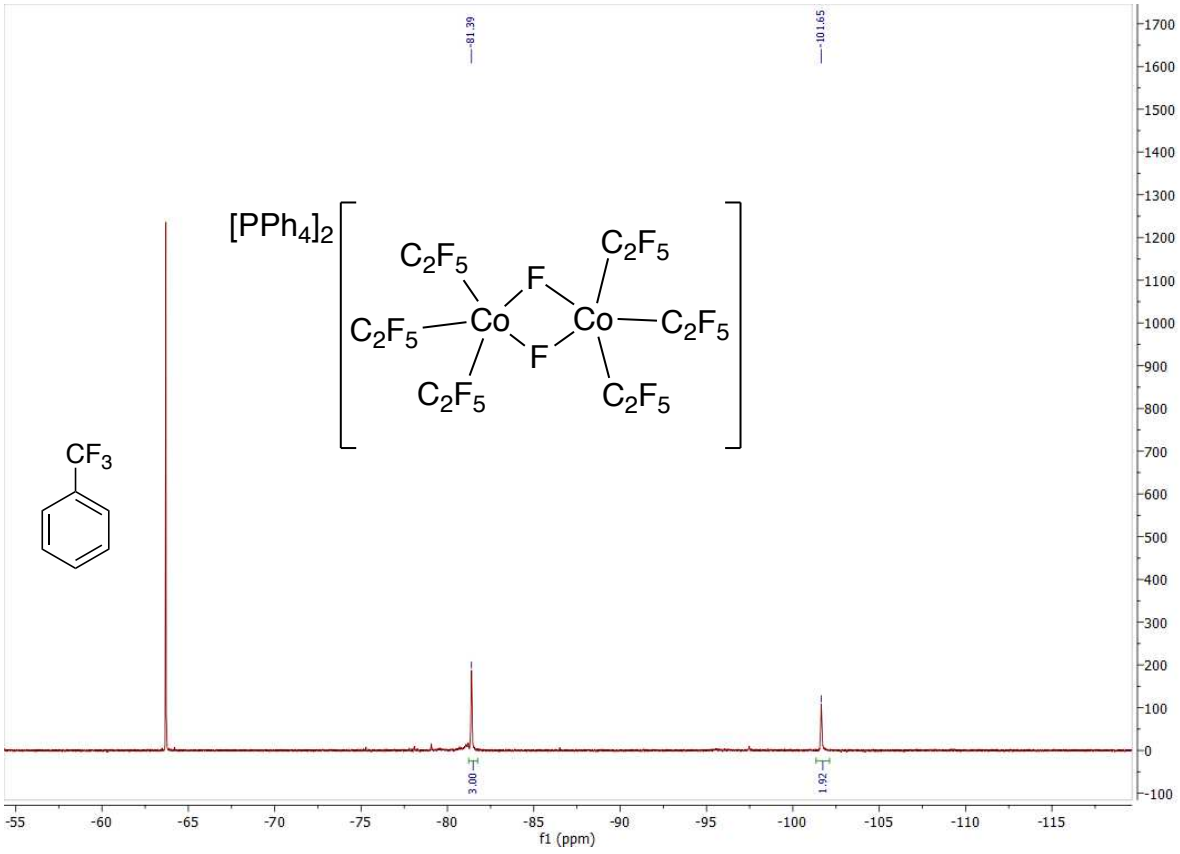

Figure D5. Expanded ^{19}F NMR of $[PPh_4]_2[(C_2F_5)_3Co(\mu\text{-}F)_2Co(C_2F_5)_3]$ **(5b)** in CD_2Cl_2 at room temperature

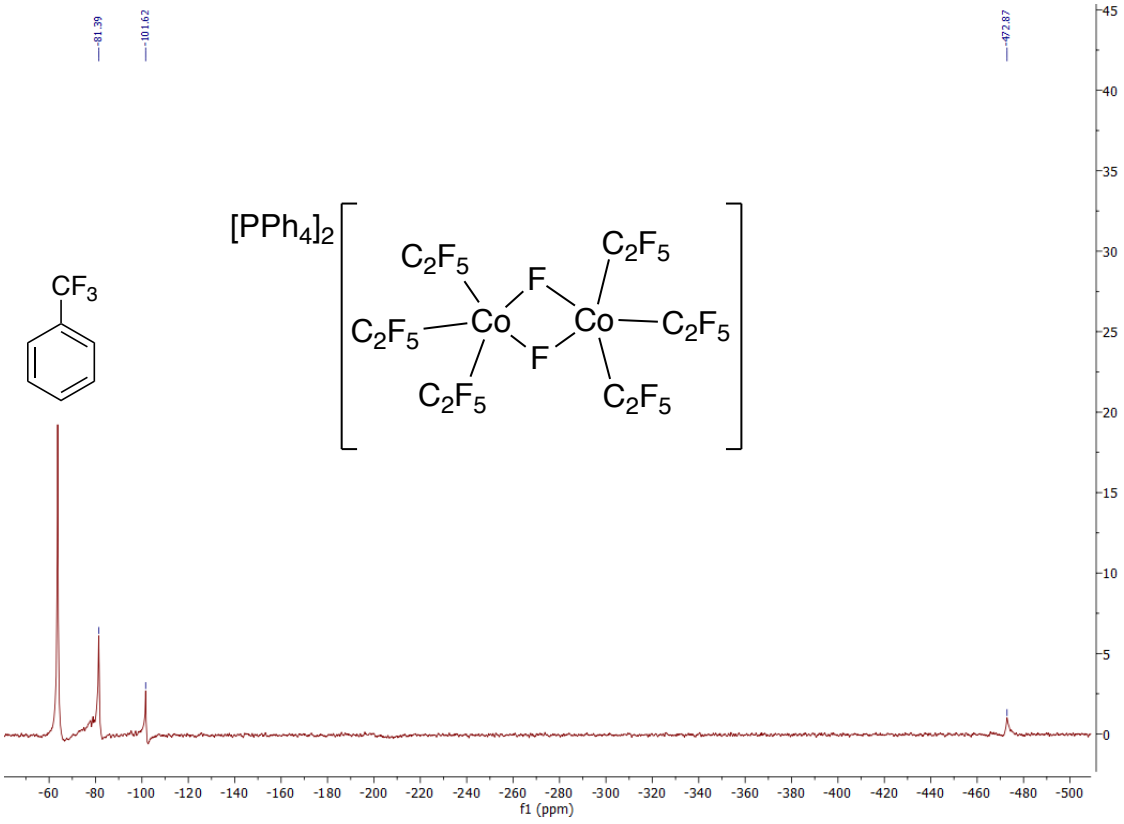

Figure D6. ^{1}H NMR of $[PPh_4]_2[(C_2F_5)_3Co(\mu\text{-}F)_2Co(C_2F_5)_3]$ **(5b)** in CD_3CN

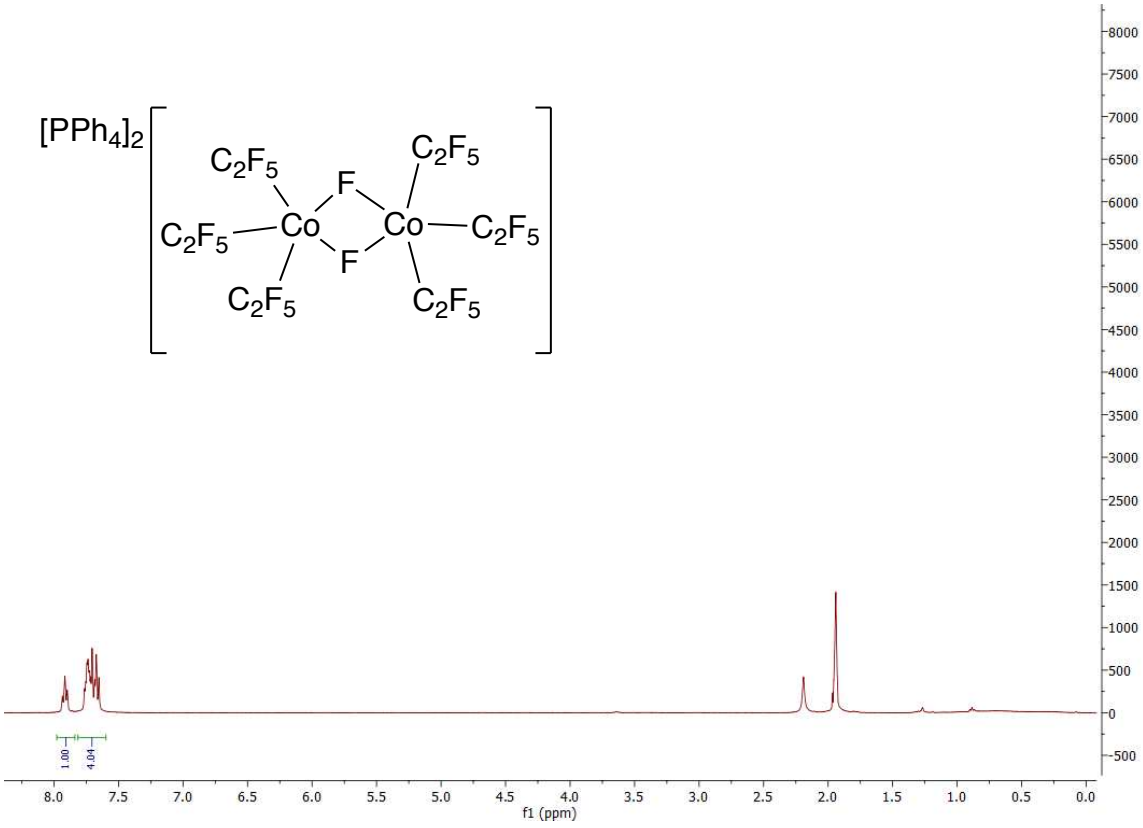

Figure D7. $^{31}P\{H\}$ NMR of $[PPh_4]_2[(C_2F_5)_3Co(\mu\text{-}F)_2Co(C_2F_5)_3]$ **(5b)** in CD_3CN

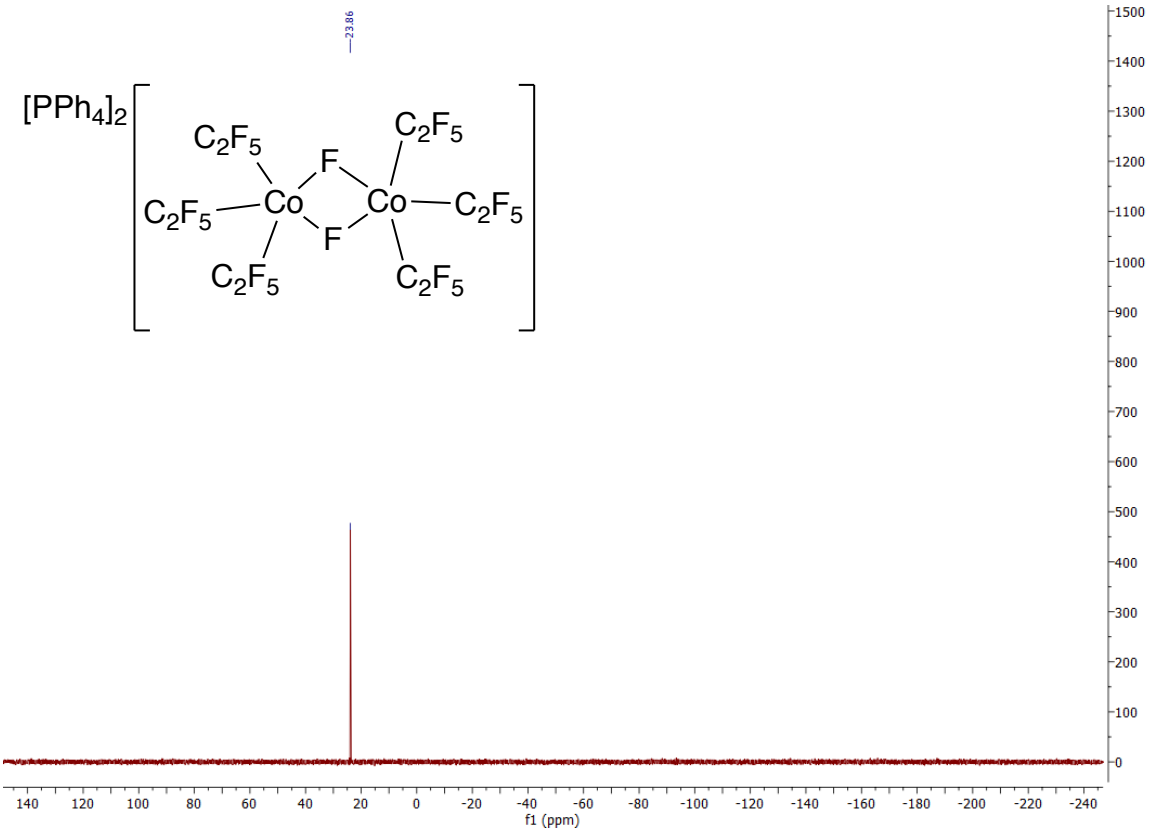

Figure D8. ^{19}F NMR of $[PPh_4]_2[(C_2F_5)_3Co(\mu\text{-}F)_2Co(C_2F_5)_3]$ **(2)** in CD_3CN over time

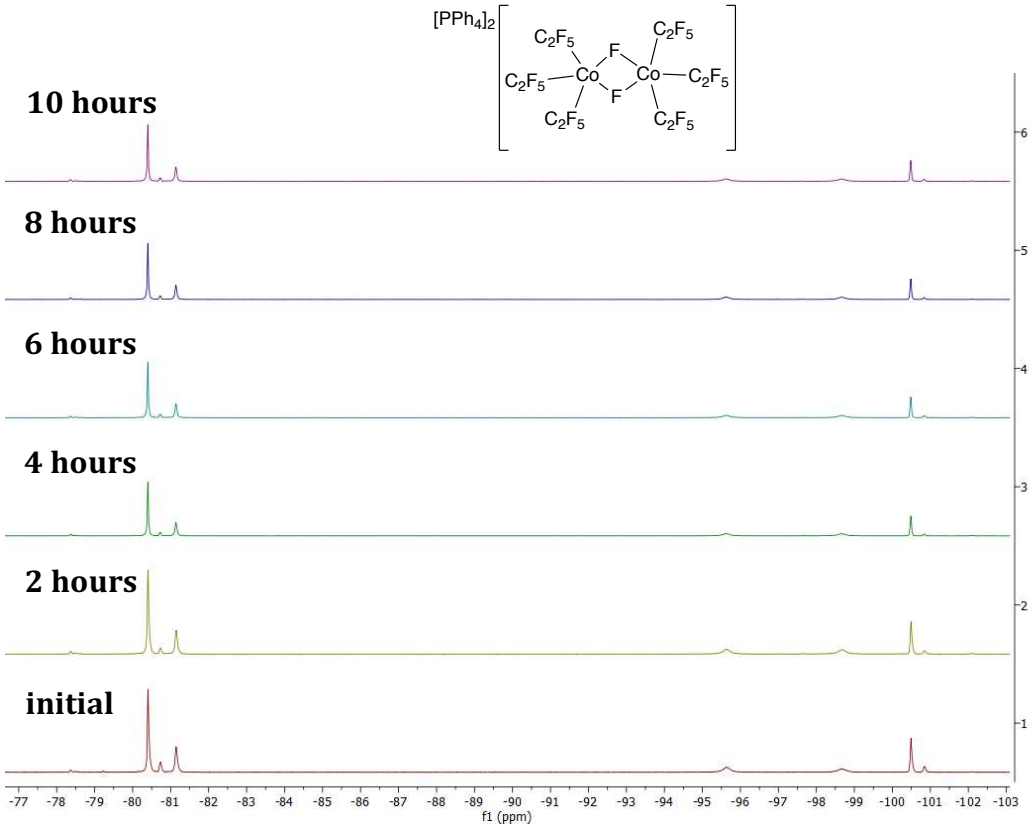

Figure D9. ^{19}F NMR of $[PPh_4]_2[(C_2F_5)_3Co(\mu\text{-}F)_2Co(C_2F_5)_3]$ **(5b)** in CD_3CN at elevated temperatures

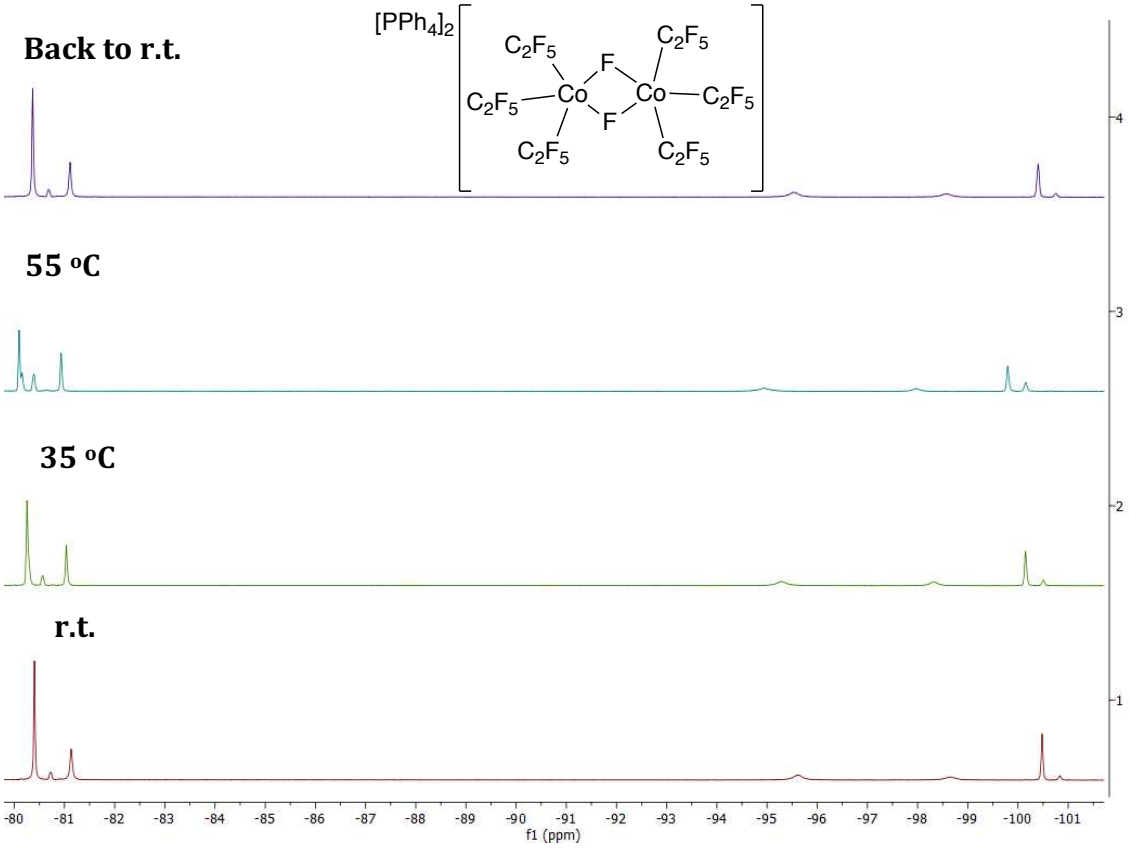

Figure D10. ^{19}F NMR of $[PPh_4]_2[(C_2F_5)_3Co(\mu\text{-}F)_2Co(C_2F_5)_3]$ **(5b)** in CD_3CN at -30 °C and room temperature

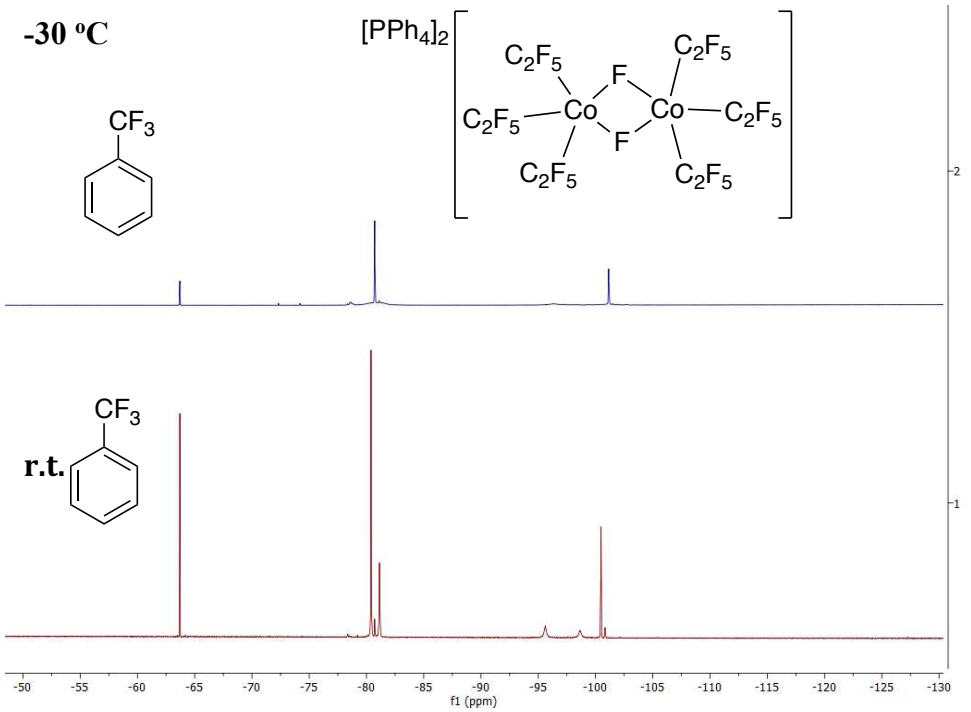

Figure D11. ^{19}F NMR of $[PPh_4]_2[(C_2F_5)_3Co(\mu\text{-}F)_2Co(C_2F_5)_3]$ **(5b)** in CD_3CN at room temperature with integrations

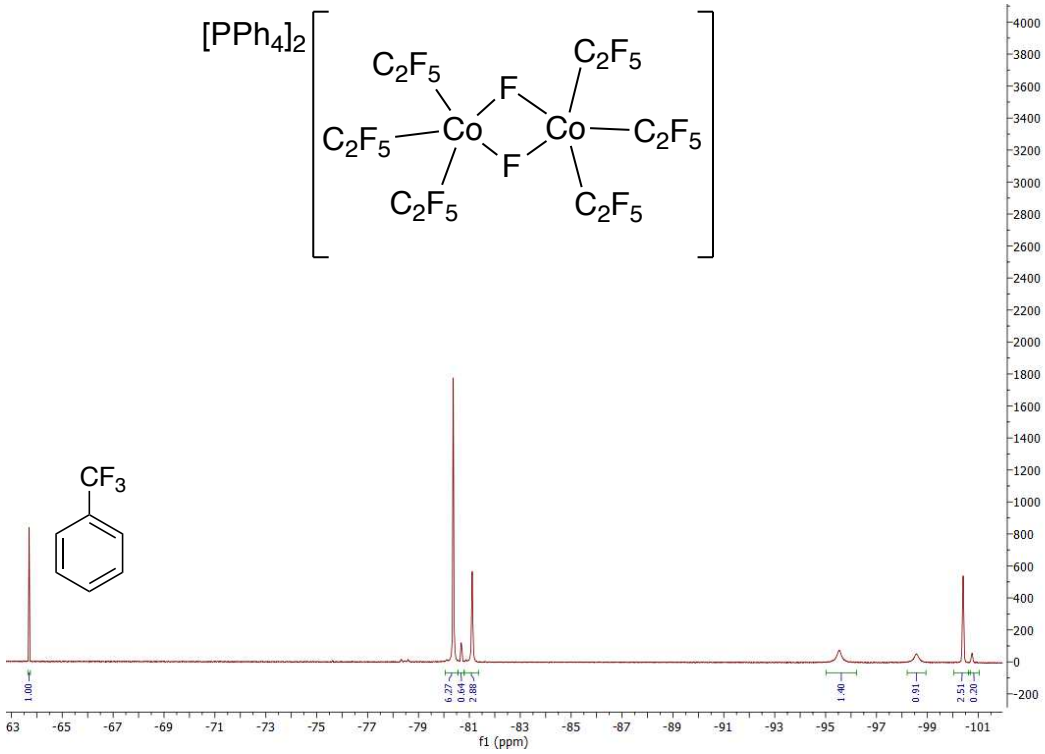

Figure D12. ^{19}F NMR of $[PPh_4]_2[(C_2F_5)_3Co(\mu\text{-}F)_2Co(C_2F_5)_3]$ **(5b)** in CD_3CN 35 °C with integrations

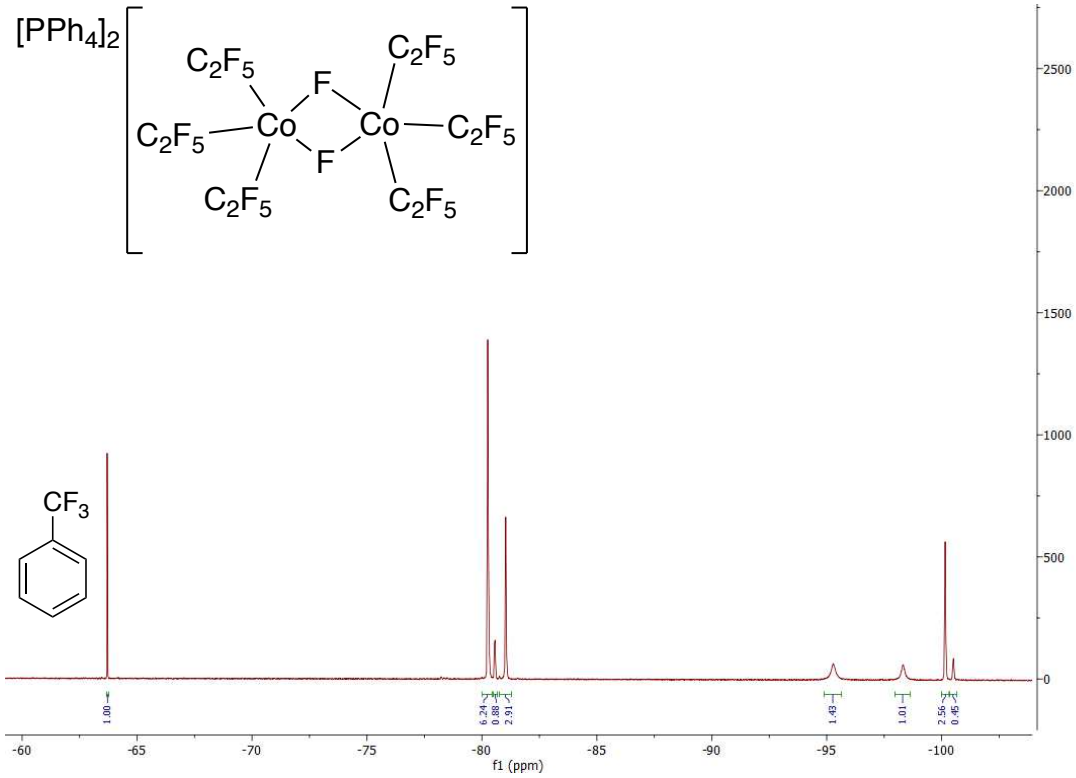

Figure D13. ^{19}F NMR of $[PPh_4]_2[(C_2F_5)_3Co(\mu\text{-}F)_2Co(C_2F_5)_3]$ **(5b)** in CD_3CN 55 °C with integrations

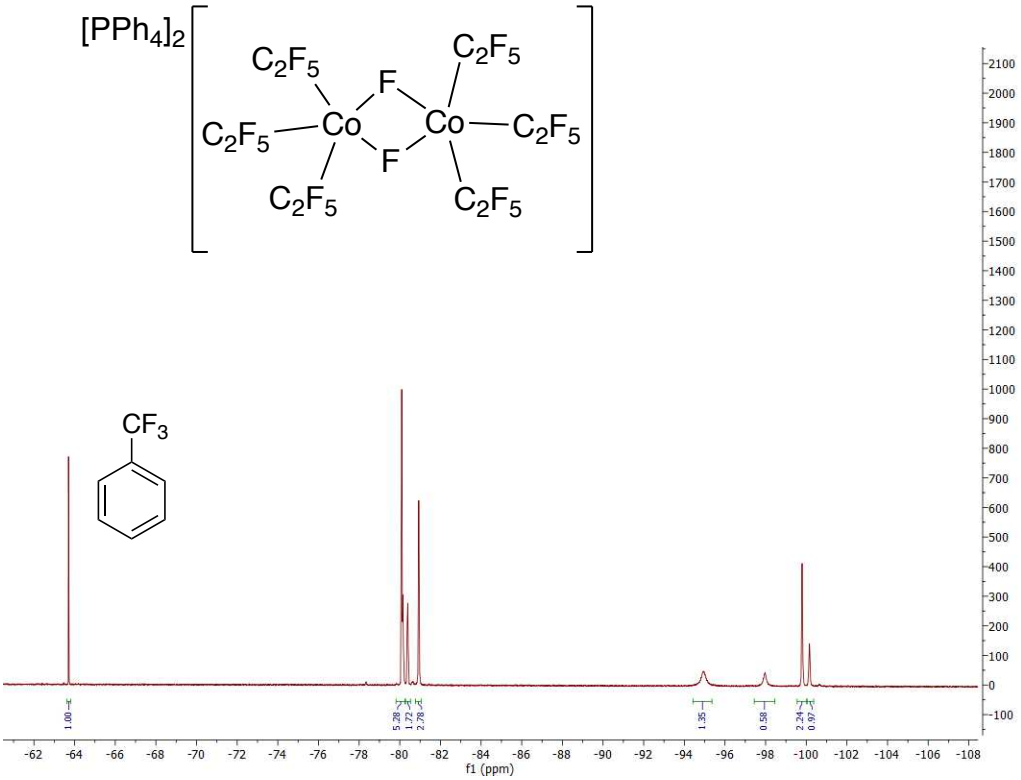

DFT optimized geometry of 5c - *fac*

Co	-0.72264103	-0.09367642	0.22627185
C	1.26129080	-0.10442704	-0.07079727
C	2.23057795	1.08973570	-0.21834036
C	-0.56108106	-0.01235992	2.17916149
C	-0.61600001	-1.31541120	3.01172201
C	-0.99252506	1.84053539	0.15349290
C	-2.44273480	2.37025414	0.02798840
F	0.42051192	-2.14217305	2.77545225
F	-0.57926865	-1.02928043	4.34026015
F	-1.75080242	-2.01125018	2.80098370
F	-1.60020611	0.72118790	2.73618577
F	0.59012613	0.60575425	2.65187361
F	1.88105322	-0.87609686	0.91291914
F	1.52946217	-0.81847558	-1.25454138
F	2.10541719	1.99865446	0.76328424
F	3.52385634	0.66577839	-0.18891306
F	2.07549044	1.72466826	-1.39768936
F	-0.39495635	2.37922558	-0.98925993
F	-0.47633422	2.59545092	1.19332420
F	-2.41133476	3.72589570	-0.14690389
F	-3.08352587	1.87554997	-1.04765258
F	-3.19867275	2.15946285	1.11338683
F	-2.55983848	-0.35321033	0.43511297
C	-0.55748139	-3.24916667	-0.01580503
C	-1.34223944	-0.20557628	-2.87782881
N	-1.06265152	-0.15822376	-1.75919322

N	-0.57674721	-2.10441621	0.12947218
C	-0.52481269	-4.69502757	-0.18303678
H	0.28716913	-4.97291211	-0.85988015
H	-0.36168454	-5.17437181	0.78572420
H	-1.47274769	-5.04475096	-0.59963130
C	-1.69862568	-0.25386447	-4.28907739
H	-0.80988660	-0.09222602	-4.90426638
H	-2.12862099	-1.22879668	-4.53222160
H	-2.43308467	0.52461277	-4.51125995

DFT optimized geometry of 5c - *mer*

Co	-0.83871669	-0.16901581	0.13682959
C	1.21147929	-0.17571746	-0.25475895
C	2.23495491	0.97269783	-0.39630985
C	-0.98259483	1.80075302	0.16623526
C	-2.26396159	2.64380484	-0.06034116
F	1.80671864	-0.95505220	0.73963675
F	1.45097621	-0.89755274	-1.44106083
F	2.13866427	1.87932630	0.59579647
F	3.51089171	0.49526028	-0.35134093
F	2.13309369	1.61969838	-1.57459047
F	-0.18131444	2.31850776	-0.85694393
F	-0.47635302	2.33590258	1.33360183
F	-1.94214585	3.96643622	-0.05889097
F	-2.83166339	2.39479729	-1.25632061
F	-3.19266998	2.48883948	0.89591996
C	-0.27545793	-3.28052338	-0.01995666
C	-1.50620536	-0.14664799	-2.85140745
N	-1.24869353	-0.15734107	-1.72728134
N	-0.53914141	-2.15903420	0.03721501
C	0.03627307	-4.70073792	-0.07986600
H	0.18218907	-5.00686763	-1.11886068
H	0.94992391	-4.90551601	0.48396102
H	-0.78701424	-5.27681501	0.35054163
C	-1.83219574	-0.12414018	-4.26922363
H	-0.92145886	-0.23387218	-4.86348830
H	-2.51575523	-0.94311427	-4.50742364
H	-2.31170425	0.82533100	-4.52130761
C	-2.79806133	-0.46576477	0.61115009
C	-3.36993468	-1.89235296	0.72324054
F	-0.47658681	-0.22086372	1.92304066

F	-3.13519325	0.07642315	1.84509196
F	-3.69397327	0.11103166	-0.29879654
F	-4.68916421	-1.87026109	1.04593605
F	-3.27627384	-2.56708432	-0.44434785
F	-2.75954090	-2.62545327	1.67717640

DFT optimized geometry of 5b

Co	10.33634348	14.59078754	10.18018026
C	8.64269889	13.99198771	10.93355938
F	10.57994552	15.84441537	11.62613254
C	7.40539268	14.74405743	10.38956373
F	8.60516080	14.28130161	12.29265446
F	8.29516660	12.65792694	10.85424645
C	11.33255759	13.09212915	10.78681657
F	7.64939350	16.07176659	10.30828174
C	11.63346312	12.91917593	12.29316813
F	6.33013547	14.58768343	11.19585354
C	9.99531674	13.83281489	8.44173176
F	7.04060101	14.31915826	9.16799526
C	11.09462320	13.44976317	7.42618860
F	10.83468404	11.86673663	10.40809473
F	12.59336827	13.17777167	10.22002625
F	12.49009446	11.88268608	12.47031752
F	12.21613866	14.00529376	12.82330584
F	10.53064218	12.63802892	13.00414576
F	9.33984901	14.91072635	7.82502913
F	9.12386262	12.76658788	8.34710688
F	12.00908811	14.41090484	7.23335123
F	11.73818963	12.32736986	7.79671206
F	10.53345470	13.19754126	6.21465211
Co	12.05212038	16.92416223	10.98428737
C	13.74566120	17.52348589	10.23126602
F	11.80853200	15.67053900	9.53821877
C	14.98380536	16.77352356	10.77627922
F	13.78376662	17.23265431	8.87250787
F	14.09153685	18.85807779	10.30923389
C	11.05590055	18.42258889	10.37671203
F	14.74118214	15.44568158	10.85963289
C	10.75800488	18.59660925	8.86983542
F	16.05877089	16.92973711	9.96955327
C	12.39283491	17.68232294	12.72271411
F	15.34838436	17.20072164	11.99709346
C	11.29300842	18.06262670	13.73872453
F	11.55189712	19.64809556	10.75759164
F	9.79399559	18.33543493	10.94067284
F	9.90036069	19.63215631	8.69193412
F	10.17790268	17.51022667	8.33742791
F	11.86188396	18.87996134	8.16136699
F	13.05081988	16.60582957	13.33927323
F	13.26198467	18.75042155	12.81688252
F	10.38273449	17.09796124	13.93393183
F	10.64442989	19.18178975	13.36722321
F	11.85429689	18.31893492	14.94935285

Table D1. Relative energies for DFT optimized structures of **5b** and **5c**

Compound	Electronic Energy (Hartree)
[fac-$(MeCN)_2(F)Co(C_2F_5)_3]^-$	– 3474.373133
[*mer*-$(MeCN)_2(F)Co(C_2F_5)_3]^-$	– 3474.357040
$[(C_2F_5)_3Co(\mu\text{-}F)_2Co(C_2F_5)_3]^{2-}$	– 6417.710363

Appendix E: Supporting Information and Spectral Data for Chapter 6

Figure E1. Cyclic voltammogram of $[NBu_4][Cu(CF_3)_4]$ (20 mM) in MeCN. Working and counter electrodes are platinum with a Ag pseudo reference. Electrolyte: $[Bu_4N][PF_6]$ (100 mM). Scan rate: 100 mV s^{-1}.

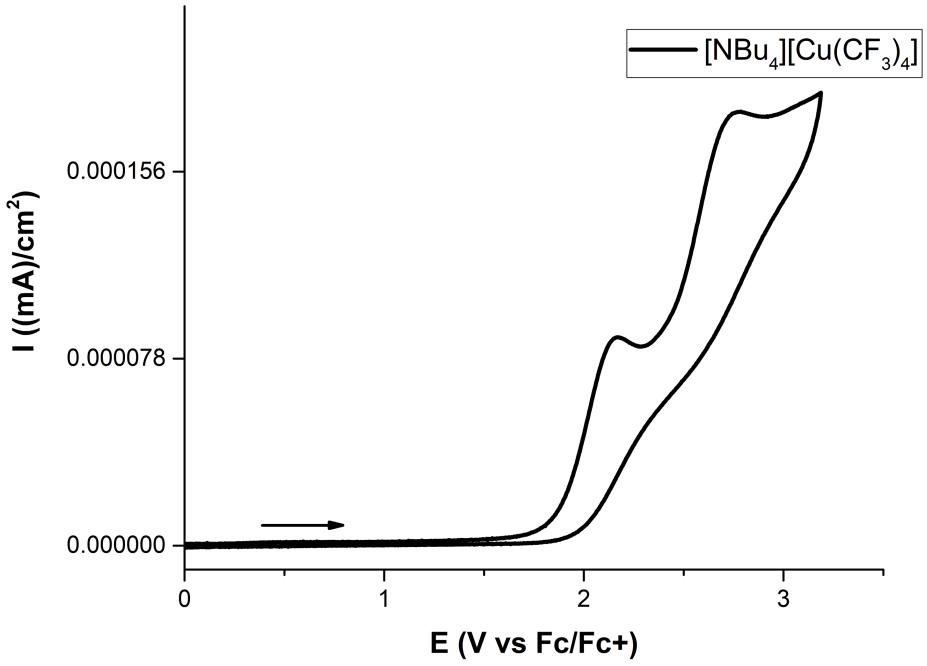

Figure E2. ^{19}F NMR of $[PPh_4][(MeCN)Ni(CF_3)_3]$ (**6e**) in CD_3CN

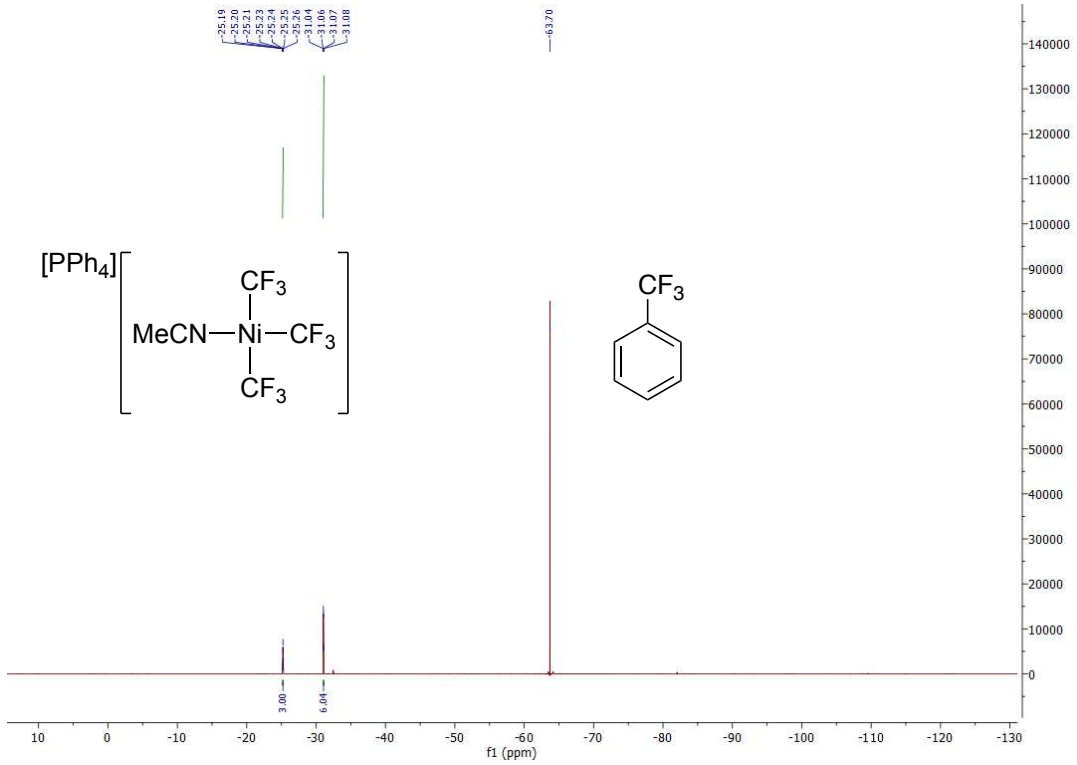

Figure E3 – ^{1}H NMR of $[PPh_4][(MeCN)Ni(CF_3)_3]$ (**6e**) in CD_3CN

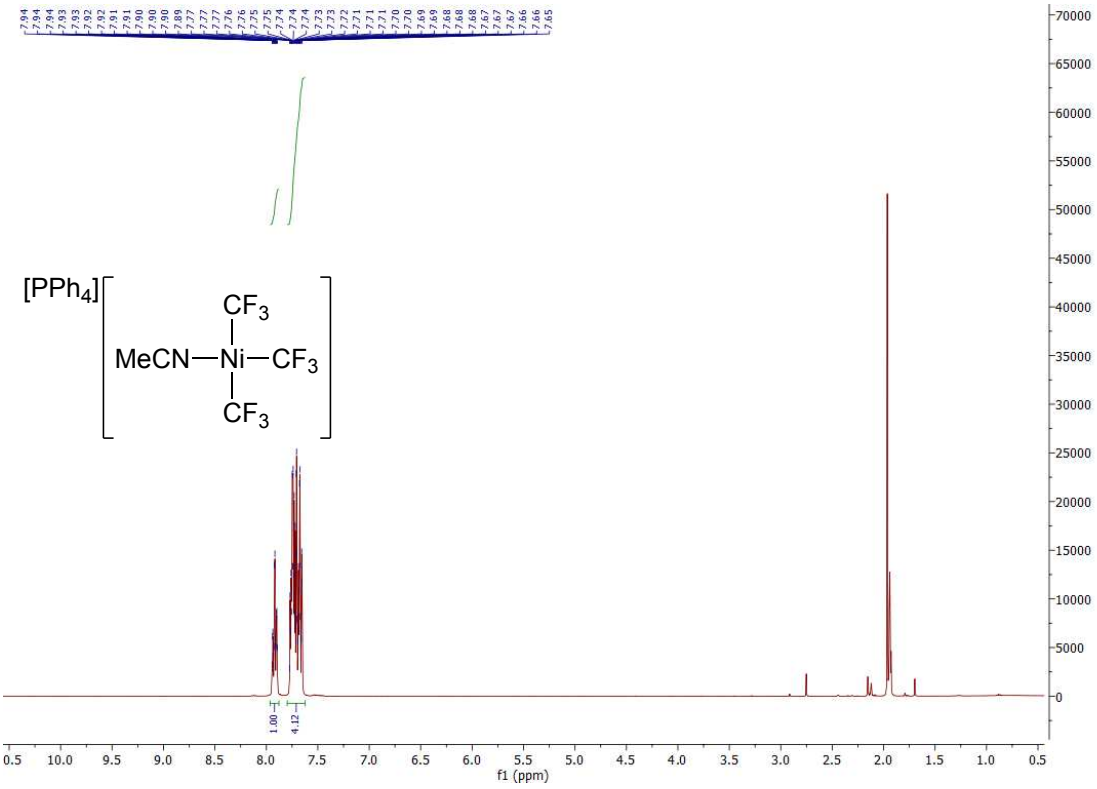

Figure E4. $^{31}P\{^{1}H\}$ NMR of $[PPh_4][(MeCN)Ni(CF_3)_3]$ (**6e**) in CD_3CN

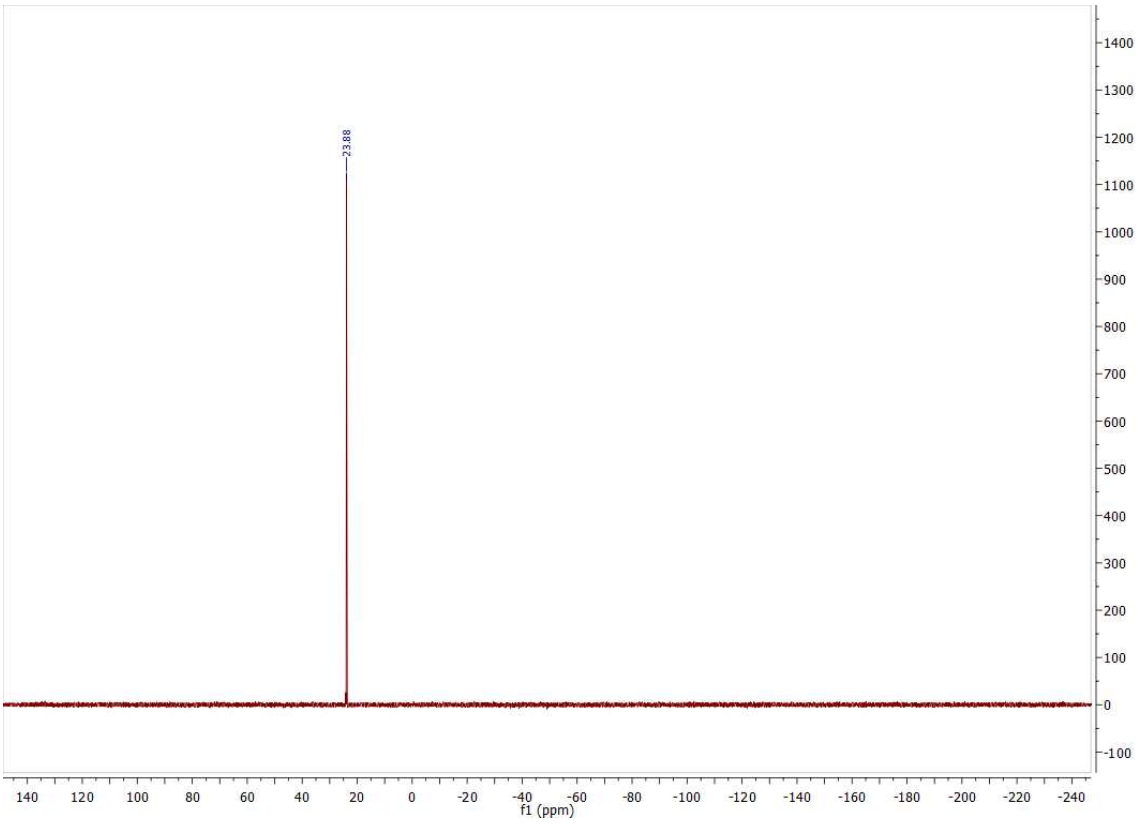

Figure E5. ^{19}F NMR of $[PPh_4]_2[Ni(CF_3)_4]$ (**6f**) in CD_3CN

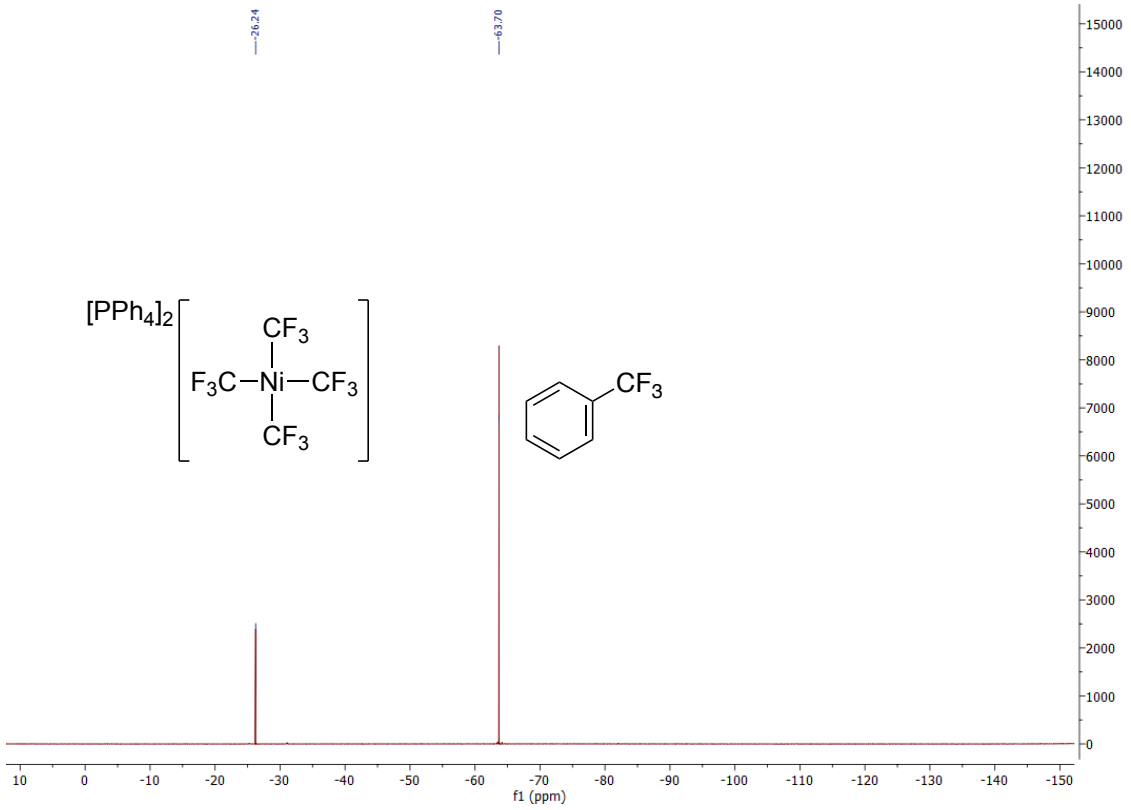

Figure E6. ^{1}H NMR of $[PPh_4]_2[Ni(CF_3)_4]$ (**6f**) in CD_3CN

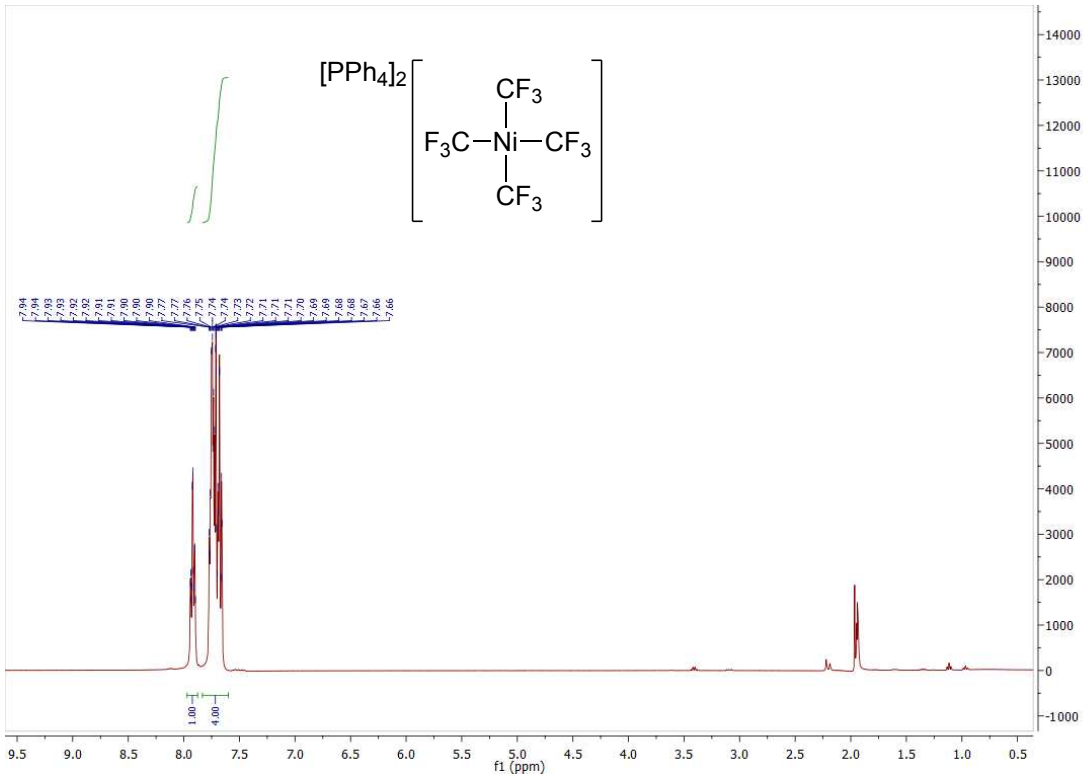

Figure E7. $^{31}P\{H\}$NMR of $[PPh_4]_2[Ni(CF_3)_4]$ (**6f**) in CD_3CN

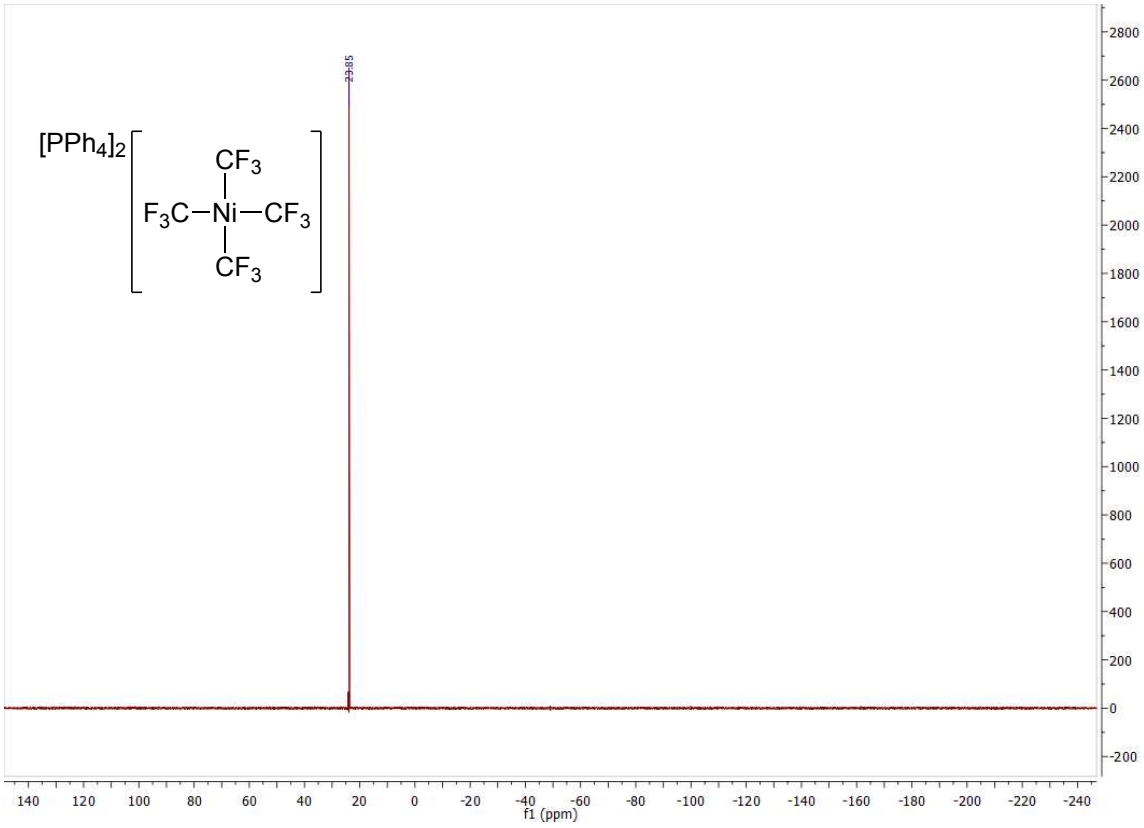

Figure E8. ^{19}F NMR of $[PPh_4]_2[(PhO)Ni(CF_3)_3]$ (**6g**) in CD_3CN at -30 °C

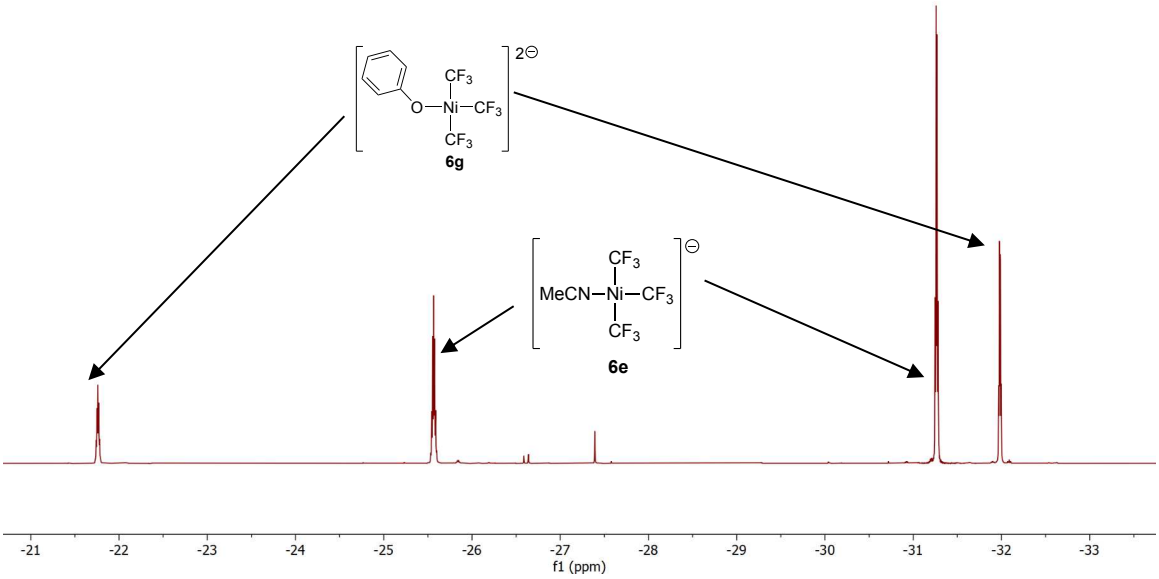

Figure E9. ^{1}H NMR spectra highlighting the decomposition of **$[PPh_4]_2[(ArO)Ni(CF_3)_3]$**. All spectrum were recorded in CD_3CN

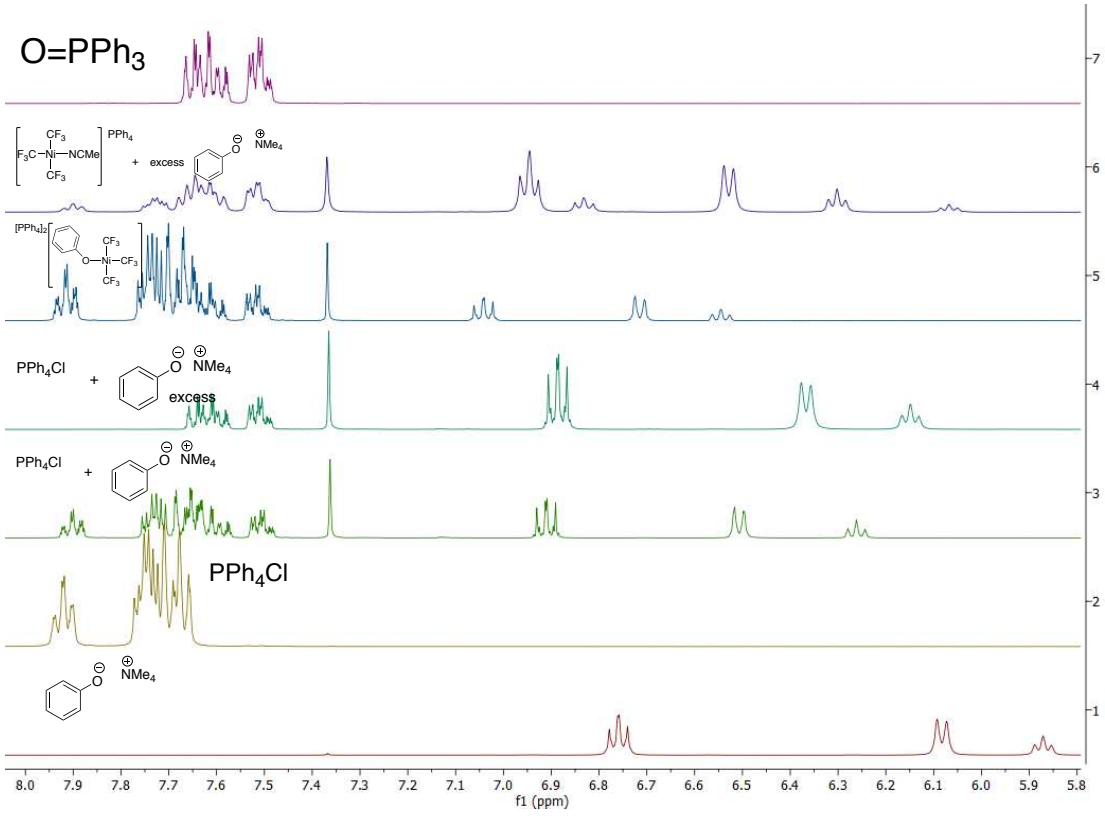

Figure E10. $^{31}P\{^{1}H\}$ NMR spectra highlighting the decomposition of **$[PPh_4]_2[(ArO)Ni(CF_3)_3]$**. All spectrum were recorded in CD_3CN.

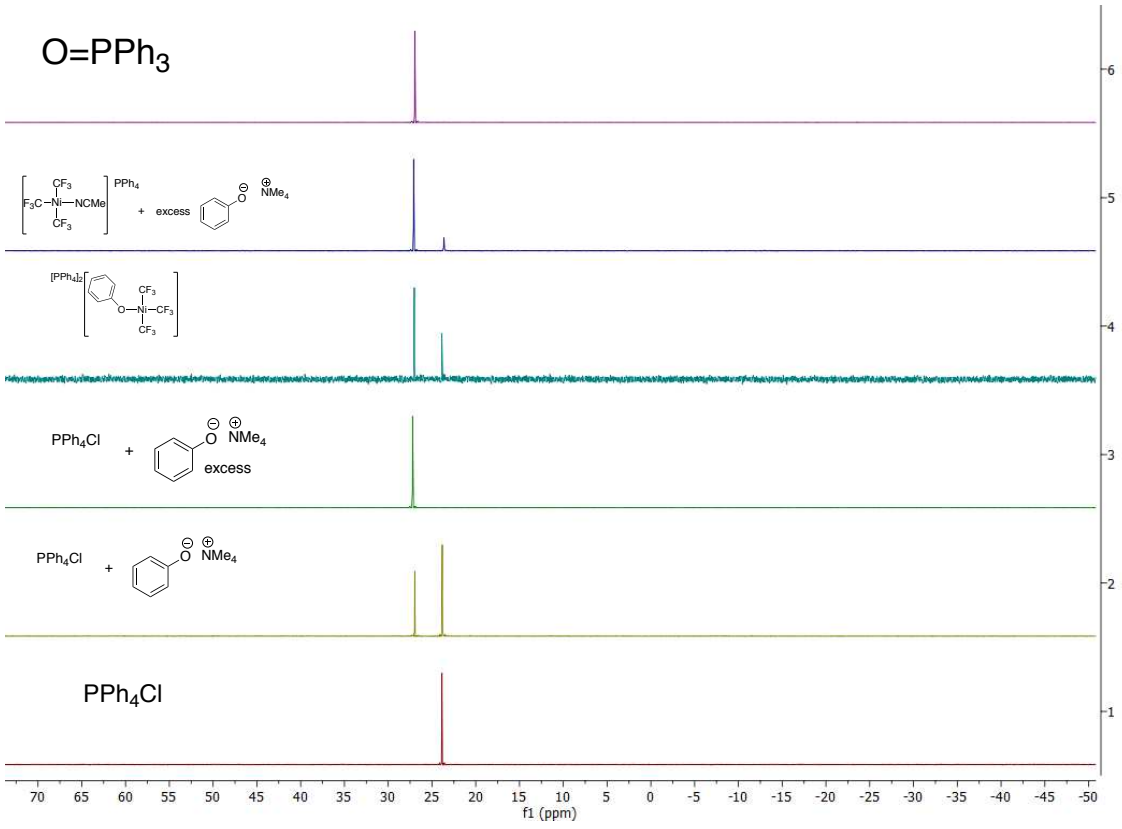

Figure E11. ^{19}F NMR spectrum (CD_3CN) of the products of oxidation of **6f** with potassium persulfate. After oxidation, the insoluble materials were filtered and discarded, and the volatiles were removed under vacuum. Dissolution of the solids in CD_3CN then gave the below spectrum. The two singlets at –25.0 and –25.1 ppm were initially proposed to correspond to $[(SO_4)Ni(CF_3)_2(MeCN)_2]$ and $[Ni(CF_3)_4(MeCN)_2]$, respectively. However, $[Ni(CF_3)_4(MeCN)_2]$, has now been independently prepared and found to have a different splitting pattern (see Chapter 7). Further based on newer data, the singlet at -25.1 ppm was proposed to correspond to $[Ni(CF_3)_6]^{2-}$ (see Chapter 7). $[(MeCN)Ni(CF_3)_5]^-$ is proposed to give rise to the apparent nonet (J = 8.3 Hz) at δ –19.5 and quartet (J = 8.2 Hz) at δ –28.7, and newer data further supported this assignment (see Chapter 7).

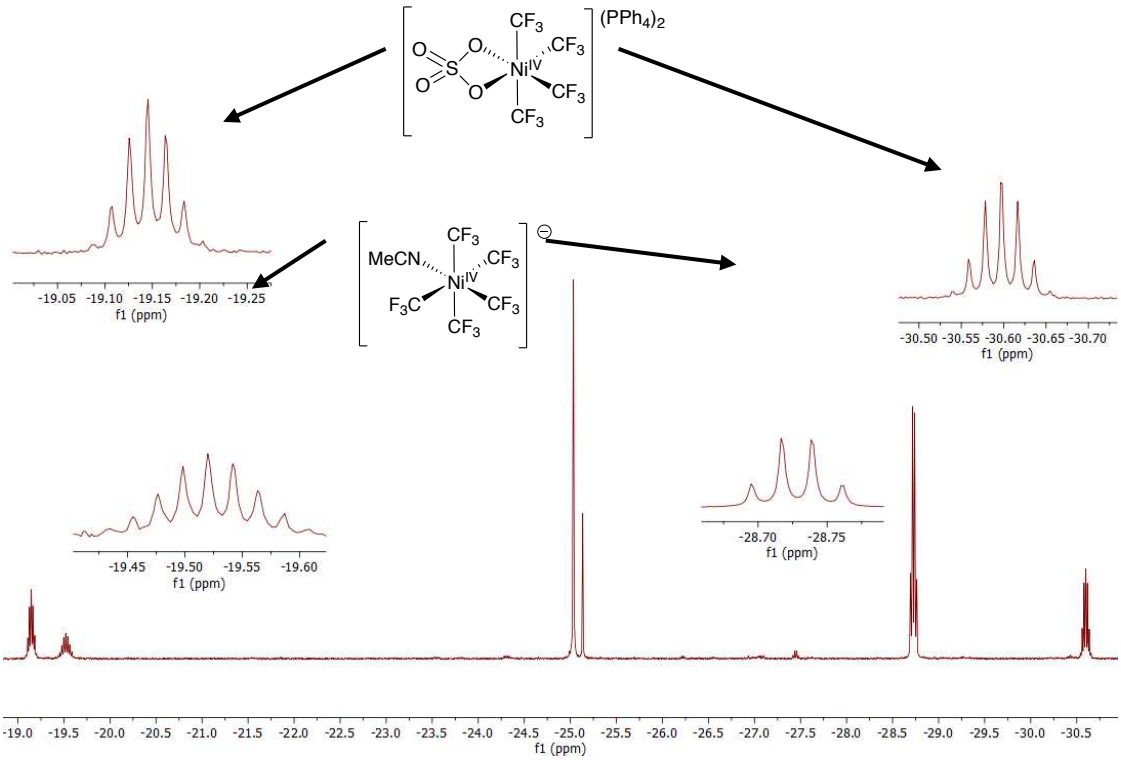

Figure E12 – ^{1}H NMR of $[NMe_4]_2[(C_7H_5N_2)Ni(CF_3)_3]$ in CD_3CN

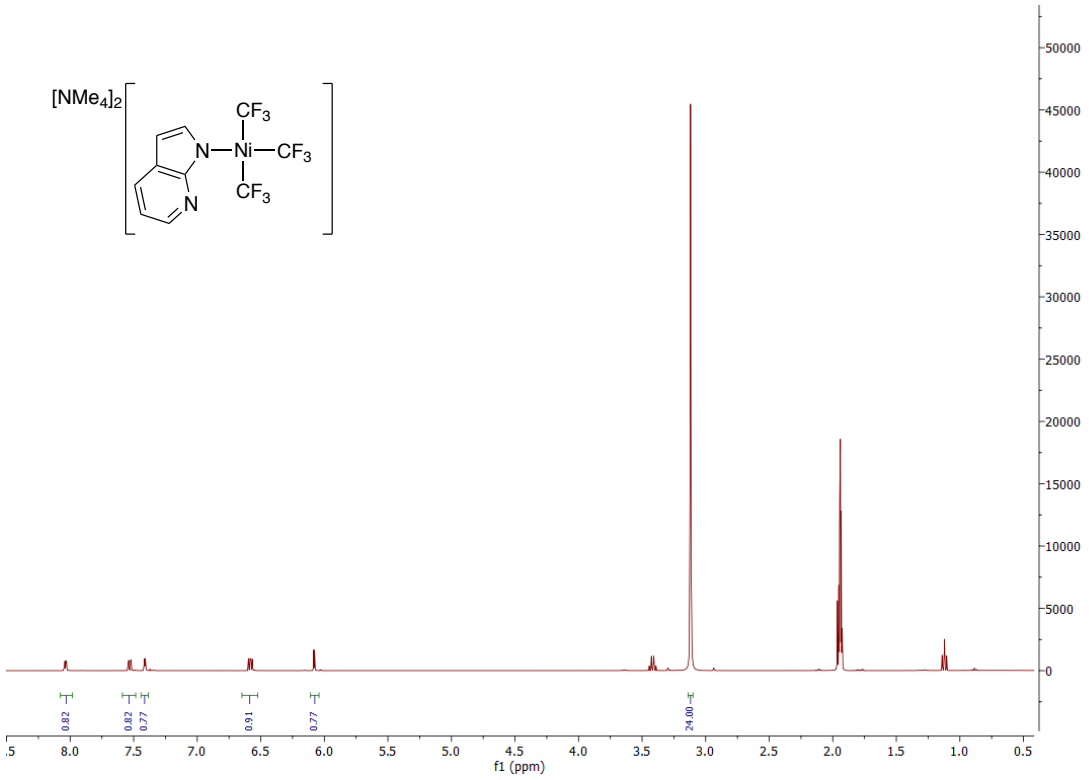

Figure E13 – ^{19}F NMR of $[NMe_4]_2[(C_7H_5N_2)Ni(CF_3)_3]$ in CD_3CN

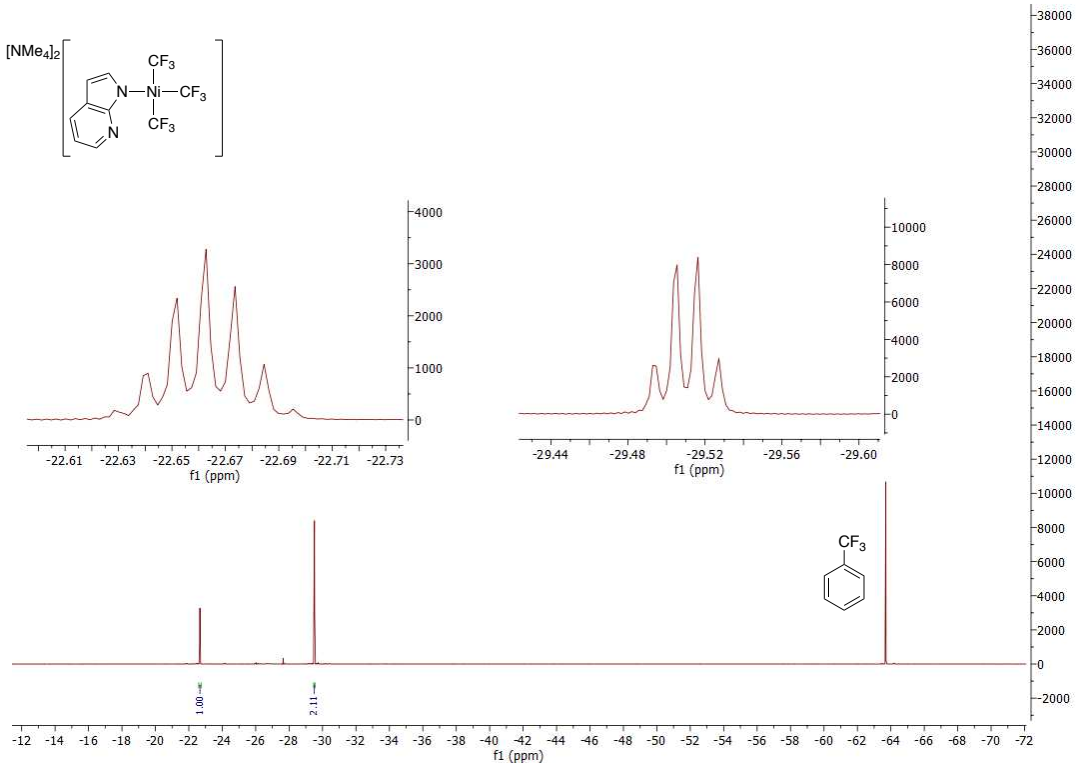

Appendix F: Supporting Information and Spectral Data for Chapter 7

Table F1: Additional optimizations for catalytic trifluoromethylation

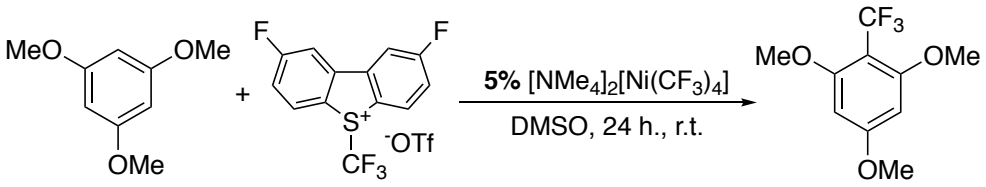

In a nitrogen-filled glovebox, (hetero)arene substrate (0.25 mmol, 5 equiv) and Umemoto Reagent II (**7k**) (22 mg, 0.05 mmol) were dissolved in DMSO (0.9 mL). The catalyst was added as 100 μL of a 0.025 M stock solution in DMSO). The reaction was stirred for 24 hours at room temperature and trifluorotoluene was added as an internal standard and the yield was determined by ^{19}F NMR spectroscopy.

entry	modification	Yield (%)
1	none	96
2	2 equiv arene	66
3	2 equiv. arene + 1 equiv DIPEA	36
4	THF solvent	7
5	MeCN solvent	51
6	1,4 – dioxane solvent	10
7	**18 h.**	**96**
8	CF_3CO_2H as catalyst	6

Figure F1. ^{19}F NMR of $[NMe_4][(MeCN)Ni(CF_3)_3]$ (**7b**) in CD_3CN

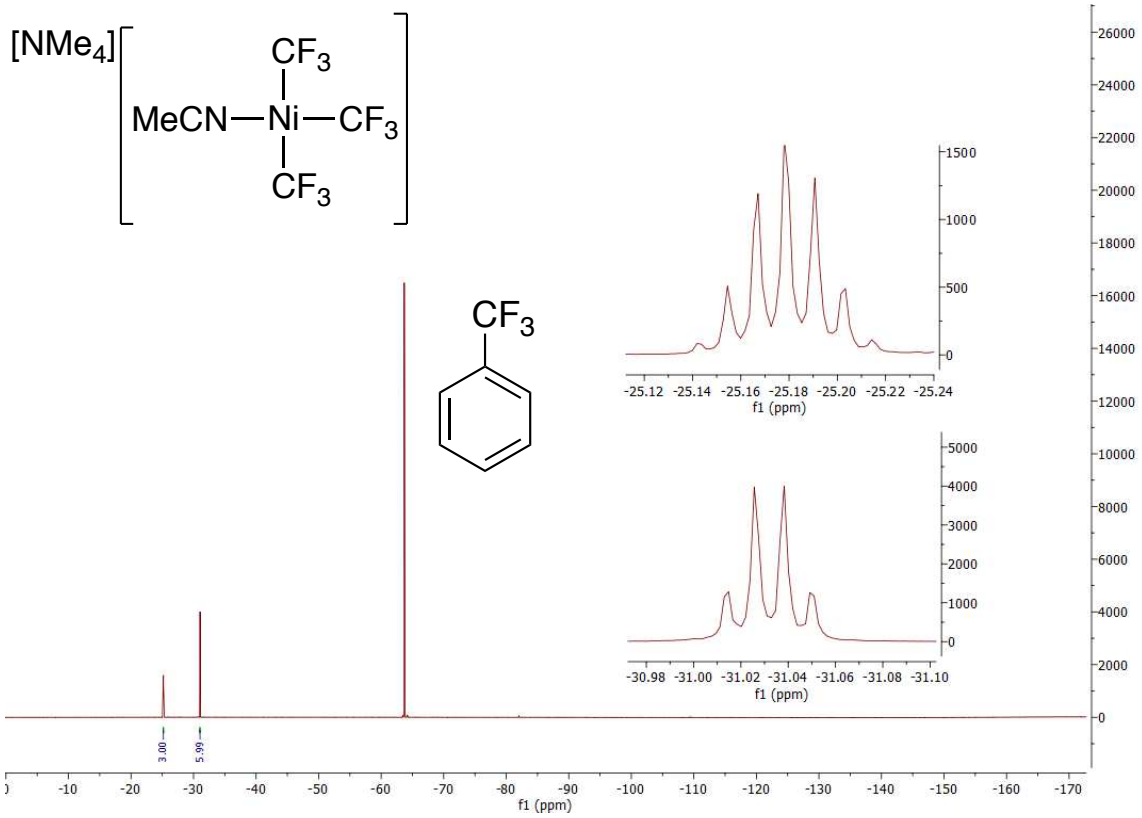

Figure F2. ^{1}H NMR of $[NMe_4][(MeCN)Ni(CF_3)_3]$ (**7b**) in CD_3CN

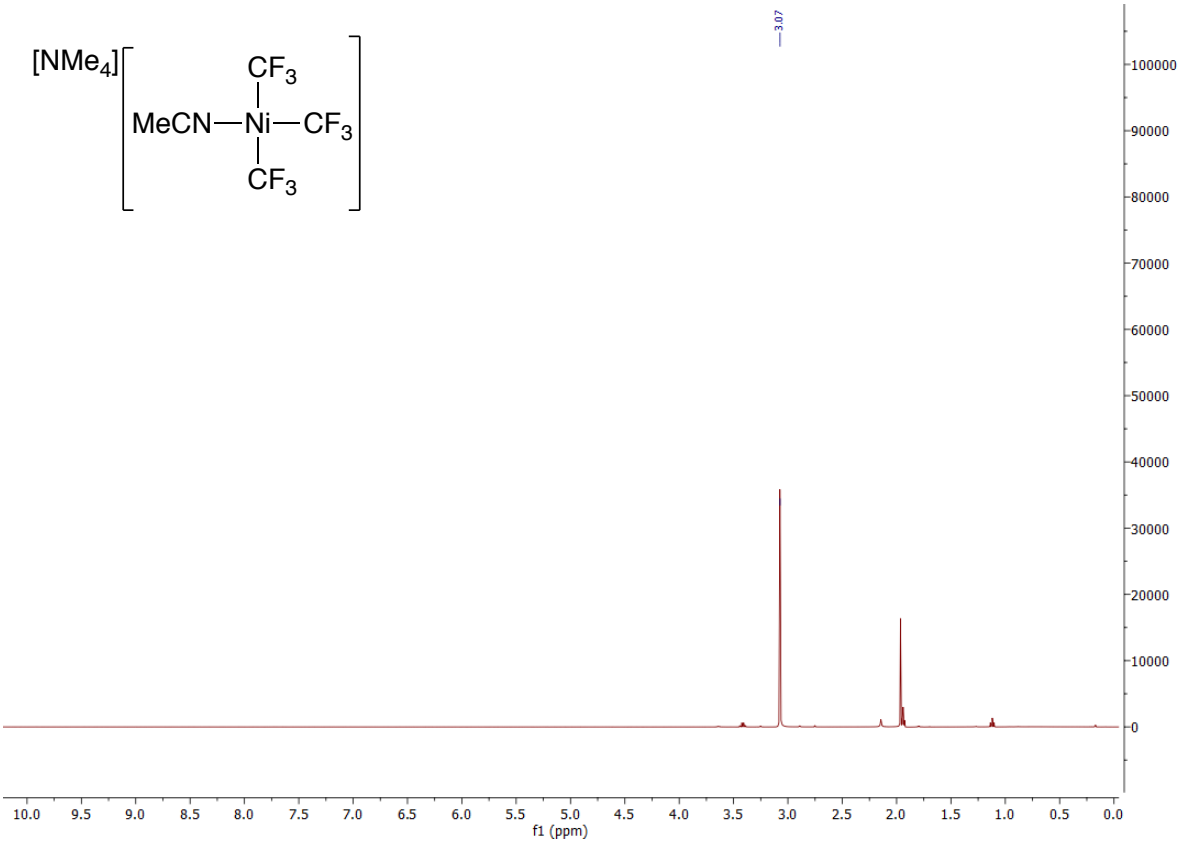

Figure F3. ^{19}F NMR of $[NMe_4]_2[Ni(CF_3)_4]$ (**7c**) in CD_3CN

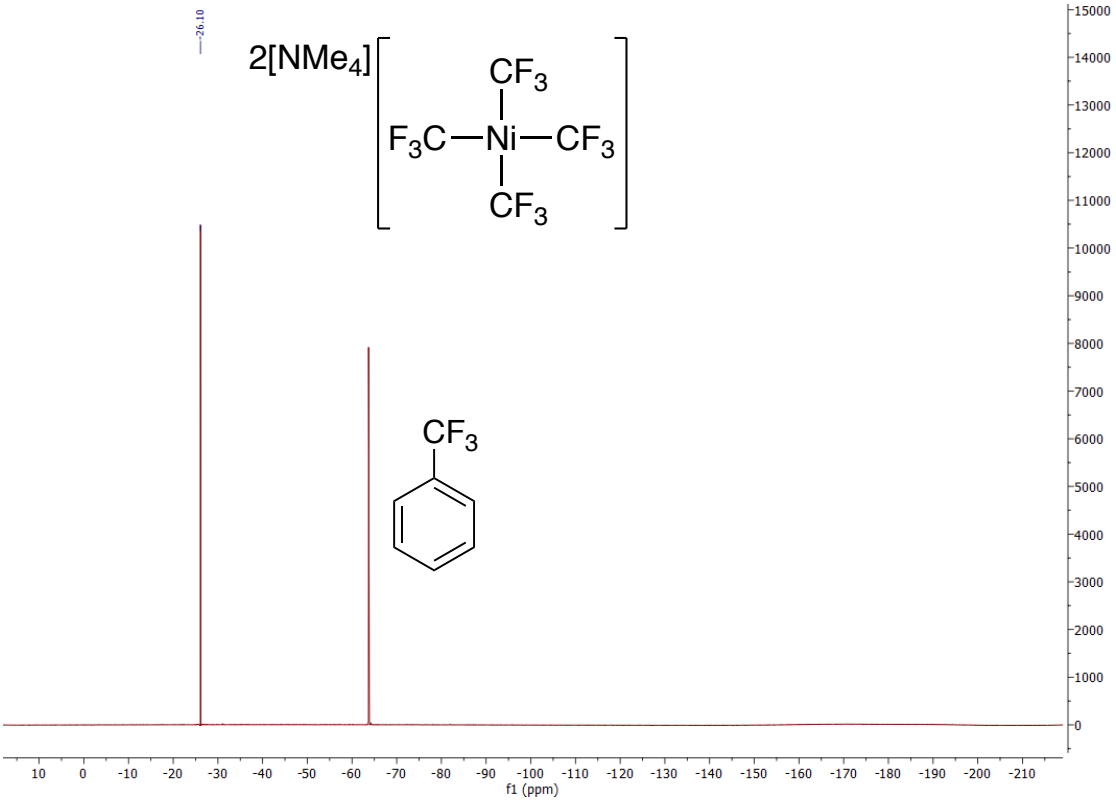

Figure F4. ^{1}H NMR of $[NMe_4]_2[Ni(CF_3)_4]$ (**7c**) in CD_3CN

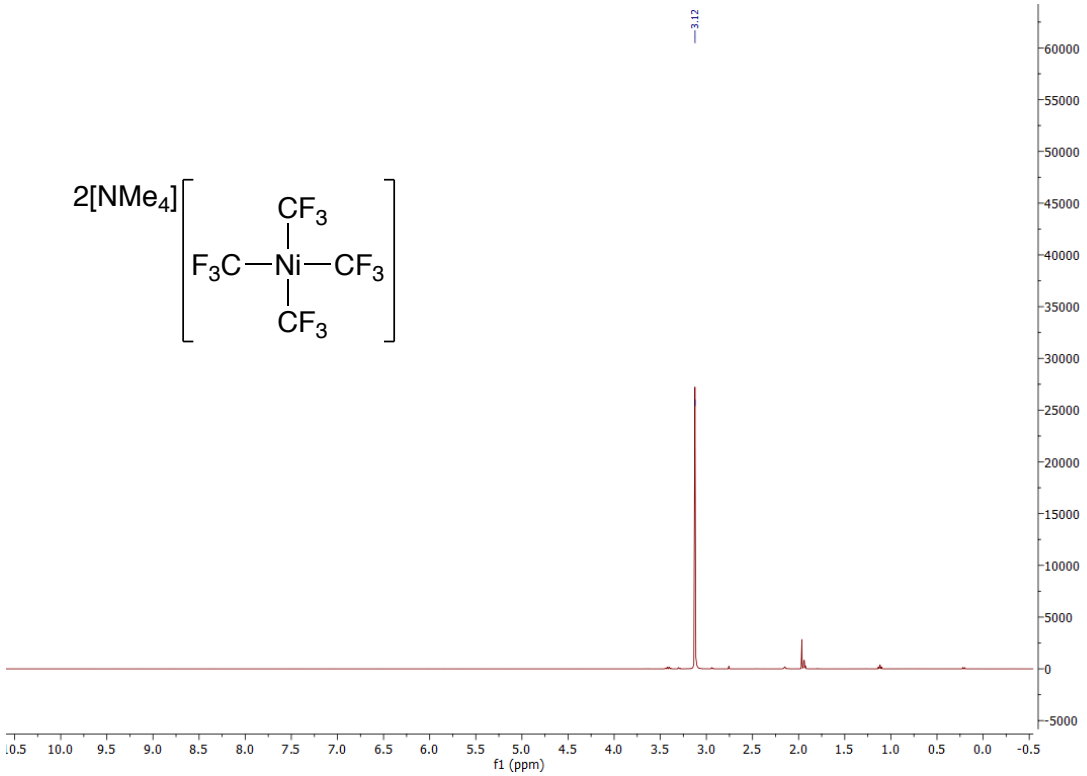

Figure F5. ^{19}F NMR of $[NMe_4][(MeCN)Ni(C_2F_5)_3]$ (**7e**) in CD_3CN

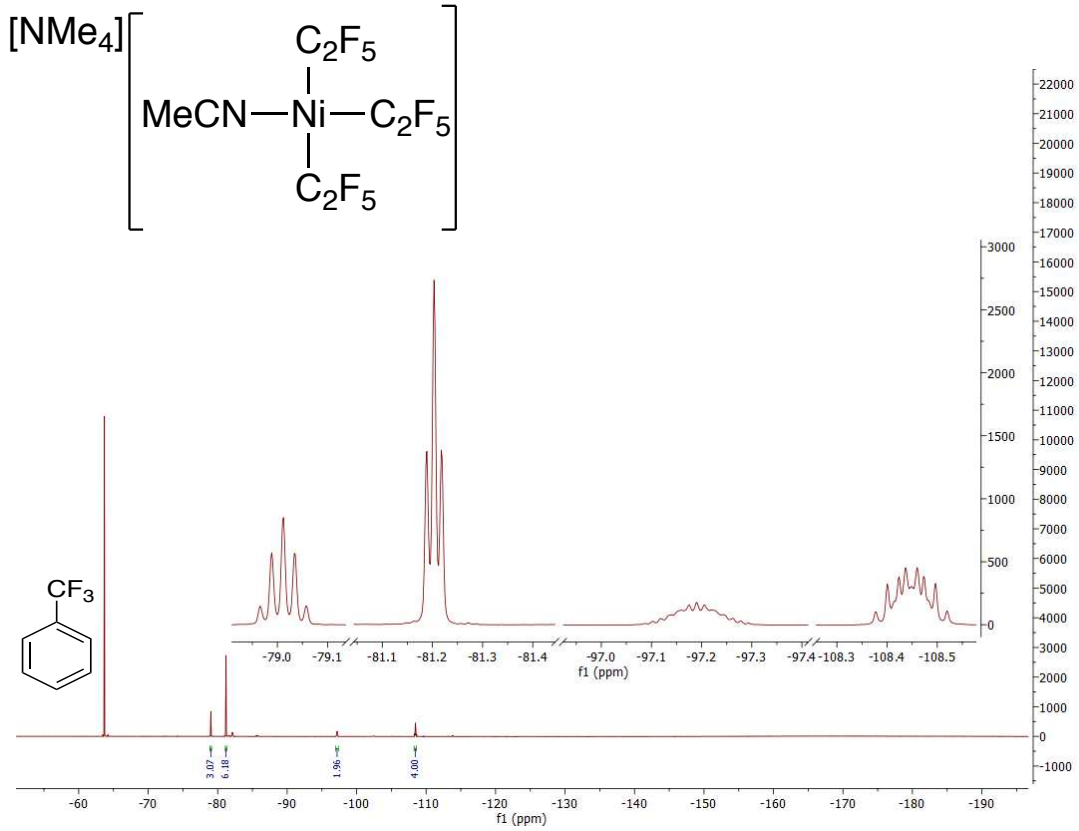

Figure F6. ^{1}H NMR of $[NMe_4][(MeCN)Ni(C_2F_5)_3]$ (**7e**) in CD_3CN

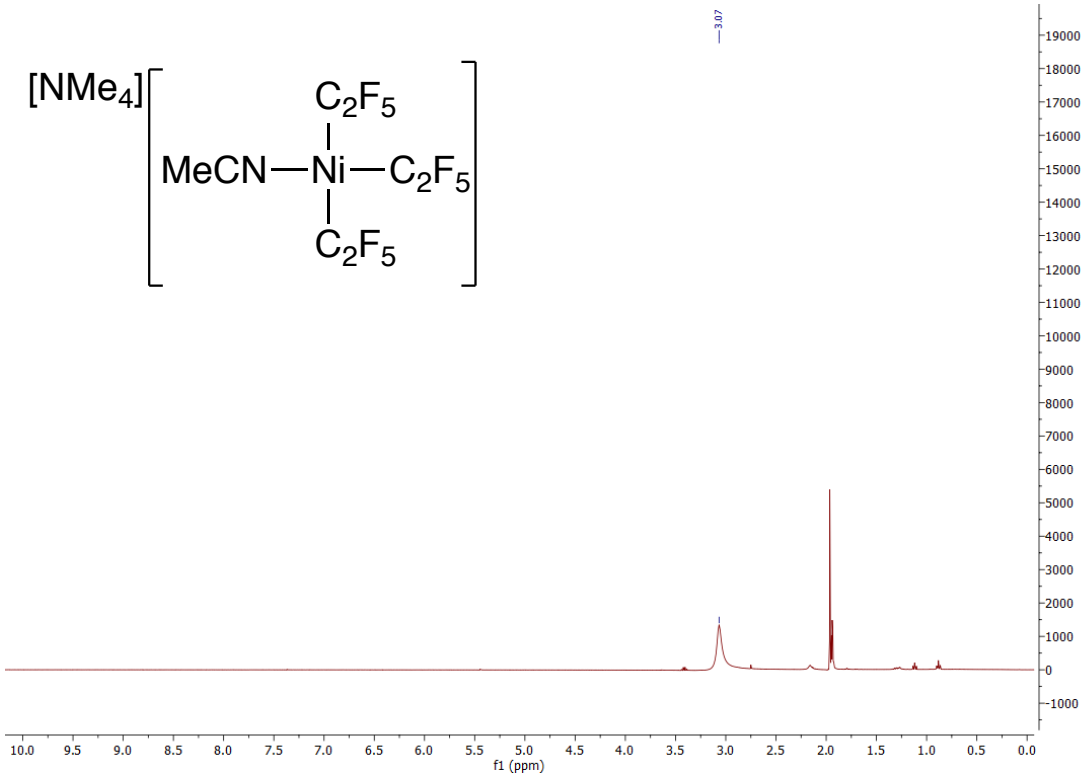

Figure F7. ^{19}F NMR of the oxidation of $[NMe_4]_2[Ni(CF_3)_4]$ with Umemoto's Reagent II (**7k**) in CD_3CN/CH_3CN. The identified products were consistent with $[(MeCN)_2Ni(CF_3)_4]$ (**7i**) (2%), $[(MeCN)Ni(CF_3)_5]^-$ (**7o**) (51%), $[Ni(CF_3)_6]^{2-}$ (**7n**) (12%), $[(MeCN)_2Ni(CF_3)_2]$ (**7a**) (5%), and unreacted Umemoto's reagent II (**7k**) (13%).

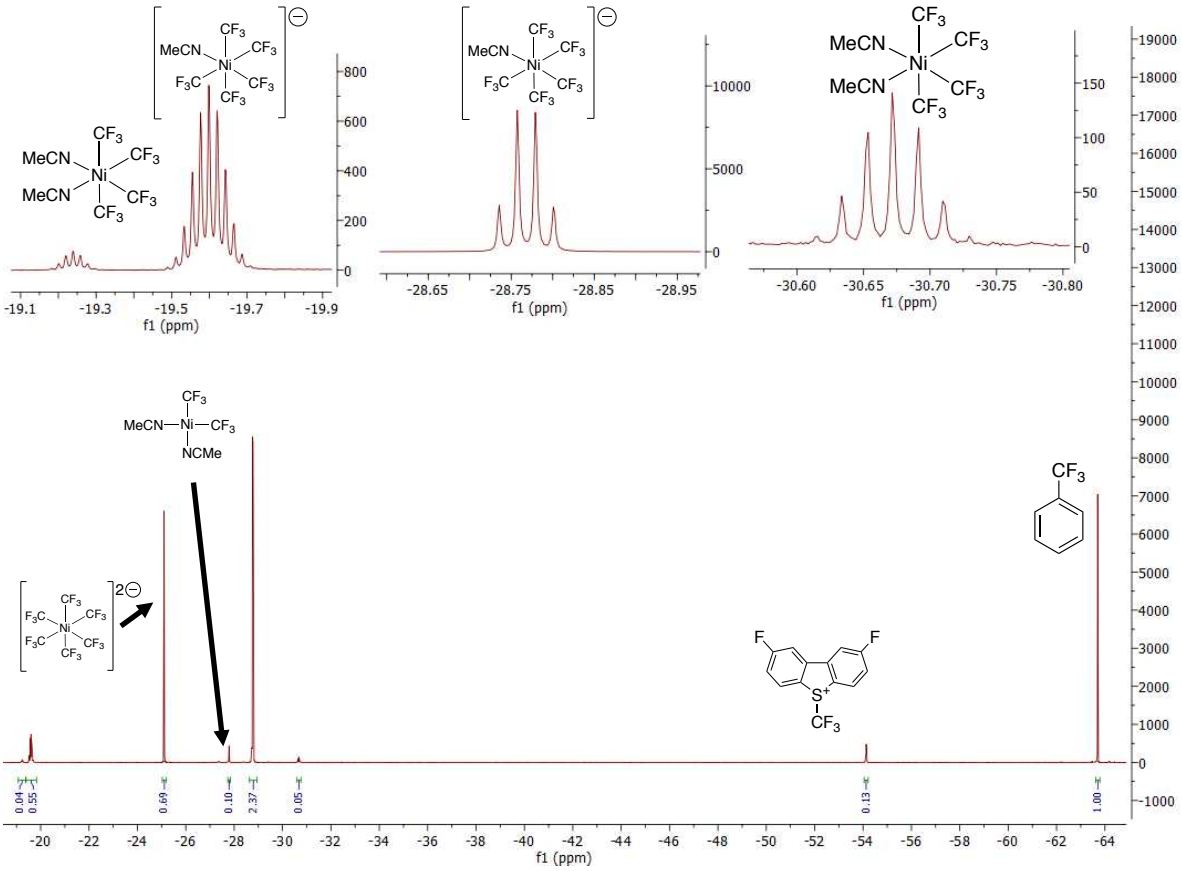

Figure F8. ^{19}F NMR of $[(MeCN)_2Ni(CF_3)_4]$ (**7i**) in CD_3CN

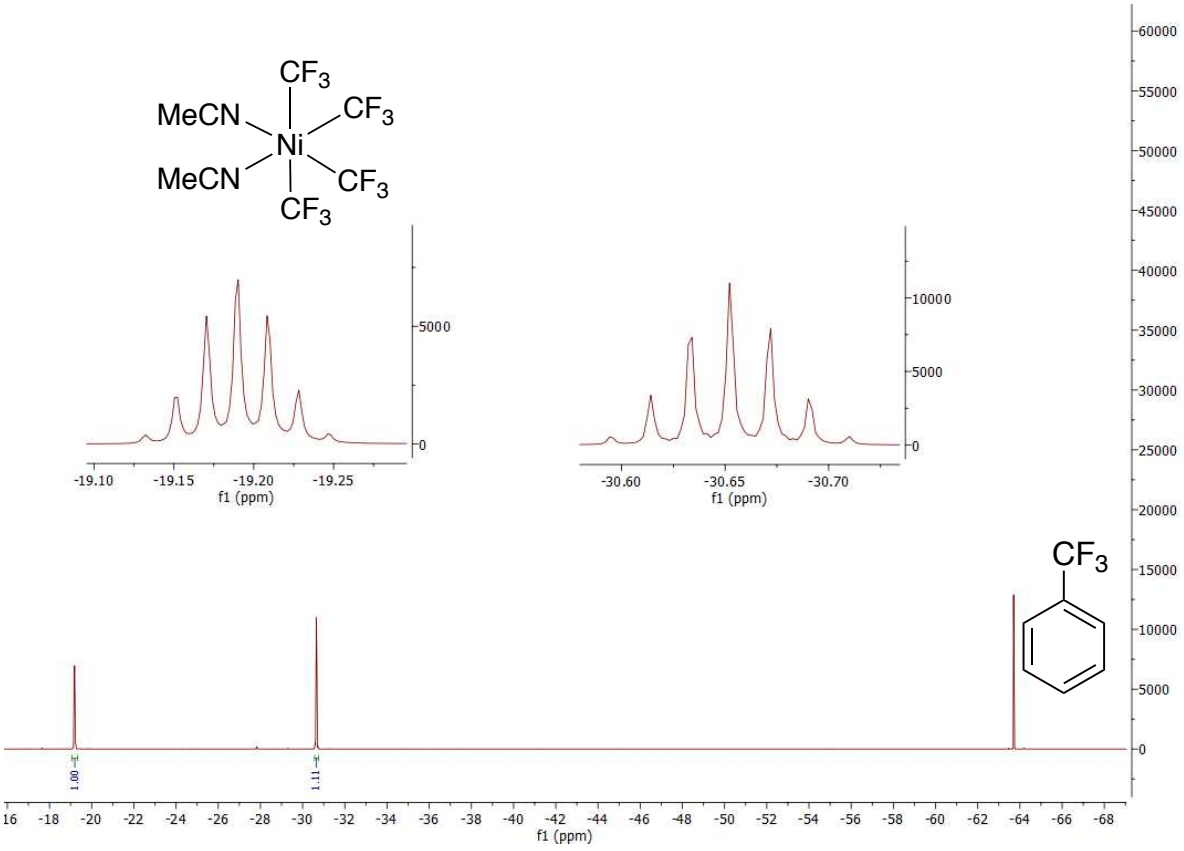

Figure F9. ^{19}F NMR spectrum of the products of the reaction of **7g** and **7b** in CD_3CN/CH_3CN

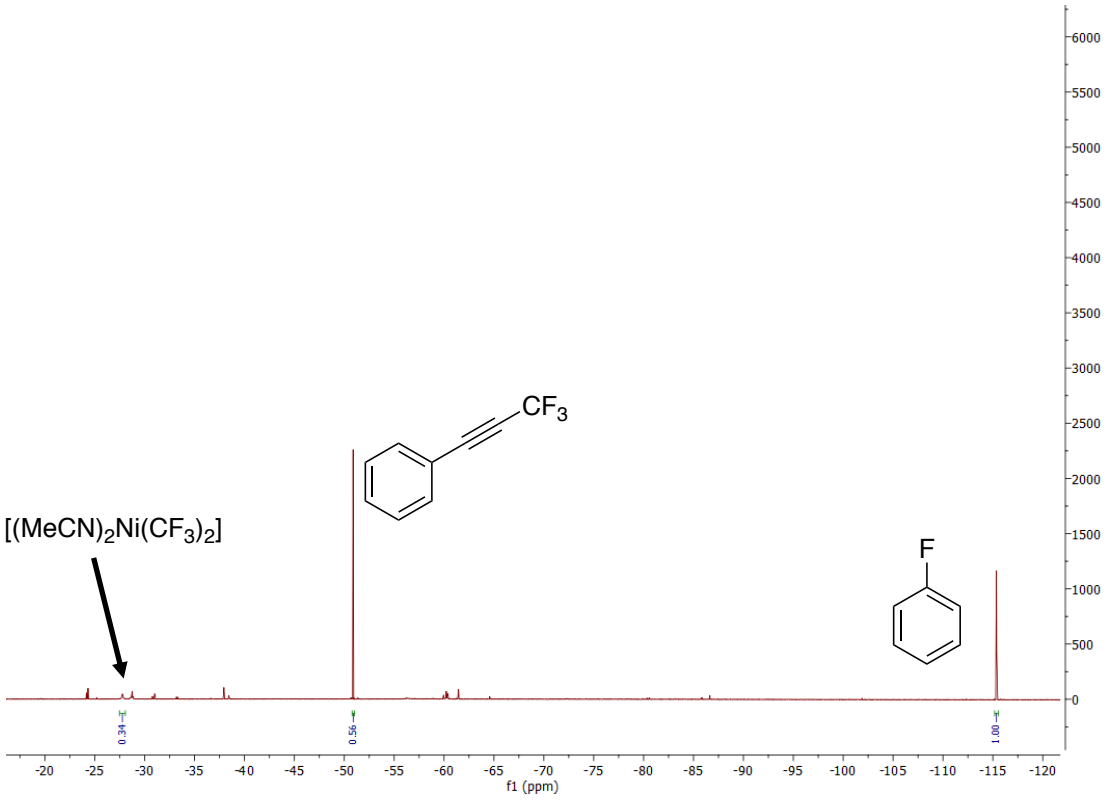

Figure F10. ^{19}F NMR spectrum of the products of the reaction of **7h** and **7e** in CD_3CN/CH_3CN

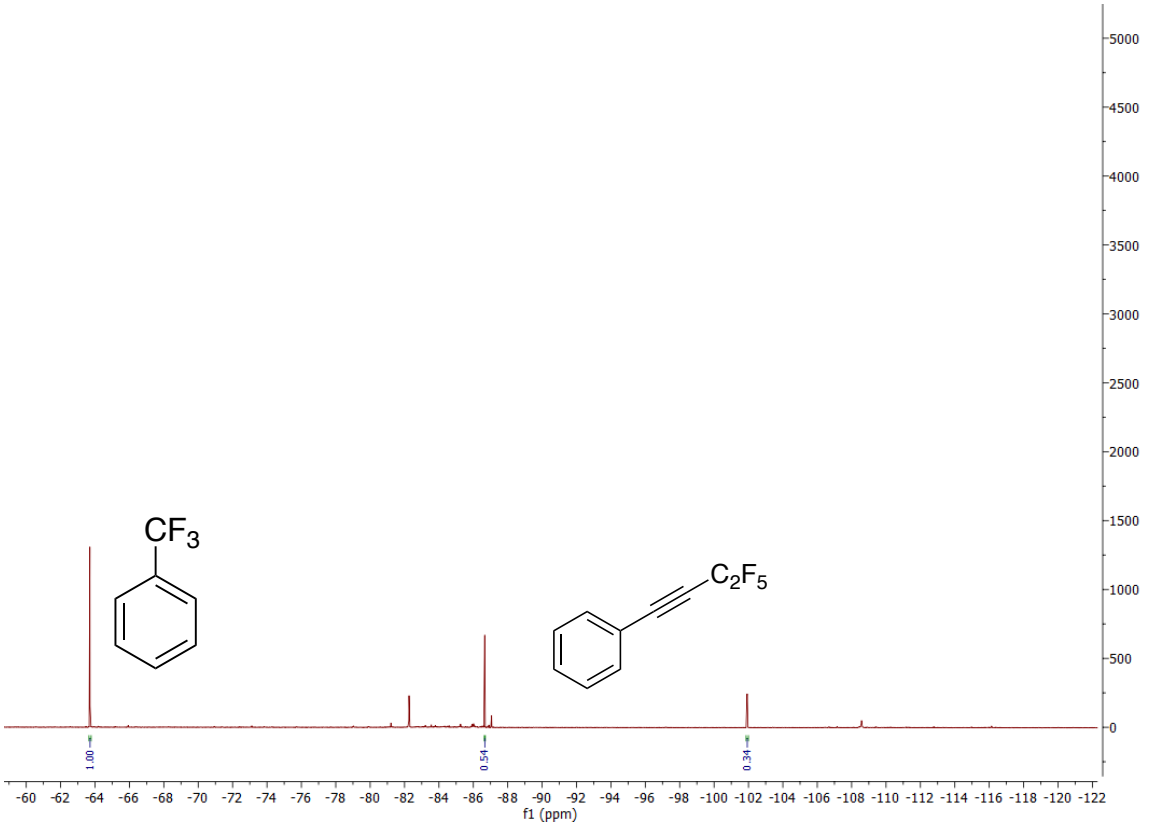

Figure F11. ^{19}F NMR spectrum of the products of the reaction of bis(4-tert-butylphenyl)iodonium hexafluorophosphate and **7e** in CD_3CN/CH_3CN

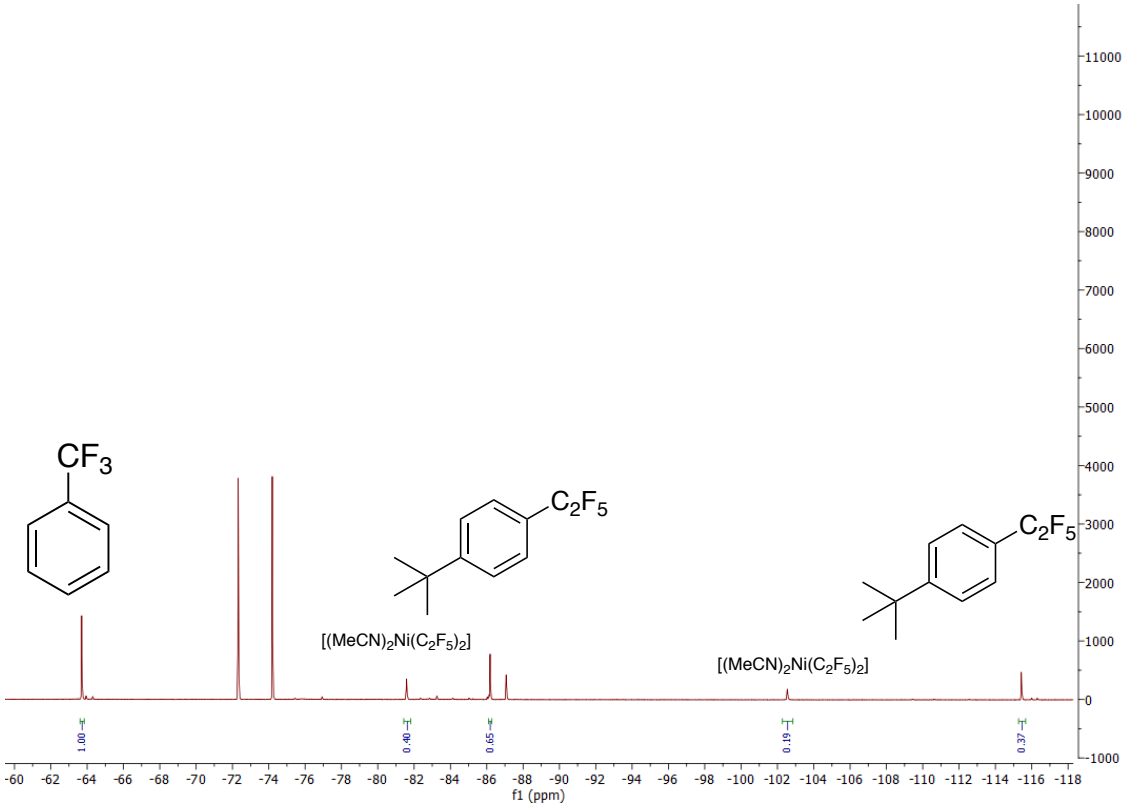

Figure F12. ^{19}F NMR spectrum of the products of the reaction of 3,5 – dichlorophenyldiazonium tetrafluoroborate and **7b** in CD_3CN/CH_3CN

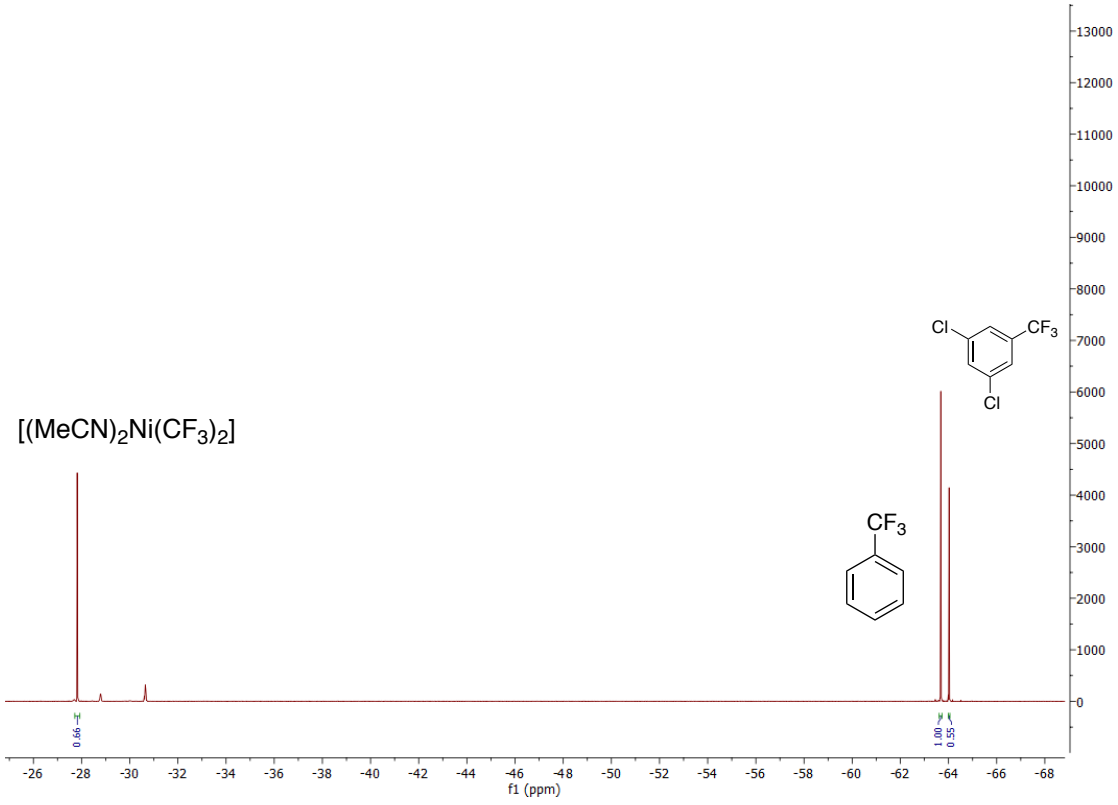

Figure F13. ^{19}F NMR spectrum of the products of the reaction of 3,5 – dichlorophenyldiazonium tetrafluoroborate and **7e** in CD_3CN/CH_3CN

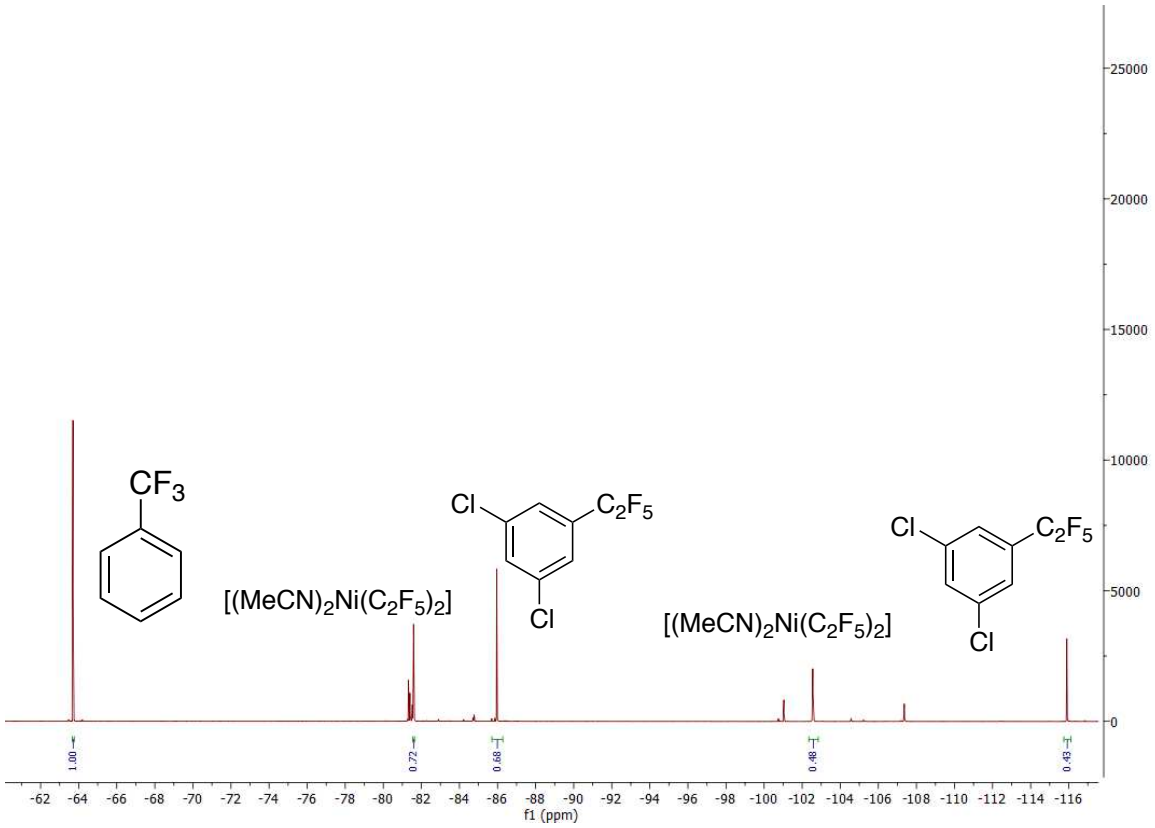

Figure F14. ^{19}F NMR spectrum of the products of the reaction of 4 – methoxybenzenediazonium tetrafluoroborate and **7b** in CD_3CN/CH_3CN

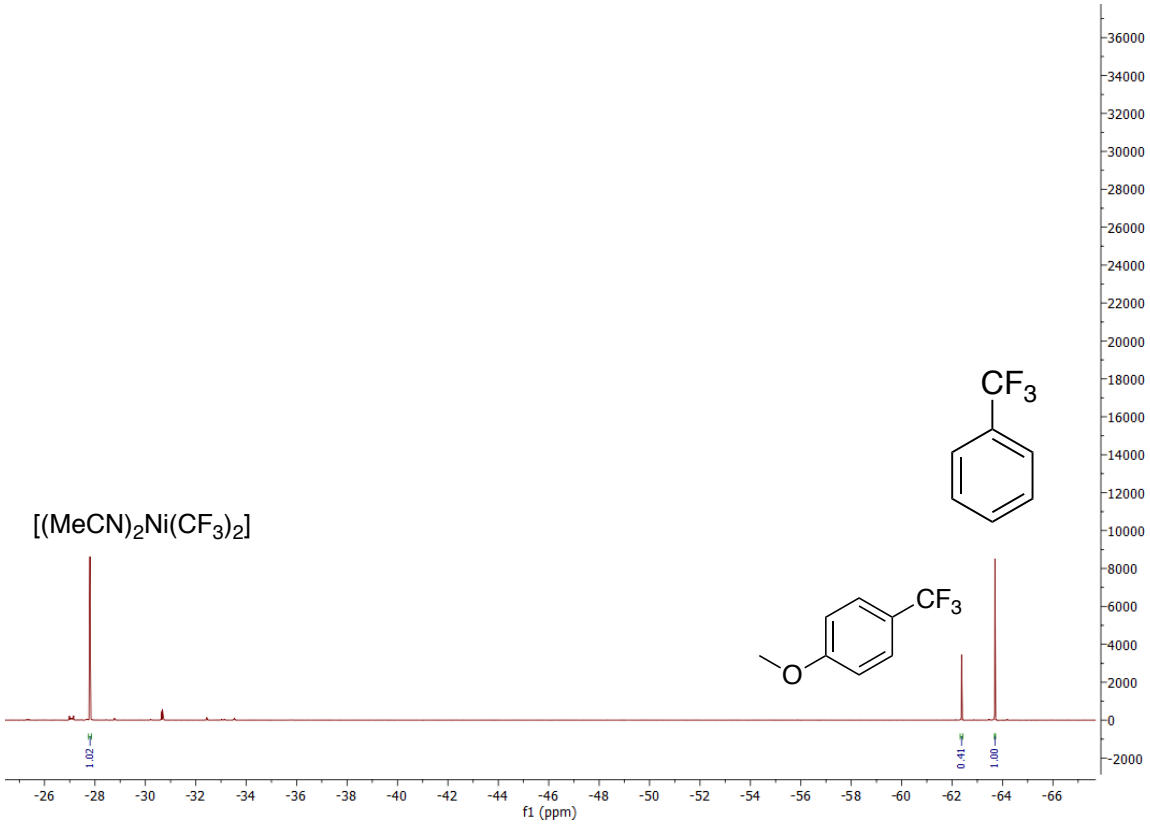

Figure F15. ^{19}F NMR spectrum of the products of the reaction of 4 – methoxybenzenediazonium tetrafluoroborate and **7e** in CD_3CN/CH_3CN

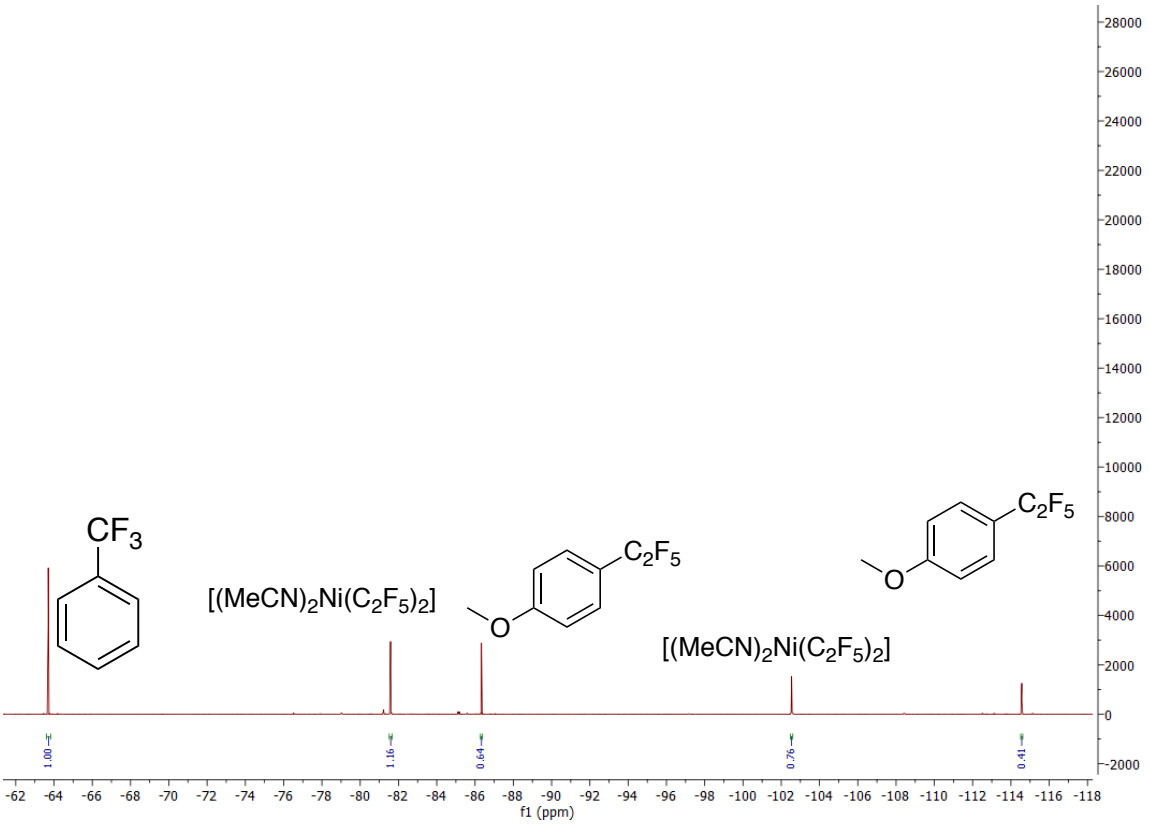

Figure F16. ^{19}F NMR spectrum of the products of the reaction of 4 – nitrobenzenediazonium tetrafluoroborate and **7b** in CD_3CN/CH_3CN

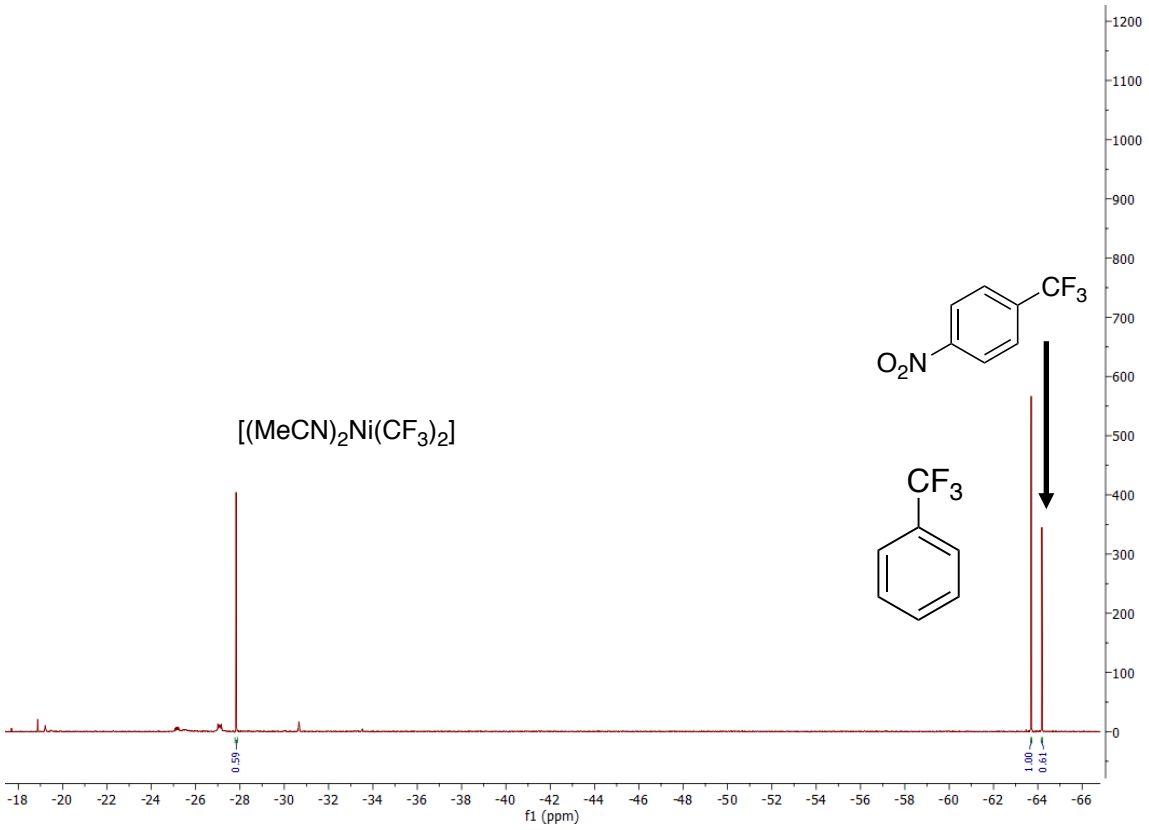

Figure F17. ^{19}F NMR spectrum of the products of the reaction of 4 – nitrobenzenediazonium tetrafluoroborate and **73** in CD_3CN/CH_3CN

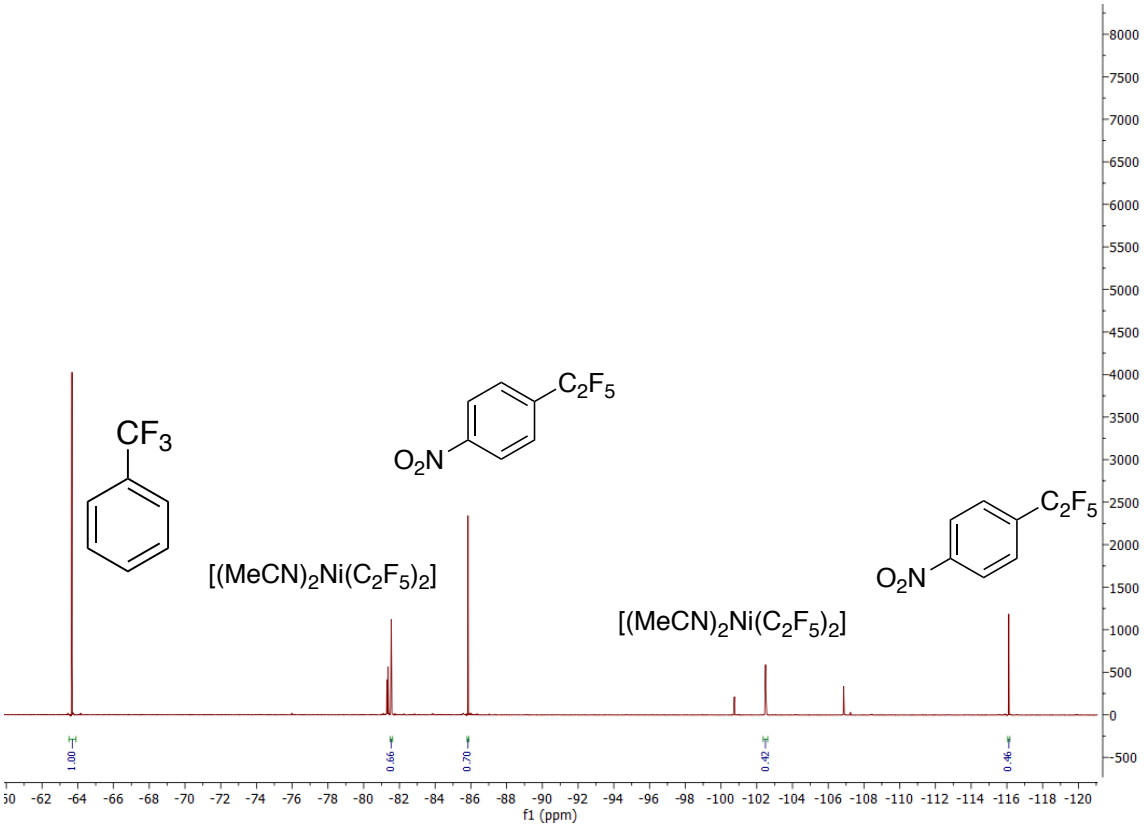

Figure F18. ^{19}F NMR spectra of catalytic trifluoromethylation forming **7ma**

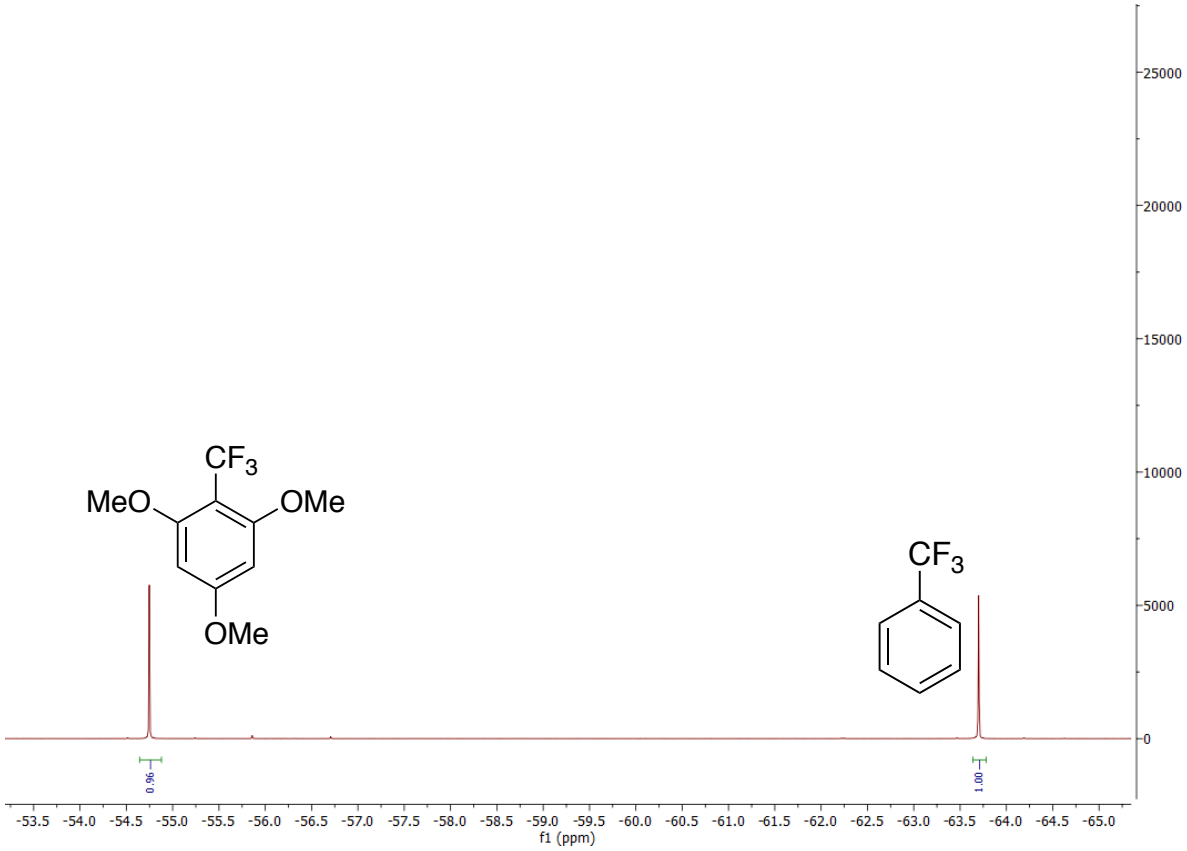

Figure F19. ^{19}F NMR spectra of catalytic trifluoromethylation forming **7mb**

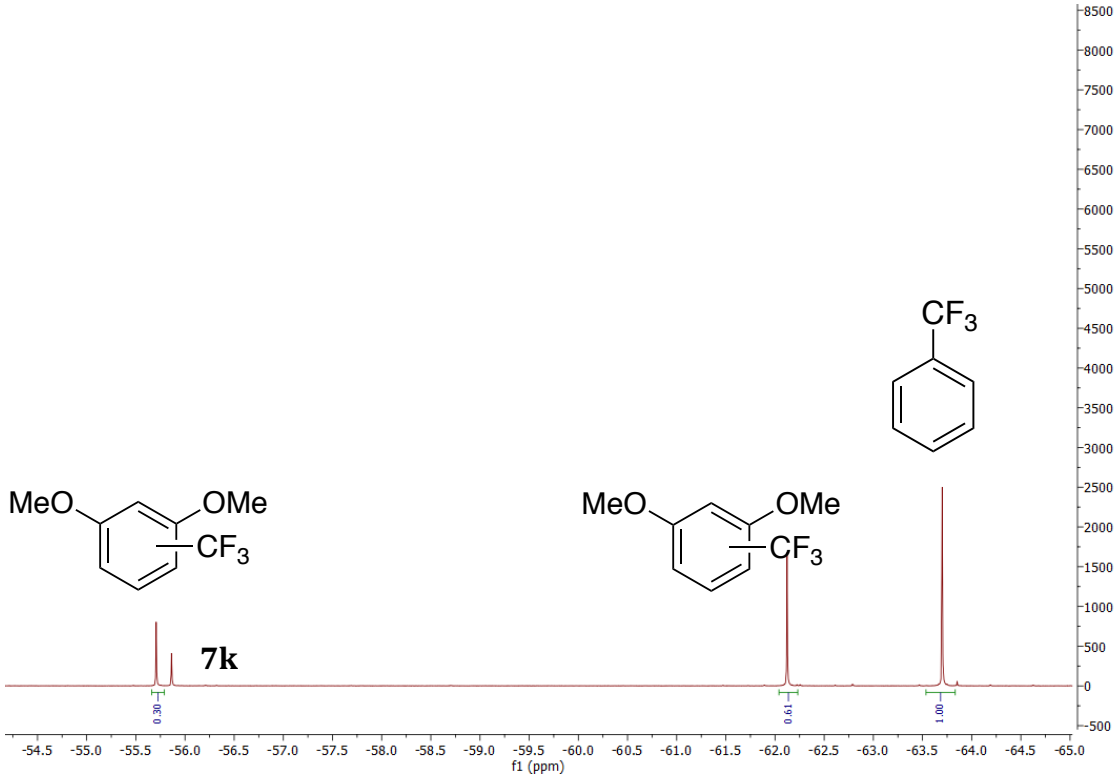

Figure F20. ^{19}F NMR spectra of catalytic trifluoromethylation forming **7mc**

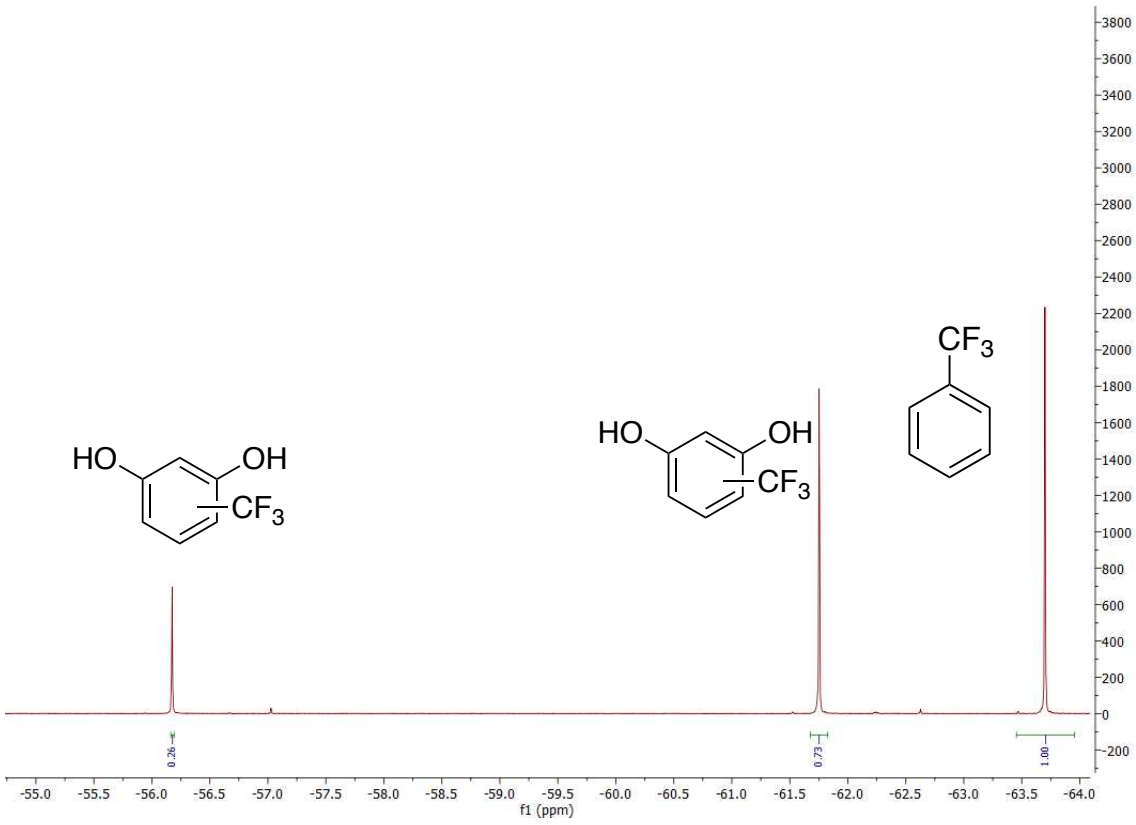

Figure F21. ^{19}F NMR spectra of catalytic trifluoromethylation forming **7md**

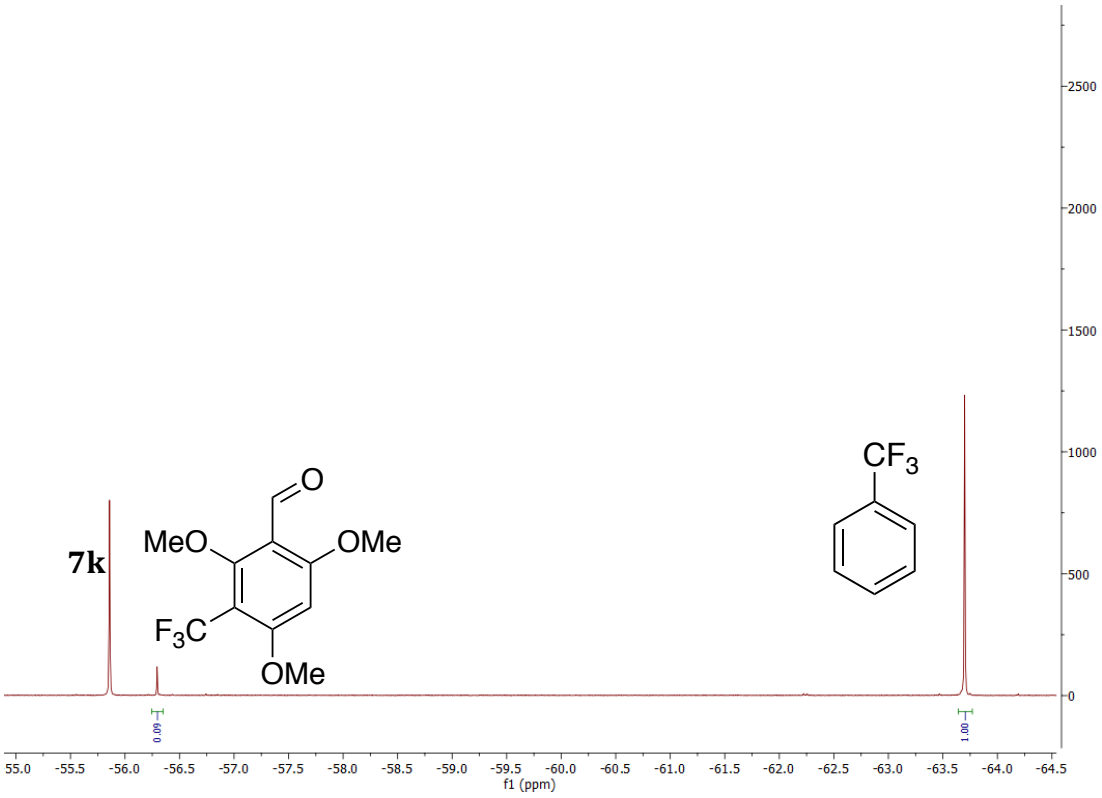

Figure F22. ^{19}F NMR spectra of catalytic trifluoromethylation forming **7me**

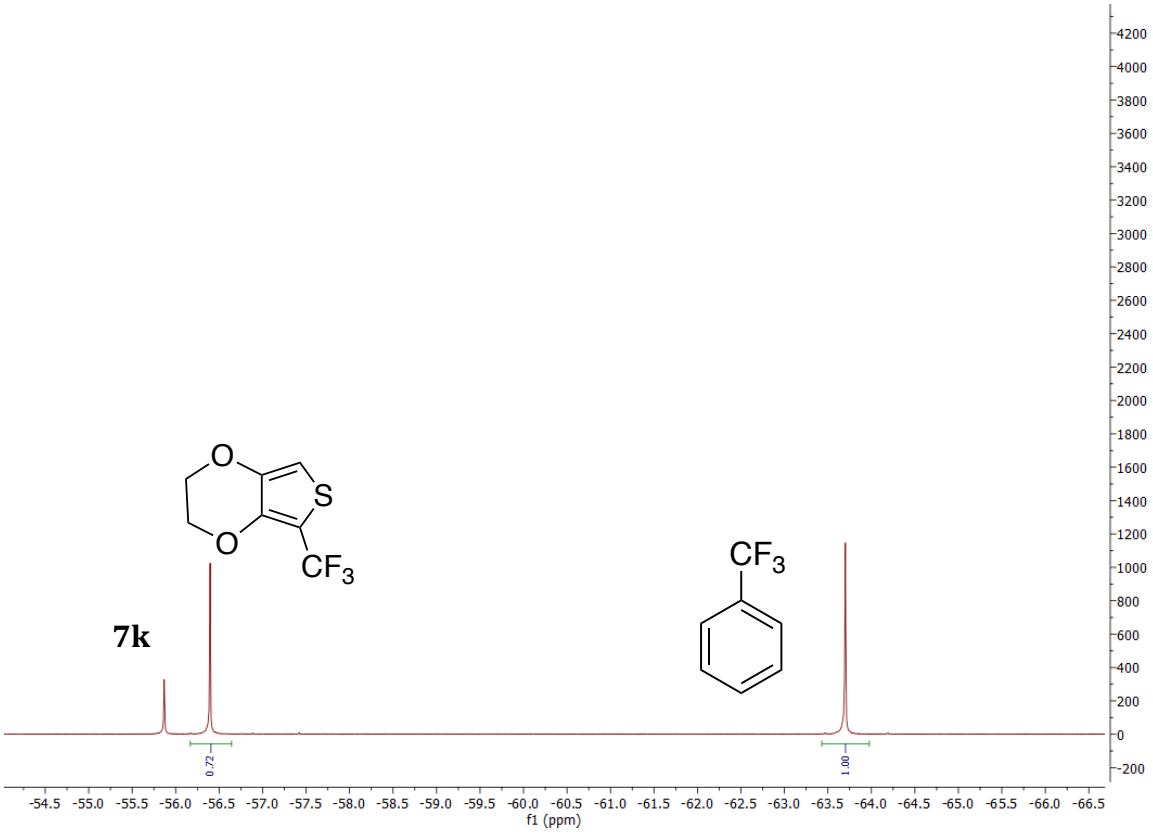

Figure F23. ^{19}F NMR spectra of catalytic trifluoromethylation forming **7mf**

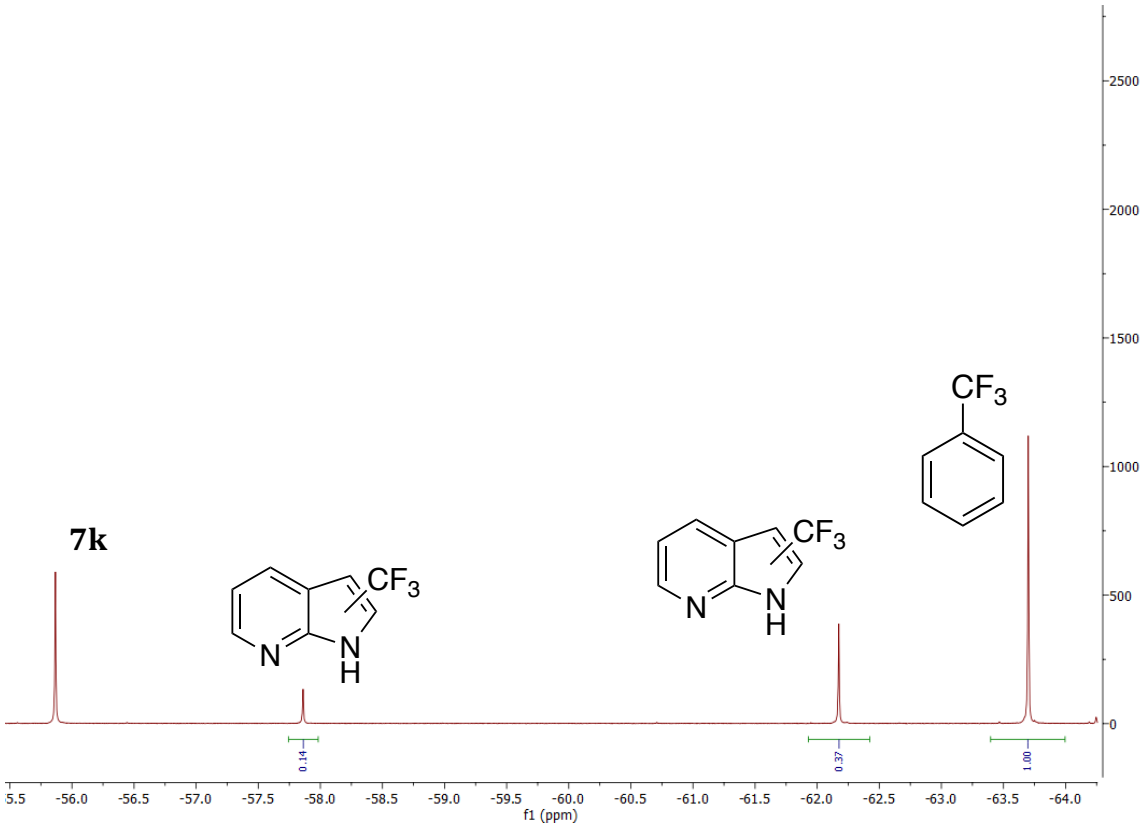

Figure F24. ^{19}F NMR spectra of catalytic trifluoromethylation forming **7mg**

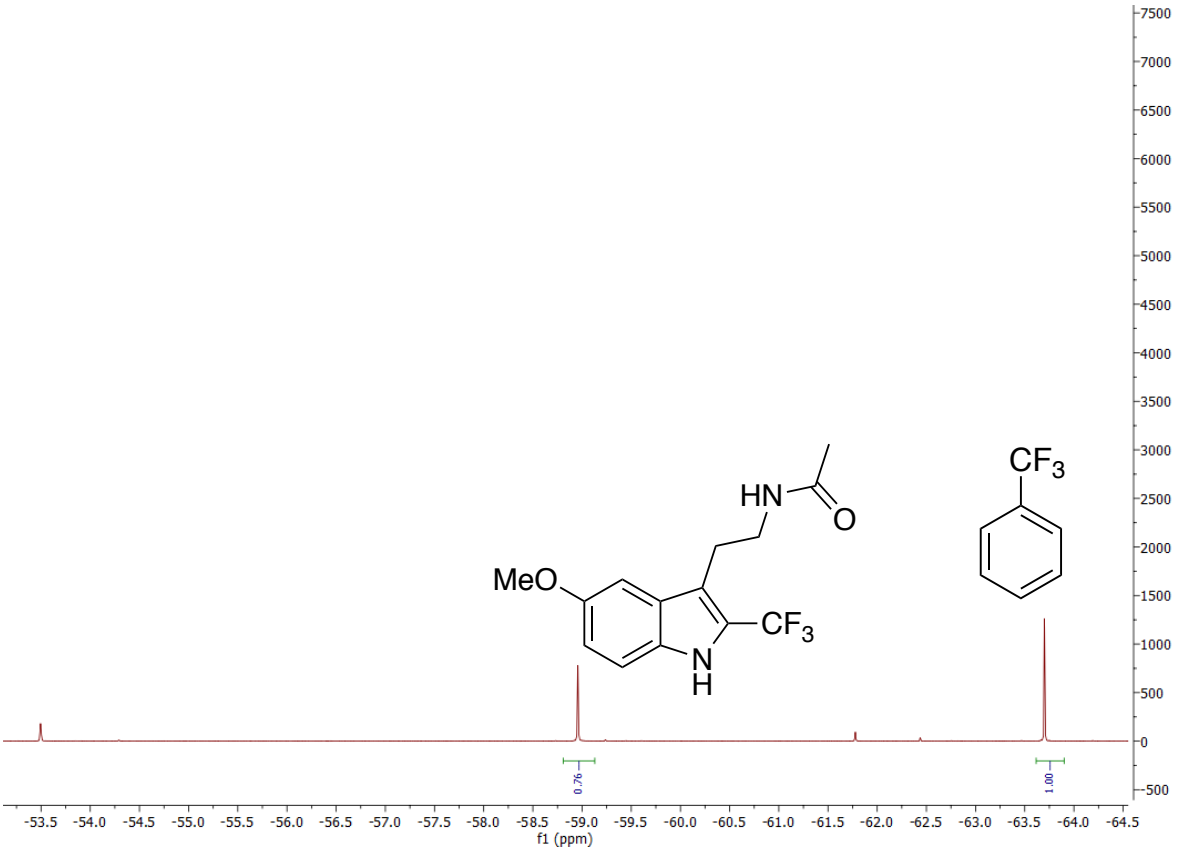

Figure S25 – ^{19}F NMR spectra of Table 7a – entry 2, trifluoromethylation of trimethoxybenzene with no catalyst

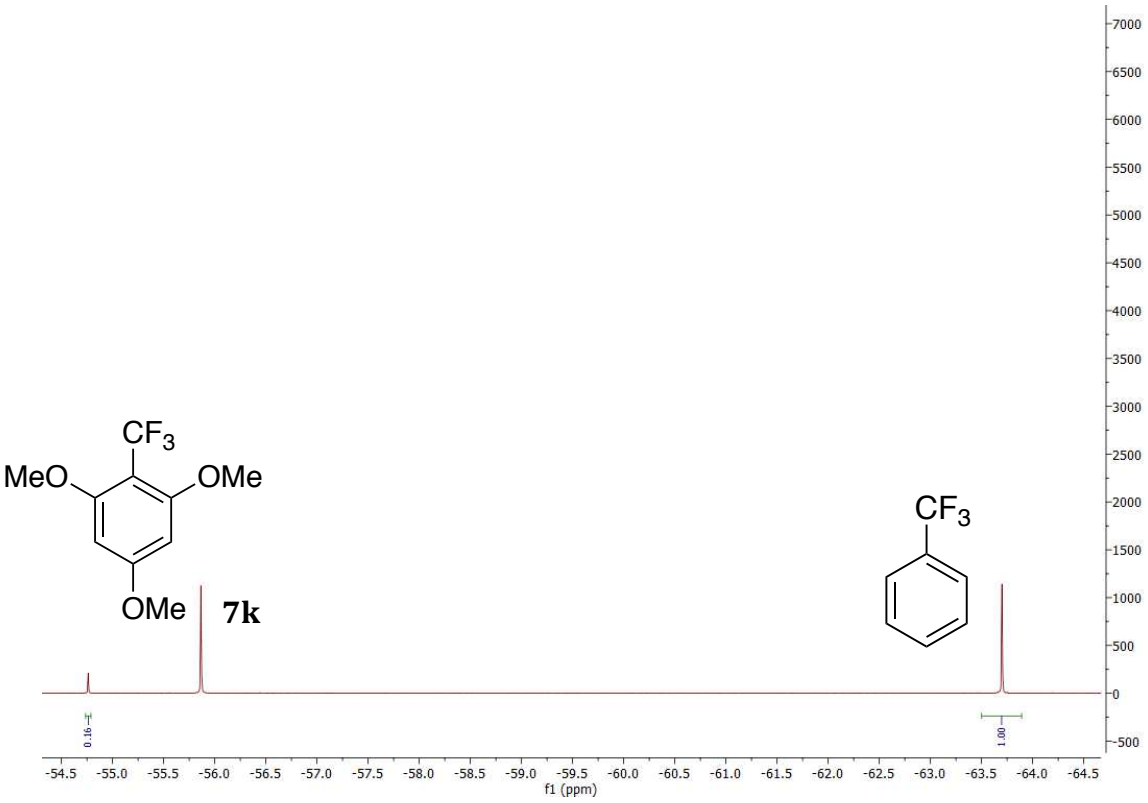

Figure F26. ^{19}F NMR spectra of Table 7a – entry 3, trifluoromethylation of trimethoxybenzene with **7b** as catalyst

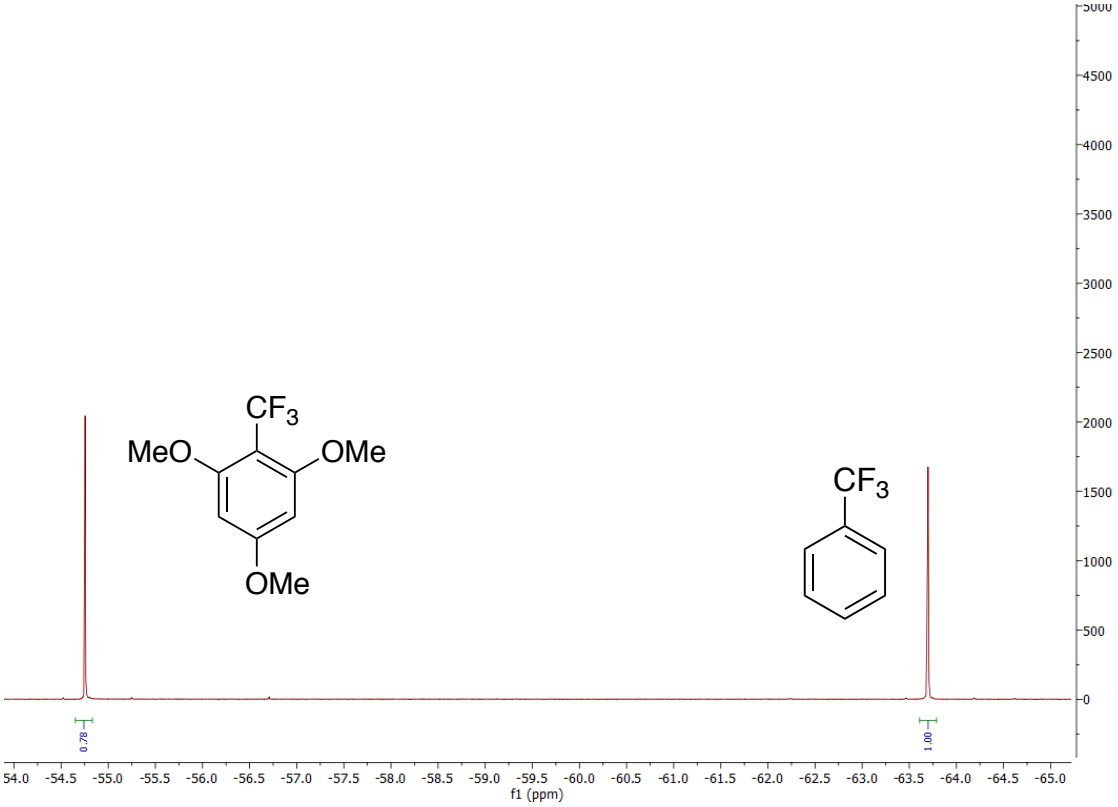

Figure F27. ^{19}F NMR spectra of Table 7a – entry 4, trifluoromethylation of trimethoxybenzene with **7c** as catalyst

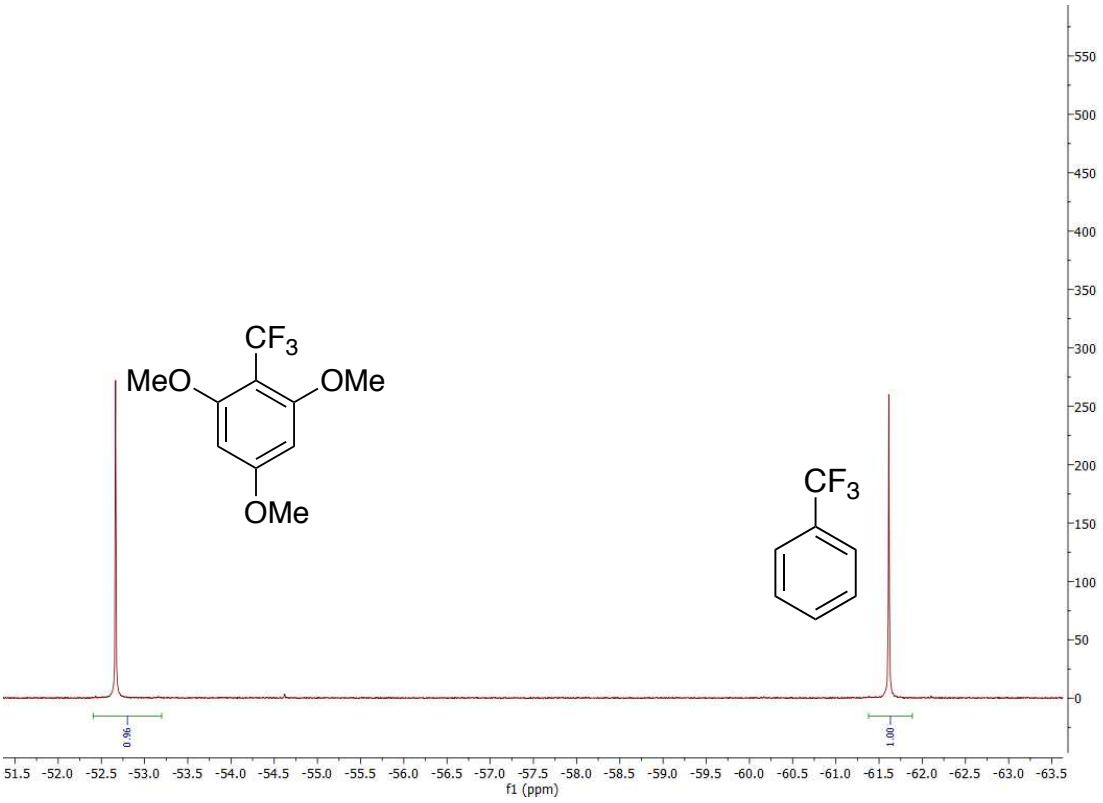

Figure F28. ^{19}F NMR spectra of Table 7a – entry 5, trifluoromethylation of trimethoxybenzene with **7l** as catalyst

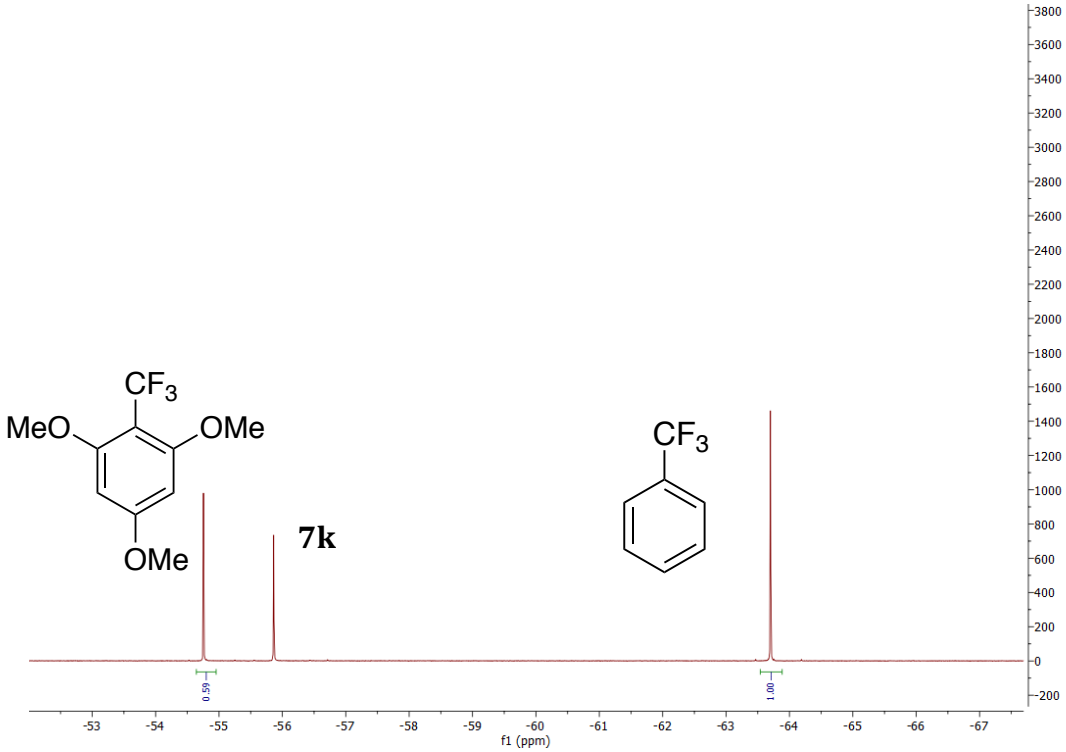

Figure F29. ^{19}F NMR spectra of Table F1 – entry 2, trifluoromethylation of trimethoxybenzene with 2 equiv. of arene

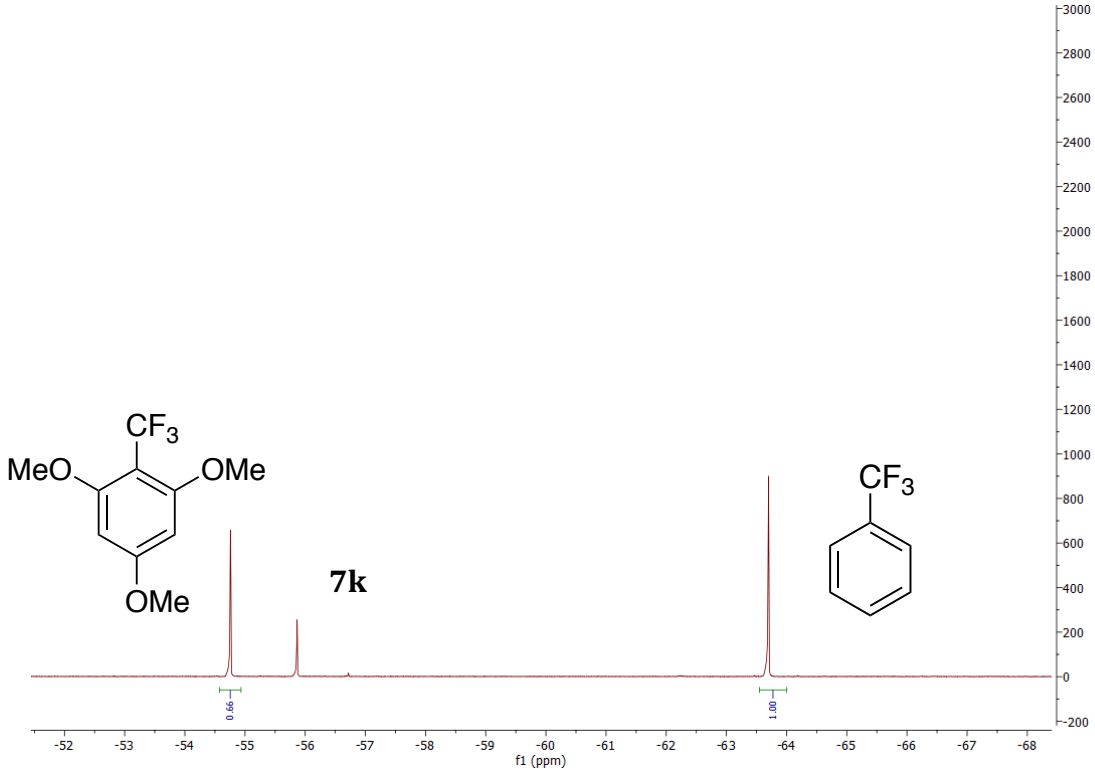

Figure F30. ^{19}F NMR spectra of Table F1 – entry 3, trifluoromethylation of trimethoxybenzene with 2 equiv. of arene and 1 equiv. of DIPEA

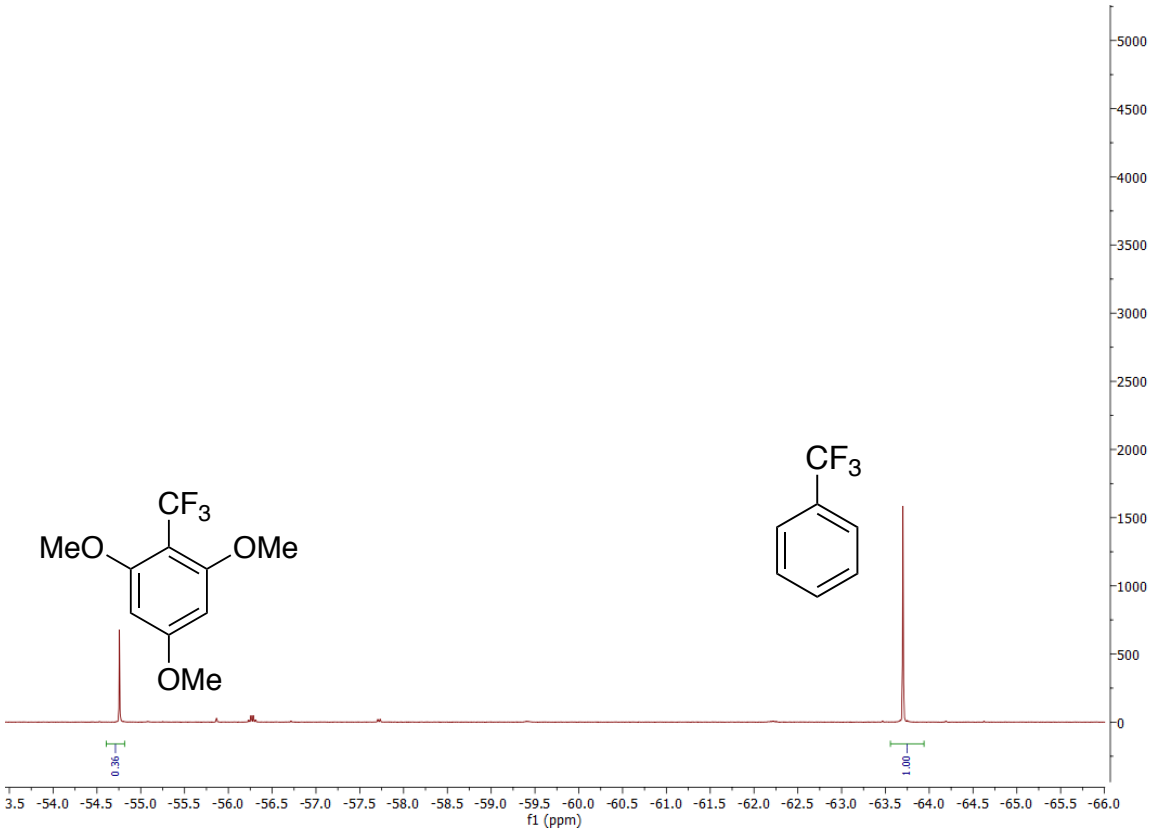

Figure F31. ^{19}F NMR spectra of Table F1 – entry 4, trifluoromethylation of trimethoxybenzene using THF solvent

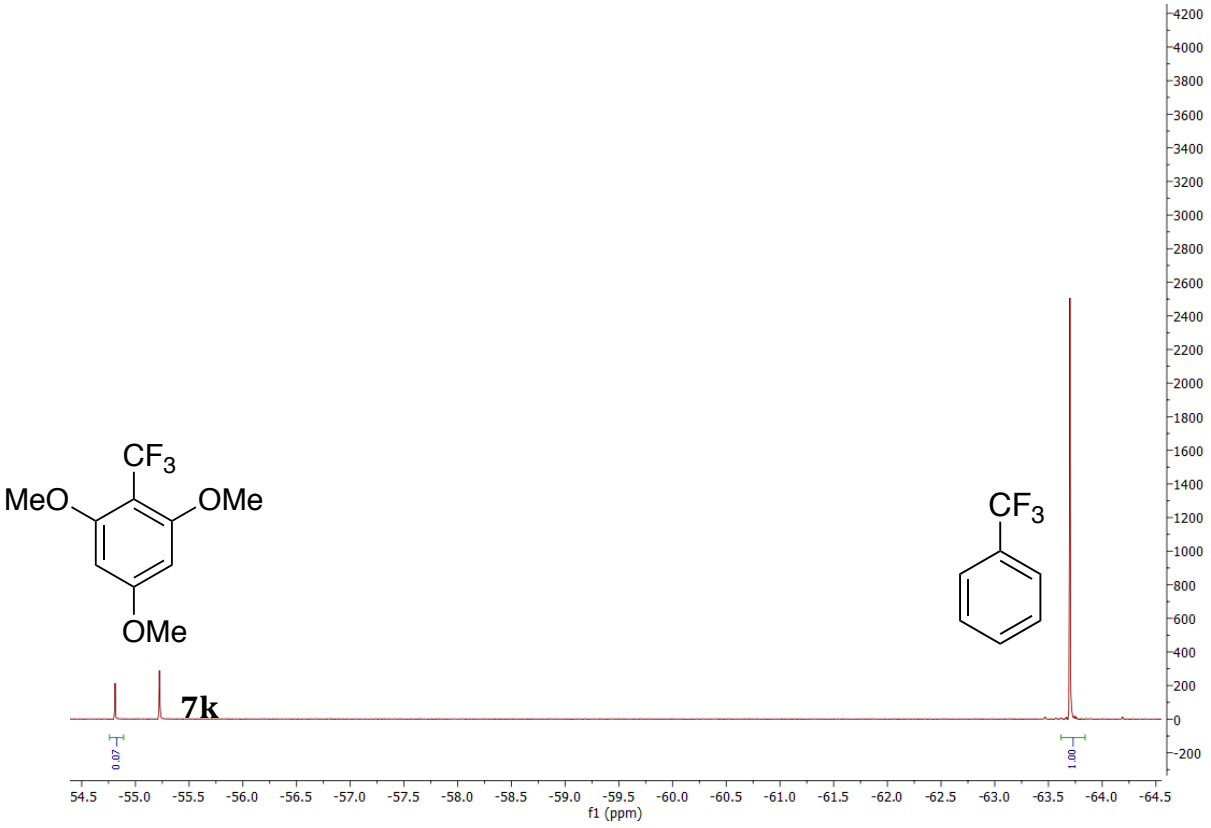

Figure F32. ^{19}F NMR spectra of Table F1 – entry 5, trifluoromethylation of trimethoxybenzene using MeCN solvent

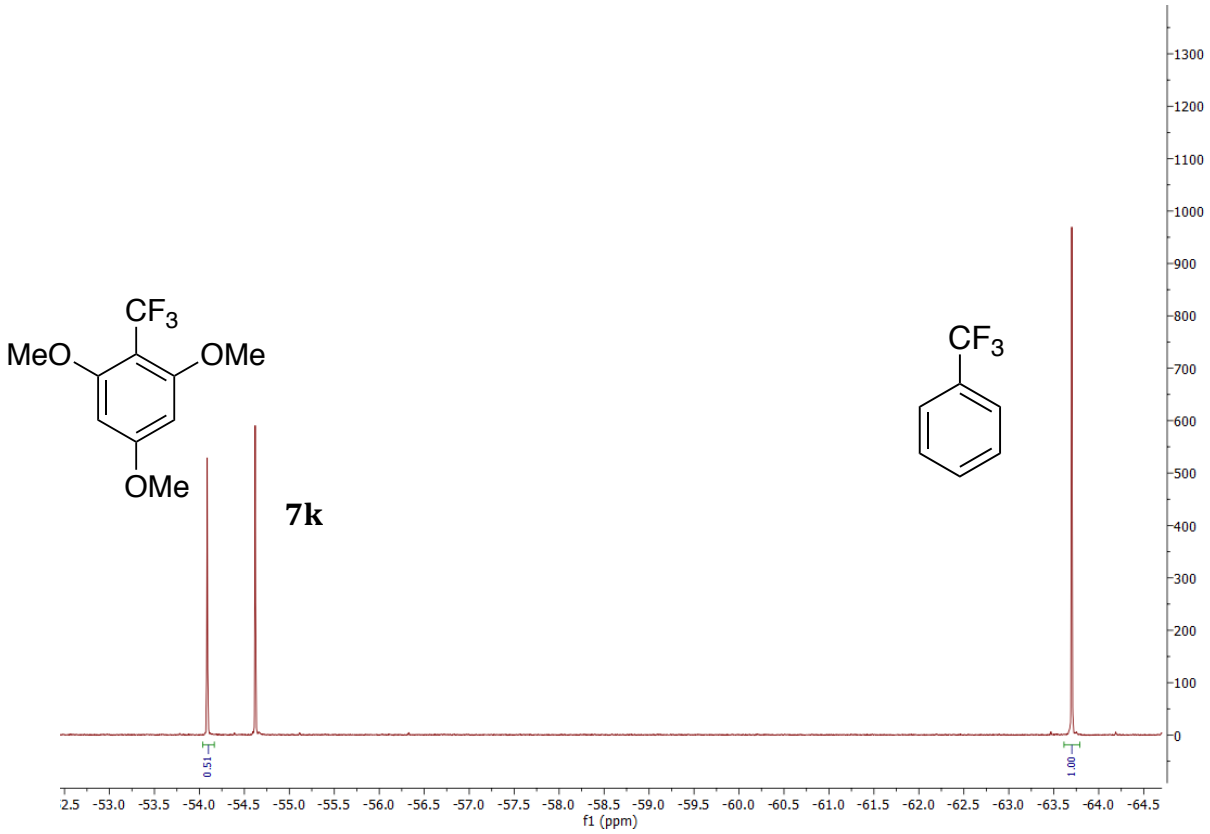

Figure F33. ^{19}F NMR spectra of Table F1 – entry 6, trifluoromethylation of trimethoxybenzene using 1,4 – dioxane solvent

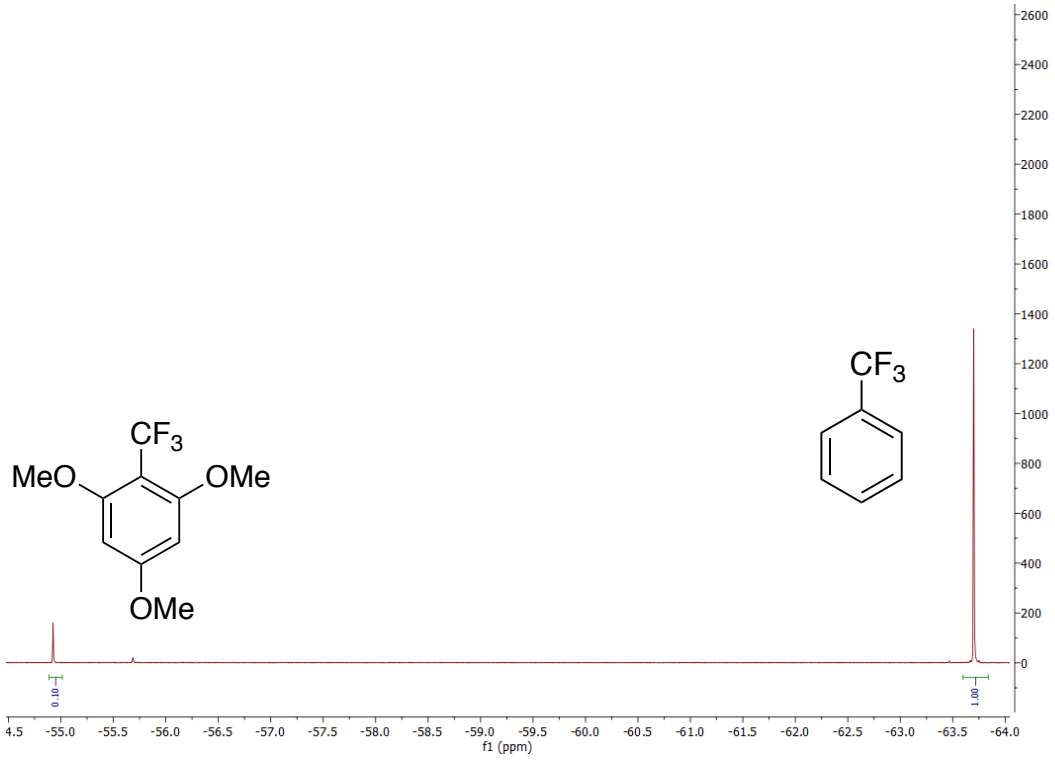

Figure F34. ^{19}F NMR spectra of Table F1 – entry 7, trifluoromethylation of trimethoxybenzene running the reaction for 18 h.

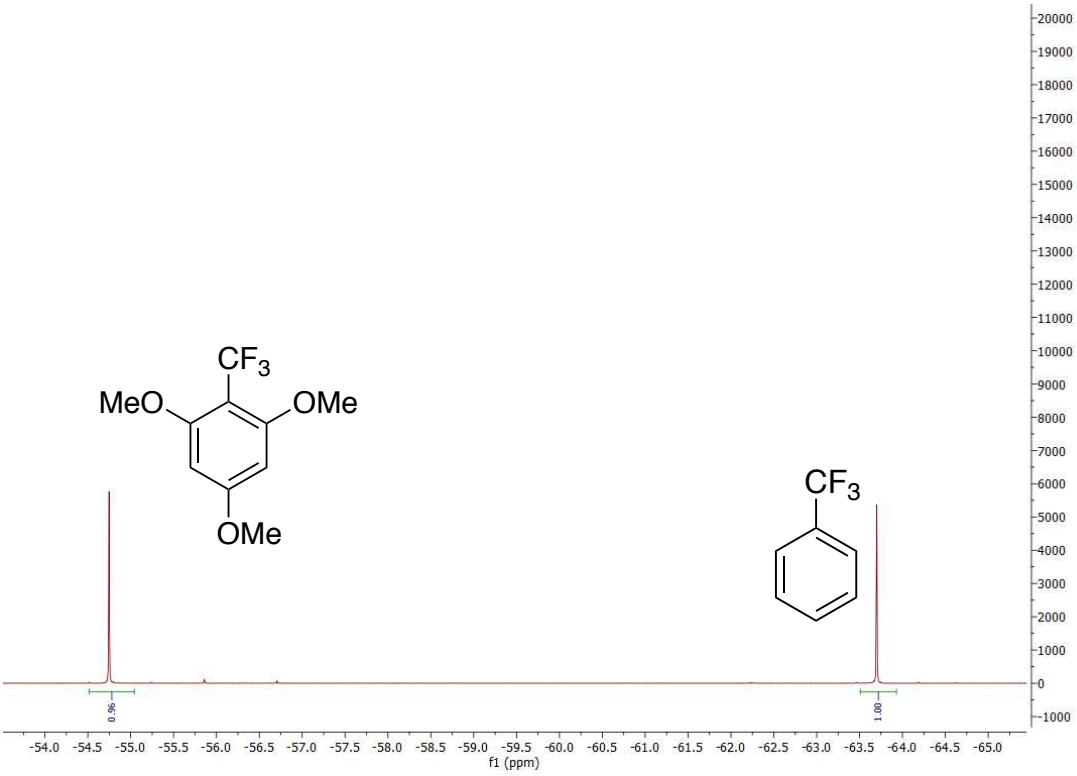

Figure F35. ^{19}F NMR spectra of Table F1 – entry 8, trifluoromethylation of trimethoxybenzene using CF_3CO_2H as cat. and running the reaction for 18 h.

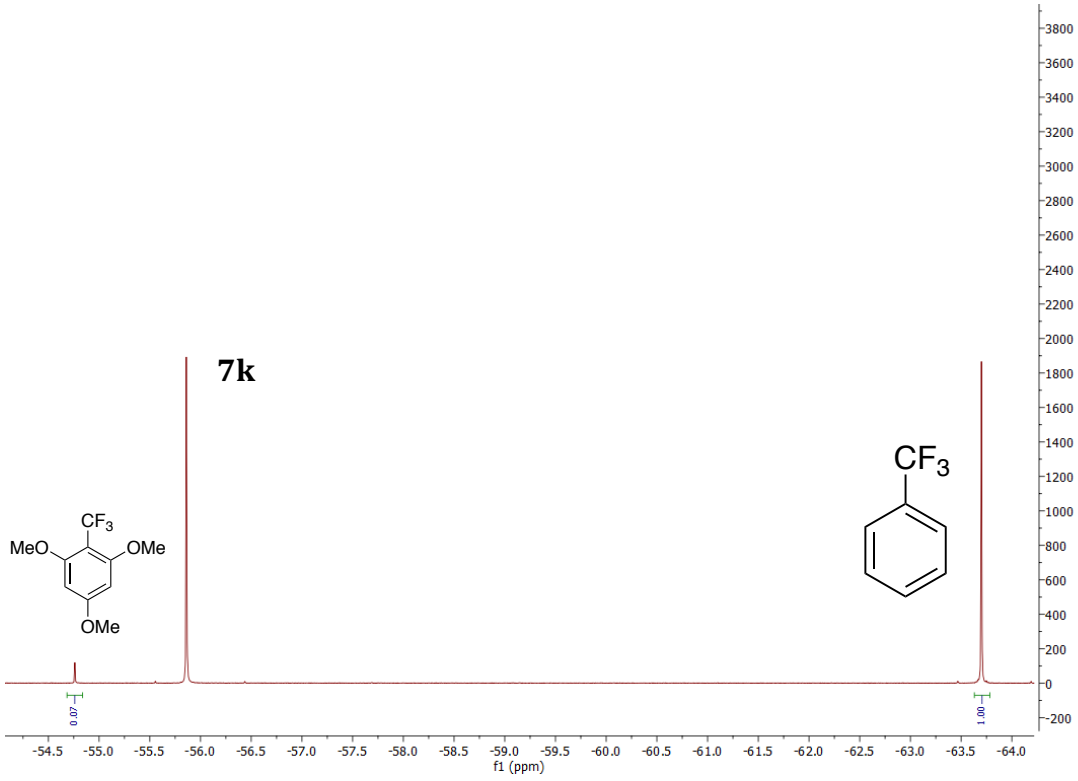

Figure F36. ^{19}F NMR spectra of crude products during the synthesis of **7c**. Two different types of nickel bearing five trifluoromethyl groups were identified in trace amounts, $[(MeCN)Ni(CF_3)_5]^-$ (**7o**) and $[(NCCH_2)Ni(CF_3)_5]^{2-}$ (**7p**) : ^{19}F NMR (CD_3CN, 376 MHz): δ -24.3 (app. septet, J = 7.5 Hz, 3 F), -27.4 (quartet, J = 7.5 Hz, 12 F).

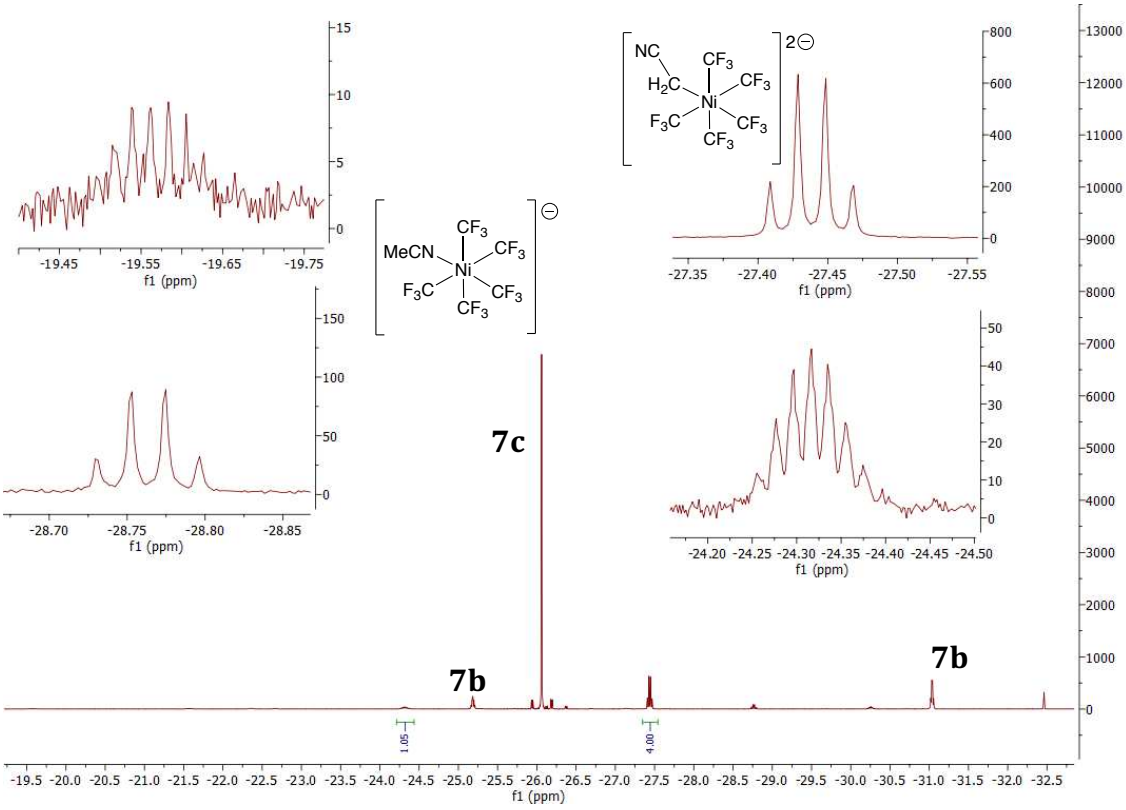

Figure F37. ^{19}F NMR spectra of reaction of aryl iodonium with $[NMe_4][(MeCN)Ni(CF_3)_3]$ in the presence of TEMPO in CD_3CN/CH_3CN.

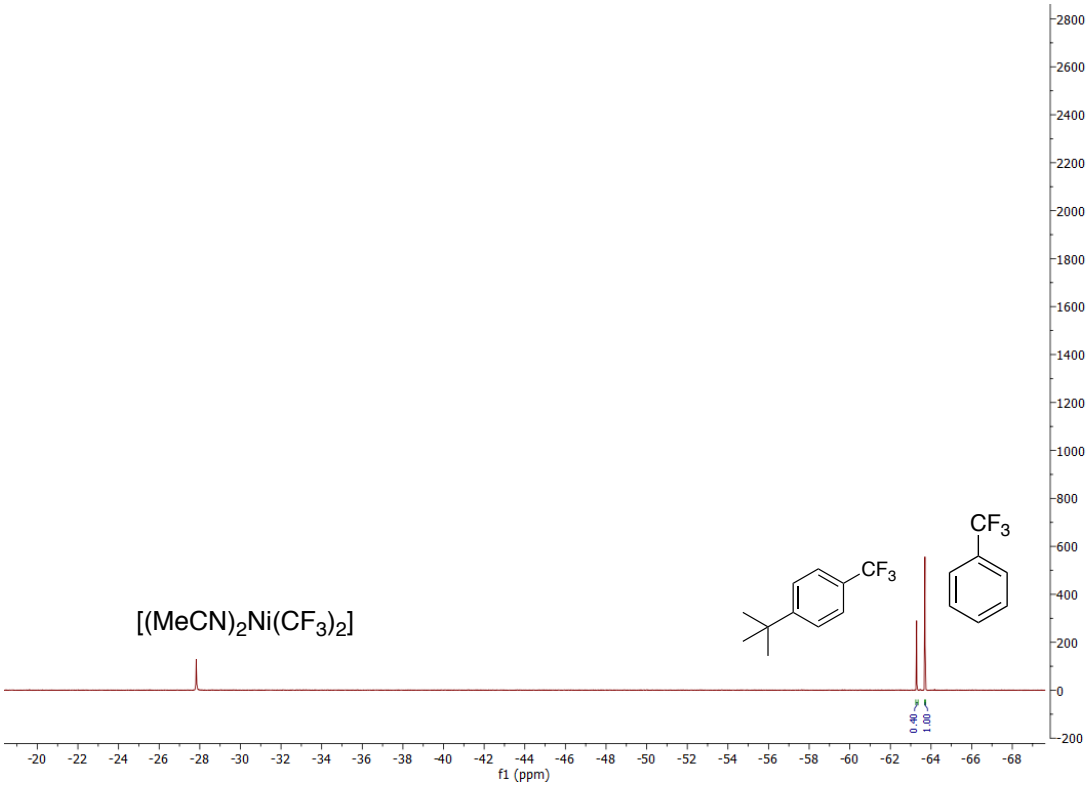

Figure F38. ^{19}F NMR spectra of reaction of alkynyl iodonium with $[NMe_4][(MeCN)Ni(CF_3)_3]$ in the presence of TEMPO in CD_3CN/CH_3CN.

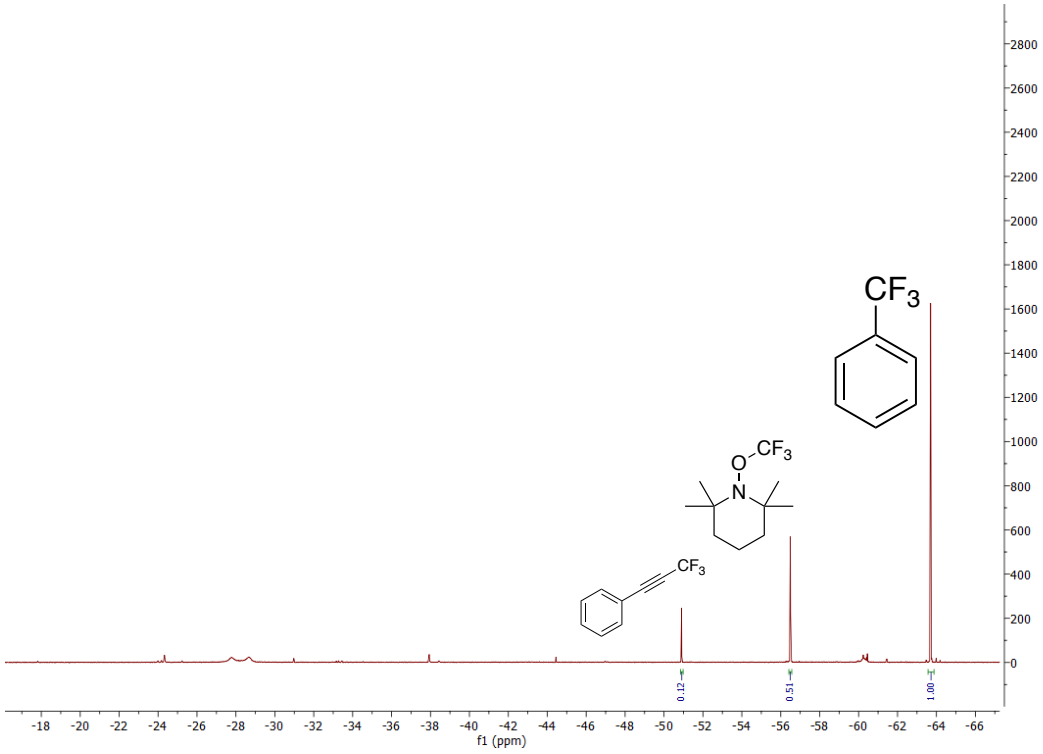

Figure F39. ^{19}F NMR spectra of reaction of 3,5-dichlorophenyldiazonium tetrafluoroborate with $[NMe_4][(MeCN)Ni(CF_3)_3]$ in the presence of TEMPO in CD_3CN/CH_3CN.

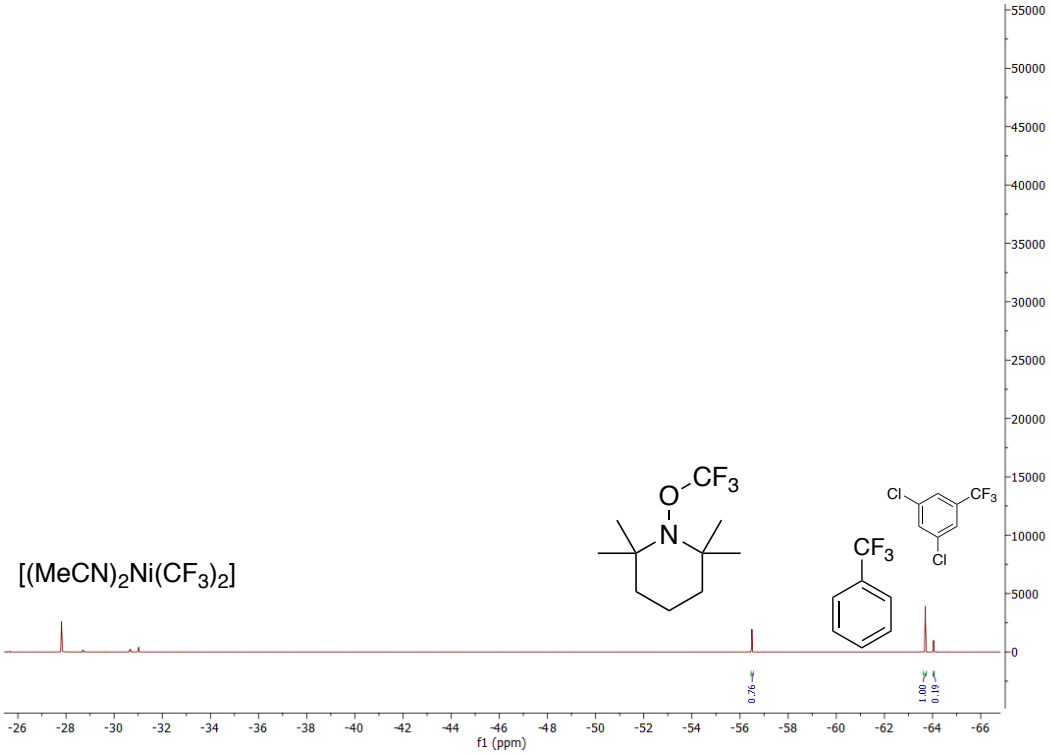

Figure F40. ^{19}F NMR spectra of reaction of $[NMe_4]_2[Ni(CF_3)_4]$ and 'magic blue' oxidant in the presence of TEMPO in CD_3CN/CH_3CN.

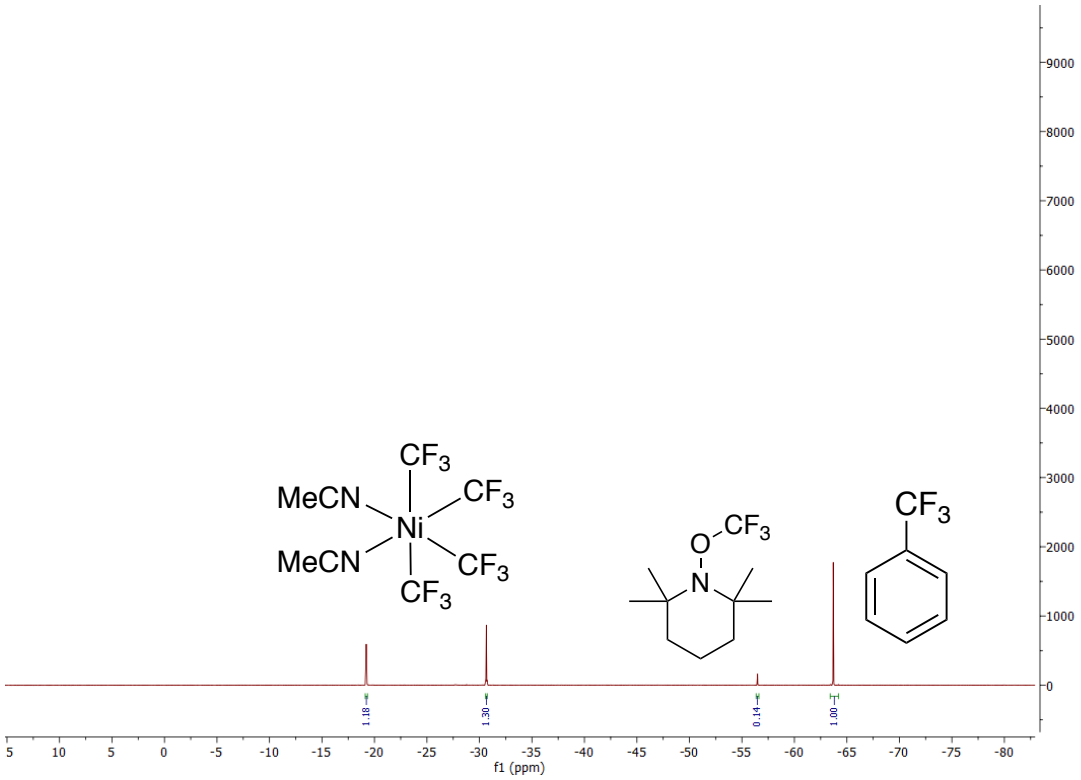

Figure F41. ^{19}F NMR spectra of the catalytic trifluoromethylation in the presence on TEMPO.

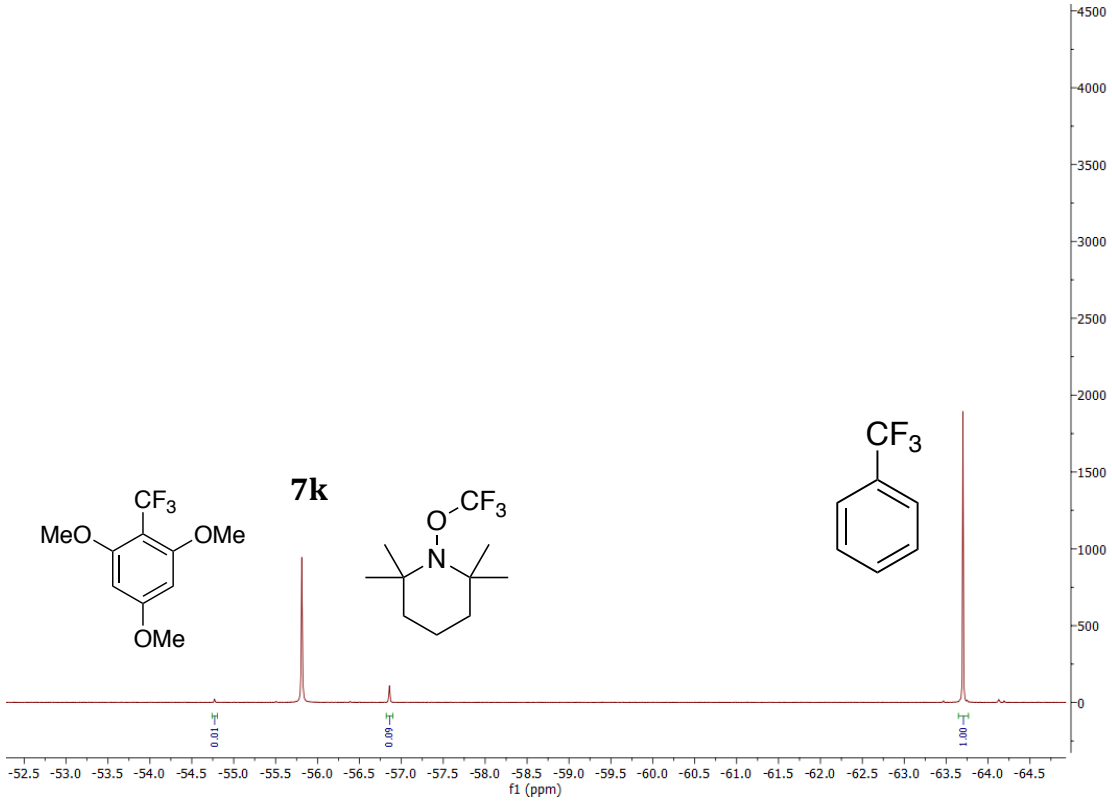

Figure F42. ^{19}F NMR spectra of the catalytic trifluoromethylation in the presence on TEMPO without any nickel catalyst.

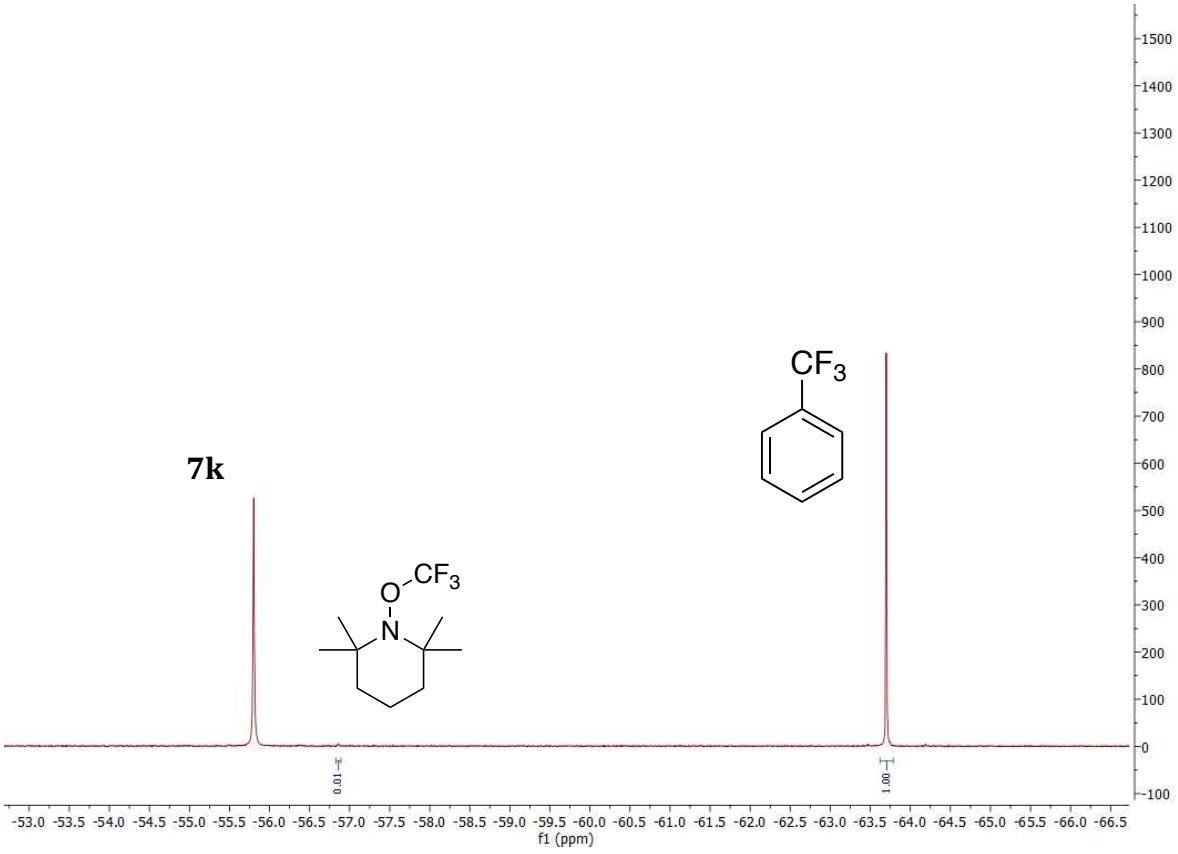

Figure F43. ^{19}F NMR spectra of the catalytic trifluoromethylation in the presence on TEMPO without any nickel catalyst, or 1,3,5-trimethoxybenzene

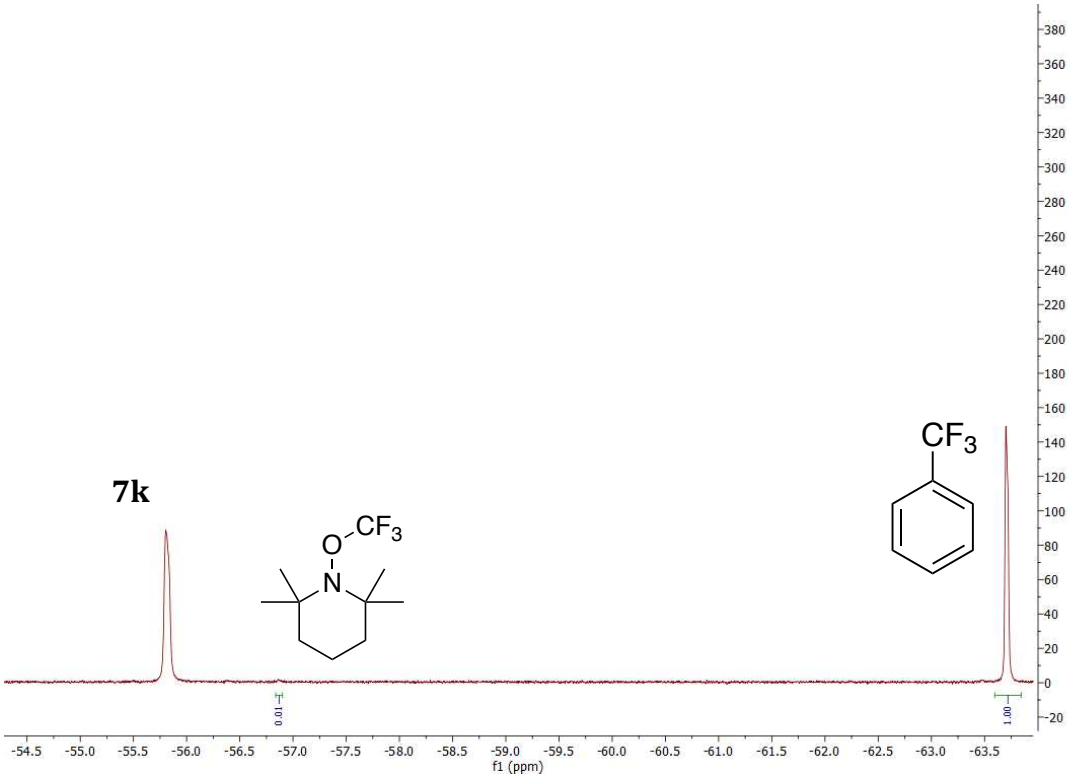

Figure F44. ^{19}F NMR spectra of Table 7a – entry 1, trifluoromethylation of trimethoxybenzene with **7j** as catalyst

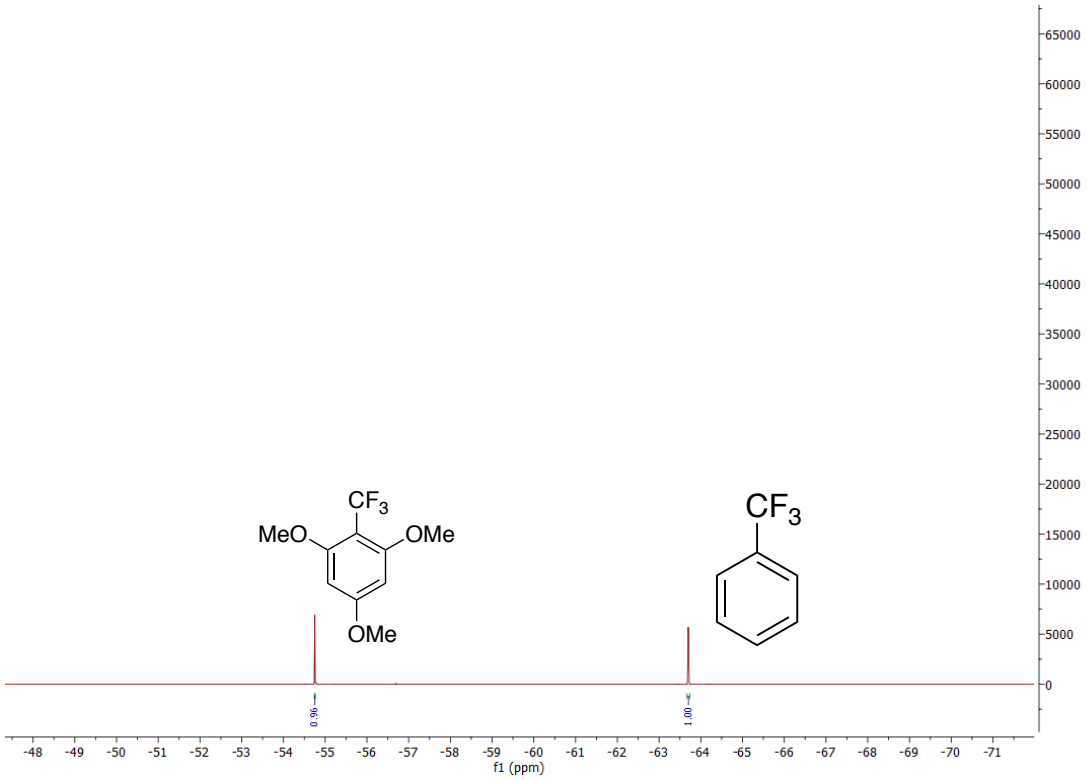

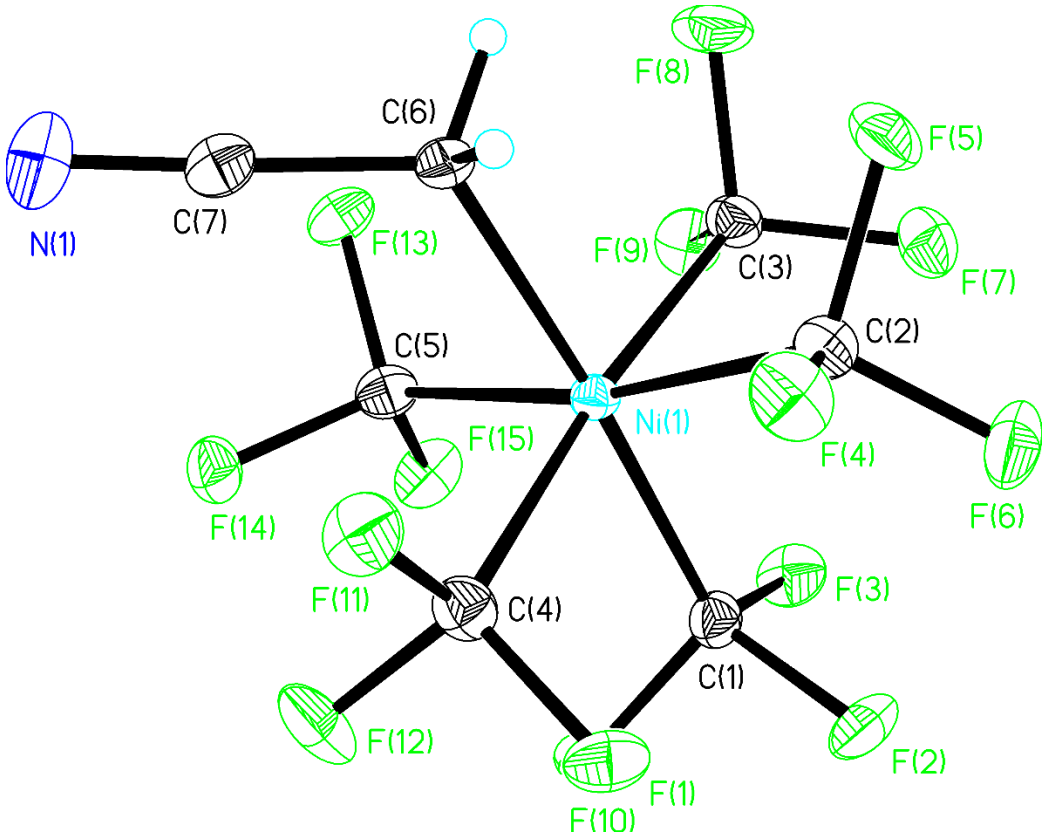

Figure F45. ORTEP diagram of $[(NCCH_2)Ni(CF_3)_5]^{2-}$ (**7p**). The two NMe_4 counterions are omitted for clarity. Selected bond lengths (Å): Ni1-C5 1.993(4); Ni1-C4 1.997(4); Ni1-C1 2.002(4); Ni1-C2 2.003(4); Ni1-C3 2.004(4); Ni1-C6 2.041(3). Selected bond angles (°): C5-Ni1-C4 96.67(15); C5-Ni1-C1 91.26(15); C4-Ni1-C1 86.50(16); C5-Ni1-C2 169.87(15); C4-Ni1-C2 89.32(15); C1-Ni1-C2 97.27(15); C5-Ni1-C3 87.40(16); C4-Ni1-C3 174.54(16); C1-Ni1-C3 89.79(15); C2-Ni1-C3 87.18(16); C5-Ni1-C6 87.50(15); C4-Ni1-C6 89.92(16); C1-Ni1-C6 176.05(15); C2-Ni1-C6 84.33(15); C3-Ni1-C6 93.91(15).

Appendix G: Supporting Information and Spectral Data for Chapter 8

Figure G1: ^{19}F NMR of $[NMe_4][(MeCN)(CF_3)Ni(C_4F_8)]$ in CD_3CN

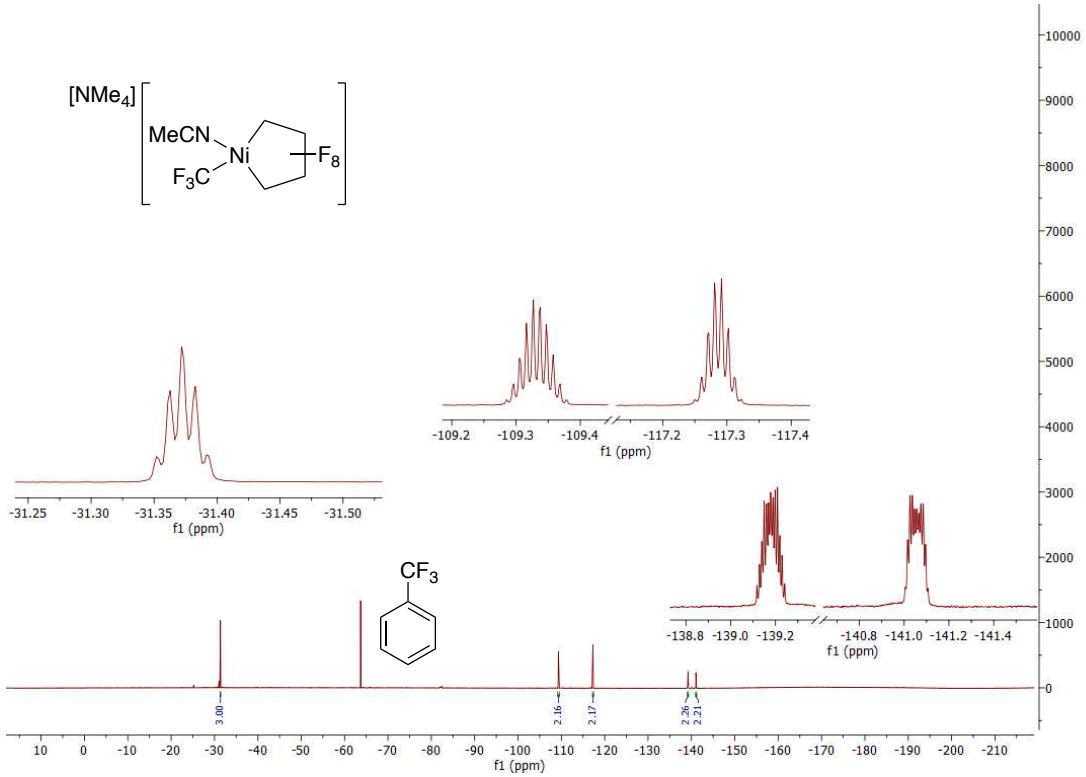

Figure G2: ^{1}H NMR of $[NMe_4][(MeCN)(CF_3)Ni(C_4F_8)]$ in CD_3CN

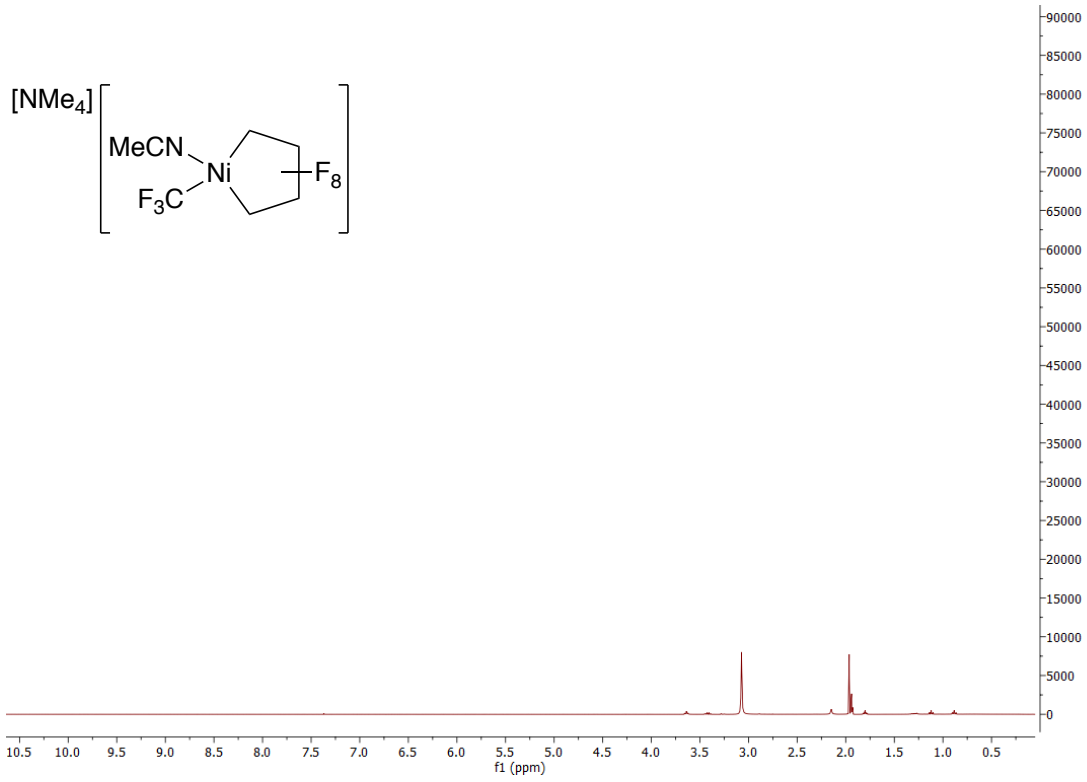

Figure G3: ^{19}F NMR of $[NMe_4][(MeCN)(C_2F_5)Ni(C_4F_8)]$ in CD_3CN

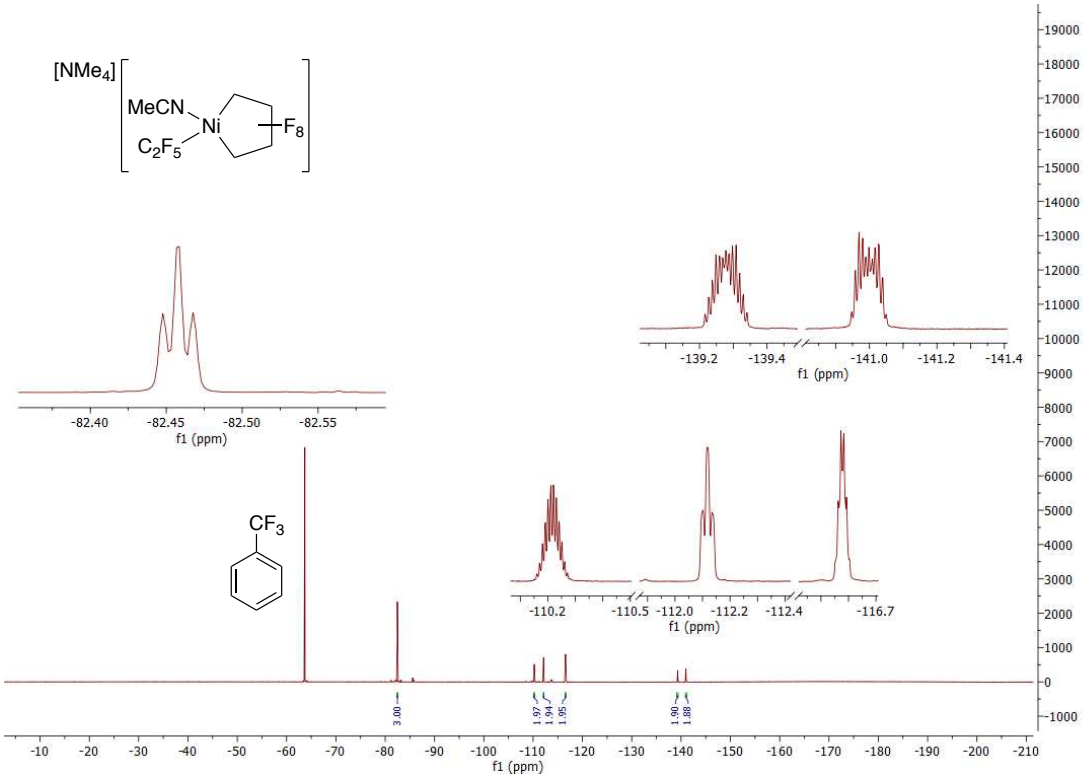

Figure G4: ^{1}H NMR of $[NMe_4][(MeCN)(C_2F_5)Ni(C_4F_8)]$ in CD_3CN

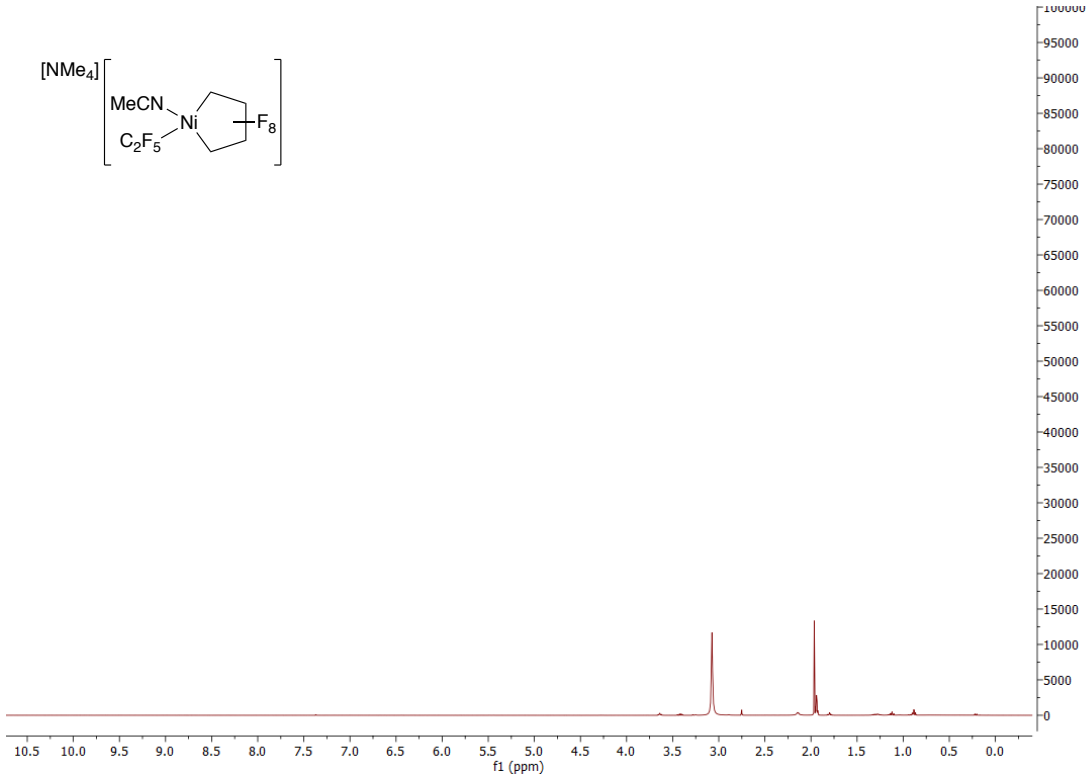

Figure G5: ^{19}F NMR of $[NMe_4][(IMes)(CF_3)Ni(C_4F_8)]$ in CD_3CN

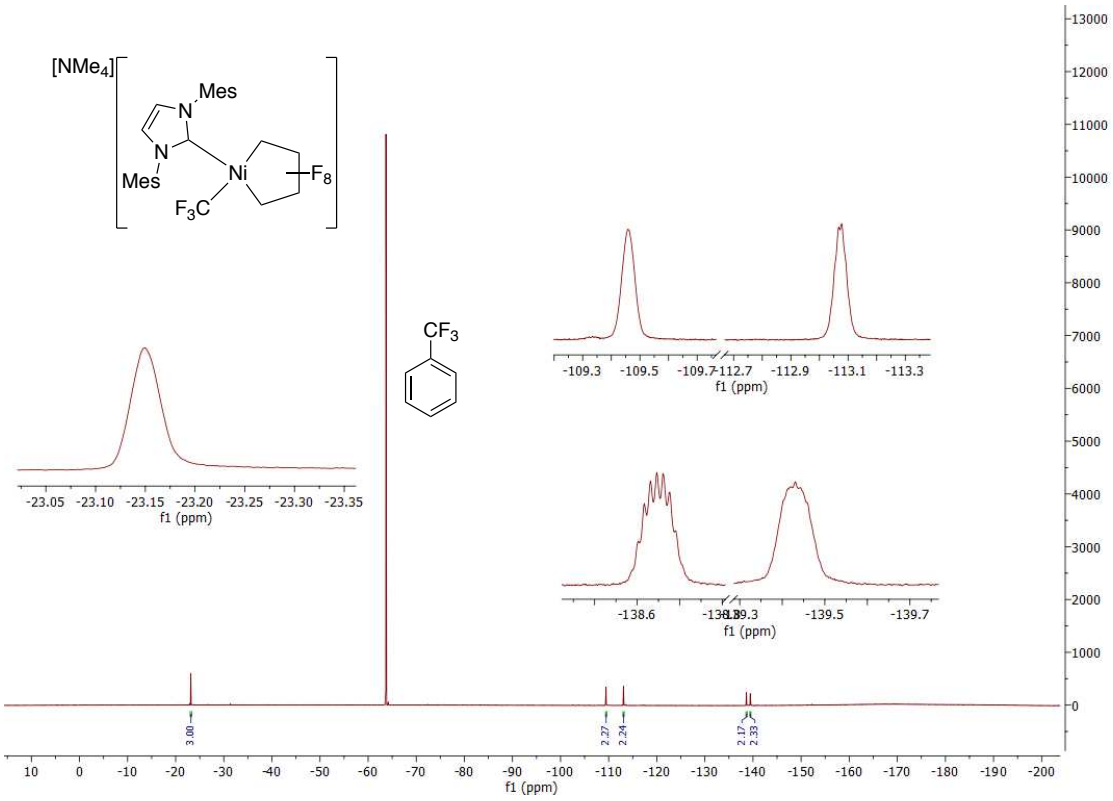

Figure G6: ^{1}H NMR of $[NMe_4][(IMes)(CF_3)Ni(C_4F_8)]$ in CD_3CN

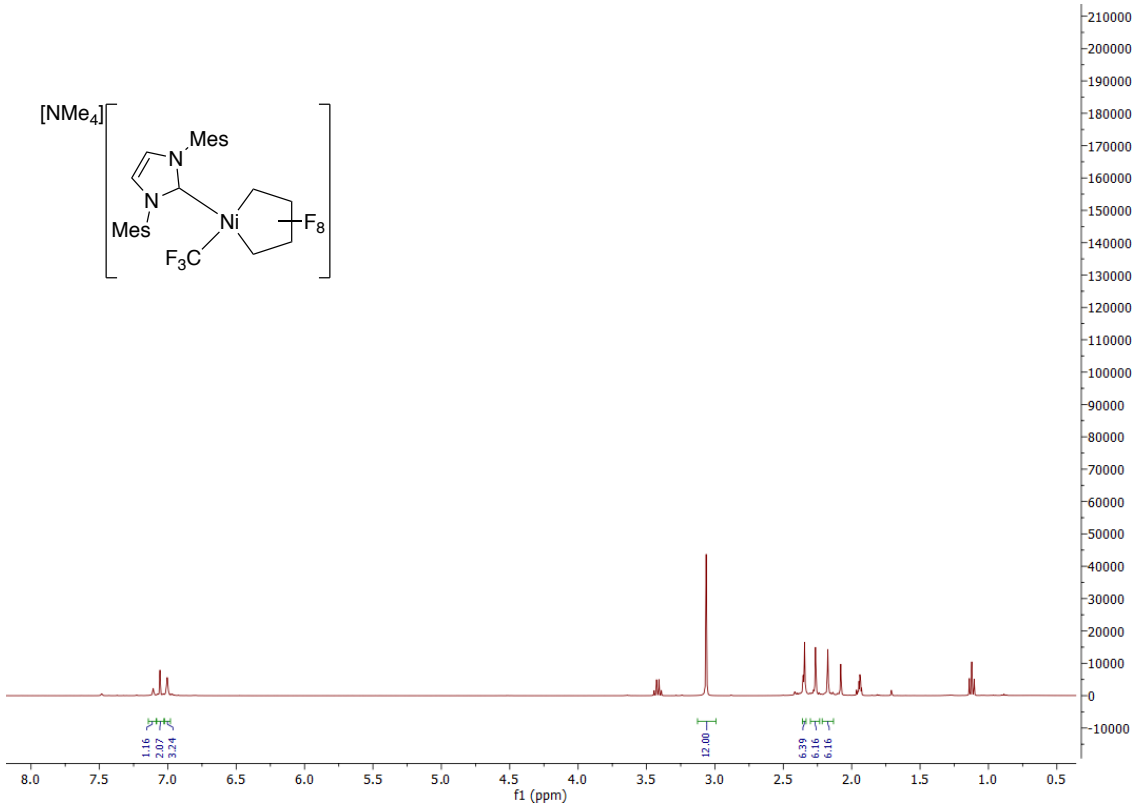

Figure G7 – ^{19}F NMR of $[NMe_4][(IMes)Ni(CF_3)_3]$ in CD_3CN

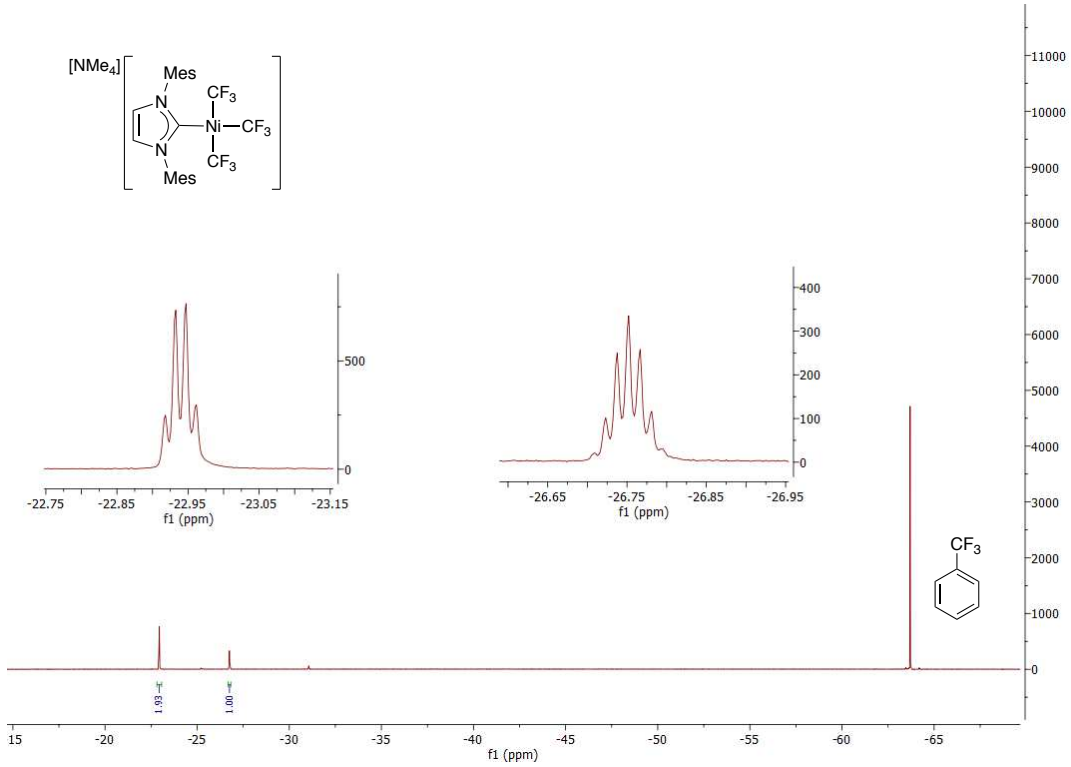

Figure G8 – ^{1}H NMR of $[NMe_4][(IMes)Ni(CF_3)_3]$ in CD_3CN

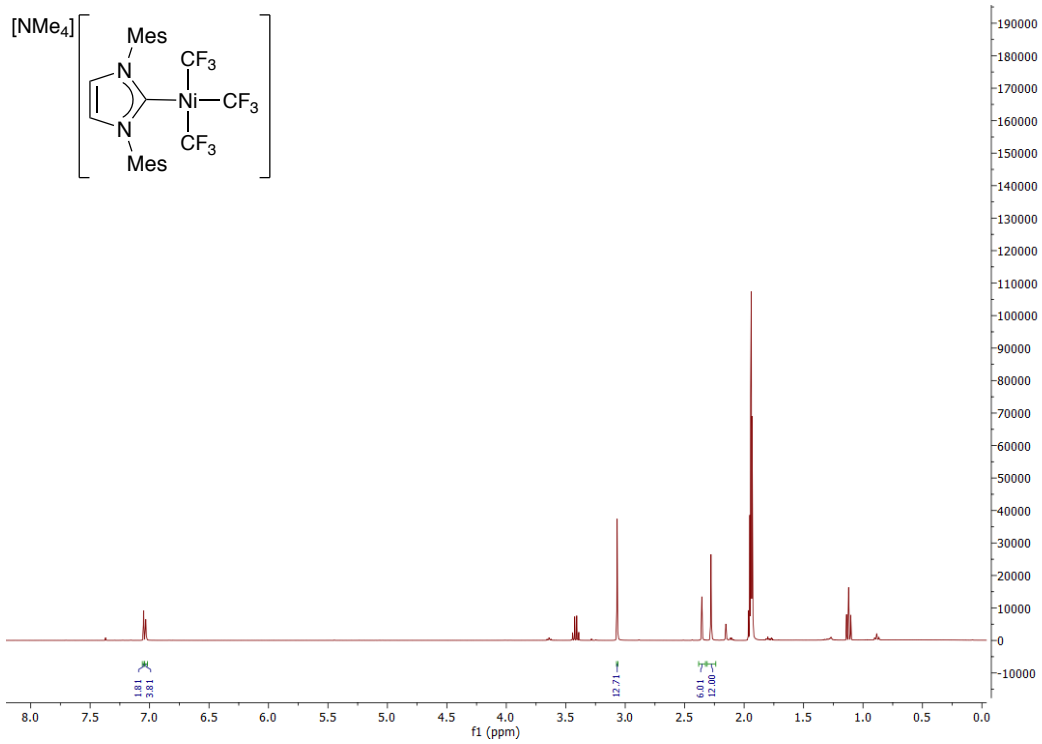

Figure G9: ^{19}F NMR spectra from the trifluoromethylation of 1,3,5 – trimethoxybenzene with Umemoto Reagent II and catalytic $[NMe_4][(MeCN)(CF_3)Ni(C_4F_8)]$ in DMSO – d_6

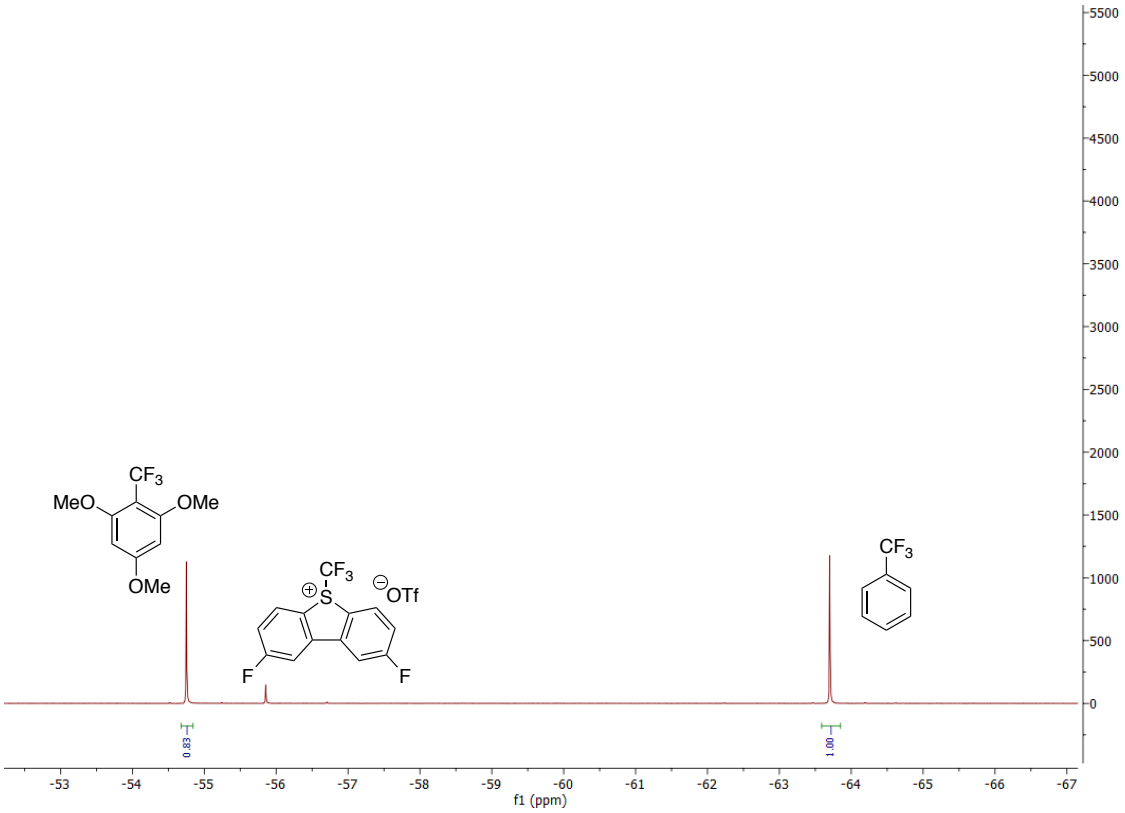

Figure G10: Cyclic voltammograms of **8d** (orange), and **8f** (blue) in MeCN. Metal complex, 10 mM; electrolyte, 100 mM [NBu_4][PF_6]; working and counter electrode, platinum; silver psuedoreference; scan rate, 100 mV/s.

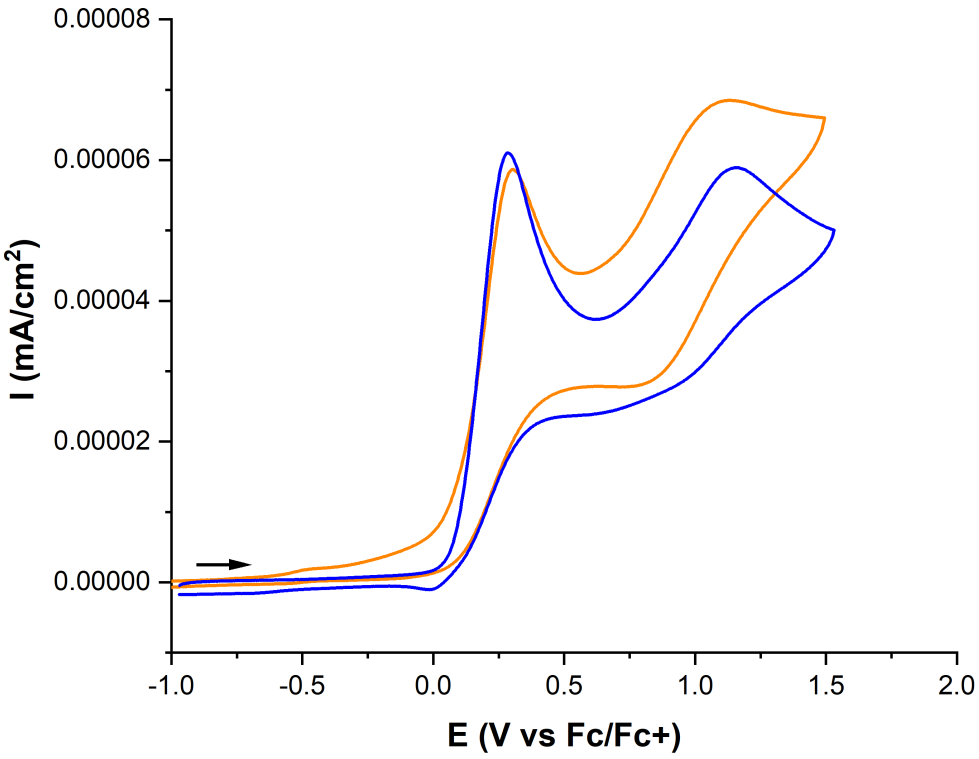

Figure G11: Preliminary X-ray data for compound 8d.

Only a poorly refined data set with two co-crystallized benzene molecules and one co-crystallized pentane could been obtained for compound **8d**. The preliminary structure shown here is only provided as additional support of the connectivity assignment in the text.

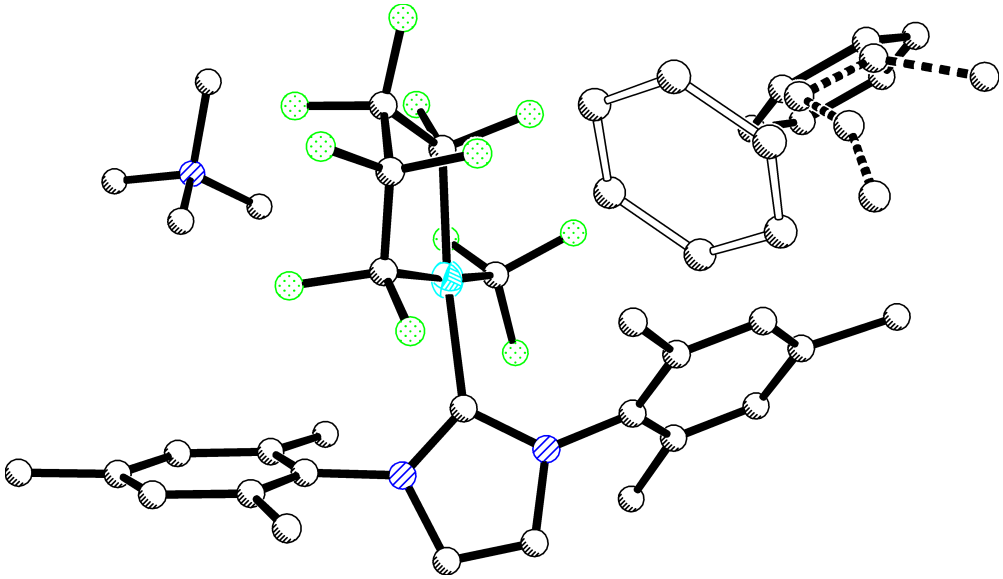

Appendix H: Supporting Information and Spectral Data for Chapter 9

Optimizations of the trifluoromethylation of brucine

Investigating excess Brucine vs. excess Umemoto Reagent II

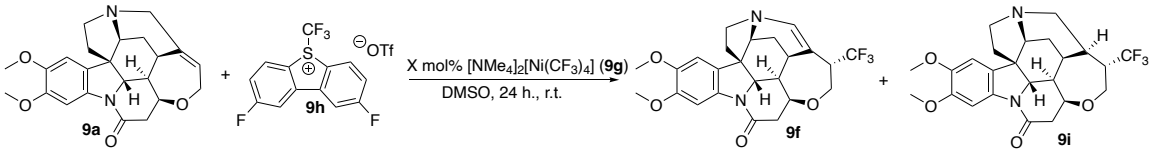

In a nitrogen filled glovebox, a vial was charged with Brucine, Umemoto reagent II, and 0.9 mL of DMSO (1 mL of DMSO was added to reactions that did not have nickel catalyst). To reactions with catalyst, 100 μL of a 0.025 M stock solution of $[NMe_4]_2[Ni(CF_3)_4]$ was added, and the reactions were stirred for 24 hours. Trifluorotoluene (0.05 mmol) was added, and the ^{19}F NMR was recorded.

Table H1: Effect of excess brucine vs. excess Umemoto reagent

Equiv. Brucine	Equiv. Umemoto	Ni Catalyst	Yield 9f	Yield 9i
0.5 (0.05 mmol)	1 (0.10 mmol)	5 %	29 %	7 %
0.5 (0.05 mmol)	1 (0.10 mmol)	0 %	8 %	3 %
0.5 (0.05 mmol)	1.5 (0.15 mmol)	5 %	27 %	7 %
1 (0.10 mmol)	1 (0.10 mmol)	5 %	38 %	9 %
1 (0.10 mmol)	1 (0.10 mmol)	0 %	13 %	6 %
1.5 (0.15 mmol)	1 (0.10 mmol)	5 %	45 %	10 %
2 (0.20 mmol)	1 (0.10 mmol)	5 %	51 %	11 %
2.5 (0.25 mmol)	1 (0.10 mmol)	5 %	59 %	10 %

Investigating different bases

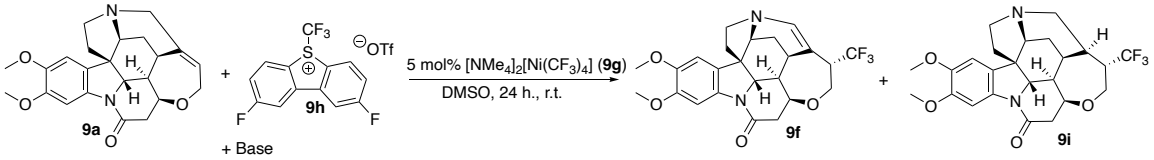

In a nitrogen filled glovebox, a vial was charged with Brucine (0.10 mmol), Umemoto reagent II (0.05 mmol), base (0.05 mmol) and 0.9 mL of DMSO (1 mL of DMSO was added to reactions that did not have nickel catalyst). To the reactions with catalyst, 100 μL of a 0.025 M stock solution of $[NMe_4]_2[Ni(CF_3)_4]$ was added, and the reactions were stirred for 24 hours. Trifluorotoluene (0.05 mmol) was added, and the ^{19}F NMR was recorded. *Note: NaH used was in the form of 60% dispersion in mineral oil.*

Table H2: Effect of different bases

Base	Ni Catalyst	Yield 9f	Yield 9i
Umemoto Reagent II	5 %	38 %	9 %
Umemoto Reagent II	0 %	13 %	6 %
DIPEA	5 %	31 %	5 %
DIPEA	0 %	13 %	5 %
NaH	5 %	38 %	4 %
NaH	0 %	15 %	4 %
KO^{t}Bu	5 %	9 %	n.d.
KO^{t}Bu	0 %	8 %	n.d.
NaO^{t}Bu	5 %	7 %	n.d.
NaO^{t}Bu	0 %	5 %	n.d.

Investigating the effect of excess Brucine with NaH as base, and effect of heat

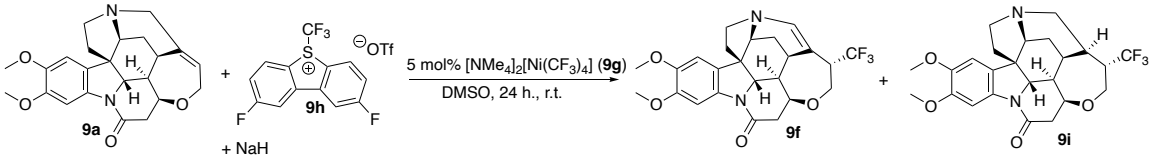

In a nitrogen filled glovebox, a vial or ampule was charged with Brucine, Umemoto reagent II, NaH, and 0.9 mL of DMSO. 100 μL of a 0.025 M stock solution of $[NMe_4]_2[Ni(CF_3)_4]$ was added, and the reactions were stirred for 24 hours at either room temperature or 50 °C. Trifluorotoluene (0.05 mmol) was added, and the ^{19}F NMR was recorded. *Note: NaH used was in the form of 60% dispersion in mineral oil.*

Table H3: Effect of excess brucine with NaH and effect of heat

Equiv. Brucine	Equiv. Umemoto	Equiv. NaH	Temp.	Yield 9f	Yield 9i
1 (0.10 mmol)	1 (0.10 mmol)	0	r.t.	38 %	9 %
2.5 (0.25 mmol)	1 (0.10 mmol)	0	r.t.	58 %	10 %
1 (0.10 mmol)	0.5 (0.05 mmol)	0.5 (0.05 mmol)	r.t.	38 %	4 %
2.5 (0.25 mmol)	0.5 (0.05 mmol)	0.5 (0.05 mmol)	r.t.	36 %	4 %
1 (0.10 mmol)	1 (0.10 mmol)	0	50 °C	41 %	7 %
1 (0.10 mmol)	0.5 (0.05 mmol)	0.5 (0.05 mmol)	50 °C	31 %	4 %

Investigating catalyst loading amount

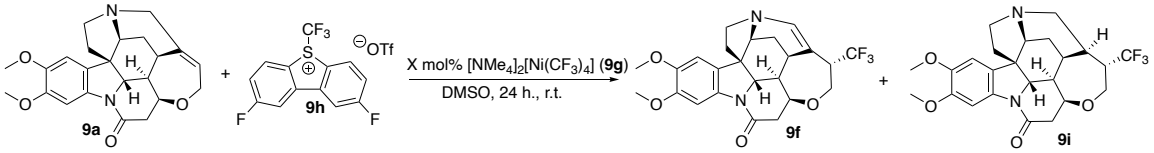

In a nitrogen filled glovebox, a vial was charged with Brucine, Umemoto reagent II, and DMSO (0.9 mL added to reactions at 5 mol% catalyst, and 0.8 mL added to reaction with 10 mol% catalyst). 100 μL of a 0.025 M stock solution of $[NMe_4]_2[Ni(CF_3)_4]$ was added to reactions with 5 mol% catalyst, and 200 μL of a 0.025 M stock solution of $[NMe_4]_2[Ni(CF_3)_4]$ was added to reactions with 10 mol% catalyst. The reactions were stirred for 24 hours. Trifluorotoluene (0.05 mmol) was added, and the ^{19}F NMR was recorded.

Table H4: Effect of different catalyst loadings

Equiv. Brucine	Equiv. Umemoto	Ni	Temp.	Yield 9f	Yield 9i
1 (0.10 mmol)	1 (0.10 mmol)	5 %	r.t.	38 %	9 %
2.5 (0.25 mmol)	1 (0.10 mmol)	5 %	r.t.	58 %	10 %
1 (0.10 mmol)	1 (0.10 mmol)	10 %	r.t.	59 %	10 %
2.5 (0.25 mmol)	1 (0.10 mmol)	10 %	r.t.	81 %	12 %

Investigating different metals

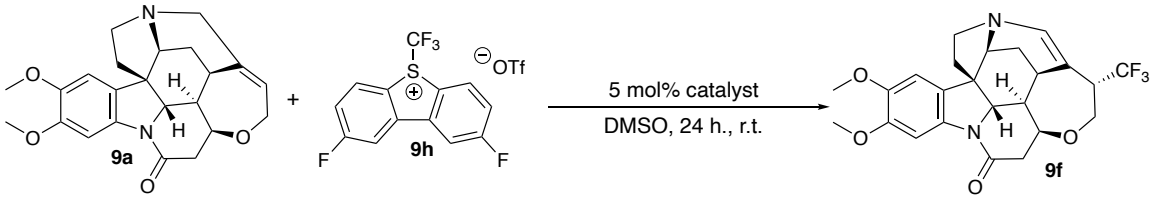

In a nitrogen filled glovebox, a vial was charged with Brucine (0.10 mmol, 1 equiv.), Umemoto reagent II (0.10 mmol, 1 equiv.), and 0.9 mL of DMSO (1 mL of DMSO was added to reactions that did not have a catalyst). To the reactions with catalyst, 100 μL of a 0.025 M stock solution of catalyst was added, and the reactions were stirred for 24 hours. Trifluorotoluene (0.05 mmol) was added, and the ^{19}F NMR was recorded.

Table H5: Effect of different metal catalyst

Metal Catalyst	**Yield**
No catalyst	13 %
$[(MeCN)_3Co(CF_3)_3]$	13 %
$[NMe_4]_2[Ni(CF_3)_4]$	38 %
$[NBu_4][Cu(CF_3)_4]$	15 %

Reaction of trifluoromethylation of brucine with tributyltin hydride: In a nitrogen filled glovebox, a vial was charged with brucine (395 mg, 1.00 mmol), Umemoto Reagent II (220 mg, 0.50 mmol), and 9 mL of DMSO. Tributyltin hydride (0.14 mL, 0.52 mmol) was added with stirring, followed by 1 mL of a 0.025 M solution of $[NMe_4]_2[Ni(CF_3)_4]$ in DMSO. The reaction was stirred for 24 hours. The reaction was then added to seperatory funnel with ether (60 mL), and extracted with water (2 x 25 mL). The aqueous layers were combined and re-extracted with ether (60 mL). The organic layers were combined and washed with water (3 x 25 mL), brine (1 x 25 mL) and dried over $MgSO_4$. The solvent was removed by rotary evaporator, and the crude product was purified by flash column chromatography. The proposed minor product was isolated from this reaction in trace amounts, and the following NMR data (Fig. H1) was obtained.

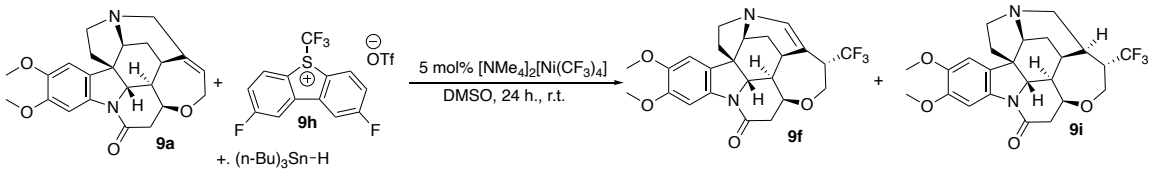

Figure H1: NMR spectral data of the minor product from the reaction described on page S9

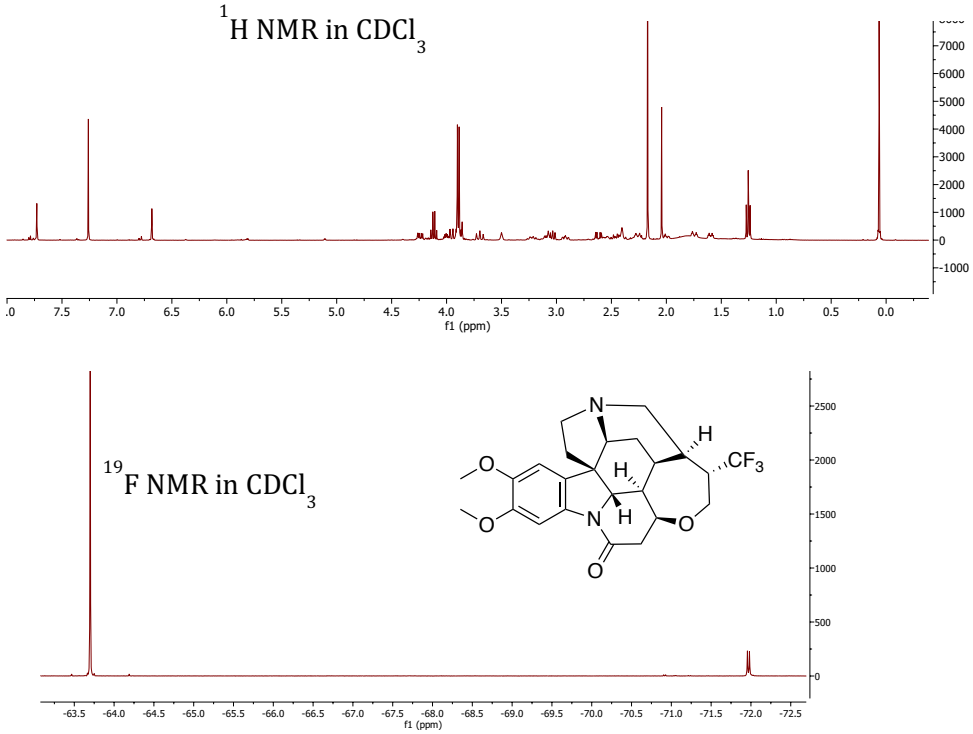

Figure H2: ^{1}H NMR of **9f** in C_6D_6

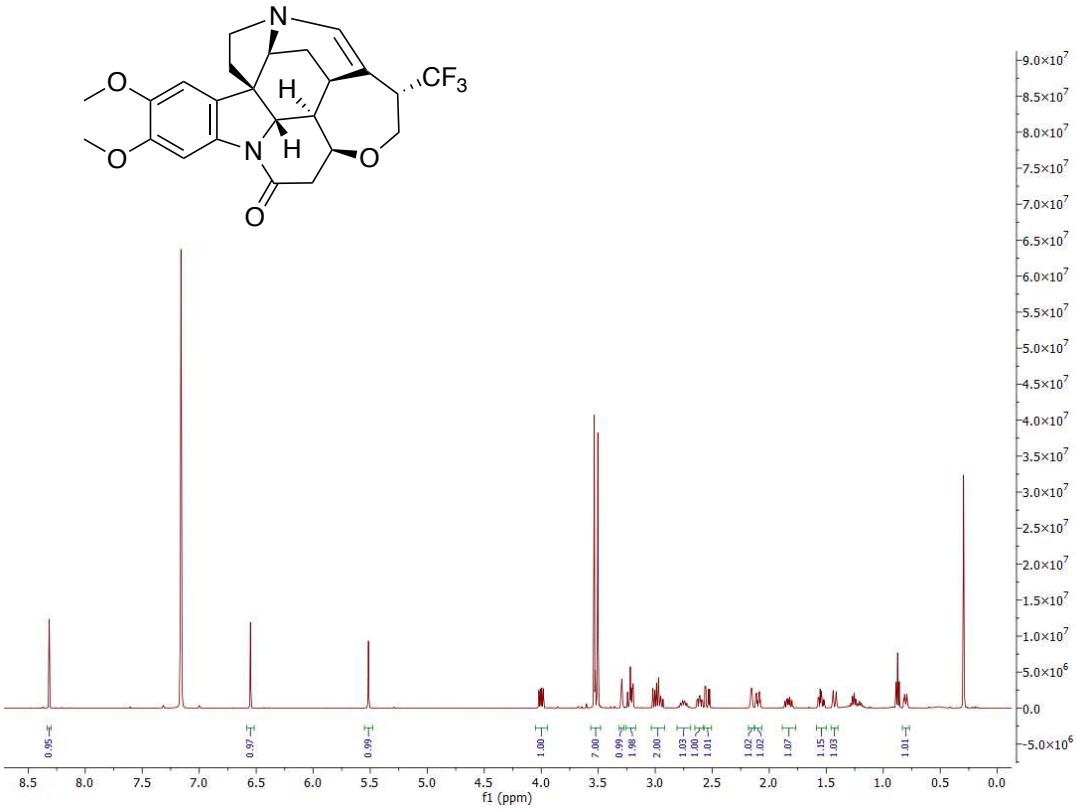

Figure H3: ^{13}C $\{^{1}H\}$ NMR of **9f** in C_6D_6

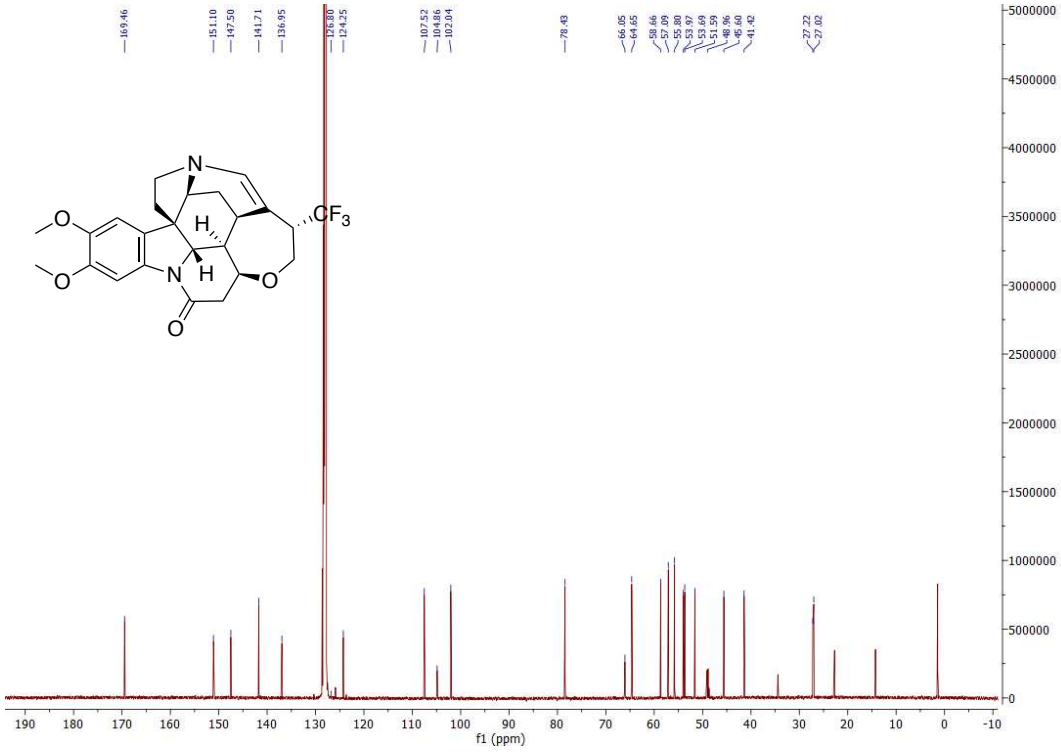

Figure H4: ^{19}F NMR of **9f** in C_6D_6

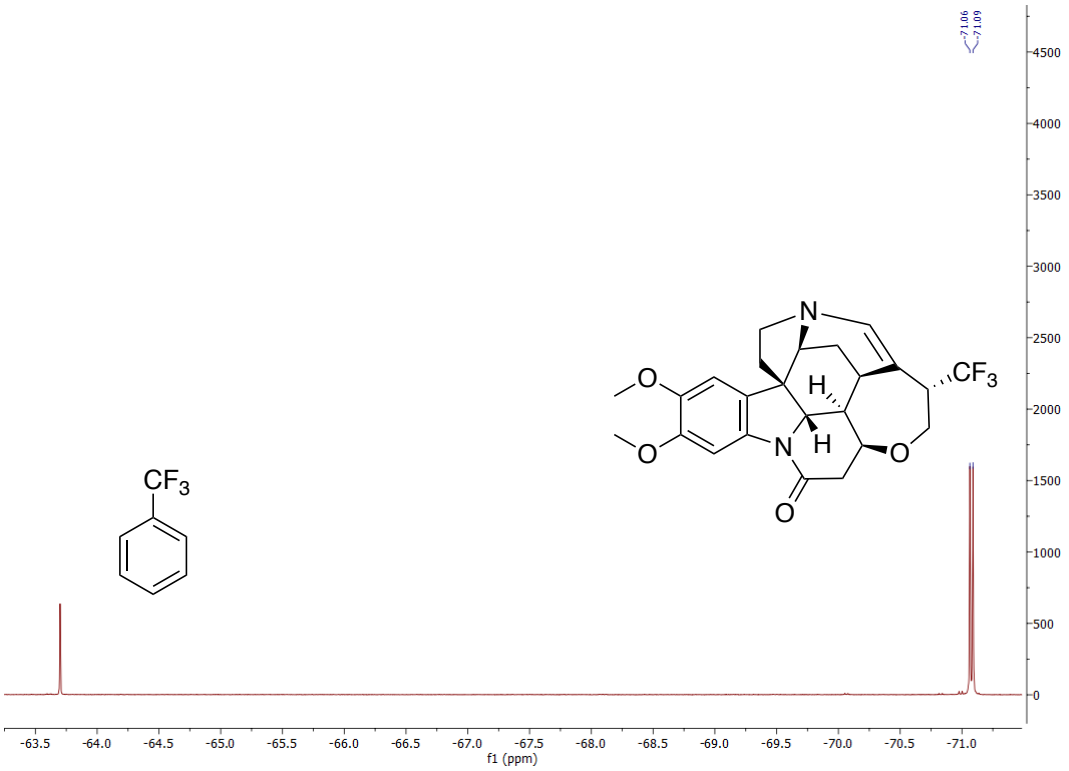

Figure H5: ^{1}H-^{1}H COSY NMR of **9f** in C_6D_6

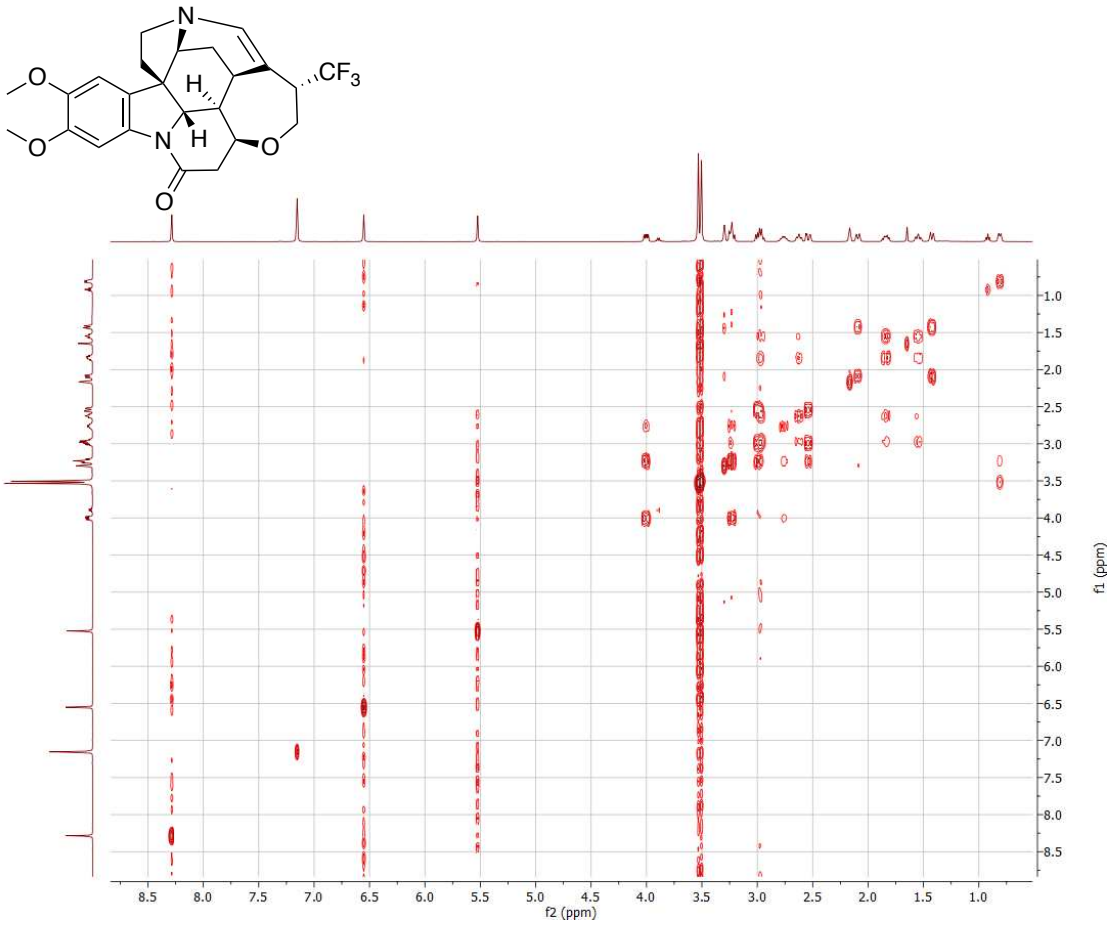

Figure H6: ^{13}C $\{^{1}H\}$ – DEPT135 NMR of **9f** in C_6D_6

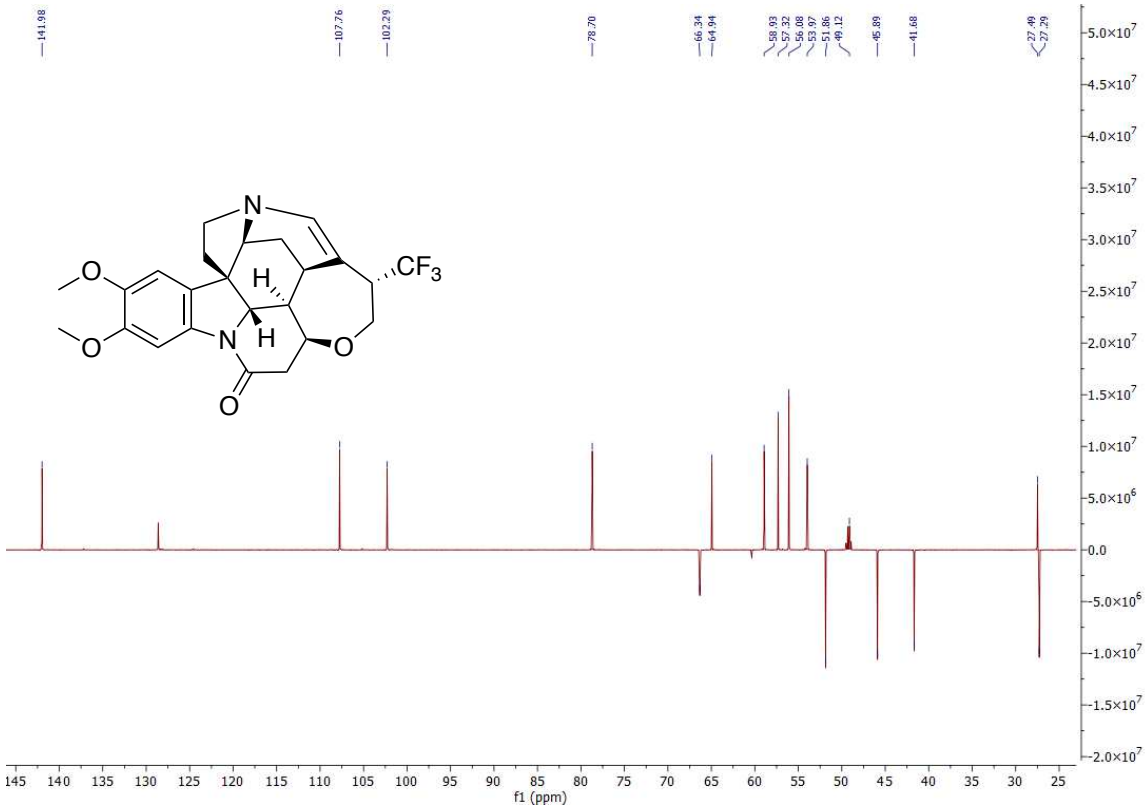

Figure H7: ^{1}H-^{13}C {^{1}H} HSQC NMR of **9f** in C_6D_6

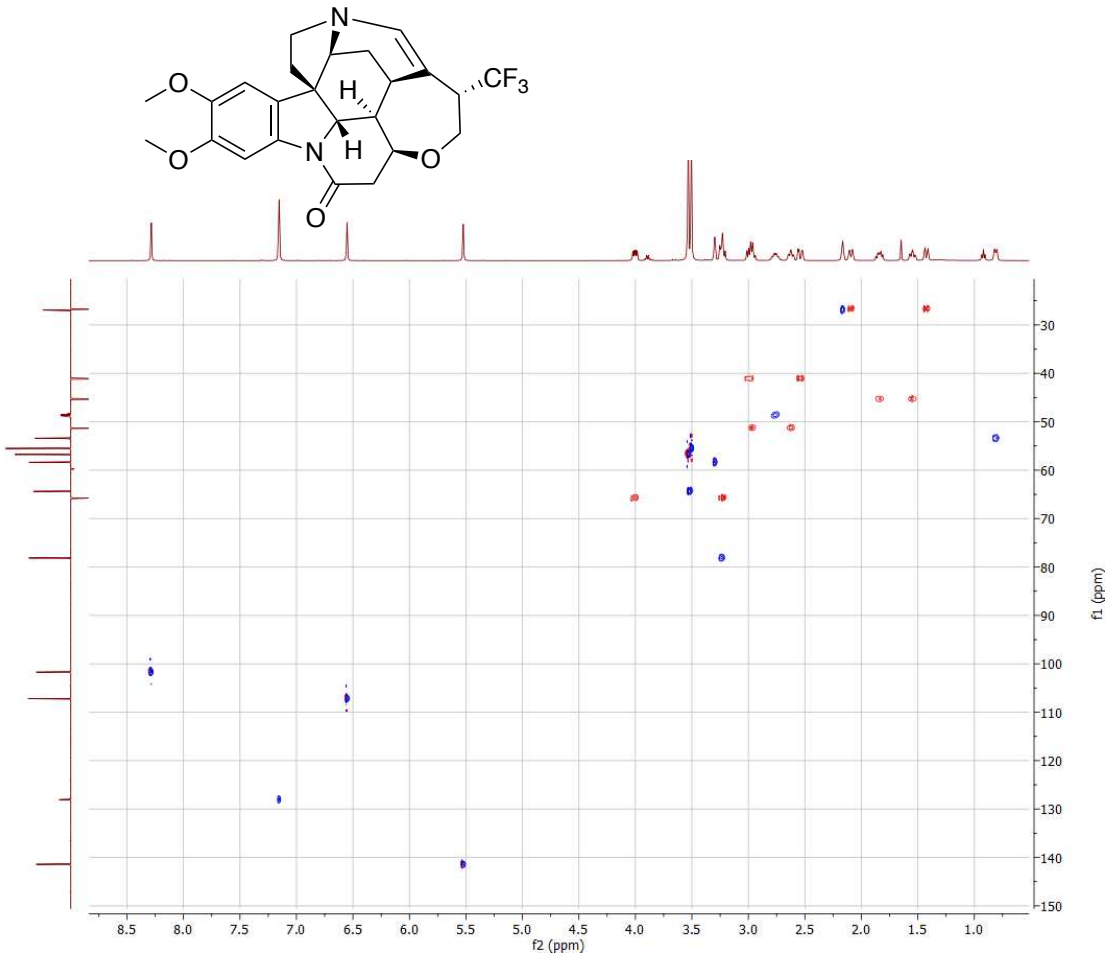

Figure H8: ^{1}H-^{13}C {^{1}H} HMBC NMR of **9f** in C_6D_6

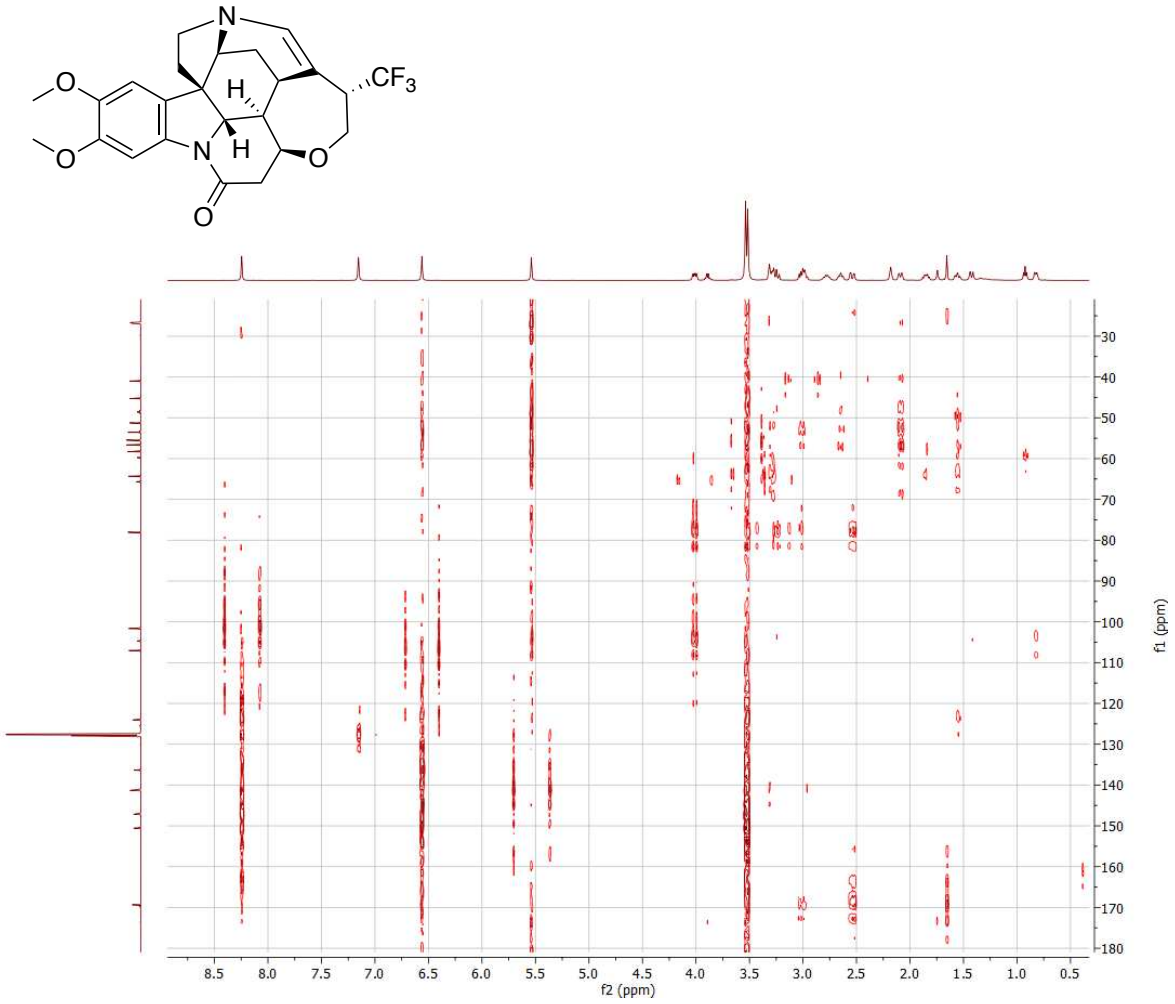

Figure H9: ^{1}H-^{1}H NOESY NMR of **9f** in C_6D_6

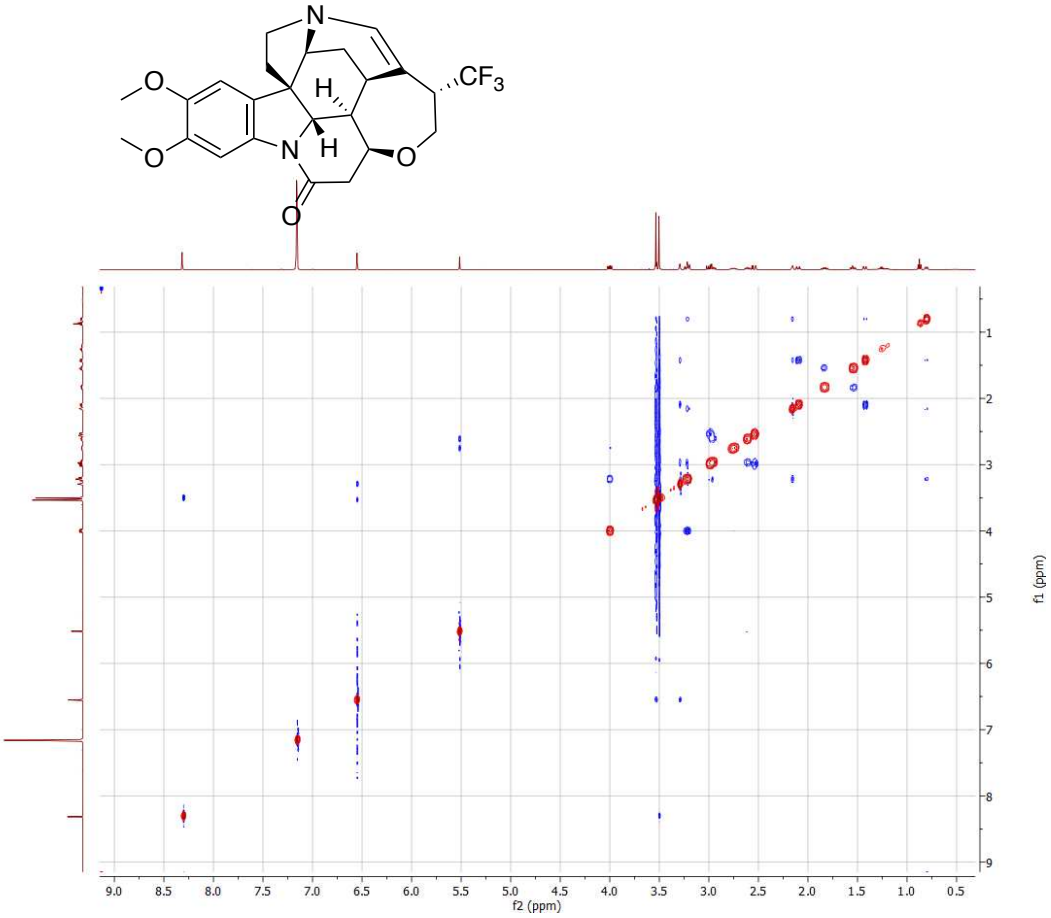

Figure H10: ^{19}F NMR after the reaction of brucine with $[(MeCN)_2Ni(CF_3)_4]$ in MeCN. Identified products labeled.

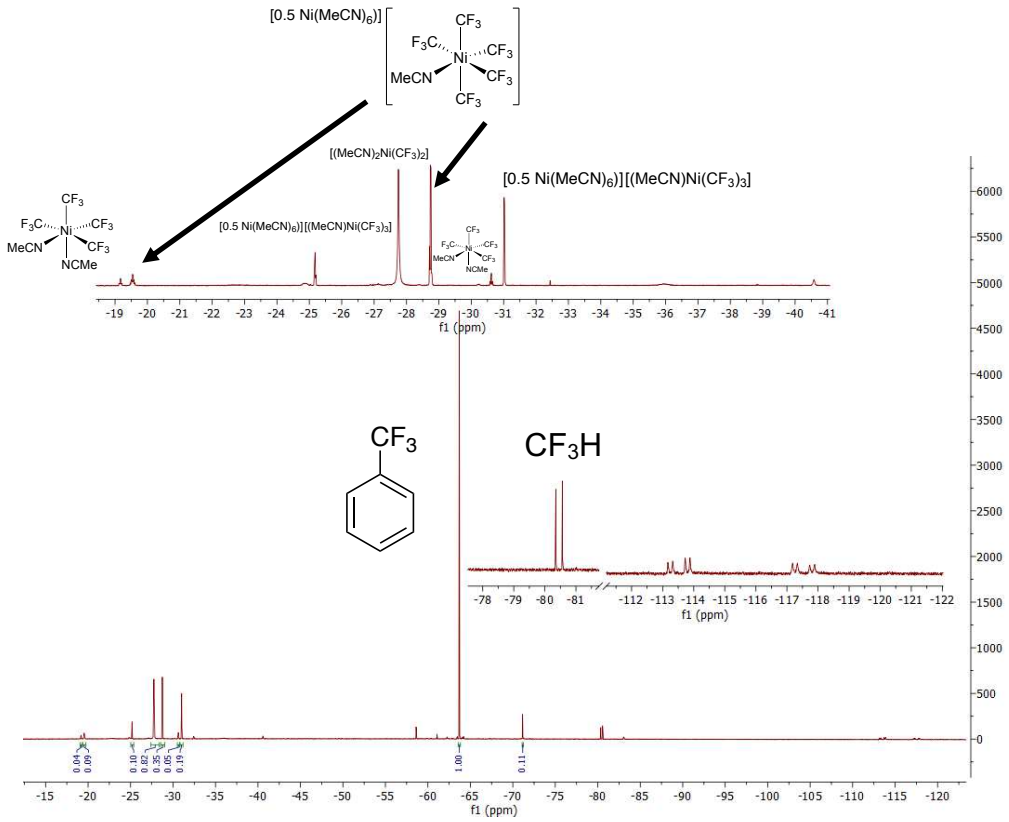

Computational details: Density functional theory (DFT) calculations were done on the different possible diastereomers of **9i** using Gaussian09.[1] Geometry optimizations and frequency calculations were done using the B3LYP functional[2,3] with a 6-31+(d,p) basis set. The IEFPCM solvation model with DMSO was employed. The true minima were confirmed by the presence of no imaginary frequencies.

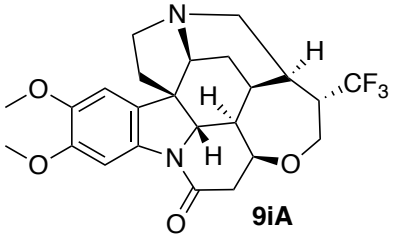

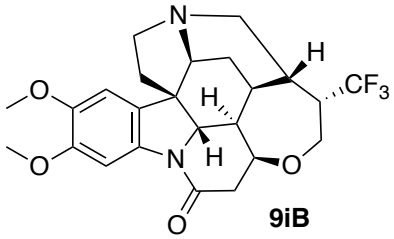

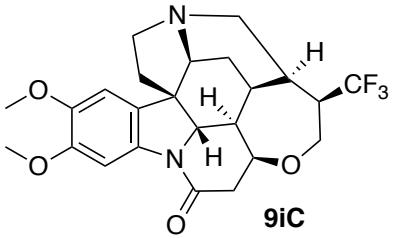

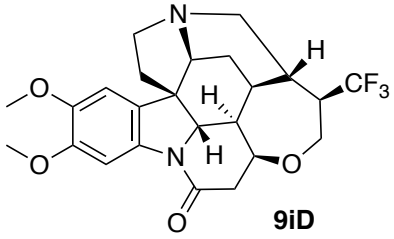

Table H6: Calculated energies of different diastereomers of **X**

Compound	Energy (Hartrees)	Energy difference with **A** set to 0 in kcal/mol
9iA	-1640.828978	0
9iB	-1640.821718	+4.6
9iC	-1640.823461	+3.5
9iD	-1640.822803	+3.9

DFT optimized geometry of 9iA

O	3.77433900	9.36035000	16.12405200
N	1.15610200	5.30331000	15.65377000
F	1.80086400	9.38469900	12.30446500
C	1.11599900	9.56479500	13.46852400
O	7.21830700	6.91773500	18.33329200
N	5.18836700	6.04661800	17.71066700
F	-0.10830900	9.00098700	13.28459500
C	1.84342100	8.98827600	14.67350300
H	1.20119200	9.23883400	15.52638500
O	7.71601400	1.84450600	18.45882400
F	0.90307400	10.90433300	13.58357600
C	3.16818300	9.74621000	14.89385700
H	3.86012200	9.59367400	14.05785600
H	2.96314500	10.81734900	14.96836400
O	5.73255400	0.52833000	17.40477600
C	4.84215100	8.40777500	16.00922500
H	5.53128400	8.75650000	15.22877100
C	4.35544000	6.99309400	15.65302500

H	5.25714700	6.45765800	15.32376000
C	3.38052800	6.83831100	14.46246300
H	3.86969000	7.26474400	13.57835800
C	5.56397400	8.41981100	17.38328500
H	6.39955900	9.12062600	17.38758900
H	4.83748000	8.77448200	18.12518600
C	6.08625100	7.06617800	17.85223300
C	3.92494600	6.29951700	16.96578700
H	3.30596800	6.98036000	17.55501600
C	3.21296200	5.32230100	14.25509000
H	2.62258700	5.11636800	13.35552100
H	4.18808000	4.84168300	14.12033500
C	2.50393100	4.72693200	15.46609900
H	2.35983100	3.65090400	15.30693000
C	3.22961500	4.90466200	16.84681000
C	2.03238400	4.73829200	17.85010700
H	2.11372700	3.79647800	18.39839600
H	2.02986900	5.54171800	18.59315200
C	0.75113500	4.75392500	16.96081300
H	0.38392200	3.73266500	16.81155500
H	-0.06481800	5.34213900	17.38912900
C	4.37781600	3.96444000	17.16016100
C	5.45328500	4.65438000	17.71630900
C	6.59938300	3.99395400	18.17602900
H	7.41180600	4.56057100	18.60488400
C	6.65452800	2.60290300	18.05388200
C	5.57111800	1.88498400	17.48017900
C	4.43542300	2.57234700	17.04368300
H	3.59867600	2.02868000	16.62140300
C	4.66545400	-0.24751300	16.85710700
H	5.00365500	-1.28314800	16.89513300
H	4.46337500	0.03287600	15.81697700
H	3.75089200	-0.13945900	17.45149700
C	8.83536500	2.50829100	19.05055400
H	9.54903900	1.72115000	19.29414200
H	8.54458300	3.03550800	19.96607300
H	9.29341600	3.21409100	18.34865400
C	1.95162100	7.43265400	14.56125100
H	1.47366100	7.13329900	13.62114800
C	1.13390700	6.78110200	15.68983200
H	0.08776400	7.09432000	15.59871300
H	1.48659600	7.17814400	16.65561900

DFT optimized geometry of 9iB

O	3.68448200	9.32986500	16.11047100
N	1.16591700	5.20690100	15.46823700
F	2.39380200	8.65807700	12.14022900

C	1.49098400	9.16390400	13.02479900
O	7.06231900	6.93328500	18.49892300
N	5.10794600	6.00453200	17.73410800
F	0.28929100	8.61691200	12.69752800
C	1.85272500	8.92994300	14.48093600
H	1.00356000	9.34456200	15.03689200
O	7.72687100	1.86064700	18.48525600
F	1.39133900	10.49531600	12.74268300
C	3.13261900	9.74335100	14.85856900
H	3.88943600	9.66279100	14.06959100
H	2.87405300	10.79906500	14.96796100
O	5.85236000	0.51898200	17.27328300
C	4.79552500	8.40746200	16.05502000
H	5.52104800	8.79894600	15.33056900
C	4.39633500	6.97698500	15.64565300
H	5.32611500	6.48025600	15.33634100
C	3.40244200	6.85031200	14.48743800
H	3.80236100	7.36088100	13.60744400
C	5.41982700	8.40554800	17.47802900
H	6.23014800	9.13082600	17.56028900
H	4.63278300	8.71683400	18.17632300
C	5.95823800	7.05375600	17.95115000
C	3.89858300	6.24170500	16.90935900
H	3.22041400	6.88763100	17.47321300
C	3.27190800	5.35226600	14.16364900
H	2.72245500	5.19280800	13.23073000
H	4.26379700	4.90935400	14.02074900
C	2.55180300	4.66127100	15.31557500
H	2.48368300	3.58360200	15.11639100
C	3.24497100	4.83560300	16.70708600
C	2.02284800	4.62810700	17.64261400
H	1.82994400	3.55394100	17.73501300
H	2.18915900	5.02317500	18.64952600
C	0.86388500	5.32443600	16.91456600
H	-0.10198800	4.86377700	17.15265500
H	0.79563500	6.37856900	17.22298100
C	4.40155400	3.91799900	17.05598300
C	5.41795100	4.62106600	17.70446600
C	6.55555300	3.98140000	18.20999900
H	7.32157200	4.55780300	18.70623400
C	6.66548700	2.59788800	18.04362100
C	5.64296300	1.86694600	17.38168000
C	4.51358900	2.53346100	16.89791500
H	3.72463700	1.97928000	16.40377800
C	4.84792300	-0.26985100	16.63341300
H	5.21546200	-1.29574400	16.66233000

H	4.70517900	0.03765200	15.59107100
H	3.89384400	-0.20801100	17.16939200
C	8.78338900	2.53673400	19.17130400
H	9.50691600	1.76393600	19.43114800
H	8.41744500	3.01848600	20.08489500
H	9.26037800	3.28334100	18.52661200
C	2.02865700	7.45794400	14.91282200
H	2.05231200	7.57637700	15.99629700
C	0.89242400	6.43828300	14.69448200
H	-0.06432600	6.84177900	15.04002900
H	0.76101300	6.18369700	13.63880700

DFT optimized geometry of 9iC

O	3.50385600	9.02921300	16.76078700
N	1.15440100	5.39387700	15.94801900
O	7.38190100	6.80386700	18.22467200
N	5.31295400	5.96035700	17.71832000
C	2.06087600	9.00530000	14.67446200
O	7.82447000	1.71384300	18.23806300
C	2.67453200	9.77732600	15.88658200
H	3.22770400	10.64253900	15.49913300
H	1.87858500	10.15220600	16.53445800
O	5.74684200	0.43660300	17.32563000
C	4.67832500	8.40187700	16.21388000
H	5.06293200	9.00889700	15.38455600
C	4.33932300	6.97646800	15.75805300
H	5.27121400	6.53701900	15.37558800
C	3.33277800	6.80077600	14.60594200
H	3.79744300	7.21395300	13.70132600
C	5.73601700	8.35177600	17.35812600
H	6.63191800	8.91346800	17.08615500
H	5.30440300	8.85330400	18.23238500
C	6.22702000	6.96976300	17.80517800
C	4.00392000	6.23223000	17.07440200
H	3.43799500	6.90516000	17.71875900
C	3.12406100	5.29121200	14.42174800
H	2.49792100	5.09394700	13.54475300
H	4.08130500	4.78251900	14.26006500
C	2.44958700	4.73367400	15.66745200
H	2.22441800	3.67007500	15.51589800
C	3.27737900	4.85694500	16.99064700
C	2.14788300	4.71019400	18.06892100
H	2.20116400	3.72964600	18.54936600
H	2.25700200	5.45990700	18.85873200
C	0.80803500	4.86458100	17.28110900
H	0.33361000	3.88474700	17.15680000
H	0.08877100	5.52027300	17.77887400

C	4.42850100	3.89440400	17.21485900
C	5.55427200	4.56341100	17.69658000
C	6.72098300	3.88134600	18.06259500
H	7.57181900	4.43171200	18.43455400
C	6.74622300	2.49100000	17.92236300
C	5.61209200	1.79470300	17.42532900
C	4.45728000	2.50298200	17.08172400
H	3.58304600	1.97616000	16.71797400
C	4.63350300	-0.31680700	16.84276700
H	4.95868500	-1.35731100	16.84291900
H	4.36410700	-0.01819500	15.82313700
H	3.76366300	-0.20566000	17.50042100
C	8.99548400	2.35657800	18.74685600
H	9.71470600	1.55765200	18.92764800
H	8.78398000	2.87900200	19.68659300
H	9.40766700	3.06298800	18.01759600
C	1.94258400	7.45779600	14.76069800
H	1.38815400	7.15835500	13.86235600
C	1.17979700	6.88200900	15.96682700
H	0.13695400	7.21068700	15.94292400
H	1.60811800	7.27682500	16.89825500
C	0.74685600	9.67629000	14.29682100
H	2.69762100	9.19304600	13.80208600
F	0.20301200	9.16266200	13.16235700
F	0.91915400	11.00973800	14.06754000
F	-0.21192900	9.58093400	15.25867900

DFT optimized geometry of 9iD

O	3.69515700	9.33363800	16.16994600
N	1.15515100	5.20422100	15.54267500
O	7.07574300	6.90919800	18.52969300
N	5.11817000	5.98206500	17.77077000
C	1.87862800	8.92084600	14.48245400
O	7.76759400	1.84132900	18.42549400
C	3.15079300	9.72985100	14.90769900
H	3.91061900	9.63172200	14.12614700
H	2.91057100	10.79169000	14.99455800
O	5.88283800	0.50766500	17.22037100
C	4.79473900	8.40017400	16.12048700
H	5.52853900	8.78377800	15.39976600
C	4.37863100	6.97698500	15.70263300
H	5.29773300	6.47730800	15.36737400
C	3.35756700	6.87102000	14.56674800
H	3.73014900	7.40054900	13.68294900
C	5.41526000	8.38643500	17.54422200
H	6.21810100	9.11860600	17.63773600
H	4.62357800	8.67934100	18.24523700

C	5.96569900	7.03224100	17.99482800
C	3.89883200	6.22551500	16.96318500
H	3.22386800	6.86206700	17.54138100
C	3.23095900	5.37965000	14.21358600
H	2.66519100	5.23410200	13.28834900
H	4.22379300	4.94939800	14.04260900
C	2.53714900	4.66398600	15.36444700
H	2.47082700	3.58908700	15.14947600
C	3.24879500	4.81970300	16.74898400
C	2.03995200	4.59139600	17.69705900
H	1.85666500	3.51467100	17.77807500
H	2.21652200	4.97456300	18.70684000
C	0.86523000	5.28813800	16.99413700
H	-0.09194400	4.80953000	17.23232700
H	0.78622100	6.33456600	17.32385700
C	4.41382400	3.90244000	17.06978100
C	5.43472700	4.60082800	17.71624400
C	6.58204600	3.95972500	18.19733300
H	7.35163500	4.53267900	18.69202100
C	6.69660800	2.57939700	18.00914700
C	5.66889400	1.85300800	17.35028800
C	4.53038100	2.52086900	16.89030200
H	3.73805300	1.96987100	16.39796400
C	4.87092600	-0.27751700	16.58784900
H	5.24311100	-1.30209200	16.59763200
H	4.70899700	0.04232600	15.55205200
H	3.92595400	-0.22635000	17.14085700
C	8.83044100	2.51324000	19.10591600
H	9.56202200	1.74087300	19.34352500
H	8.47549100	2.97934000	20.03188100
H	9.29356900	3.27206400	18.46538800
C	1.99046400	7.47926300	15.02427900
H	2.02473900	7.61237800	16.10597600
C	0.86237600	6.44912500	14.79972600
H	-0.09825500	6.81864600	15.16318900
H	0.72735300	6.22588900	13.73574900
C	0.61081000	9.63603200	14.92610200
H	1.83252200	8.92339200	13.38642500
F	0.58674700	10.93727400	14.51993100
F	-0.51495000	9.06975500	14.41010300
F	0.45094200	9.65498300	16.27701100

Figure H11: Cyclic voltammogram of $[(MeCN)_2Ni(CF_3)_4]$ in MeCN. Metal complex, 10 mM; electrolyte, 100 mM $[NBu_4][PF_6]$; working and counter electrode, platinum, silver psuedoreference, scan rate, 100 mVs^{-1}. Cyclic voltammogram was collected in a nitrogen filled glovebox at room temperature on a PARSTAT 4000A potentiostat.

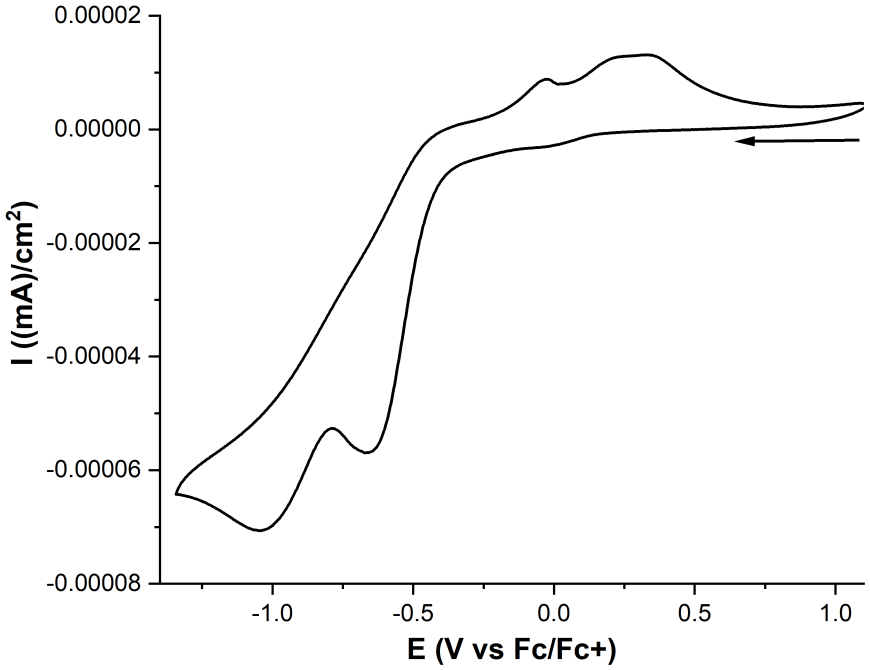

References

1) Gaussian 09, Revision D.01,
M. J. Frisch, G. W. Trucks, H. B. Schlegel, G. E. Scuseria,
M. A. Robb, J. R. Cheeseman, G. Scalmani, V. Barone, B. Mennucci,

G. A. Petersson, H. Nakatsuji, M. Caricato, X. Li, H. P. Hratchian,
A. F. Izmaylov, J. Bloino, G. Zheng, J. L. Sonnenberg, M. Hada,
M. Ehara, K. Toyota, R. Fukuda, J. Hasegawa, M. Ishida, T. Nakajima,
Y. Honda, O. Kitao, H. Nakai, T. Vreven, J. A. Montgomery, Jr.,
J. E. Peralta, F. Ogliaro, M. Bearpark, J. J. Heyd, E. Brothers,
K. N. Kudin, V. N. Staroverov, T. Keith, R. Kobayashi, J. Normand,
K. Raghavachari, A. Rendell, J. C. Burant, S. S. Iyengar, J. Tomasi,
M. Cossi, N. Rega, J. M. Millam, M. Klene, J. E. Knox, J. B. Cross,
V. Bakken, C. Adamo, J. Jaramillo, R. Gomperts, R. E. Stratmann,
O. Yazyev, A. J. Austin, R. Cammi, C. Pomelli, J. W. Ochterski,
R. L. Martin, K. Morokuma, V. G. Zakrzewski, G. A. Voth,
P. Salvador, J. J. Dannenberg, S. Dapprich, A. D. Daniels,
O. Farkas, J. B. Foresman, J. V. Ortiz, J. Cioslowski,
and D. J. Fox, Gaussian, Inc., Wallingford CT, **2013**.

2) Becke, A. D., Density-Functional Thermochemistry. III. The Role of Exact Exchange. *J. Chem. Phys.* **1993,** *98*, 5648-52.
3) Lee, C.; Yang, W.; Parr, R. G., Development of the Colle-Salvetti Correlation-Energy Formula into a Functional of the Electron Density. *Phys. Rev. B: Condens. Matter* **1988,** *37*, 785-9.

Curriculum Vitae

Scott T. Shreiber

scottshreiber1@gmail.com

Education

Lehigh University-Bethlehem, PA — August 2018 - Present
Ph.D. Chemistry — GPA: 3.92 — *Expected May 2022*
Dissertation Title
Advancing Fluoroalkylation Methodologies with Copper, Nickel, and Cobalt
Advisor: Dr. David A. Vicic

Lock Haven University-Lock Haven, PA — August 2014 – May 2018
B.S. *summa cum laude* in Chemistry — GPA: 3.84

Publications

10) Shreiber, S.T.; Vicic, D.A. Synthesis and Electrochemical Properties of Heteroleptic Trifluoromethyl Nickelates $[(azaindole)Ni(CF_3)_3]^{2-}$ and $[(PhO)Ni(CF_3)_3]^{2-}$. **2022** *manuscript in preparation*.

9) Xue, T.; Shreiber, S.T.; Vicic, D.A. Synthesis and Characterization of Solvated Perfluoroethyl and *n*-Perfluoropropyl Cobalt(III) Complexes. **2022**, *manuscript in preparation*.

8) Shreiber, S.T.; Puchall, G.I.; Vicic, D.A. Transformation of brucine into trifluoromethyl neobrucine using the homoleptic nickel catalyst $[Ni(CF_3)_4]^{2-}$. **2022**, *submitted*.

7) Shreiber, S.T.; Amin, F.; Schäfer, S.A.; Cramer, R. E.; Klein, A.; Vicic, D.A. Synthesis, Strucure, and Electrochemical Properties of $[LNi(R_f)(C_4F_8)]^-$ and $[LNi(R_f)_3]^-$ Complexes. *Dalton Trans.* **2022**, *in press*.

6) Shreiber, S.T.; Vicic, D.A. Synthesis and Characterization of the Dinuclear Cobalt(III) Complex: $[(C_2F_5)_3Co(\mu\text{-}F)]_2^{2-}$. *J. Organomet. Chem.* **2021**, *949*, 121974.

5) Shreiber, S.T.; Vicic, D.A. Solvated Nickel Complexes as Stoichiometric and Catalytic Perfluoroalkylation Agents. *Angew. Chem. Int. Ed.* **2021**, *60*, 18162-18167. *Article also appears in "Hot Topic: Fluorine Chemistry"*

4) Shreiber, S.T.; Vicic, D.A. Synthesis and Oxidative Stability of an Anionic Perfluoroethyl Cobalt(III) Complex. *Helv. Chim. Acta* **2020**, *103,* e2000149. *Part of a special issue dedicated to Antonio Togni.*

3) Shreiber, S.T.; DiMucci, I.M.; Khrizanforov, M. N.; Titus, C. J.; Nordlund, D.; Dudkina, Y.; Cramer, R.E.; Budnikova, Y.; Lancaster, K. M.; Vicic, D.A. $[(MeCN)Ni(CF_3)_3]^-$ and $[Ni(CF_3)_4]^{2-}$: Foundations toward the Development of Trifluoromethylations at Unsupported Nickel. *Inorg. Chem.* **2020**, *59*, 9143-9151. *This work was listed as one of the 'most-read' articles of the journal during the month of June 2020.*

2) Shreiber, S.T.; Kaplan, P.T.; Hughes, R.; Vasiliu, M.; Dixon, D.A.; Cramer, R.E.; Vicic, D.A. Synthesis, Solution Behavior, and Computational Bond Length Analyses of Trifluoromethyl and Perfluoroethyl Cuprate Salts. *J. Fluorine Chem.* **2020**, *234,* 109518.

1) Shreiber, S.T.; Scudder, J.J.; Vicic, D.A. $[(MeCN)_3Co(C_2F_5)_3]$: A Versatile Precursor to Cobalt (III) Perfluoroethyl Complexes. *Organometallics* **2019**, *38*, 3169-3173. *This work was listed as one of the 'most-read' articles of the journal during the month of August 2019.*

Presentations

Winter Fluorine Conference – Clearwater, FL January 2022

- Oral – Use of Solvated Nickel in Perfluoroalkylation Reactions

Pacifichem 2021 – Honolulu, HI December 2021

- Oral – Use of Solvated Nickel in Perfluoroalkylation Reactions (*Virtual)*

European Symposium of Fluorine Chemistry – Warsaw, Poland
August 2019

- Poster – New Chemistry of First-Row Metals Bearing Fluoroalkyl Substituents
    - *Awarded as one of the best poster presentations*

American Chemical Society National Meeting – New Orleans, LA
March 2018

- Poster – Divergent Transmetalation between Boron and Tin Reagents
- Poster – Lock Haven University Chemistry Club

American Chemical Society National Meeting – San Francisco, CA
April 2017

- Poster – Development of High Performance Liquid Chromatography Methods for a
  Waters Alliance HPLC Running Empower 3 Software
- Poster – Lock Haven University of Pennsylvania Chemistry Club

American Chemical Society National Meeting – San Diego, CA
March 2016

- Poster – Lock Haven University of Pennsylvania Chemistry Club

Employment and Teaching Experience

Lehigh University June 2018 – Present

- Roy G. Hornor Fellow
    - May 2021 - *present*
- Graduate Teaching Assistant
    - Organic Chemistry II Recitation Instructor
        - Feb. 2021 –May 2021
    - General Chemistry II Lab TA
        - Jan. 2020 – May 2020
- Graduate Research Assistant
    - Aug. 2019 – Jan. 2020, June 2020 –Jan. 2021
- Lehigh Presidential Fellow
    - Aug. 2018 – Aug. 2019
- Graduate Student Summer Researcher
    - June 2018 – Aug. 2018

Montana State University June 2017-Aug. 2017

- Researcher funded by National Science Foundation (NSF) research experience for undergraduate (REU) grant
    - Worked in the Neufeldt Group

Avery Dennison Performance Polymers

- Laboratory Intern in the Performance Polymer Division
  Feb. 2016 – May 2018

Lock Haven University

- Tutorial Services – Chemistry Tutor Aug. 2015 – May 2017
- Course Assistant – Principles of Chemistry 1, Basic Chemistry
  Aug. 2015 – Dec. 2016

Honors and Awards

Lehigh University

- Roy G. Hornor Fellowship May 2021
- Graduate Student Senate Travel Grant August 2019
- Lehigh Presidential Fellowship August 2018

Lock Haven University

- Syed R. Ali-Zaidi Award Nominee April 2018
- Chemistry Faculty Award Fall 2015 – Spring 2018 (6x)
- Deans List 8 of 8 semesters
- Organic Chemistry 1 & 2 Award
  - Highest Achievement in Organic Chemistry 1 & 2
    December 2016
- CRC Press Chemistry Achievement Award
  - Highest Achievement in Principles of Chemistry 1 & 2
    November 2015
- Intermediate General Physics 1 & 2 Award
  - Highest Achievement in Physics (Calculus Based) 1 & 2
    November 2015

Red Land High School

- National Honor Society - member 2013-2014

Professional Affiliations

Lock Haven University – Chemistry Club President

August 2015 – May 2018

- Organized/Presented: PSU Nuclear Reactor tour, Halloween Demonstration Shows, Chemistry Camp, Journal Club

- Acquired funding (Joseph A. Dixon Travel Grant) and planned trips for ACS National Meetings (251st, 253rd, 255th)

American Chemical Society October 2015 – Present

Phi Kappa Phi – National Honor Fraternity February 2016 – Present